DEOXYNYBOQUINONES AS NQO1-TARGETED ANTICANCER COMPOUNDS AND DEOXYNYBOMYCINS AS POTENT AND SELECTIVE ANTIBIOTICS

BY

ELIZABETH IVY PARKINSON

DISSERTATION

Submitted in partial fulfillment of the requirements
for the degree of Doctor of Philosophy in Chemistry
in the Graduate College of the
University of Illinois at Urbana-Champaign, 2015

Urbana, Illinois

Doctoral Committee:

Professor Paul J. Hergenrother, Chair
Professor Martin D. Burke
Professor Wilfred A. van der Donk
Professor Douglas A. Mitchell

ABSTRACT

Cancer and antibiotic-resistant bacterial infections are currently two of the major health concerns facing the United States. Novel therapeutics capable of specifically targeting either cancer or resistant bacteria are greatly needed. Described herein are three separate efforts to address these needs.

Described in Chapter 2 is the development of a targeted anticancer agent deoxynyboquinone (DNQ) which is specifically activated by the enzyme NAD(P)H:quinone oxidoreductase-1 (NQO1). NQO1 is a 2-electron reductase that is known to be overexpressed in many solid tumors. Development of an anticancer quinone that is bioactivated by NQO1 has long been a goal of cancer therapy. Previously, several putative NQO1 substrates have been developed including mitomycin C, RH1, streptonigrin, and β-Lapachone (β-Lap). Recently the Hergenrother laboratory discovered the small molecule DNQ which has potent anticancer activity. Due to its quinone moiety and the fact that it causes reactive oxygen species (ROS) dependent cell death, we hypothesized that its activity was due to activation by NQO1.

Described herein is a set of assays that was developed to determine the NQO1-dependence of anticancer compounds. Of the putative NQO1 substrates, only β-Lap and DNQ were found to be selectively activated by NQO1. Due to its excellent potency and pharmacokinetic profile, DNQ was explored further. Mechanistic evaluation of DNQ revealed that after reduction by NQO1, DNQ undergoes reduction-oxidation cycling which concurrently results in the formation of ROS. ROS causes extensive DNA damage that then activates poly(ADP-ribose) polymerase-1 dependent cell death. DNQ was found to be efficacious a murine model of lung cancer. Utilizing a modified version of the DNQ synthesis previously developed by the Hergenrother laboratory, derivatives were synthesized and evaluated. Several were found that have potent activity against a panel of breast and lung cancers along with improved solubility and toxicity profiles compared to DNQ. These derivatives are currently under investigation for *in vivo* activity.

Described in Chapter 3 is the development of deoxynybomycin (DNM) as an antibiotic with potent activity against fluoroquinolone-resistant (FQR) bacteria. DNM is a natural product that has been shown previously to have antibiotic activity. Recently DNM was found to have potent activity against FQR Methicillin-resistant *S. aureus* (MRSA). This activity is due to the ability of DNM to inhibit the mutant DNA gyrase (specifically S84L gyrA) responsible for FQR. At the start of the studies described here, two main challenges to the further development of DNM existed: 1) Difficulty in attaining significant quantities of pure DNM for biological evaluation and 2) The poor solubility of DNM. The first issue was addressed by the development of a synthesis of DNM. A single reaction from a late stage intermediate of the DNQ synthesis allowed for the generation of DNM. The modular nature of the synthesis also allowed for the synthesis of a variety of derivatives some of which showed similar potency against FQR MRSA and greatly improved solubility.

DNM and its derivative DNM-2 were tested against a variety of bacterial species to determine the activity profile for this class of compounds. The best activity was observed for FQR MRSA with S84L mutant of DNA gyrase and FQR VRE with S84I mutation. Less potent activity was observed for bacteria that commonly have other mutations such as S84F or S84Y. *In vitro* inhibition assays suggest that DNM is less potent against DNA gyrase with these mutations, but further studies need to be performed to confirm this. Additionally, DNM is inactive against Gram-negative bacteria likely due to its inability to traverse the outer membrane. Further studies to identify compounds active against Gram-negative bacteria are ongoing. Resistance to DNM was found to occur via regeneration of the WT DNA gyrase, thus re-sensitizing bacteria to FQs. This resistance cycling suggests that bacteria which develop resistance to DNM would be treatable.

After determining that DNM and DNM-2 have good potency against FQR MRSA, studies evaluating their *in vivo* activity were performed. Initial pharmacokinetic analysis revealed that oral administration of DNM is not a useful administration route likely due to its poor solubility.

However, DNM-2 has excellent oral absorption with area under the curve values which predict good *in vivo* efficacy. DNM-2 was used in further studies. Toxicity studies revealed no significant effects of DNM-2 on mice when treated at 50 mg/kg for ten consecutive days. Excitingly, DNM-2 was the first compound in the deoxynybomycin class to show *in vivo* activity, saving mice with FQR MRSA sepsis.

Described in Chapter 4 is the analysis of the anticancer compound ersindole, an actiniophyllic acid analogue synthesized by the Martin laboratory. The anticancer activity of ersindole was discovered by the Hergenrother laboratory via a high throughput screen for compounds which induce breast cancer cell death. One of the most striking features of ersindole-induced cancer cell death is the shape of the dose response curve. Specifically, it has a very steep Hill slope and high E_{max}. These attributes reflect consistent and efficient induction of cancer cell death and suggest that ersindole is a very promising anticancer drug. Analysis of multiple cell lines and timepoints reveal that the steep Hill slope and high E_{max} of the ersindole dose response curve are general attributes of the compound. Previous mechanistic studies with ersindole suggested that it induced cancer cell death via induction of endoplasmic reticulum stress. This was further confirmed here via Western blot analysis and siRNA knockdown studies. Future efforts should focus on determining the molecular target of ersindole.

Unfortunately, ersindole was found to induce hemolysis of red blood cells. A set of derivatives was investigated in an effort to find compounds that do not lyse red blood cells. Ersindole-9 was found to be nearly as potent as ersindole against a panel of cancer cell lines and to have a similarly shaped dose-response curve. Gratifyingly, ersindole-9 does not induce significant hemolysis. For this reason, ersindole-9 was studied in a murine model of breast cancer where it was found to have good efficacy. Evaluation of a second set of derivatives was then performed in order to find additional derivatives that are potent and do not induce hemolysis. Several leads were discovered. Further analysis of these compounds is needed to determine the best compound for future evaluation.

ACKNOWLEDGEMENTS

I am extremely grateful to those who have helped me complete this work. First, I would like to thank my advisor, Paul Hergenrother, who has been a wonderful source of support, guidance, and inspiration. I am so appreciative that he was willing to accept me into his lab and support me over the years. I am especially thankful for his patience with me and his commitment to my education which has allowed me to become the scientist I am today.

I would like to thank my committee, Professors Burke, Mitchell, and van der Donk, who have provided me with valuable advice both about my projects as well as my future goals. I have also benefited greatly from the support of other faculty members including Professors Zimmerman and Beak. During my time at UIUC, I have had the privilege to collaborate with a number of professors including Professor David Boothman, Stephen Martin, Sarah Reisman, Mo Movassaghi, Gee Lau, Tim Fan, John Katzenellenbogen, and Benita Katzenellenbogen. I am very appreciative to them and their students for their help and advice with these projects. I also thank my undergraduate research advisor Dr. Phil Potter, my undergraduate academic advisor Prof. David Jeter, my chemistry and biology professors from Rhodes College, and my high school biology teachers Mr. O'Connell and Mrs. Hugie. Without them I would never have pursued this path. Also, thank you to the National Science Foundation and the American Chemical Society Division of Medicinal Chemistry for providing me with pre-doctoral fellowships.

Thank you to the Hergenrother group, past and present, both for your friendship and your assistance in lab. I am especially thankful to Joe Bair who was very patient with me from the beginning and has continued to help me even long after he graduated. I am thankful to all members of my subgroup, previous and current, who have challenged me with questions and given me advice on how to overcome problems. I am also extremely appreciative of the high school, undergraduate, and veterinary medicine students who I have had the opportunity to work with and who have helped to push projects forward. Finally, thank you to my family and friends who have encouraged me throughout this process. I would not have made it without you.

TABLE OF CONTENTS

Chapter 1. Introduction

Portions of this Chapter are reprinted with permission from Parkinson, E.I.; Hergenrother, P.J. "Deoxynyboquinones as Personalized Anticancer Therapeutics" *Acc. Chem. Res.* Submitted **2015**., Parkinson, E. I.; Hergenrother, P. J. "Runaway ROS as a Selective Anticancer Strategy" *Chem Med Chem* **2011**, *6*, 1957-1959., and Bair, J. S.; Palchaudhuri, R.; Hergenrother, P. J. "Chemistry and Biology of Deoxynyboquinone, a Potent Inducer of Cancer Cell Death" *J. Am. Chem. Soc.* **2010**, *132,* 5469-5478.

1.1 Deoxynyboquinones as personalized cancer therapeutics

Cancer is the second-leading cause of death in the United States and is expected to surpass heart disease as the leading cause of death within the next few years.[1] It is estimated that there will be 1,658,370 new cancer cases and 589,430 cancer deaths in 2015.[1] Treatment of cancer typically relies on a combination of surgery, radiotherapy, and chemotherapeutics.[2] The majority of chemotherapeutics used in the clinic target macromolecules important for general cell survival, such as DNA, topoisomerase, and tubulin (e.g., cisplatin, doxorubicin, and paclitaxel, respectively). While these agents are effective at killing many types of cancer cells, they also affect rapidly dividing normal cells, such as those in the intestinal lining and bone marrow, resulting in dose-limiting toxicities that reduce efficacy against many solid tumors and metastatic disease. A goal of personalized therapy as applied to cancer is to understand the precise defects in the cancer cell, which may only be present in one particular type of cancer and/or a small subset of patients, and to develop drugs that exploit these differences. A small number of such cancer-specific therapies exist. These treatments commonly target a unique characteristic of cancer, such as a translocation, mutation, or protein with elevated expression.[3] The poster child for this approach is imatinib (Gleevec), which inhibits the tyrosine kinase domain of the Bcr-abl protein, the product of a translocation between chromosomes 9 and 22 often observed in patients with chronic myeloid leukemia. Analogous success stories have appeared, including erlotinib

(Tarceva), which inhibits a mutated version of the epidermal growth factor receptor (EGFR) protein found in some non-small-cell lung cancers,[3] and trastuzumab (Herceptin), a monoclonal antibody that targets the Her-2/neu receptor that is overexpressed in some breast cancers.[3] As effective as these therapies are for their target populations, they are only useful for a subset of cancer patients. One of the major goals of cancer research is the identification of novel targets and associated targeted therapeutics that would be effective against other groups of cancer patients.

1.1.1 NQO1 and cancer

NQO1 is a 2-electron reductase responsible for the detoxification of xenobiotics such as quinones.[4] It is known to be overexpressed in many solid tumors including non-small cell lung carcinoma,[5-13] breast cancer,[5,8-9,14] colon cancer,[5,9,15-16] pancreatic cancer,[17-20] and ovarian cancer,[9,21] among others.[5,9,22-24] High NQO1 expression correlates with later clinical stage, metastasis, lower disease-free survival, and lower overall survival.[12-14,16,21-23] While the reason for NQO1 overexpression in cancer is not fully understood, it possibly enables cancer cells to cope with increased oxidative stress.[25] NQO1 expression is under the control of the transcription factor Nrf2, which with its repressor KEAP1 makes up one of the major signaling cascades for stress response.[26] Normally Nrf2 is bound to KEAP1 and cannot induce expression of its target proteins. Upon exposure to electrophiles or ROS, KEAP1 is inactivated, thus allowing for activation of Nrf2.[25-26] In cancers including lung,[27-28] breast,[29] and ovarian,[30] Nrf2 is often constitutively activated by mutations to itself or KEAP1 or by changes in copy number.[25] These mutations and their downstream effects (e.g. overexpression of NQO1) are hypothesized to be drivers of oncogenesis.[28,31-32] Based on this alteration of NQO1 in cancer, it was speculated that inhibiting NQO1 would be an effective anticancer strategy as this inhibition could lead to toxic oxidative stress levels.[33] However, studies with NQO1 inhibitors indicate that there is no correlation between NQO1 inhibition and cancer cell cytotoxicity.[34-35]

NQO1 has two characterized polymorphisms, NQO1*2 and NQO1*3, either of which results in inactivation of the enzyme.[4] NQO1*2 is the more common polymorphism with ~4% of Caucasians and ~20% of Asians homozygous for it.[36] While some studies suggest that individuals with the NQO1*2 polymorphism have a higher risk of developing cancer, others suggest that the effect is small if it does exist.[37-38] Regardless, individuals with these polymorphisms that have cancer would not benefit from a therapy that targets overexpression of NQO1; facile methods exist for the detection of this polymorphism allowing for convenient patient screening for NQO1 status.[39]

1.1.2 NQO1 substrates as reduction-oxidation cyclers and anticancer agents

Given its dramatic overexpression in most solid tumors, exploitation of the ability of NQO1 to *activate* certain compounds to toxic species has been explored. NQO1 catalyzes a 2-electron reduction of a variety of substrates including quinones (to give hydroquinones, Figure 1.1), quinoneimines, nitroaromatics and azo dyes.[40] The 2-electron reduction of quinones, including endogenous quinones (e.g. estradiol-3,4-quinone[40] and ubiquinone,[41] Figure 1.2A) and exogenous quinones (menadione[41] and benzo[*a*]pyrene 3,6-quinone[41], Figure 1.2A), is generally believed to be a detoxification process as most hydroquinones are stable (or at least more stable than their semiquinone counterpart) and easily conjugated to glutathione or glucuronic acid and excreted.[41-42] However, certain hydroquinones are not stable and have the potential to induce cell death (Figure 1.1).[4] Three main mechanisms of NQO1-dependent death been proposed. The first is a direct alkylation of DNA by the hydroquinones.[36,43-45] While there is evidence that some quinones (e.g. mitomycin C and RH1, Figure 1.2B) are activated by NQO1 to DNA alkylators,[36,43-45] there is controversy over the importance and magnitude of this effect.[4,36,46-48] Recent head-to-head comparisons (as discussed herein) indicate that most of these compounds are not bioreductively activated by NQO1 in cancer cells in culture.[49] The second mechanism is inhibition of Hsp90 by hydroquinones.[50-51] It appears that certain quinones (e.g. geldanamycin and its

derivative 17-AAG, Figure 1.2B) upon reduction to their corresponding hydroquinones by NQO1 become potent inhibitors of Hsp90.[4,50-51] However, the NQO1 dependence of this conversion has been questioned in other studies.[52]

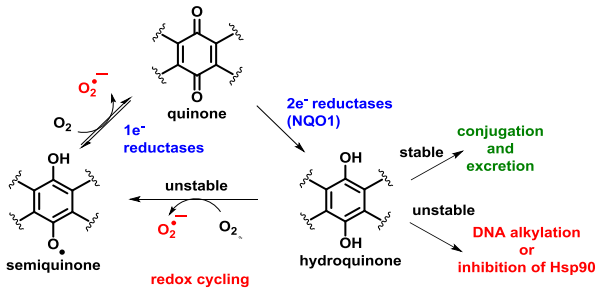

Figure 1.1. Reduction pathways and subsequent reactions of quinones.

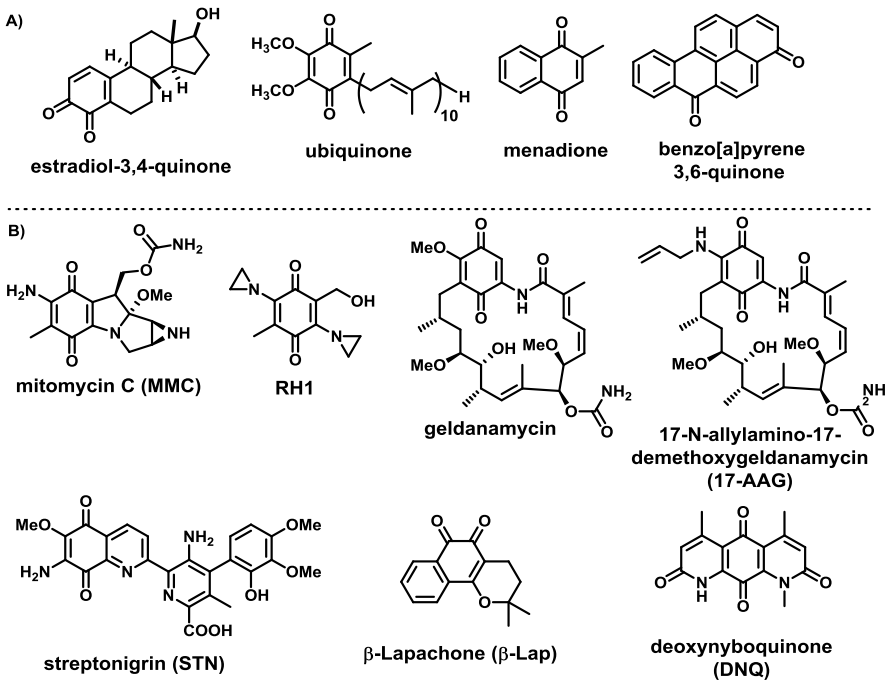

Figure 1.2. A) Quinones detoxified by NQO1. B) Quinones reported to be bioactivated by NQO1.

The final and most substantiated NQO1-dependent mode-of-action for anticancer agents is the redox cycling quinones (Figure 1.1 and 1.2B).[11,49,53] Upon reduction by NQO1, the respective hydroquinones rapidly react with molecular oxygen in the cell to give two moles of

superoxide and regenerate the quinone. Because these compounds rapidly and catalytically generate large quantities of toxic ROS only in NQO1-expressing cells, they have considerable potential as anticancer agents. Three main NQO1 substrates that are redox cyclers have been described (Figure 1.2B), streptonigrin (STN), β-lapachone (β-Lap), and deoxynyboquinone (DNQ, described further in Chapter 2). STN is a moderate NQO1 substrate,[49,54] but is also activated by other enzymes[55] and likely because of this has severe *in vivo* toxicity.[56] β-Lap is a good substrate for NQO1[49,57] that has been convincingly shown to induce NQO1-dependent death of cancer cells[49,57-63] and has shown promise in initial clinical trials.[4,64] As described in detail herein, DNQ has also been found to be activated by NQO1 and undergo redox cycling.[49,53]

1.1.3 Tools for determining NQO1 dependence

Two general methods exist for determining whether a compound induces NQO1-dependent cancer cell death. The first is a chemical method. With this method, cells are treated with compound of interest alone or are co-treated with compound of interest and an NQO1 inhibitor. If the compound must be activated by NQO1 to induce cancer cell death, co-treatment with an NQO1 inhibitor should result in greatly reduced cell death (Figure 1.3A).

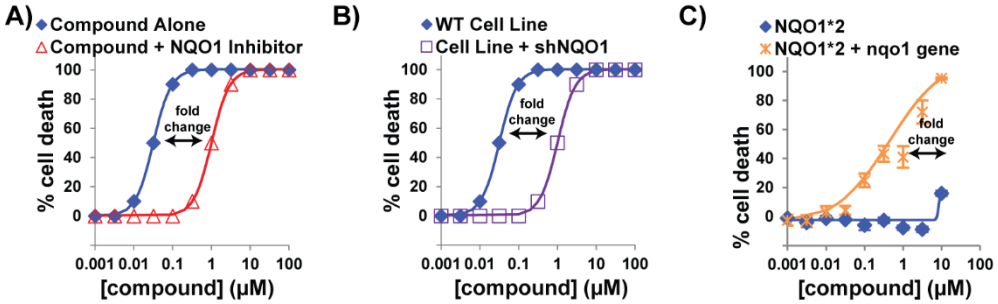

Figure 1.3. (**A**) Dose-response curve for an NQO1-overexpressing cell line is treated with compound in the presence (red) and absence (blue) of an NQO1 inhibitor. (**B**) Dose-response curve for isogenic NQO1-overexpressing cell lines transfected with either nonsense shRNA (WT Cell Line, blue) or shRNA against NQO1 (Cell Line + shNQO1, purple) and treated with compound. (**C**) Dose-response curve for isogenic NQO1*2-cell lines transfected with either empty vector (NQO1*2, blue) or the gene for NQO1 (NQO1*2 + nqo1 gene, yellow) and treated with compound.

Two NQO1 inhibitors are commonly used in these types of assays. The first is dicoumarol (DIC, Figure 1.4), a coumarin which originally was used as an anticoagulant.[65] DIC is a competitive inhibitor of NQO1 (K_I = 1-10 nM) that interacts with the NAD(P)H binding site.[66] The second inhibitor is ES936 (Figure 1.4), a potent mechanism based inhibitor which alkylates key tyrosine residues within the NQO1 active site.[34] While neither DIC nor ES936 has perfect specificity for NQO1,[34,67-68] both DIC and ES936 are widely used in studies of NQO1-mediated cell death,[53,57-58,69-70] as incubation of cells with these inhibitors is effective in blocking the enzymatic activity of NQO1.[33,70-72]

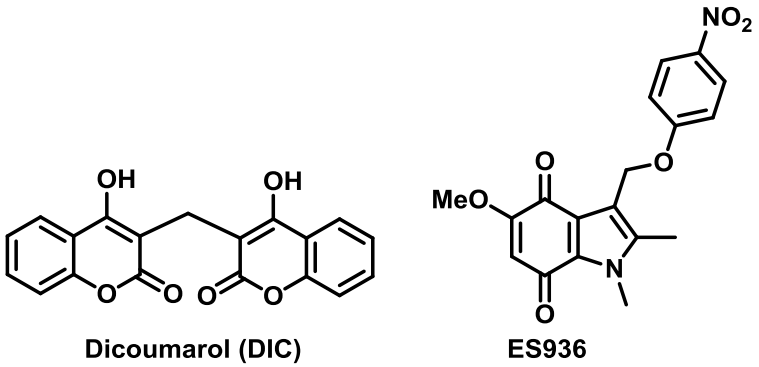

Figure 1.4. NQO1 inhibitors

The second method for determining whether an anticancer compound requires activation by NQO1 is the genetic method. The first example of the genetic method is utilizing a cell line which normally expresses high levels of NQO1 and knocking down NQO1 using shRNA against it. The WT cell line should be sensitive to the compound while the NQO1-knockdown cell line should have greatly reduced sensitivity (Figure 1.3B). This strategy was previously used with the pancreatic cell line MIA PaCa-2 to demonstrate that NQO1-dependence of β-Lap.[61] The second strategy uses cell lines derived from individuals with the NQO1*2 polymorphism described earlier in section 1.1.1 which results in undetectable NQO1 activity. Testing of isogenic cell line pairs of the NQO1*2 cell line transfected with either empty vector or the gene for NQO1 is another excellent way to determine the NQO1 dependence of a compound. The compound should show

little-to-no activity against the NQO1*2 cell line and greatly improved activity against the NQO1*2 cell line transfected with the *nqo1* (Figure 1.3C). This technique is commonly used to determine NQO1 dependence of a compound.[11,73-74]

1.1.4 Discovery and synthesis of DNQ

DNQ was initially synthesized in 1961 by Rinehart and Renfroe as part of studies aimed at elucidating the structure of the natural product nybomycin,[75] and in 2012 was found to be a natural product.[76-77] The potent anticancer activity of DNQ was discovered during a high throughput screen of the UIUC Heritage library[78] as well as in a study by the National Cancer Institute.[79]

To further study its activity and generate derivatives, a scalable synthetic route to DNQ was required. While Rinehart and coworkers developed a synthesis of the structurally related compound deoxynybomycin (DNM)[80-81] that could then be converted to DNQ using concentrated nitric acid,[75] this route was low yielding (<0.8% overall yield) and not amenable to derivative synthesis. For this reason the Hergenrother laboratory developed a novel, modular route to DNQ that could provide the large quantities of compound required for animal studies and allow construction of derivatives. This route involves a mixed Suzuki cross-coupling followed by ring closing to afford the core, deprotection, and salcomine-catalyzed oxidation to the quinone (Scheme 1.1).[82] Using this route significant quantities of compound was generated for biological evaluations, and 25 novel derivatives were synthesized that will be discussed further below.[49] As described in Chapter 3, a variation of this route can be used to construct DNM, and through derivative synthesis and screening we identified a non-natural version of DNM that has impressive antibacterial activity in mice infected with MRSA.[83]

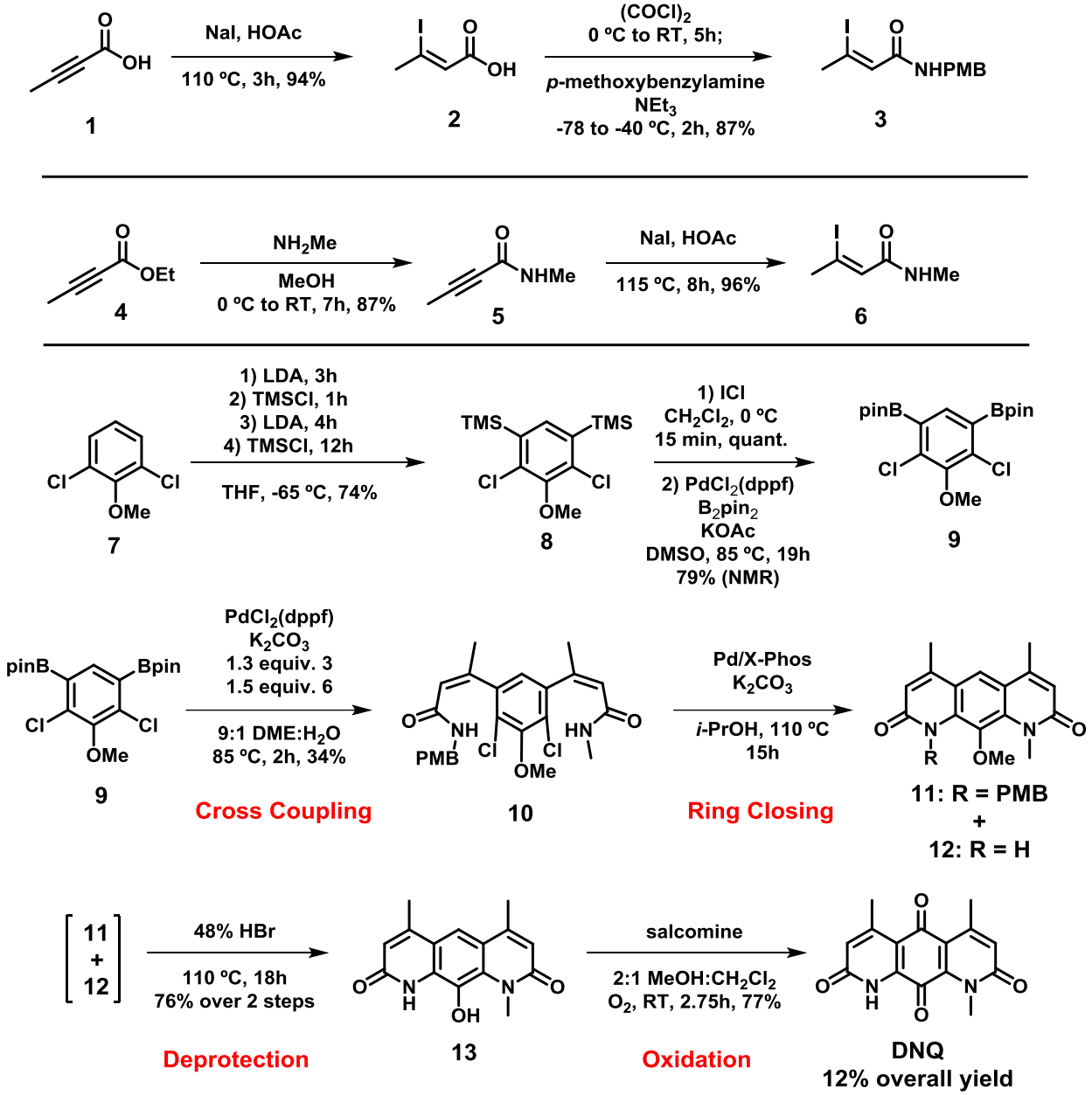

Scheme 1.1. Synthesis of DNQ.[82]

1.1.5 Mode of action of DNQ

When certain cancer cells are treated with DNQ, large amounts of ROS are generated,[53,82,84] and the potency of DNQ is reduced either in co-treatments with antioxidants (e.g.

N-acetylcysteine) or treatment under reduced oxygen atmosphere (hypoxia), suggesting that its mechanism is dependent upon ROS generation (Figure 1.5).[82] This mechanism was further supported by transcript profiling data of cells treated with DNQ where the top up-regulated genes were *HMOX1*, the gene that encodes for the antioxidant enzyme heme oxygenase-1, and other oxidative stress related genes.[82,84]

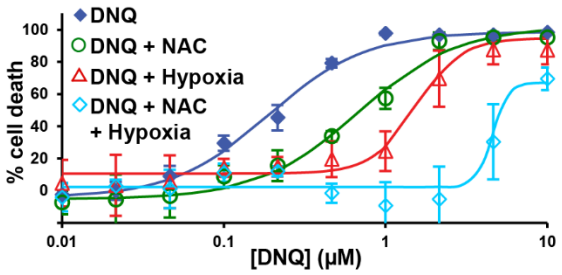

Figure 1.5. Effect of DNQ on HeLa cells in hypoxia and normoxia, and in the presence of *N*-acetylcysteine (NAC).[82]

For quinones, two major pathways for ROS generation exist: 1) 2-electron reduction by NQO1 followed by redox cycling of the unstable hydroquinone as described earlier or 2) 1-electron reduction by one of the various 1-electron reductases to an unstable semiquinone that then redox cycles (Figure 1.1).[82,85]

When I joined the Hergenrother laboratory, the mechanism by which DNQ induces ROS was unknown. We hypothesized that DNQ was activated by NQO1. As described earlier in Section 1.12, many compounds have been hypothesized to be NQO1-activated anticancer compounds. These studies often utilized only a single technique to "prove" NQO1-activation of a compound. Additionally, few studies directly compare compounds making it difficult to assess which putative NQO1-substrate is the most promising. In order to determine if DNQ is activated by NQO1, we chose to examine it in a variety of assays including *in vitro* activation, cell culture studies with chemical inhibitors, and cell culture studies with genetic modulation of NQO1 levels. Utilization of these different techniques decreases the possibility of false positive results.

Additionally, we examined other putative NQO1 substrates in the same set of assays at the same time in order to directly compare them. This allows us to definitely determine which of the NQO1-substrates is the most promising.

As is shown in Chapter 2, we found that DNQ is an excellent substrate for NQO1 and potently induces NQO1-dependent cell death in a variety of cancer cell lines. Additionally, we found that many of the other compounds (e.g. MMC, RH1, and STN) are activated by reductases other than NQO1. β-Lap was found to be a good substrates for NQO1 and induced NQO1-depedent cell death. However, the studies performed here suggest that DNQ is the most promising of the putative NQO1 substrates. With this data in hand, we chose to perform a full mechanistic analysis and determine the *in vivo* activity of DNQ in murine models of cancer. While DNQ showed good activity in a murine model of lung cancer, its low solubility combined with its dose-limiting toxicity mean that it is likely not the best lead compound. For this reason, another goal of my project was to design DNQ derivatives that retain activity but have increased solubility and tolerability.

1.1.6 Summary

Due to the widespread prevalence of cancer and the large number of deaths that it causes each year, more effective anticancer drugs are needed. One strategy to develop novel anticancer agents is to find compounds capable of specifically targeting cancer cells over normal cells. NQO1-mediated activation of an anticancer agent is an excellent targeted strategy as NQO1 is often dramatically overexpressed in cancer cells compared to normal cells. Discovery of a small molecule substrate that is capable of redox cycling back to the parent molecule is particularly promising both because of the targeted nature of the activation and the low amount of compound that is required. As described in Chapter 2, DNQ is just such a substrate. The quinone was discovered to be a potent inducer of cancer cell death during a high throughput screen. Development of a modular synthesis of DNQ allowed for further biological characterization.

Preliminary mechanistic studies found it to induce ROS dependent cell death consistent with activation by NQO1 and subsequent redox cycling. In Chapter 2, we provide evidence that DNQ is in fact an excellent substrate for NQO1. Utilizing DNQ and other active derivatives, we demonstrate that an NQO1-activated compound has great potential as a targeted anticancer agent.

1.2 Development of antibiotics that target antibiotic resistant bacteria

"There is the danger that the ignorant man may easily underdose himself [with antibiotics] and by exposing his microbes to non-lethal quantities of the drug make them resistant."

-Alexander Fleming, Nobel Lecture, Dec. 11, 1945

This warning presented by Sir Alexander Fleming during his acceptance speech of the 1945 Nobel Prize in Physiology and Medicine[86] highlights the strong possibility for the development of clinically significant antibiotic resistant bacteria. Unfortunately, since then, widespread antibacterial resistance has occurred with clinically relevant resistance being observed for all major classes of antibiotics.[87] The CDC estimates that there were 2 million illnesses and 23,000 deaths due to antibiotic resistant bacteria in the United States in 2013.[88] Additionally, many bacteria are resistant to multiple (and in some rare cases all) available antibiotics prompting the CDC to warn of a potential post-antibiotic era.[89] While underdosing patients is one of the causes of resistance, many other factors contribute to resistance including natural resistance already present in the environment, use of antibiotics for diseases not caused by bacteria, and the widespread use of antibiotics in livestock.[90] Regardless of the cause, resistance has emerged as a major world-wide health concern leading to a desperate need for novel antibiotics.

To overcome antibiotic resistance, there has been a push to develop antibiotics with orthogonal mechanisms that would retain activity against the resistant bacteria.[91] While new

antibiotics with previously unexplored targets would be useful, this strategy continues the cycle which has been termed the "resistance treadmill".[92] This treadmill refers to the constant arms race between humans and bacteria where "[r]esistance development limits the useful lifespan of antibiotics and results in the requirement for a constant introduction of new compound."[93] As soon as humans develop a novel antibiotic (i.e. run faster on the treadmill), it is only a matter of time until the bacteria develop resistance (i.e. turn up the speed on the treadmill) leaving us in same desperate position we were in before. Co-treatment of bacterial infections with antibiotics having distinct mechanisms has been proposed as a way to slow the treadmill.[94] While this is likely to delay the development of resistance, it is unlikely to completely prevent it (e.g. multi-drug resistant *M. tuberculosis* has occurred despite the fact that the bacteria is routinely treated with a combination of antibiotics).[88] Another proposal to slow resistance development is to inhibit the machinery necessary for infecting the host such as virulence factors rather than trying to kill the bacteria.[95] This is advantageous because the selective pressure to develop resistance is much lower compared to when the goal of the therapeutic is bacterial cell death. Here we explore an alternative strategy: developing antibiotics that inhibit the modulated targets which cause antibiotic resistance. This may be a way to get off the treadmill completely by pressuring bacteria to return to the wild type phenotype and thus become re-sensitized to the older antibiotics. In order to explore this possibility further, we will first examine the most common antibiotic resistance mechanisms.

1.2.1 Antibiotic resistance mechanisms

Three main causes of antibiotic resistance exist[96]:

1) Reduced permeability and/or efflux of the antibiotic
2) Inactivation of the antibiotic
3) Modification of the target of the antibiotic

These mechanisms are prevalent across the different classes of antibiotics as can be seen in Table 1.1. They are discussed in more detail below along with previous attempts to develop novel antibiotics that target them.

1.2.1.1 Resistance via reduced permeability and/or efflux of antibiotics

Two of the most common mechanisms of antibiotic resistance are 1) To decrease the permeability of the bacterial cell wall to the antibiotic or 2) To increase the efflux of the antibiotic out of the cell.[97] These mechanisms are most often observed in Gram-negative bacteria (which are already intrinsically resistant to many antibiotics due to their outer membrane) but are also observed in some Gram-positive bacteria.[96] While these modes of resistance alone often do not cause clinically relevant resistance,[97-98] there are cases where they do.

Reduced Permeability. Antibiotics that are active against Gram-negative bacteria generally enter the cell via porins.[96] Bacteria can develop resistance to these agents via downregulation of these porins or even complete replacement of the porins with more selective channels resulting the compounds being unable to enter the cell (and thus unable to kill the bacteria).[96] Mutations of porins and/or reduction in their production have been found to cause clinically relevant resistance to carbapenems in *E. coli* and *K. pneumoniae* in the absence of other mechanisms of resistance.[96]

Efflux. Both Gram-negative and Gram-positive bacteria develop antibiotic resistance by increasing the expression of efflux pumps to actively transport antibiotics out of the cell before they can accumulate.[96] These efflux pumps can have wide substrate tolerance such as the multidrug efflux pumps which confer resistance to a wide range of antibiotics. Alternatively, they can be very specific such as the tetracycline efflux pumps that are capable of differentiating subclasses of tetracyclines.[97] Increased efflux of tetracyclines by these pumps is one of the primary causes of tetracycline resistance seen in the clinic.[97]

Table 1.1. Mechanisms of antibiotic resistance to different antibiotic classes[96-97,99-100]

Class of antibiotic	Examples	Target	Mechanisms of Resistance		
			Reduced Permeability or Efflux	Inactivation or Degradation	Modified Target
Folate biosynthesis inhibitors	Sulfonamides	dihydropteroate synthase	X		X
	Trimethoprim	dihydrofolate reductase	X		X
Cell wall biosynthesis and membrane integrity inhibitors	β-lactams and cephalosporins	Penicillin-binding protein (PBP)	X	X	X
	Glycopeptides	D-Ala-D-Ala of peptidoglycan pentapeptide			X
	Daptomycin	Cytoplasmic membrane (Ca^{2+} dependent)			X
Translation inhibitors	Aminoglycosides	30S-subunit ribosomal proteins	X	X	X
	Tetracyclines	30S-subunit of ribosome	X	X	X
	Macrolides	50S-ribosomal RNA	X	X	X
	Chloramphenicol	50S-subunit of ribosome	X	X	X
	Oxazolidinones	23S-ribosomal RNA	X		X
Transcription inhibitors	Rifamycins	DNA-dependent RNA polymerase	X	X	X
DNA replication inhibitors	Fluoroquinolones	DNA gyrase and topoisomerase IV	X		X

Targeting Reduced Permeability and Efflux. Two main strategies have been employed to overcome these observed resistances. The first is increasing cell permeability. This strategy relies on molecules such as the polymyxins (e.g. colistin) that are capable of disrupting the outer membrane of Gram-negative bacteria.[101-102] While these drugs have shown efficacy in the clinic, they are typically used as drugs of last resort due to their nephrotoxicity.[97] Additionally, resistance to these agents via alteration of the outer membrane has been observed in the clinic further reducing their utility.[101-102] The second strategy is to develop efflux pump inhibitors with the goal

of using them as adjuvant therapies. One of the most well-studied efflux pump inhibitor is the peptidomimetic phenylalanine-arginine β-naphthylamide which shows good activity *in vitro* but significant toxicity *in vivo*.[103] Current efforts are aimed at developing compounds with similar activities and decreased toxicities.[103]

1.2.1.2 Resistance via inactivation of the antibiotic

Another common mechanism of antibiotic resistance is inactivation of the antibiotic by enzymatic degradation. β-lactamases hydrolyze the lactam ring in β-lactams antibiotics resulting in their inactivation and are the most well-studied example of this mechanism of resistance. Some β-lactamases are only active against first generation β-lactams, but others such as the extended-spectrum β-lactamases (ESBL) and the carbapenemases are capable of targeting a wider variety of substrates.[96,104] These enzymes are such a significant cause of resistance that the CDC has labeled the bacteria that express them as a serious and urgent threat.[88] Other clinically relevant examples of antibiotic inactivating enzymes include enzymes responsible for the inactivation of aminoglycosides, tetracyclines, macrolides, chloramphenicol, and rifamycin.[97]

Inhibition of antibiotic inactivating enzymes has been an area of success in targeting antibiotic resistant bacteria. Specifically, β-lactamase inhibitors such as clavulanic acid, sulbactam and tazobactam have greatly extended the lifetime of traditional β-lactams such as ampicillin and piperacillin.[97] However, these compounds are not active against all β-lactamases and do not inhibit the carbapenemases. Novel β-lactamase inhibitors such as avibactam are capable of targeting these enzymes and will likely be very valuable in the fight against bacteria that produce these antibiotic inactivating enzymes.[105]

1.2.1.3 Resistance via modification of the target of the antibiotic

The final mechanism of resistance is modification of the antibiotic target resulting in the antibiotic being unable to bind and exert its action. As can be seen in Table 1.1, this is a common

cause of resistance for all antibiotic classes. However, the type of modification of the target varies based on the antibiotic.

Sulfonamides. Sulfonamides are structural analogues of *p*-aminobenzoic acid (PABA) that act by inhibiting dihydropteroate synthase (DHPS), the enzyme responsible for converting PABA and dihydropteroate diphosphate into dihydrofolic acid, a precursor of folic acid.[97] *E. coli* resistance to sulfonamides occurs after a single base pair substitution in the folP gene (encodes dihydropteroate synthase) resulting in a mutant DHPS with either F28I or F28L mutant.[106] These mutants show greatly decreased binding to the sulfonamides (~150X) while only moderate decreases in binding to the natural substrate (~10X). Point mutations in DHPS are found in other sulfonamide resistant bacteria, but the mutations differ across species.[106] Additionally and potentially more clinically relevant, many sulfonamide resistant bacteria (e.g. *A. baumannii, E. coli*, *K. pneumoniae*, and *P. aeruginosa*) express sulfonamide resistant DHPSs via acquired plasmids containing one of two DHPS genes (*sul1* and *sul2*).[107-108]

Trimethoprim. Trimethoprim, similar to the sulfonamides, also inhibits folate biosynthesis but does so by inhibiting dihydrofolic acid reductase (DHFR), the enzyme responsible for the conversion of dihydrofolic acid to tetrahydrofolic acid.[97] In *S. aureus*, the majority of trimethoprim resistant strains have either H30N/F98Y or H149R/F98Y mutations in DHFR with the F98Y mutation believed to be responsible for the loss in affinity.[109-110] Other trimethoprim resistant bacteria also have mutations in DHFR but they differ in location (e.g. I100L for *S. pneumoniae*[111] or many different mutations for *E. coli*[112]). Additionally, many trimethoprim resistant bacteria have mutations in the promoter for DHFR resulting the overexpression of the enzyme.[113] Similar to the sulfonamides, plasmid-mediated resistance is also common for trimethoprim-resistant bacteria with multiple plasmids containing genes for trimethoprim-resistant DHFRs.[114]

β-lactams. β-lactams act by inhibiting the penicillin binding protein (PBP), the enzyme that catalyzes the transpeptidation reaction necessary to form strong cell walls.[97] While antibiotic

inactivation by β-lactamases is the most common form of resistance to β-lactams for most bacteria, development of methicillin-resistant *S. aureus* and penicillin-resistant *S. pneumoniae* and *Enterococcus* species is primarily due to an alteration of their PBPs.[97,115] For *S. aureus* the acquisition of an alternative PBP called PBP2a from a mobile genetic carrier called the staphylococcal cassette chromosome *mec* is the cause of the resistance.[115-116] PBP2a has greatly reduced affinity for methicillin compared to PBP and a lower rate of β-lactam mediated acylation.[115] *S. pneumoniae* have been found to express modified versions of their own class A and class B PBP from mosaic *pbp* genes as well as point mutations in the gene. These modified PBPs are poorly acylated by β-lactams.[116] One of the PBPs from *Enterococcus* (a class B PBP) is intrinsically β-lactam resistant and takes over when other PBPs are inhibited.[116]

Vancomycin. Vancomycin inhibits cell wall synthesis by binding to the terminal D-Ala-D-Ala of peptidoglycan pentapeptides preventing the transglycosylation and ultimately weakening the peptidoglycan layer.[97] Clinical resistance to vancomycin results from installation of D-Ala-D-Lac or D-Ala-D-Ser instead of D-Ala-D-Ala resulting in the loss of an essential hydrogen bond and a ~1000-fold decrease in binding affinity.[97,117-118] The machinery to install these alternative residues is obtained from a transposon (e.g. TN1546)[119] which likely originated from the bacteria which naturally produce vancomycin.[93,120]

Daptomycin. Daptomycin is a calcium dependent antibiotic which causes bacterial cell death via disruption of the bacterial cell membrane.[97] While the exact mechanisms of daptomycin resistance are still under investigation, they primarily involve alteration of the thickness, charge and/or composition of the cell wall.[121]

Aminoglycosides. Aminoglycosides are irreversible protein synthesis inhibitors that bind the 30S-subunit ribosomal proteins where they can either interfere with the initiation complex, cause misreading of mRNA, or disrupt polysomes into nonfunctional monosomes.[97] While the most common mechanism for clinical resistance to aminoglycosides is inactivation by transferase

enzymes, methylation of the 16S rRNA can result in high level resistance and has been found in a variety of clinical isolates.[122] The actinomycetes that produce aminoglycosides are intrinsically resistant to aminoglycosides often via methylation of specific nucleotides (either A1408 or G1405) within the A-site of rRNA.[123] Bacteria that are not intrinsically resistant (e.g. *E. coli, K. pneumoniae,* and *P. aeruginosa*) obtain the genes to produce the methylase on transferable plasmids.[124]

Tetracyclines. Tetracyclines are reversible protein synthesis inhibitors that bind the 30S subunit of the bacterial ribosome and act by blocking the binding of the aminoacyl-tRNA to the acceptor site.[97] While a variety of resistance mechanisms exist for the tetracyclines, the two most clinically relevant mechanisms are efflux pumps and the production of ribosomal protection proteins (RPPs).[97,125] The RPPs are believed to have originated from the producer of the tetracyclines *Streptomyces rimosus* and to have been transferred to other bacteria via plasmids.[126] The RPPs are capable of dislodging tetracyclines from the ribosome in a GTP dependent manner thus resulting in clinically significant resistance.[125] While this mechanism differs from many of the other target site modifications, upon binding the RPPs are believed to significantly distort the binding site for tetracyclines resulting in its dissociation and expulsion from the ribosome.[126-127]

Macrolides. Macrolides are protein synthesis inhibitors that bind the 50S rRNA and block peptide elongation.[97] Similar to the aminoglycosides, methylation of the ribosomal-binding site is a major cause of clinical resistance to macrolides.[96-97] Specifically, the erythromycin-resistance methylase (Erm) is a methyltransferase responsible for the mono- or dimethylation of the 23S rRNA at nucleotide A2058, which confers resistance to macrolides.[125] However, the Erm methyltransferase is only expressed when a macrolide is present likely due to its high fitness cost (methylation of A2058 results in different translation patterns).[125]

Chloramphenicol. Continuing the theme of protein synthesis inhibitors, chloramphenicol inhibits protein synthesis via reversible binding to the 50S subunit of the bacterial ribosome and inhibits the peptidyl transferase step.[97] As with the aminoglycosides and macrolides, chloramphenicol

resistance is mediated by methylation of its target RNA. Specifically, the chloramphenicol-florfenicol resistance (*cfr*) methyltransferase transfers a methyl to A2503 of the 23S rRNA.[128] This methylation has very little fitness cost thus explaining its widespread occurrence.[125]

Oxazolidinones. Oxazolidinones including linezolid (the first FDA-approved oxazolidinone antibiotic) are synthetic antimicrobials that bind a unique site (23S rRNA) on the 50S subunit resulting in inhibition of the initiation of protein synthesis.[97] Similar to the other protein synthesis inhibitors, methylation of its associated rRNA can result in resistance to linezolid.[125] A more common resistance mechanism to linezolid is the mutation of rRNA (C2534U) which has been observed in *S. pneumonia, S. aureus, S. epidermis, S. hominis, S. simulans, and Enterococcus*.[97,129] This mutation in combination with mutations in ribosomal proteins L3 and L4 results in a very high level linezolid resistance.[125]

Rifamycins. Rifamycin inhibits RNA synthesis by binding to the β-subunit of the DNA-dependent RNA polymerase. The major form of resistance to rifamycin is point mutations in *rpoB*, the gene for the β-subunit of the RNA polymerase.[97] For *M. tuberculosis*, almost all mutations occur at the rif I region of the protein with 41% of rifamycin-resistant clinical isolates having a mutation at S455, 36% at H440, and 9% at D430.[130]

Fluoroquinolones. FQs act by inhibiting bacterial type IIA topoisomerases, specifically DNA gyrase and topoisomerase IV, which catalyze the introduction of negative supercoils and the decatenation of interlinked chromosomes, respectively [131-132]. Both DNA gyrase and topoisomerase IV are tetramers made up of two copies of two different subunits and containing two active sites. For DNA gyrase, the subunits consist of GyrA (contains the active site tyrosine responsible for DNA strand breakages) and GyrB (responsible for hydrolyzing ATP thus providing energy for the reaction). Topoisomerase IV consists of similar subunits with ParC being equivalent to GyrA and ParE acting like GyrB [131]. The general mechanism of DNA gyrase begins with the binding of the G strand of DNA (green strand in part **1** of Figure 1.6A).[131,133] After binding, two

ATP molecules bind to the ATPase domains and the G strand of DNA is cleaved via the active site tyrosine (insert and part **2** of Figure 1.6A). Hydrolysis of one ATP results in the passage of the T-strand of DNA (purple strand) through the cleaved G strand (part **3** in Figure 1.6A). The DNA is then released (part 4 in Figure 1.6A) and hydrolysis of the last ATP resets the enzyme.

FQ inhibition of DNA gyrase is usually monitored by either the supercoiling or cleavage assay (Figure 1.6B).[134] As the names suggest, the supercoiling assay monitors the ability of a compound to inhibit the supercoiling of DNA that is catalyzed by DNA gyrase. The cleavage assay monitors the ability of a compound to stabilize an enzyme-DNA complex ultimately resulting in cleavage of the DNA (see Figure 1.6B). The FQs inhibit DNA gyrase causing double stranded breaks that appear as a buildup of L DNA in a DNA gyrase cleavage assay.[135] Maxwell and coworkers have demonstrated that FQs initially stabilize a single phosphotyrosine bond as evidenced by an initial buildup of OC DNA during the cleavage assay (Figure 1.6C).[135] However, the FQ stabilization of a single strand break causes an even faster second cleavage event that is also stabilized by FQs thus explaining the rapid buildup of linear DNA.[135] For this reason, many suggest that the FQs inhibit step **2** of the DNA gyrase mechanism (Figure 1.6A). Another DNA gyrase inhibitor, GSK299423, acts via a different mechanism [133]. Unlike FQs that bind within the two active sites, it binds between the active sites stabilizing either an uncleaved or a single-stranded cleaved DNA (step **1** of the DNA gyrase mechanism, Figure 1.6A). The stabilization induced by GSK299423 differs from that of CIP in that it does not result in a second cleavage event and instead causes a buildup of OC DNA (Figure 1.6C).

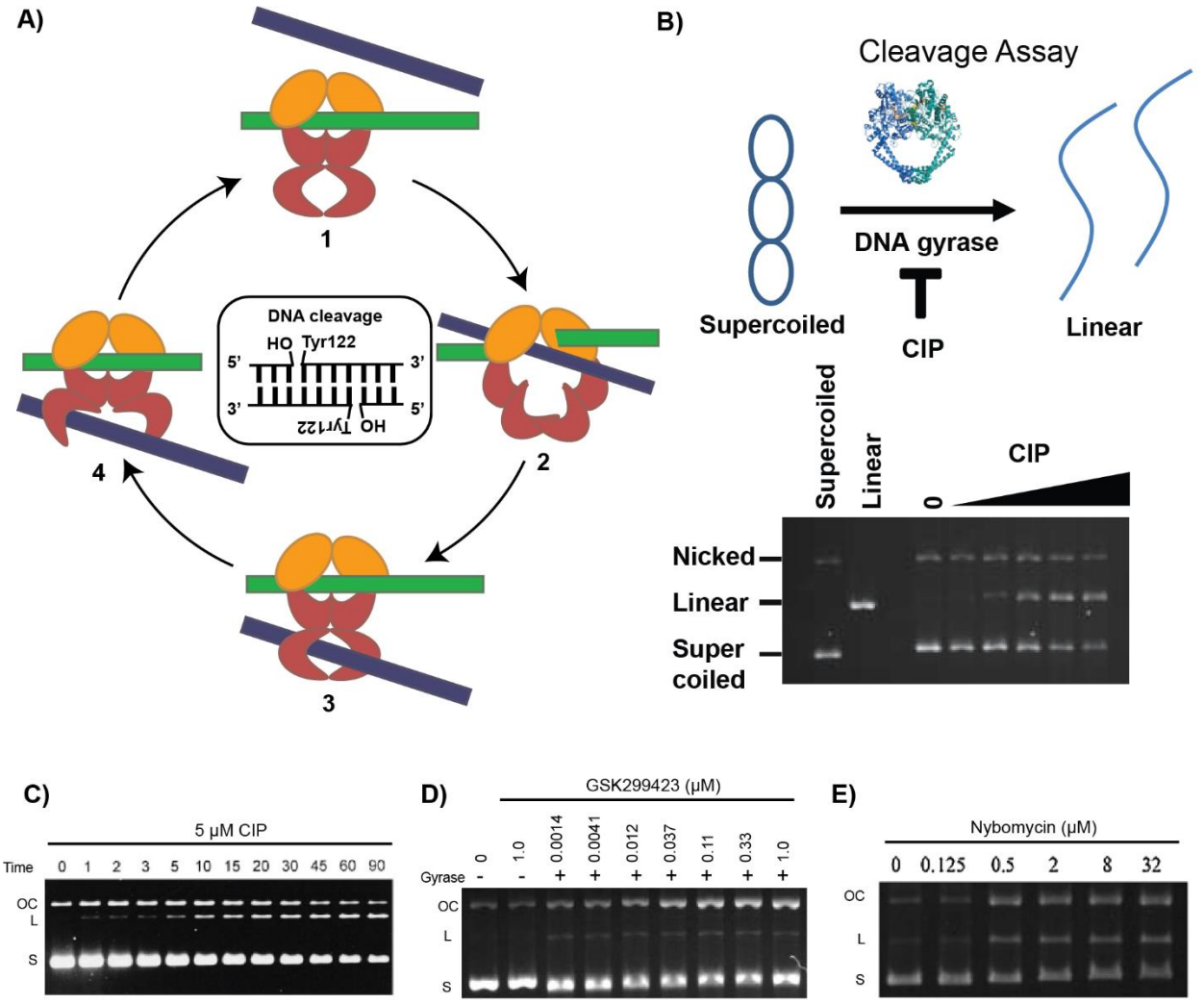

Figure 1.6. (**A**) DNA gyrase mechanism. This figure was adapted from figures in recent reviews.[131,133] **1**) The G strand of DNA (green) binds to the DNA gate. **2**) The G strand is cleaved allowing for passage of the T strand of DNA (purple). The insert shows the cleavage complex with the active site Tyr122 bound to the DNA. **3**) The G strand is re-ligated. **4**) The DNA is released. (**B**) The cleavage assay measures the ability of a small molecule to stabilize the topoisomerase-DNA complex that is normally formed during the enzyme catalyzed reaction. Supercoiled DNA is co-incubated with DNA gyrase and the compound of interest. DNA is then cleaved from DNA gyrase using SDS. The DNA is then run on agarose gel. DNA is visualized with ethidium bromide. Three different forms of DNA are observed: Supercoiled (S), Singly-nicked DNA (aka OC DNA), and linear (i.e. doubly nicked DNA). CIP causes primarily double stranded breaks and thus a buildup of linear DNA as seen in the below gel (*S. pneumoniae* gyrase with 1 – 40 μM CIP). All gels were taken from a protocol by Fisher and Pan.[134] (**C**) A timecourse analyzing the effect of CIP on DNA in the DNA cleavage assay. Initial buildup of singly nicked (OC) DNA gives way to primarily doubly nicked (linear, L) DNA. The experiment was performed by Maxwell and coworkers.[135] (**D**) A dose-response experiment analyzing the effect of GSK299423 on DNA in the DNA cleavage assay. Unlike CIP, GSK299423 results in a buildup of OC DNA, not L DNA. This experiment was performed by Gwynn and coworkers.[133] (**E**) A dose-resposne experiment analyzing the effect of nybomycin on DNA in the DNA cleavage assay. Similarly to GSK299423, it appears to result in a buildup of OC DNA. This experiment was performed by Hiramatsu and coworkers.[136]

Target site mutation is the major contributor to FQR [98,137], with high-level resistance observed in bacteria possessing key mutations in both GyrA and ParC [98]. Nearly all FQR bacteria harbor these target site mutations, with point mutations in the quinolone resistance-determining region (QRDR) of the GyrA subunit of DNA gyrase and the ParC subunit of topoisomerase IV. One of the most commonly mutated sites is the Ser84 on GyrA (*S. aureus* numbering). As discussed further in Chapter 3, this Ser is well conserved across bacterial species including Gram-positive and Gram-negative bacteria. Additionally, its mutation almost always leads to clinically relevant FQR. Another less commonly observed mechanism of resistance are the plasmid-mediated quinolone resistance genes such as *qnr.*[98] *Qnr* encodes a pentapeptide-repeat motif that binds to the bacterial topoisomerases and prevents binding FQs.

Targeting Modified Targets. Small molecules capable of targeting the first two mechanisms of resistance (reduced permeability/efflux and inactivation of the antibiotic) exist and have been relatively successful with each having clinically approved agents (colistin and the β-lactamase inhibitors, respectively). However, to the best of our knowledge, very little work has been done to develop small molecules capable of inhibiting the third mechanism of resistance (modified target). One of the few examples is work by Boger and co-workers where they developed vancomycin derivatives capable of targeting the D-Ala-D-Lac peptide responsible for vancomycin resistance.[118] Until very recently[83,136] there were no examples of small molecules that specifically target modified enzyme targets in bacteria. This idea of specifically inhibiting the modified target is particularly attractive because it is possible that resistance would develop via cycling back to the WT target thus re-sensitizing the bacteria to the original antibiotic (see Figure 1.7).[83,136,138] This drug cycling is exactly what has been observed with the small molecule deoxynybomycin (DNM), which has been shown to target the mutated DNA gyrase responsible for fluroquinolone resistance (FQR).[83,136] The rest of Chapter 1.2 and Chapter 3 will focus on our work on DNM, its derivatives, and their unique mode of action. It is likely that a similar strategy could be employed to target the mutated targets of many of the antibiotics discussed above (e.g. the mutated DHPS

responsible for sulfonamide resistance; the mutated DHFR responsible for trimethoprim resistance; the methylated rRNA responsible for resistance to aminoglycosides, macrolides, and chloramphenicol; the mutated rRNA and ribosomal protein responsible for resistance to linezolid; the mutated RNA polymerase responsible for rifamycin resistance).

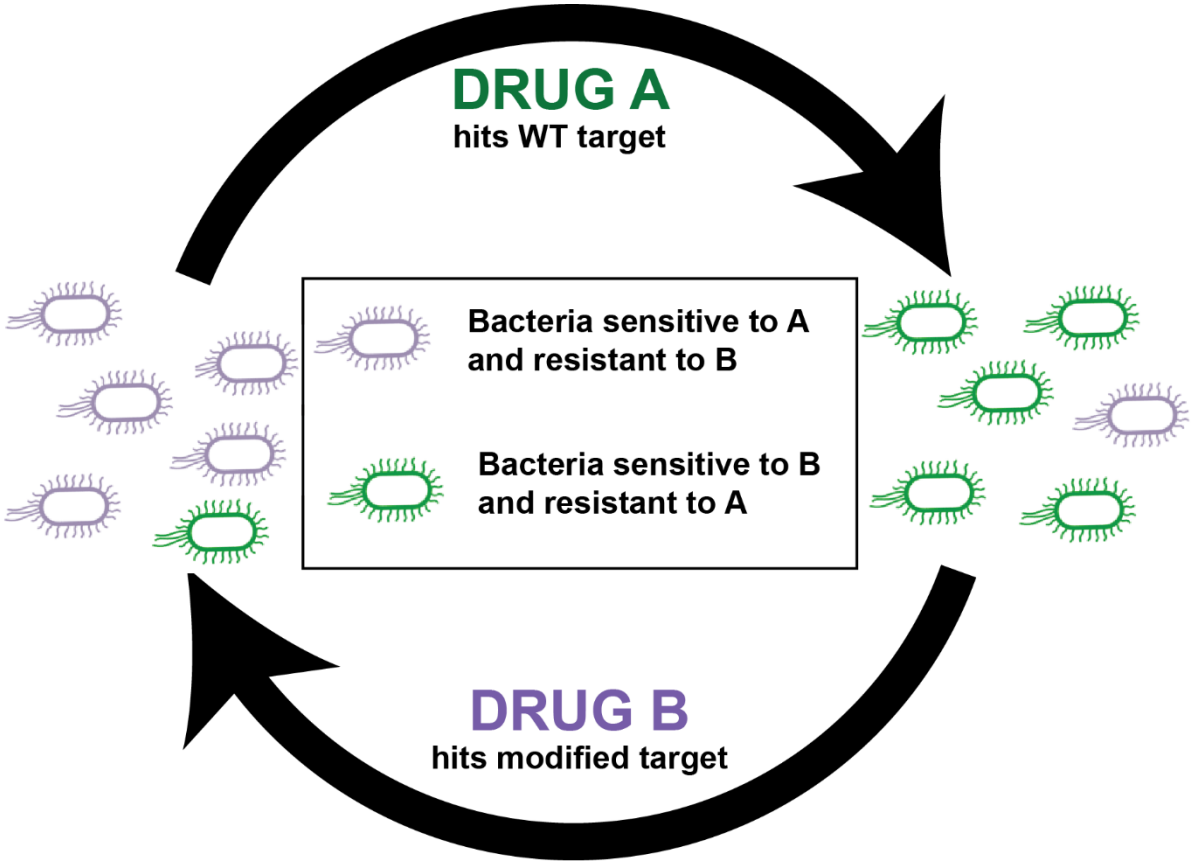

Figure 1.7. Resistance cycling with complementary antibiotics. Purple bacteria are sensitive to drug A which hits a wild type (WT) target. Upon exposure to A, selection occurs whereby bacteria resistant to drug A dominate via modification of a target (green bacteria). Green bacteria are sensitive to drug B which hits the modified target. Upon exposure to B, the bacteria develop resistance to drug B via reversion to the original WT target.

1.2.2 History of DNM

Nybomycin (NM, Figure 1.8) is a natural product first identified from a culture of a streptomycete (strain A717) isolated from a Missouri soil sample and found to have antibacterial activity including activity against *S. aureus*, *M. smegmatis,* and *Bacillus* species.[139-140] During efforts to determine its structure, Rinehart and coworkers synthesized a related compound,

deoxynybomycin (DNM, Figure 1.8), which was later found also to be a natural product and to have more potent activity than NM against a range of bacteria.[75,141]. As described above, DNM was recently found to target FQR MRSA by inhibiting mutant DNA gyrase.[83,136] Specifically, it was shown to target bacteria with a S84L mutation in gyrA. Additionally, NM was shown to inhibit the mutant DNA gyrase *in vitro* in a cleavage assay (Figure 1.6E).

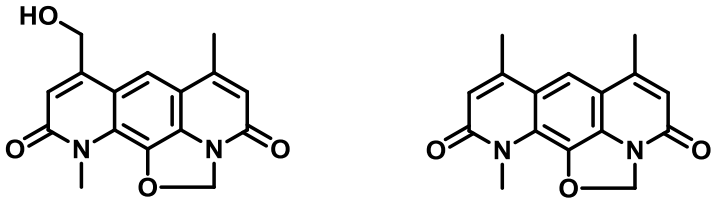

Nybomycin (NM) **Deoxynybomycin (DNM)**

Figure 1.8. Structure of nybomycin (NM) and deoxynybomycin (DNM).

1.2.3 Common mutations in DNA gyrase that result in FQR

As discussed earlier in Section 1.2.1.1, the major mechanism of FQR for bacteria involves the mutation of FQ targets DNA gyrase and topoisomerase IV. While nearly all FQR bacteria found to date have such mutations, the exact mutation can vary based on the bacterium. For MRSA, the major mutations occur at S84 of GyrA and S80 of ParC with nearly 100% have the S84L mutation in DNA gyrase.[136,142-149] Similarly, *B. anthracis,*[150] *E. coli,*[151] *Shigella* species,[152-153] and *A. baumannii*[154] also having the analogous Ser mutated to Leu. In VRE[155] the S is mutated to multiple different residues (Ile, Arg, and Tyr) while in *S. pneumoniae,*[156] *K. pneumonia,*[157] and *N. gonorrhoeae*[158] this Ser is often changed to either Phe or Tyr.[155-162] *P. aeruginosa* differs in that it naturally has a Thr instead of the Ser.[163] However, *P. aeruginosa* is similar to VRE in that the Thr is mutated to an Ile in the majority (75-96%) of FQR strains.[163-166] Finally, *Mycobacteria* species differ in that it naturally has an Ala instead of a Ser and mutates A90V in approximately 20% of FQR strains of *M. tuberculosis*.[167]

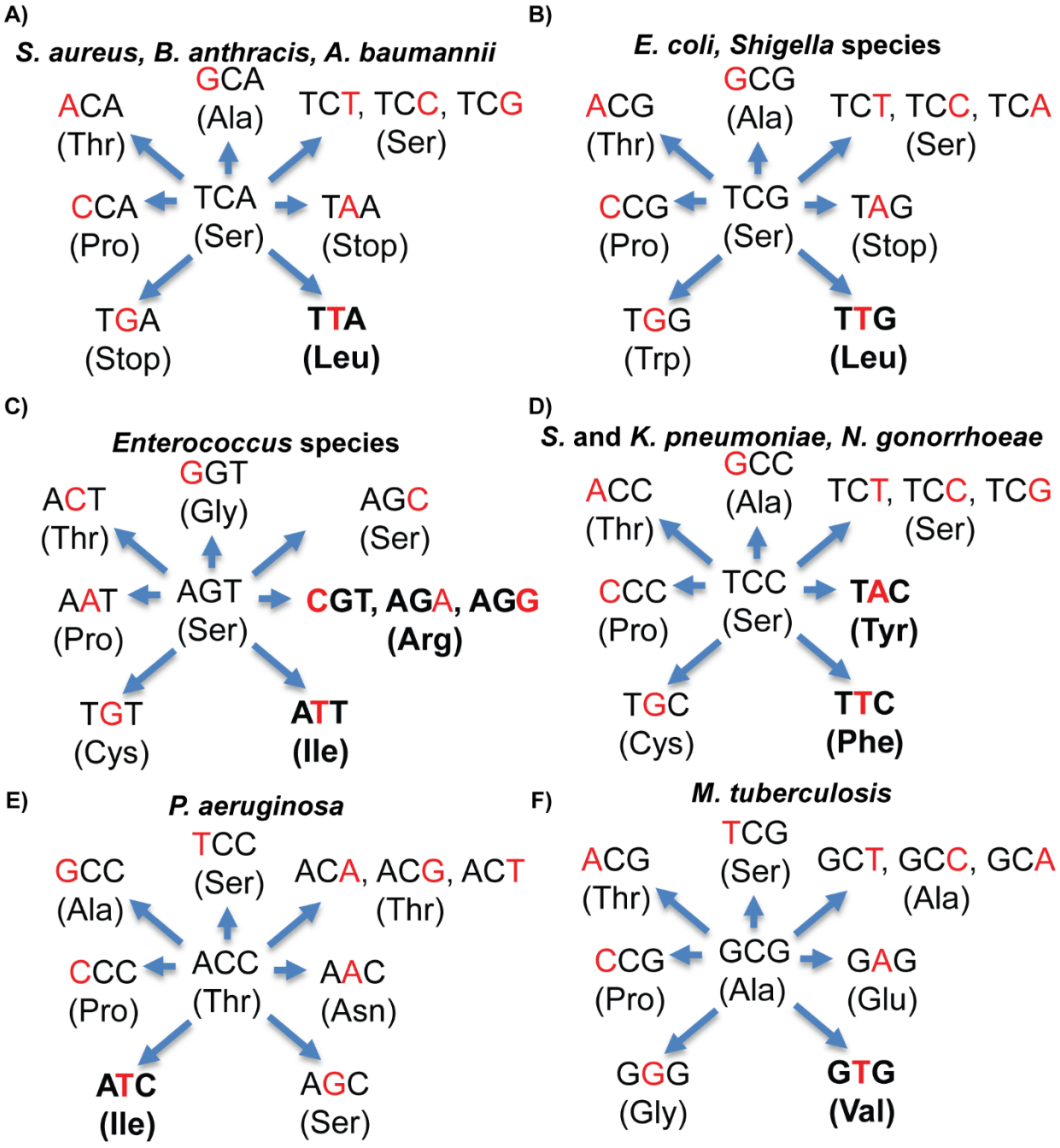

Figure 1.9. Possible gyrA mutations for different bacteria after a single base change. In the center is the WT codon (residue) at the key resistance determining position. Clinically relevant mutations are bolded. (**A**) *S. aureus, B. anthracis*, *A. baumannii*. (**B**) *E. coli* and *Shigella* species. (**C**) *Enterococcus* species. (**D**) *S. pneumoniae, K. pneumonia,* and *N. gonorrhoeae*. (**E**) *P. aeruginosa*. (**F**) *M. tuberculosis.*

The S83 (*E. coli* numbering) of gyrA is relatively well conserved across bacterial species with the exception of *P. aeruginosa* and *Mycobacteria* (See Chapter 3, Figure 3.4A). However, as evidenced by the data discussed above, development of FQR can occur via mutation of this residue to a variety of different residues (e.g. Leu, Ile, Arg, Tyr, Phe, Val) depending on the bacterial species. The reason for these different mutations in response to the same FQs is not known but may be related to the native codon that encodes the Ser in each species. Specifically, we hypothesize that the mutations are dependent upon what codons are possible after a single base change in the initial codon (Figure 1.9). For *S. aureus,*[168] *B. anthracis*,[150] and *A. baumannii*[169-172] the codon for the conserved Ser is TCA (Figure 1.9A). A single base change in this codon can result in multiple different substitutions including the clinically observed Leu. For *E. coli*[151] and *Shigella* species,[152,173-174] the codon for Ser is TCG and a single base change can also result in the commonly observed mutation, S83L (Figure 1.9B). For *Enterococcus* species,[155] the codon for Ser is AGT and a single base change can cause the frequently seen Ile and Arg (Figure 1.9C). For *S. pneumoniae,*[156,175-176] *K. pneumonia,*[157,177-179] and *N. gonorrhoeae*,[158] the codon for Ser is TCC and a single base change can result in the clinically relevant Phe and Tyr (Figure 1.9D). For *P. aeruginosa*,[163] the codon for Thr is ACC, and a single base change can result in Ile (Figure 1.9E). Finally, for *M. tuberculosis*,[167,180] the codon for Ala is GCG, and a single base change can result in Val (Figure 1.9F). It is interesting to note that for many of these bacteria a single base change could result in Ala, Thr, or Pro but none of the resistant strains have these mutations. For Ala and Thr, it may be that such enzymes would still be sensitive the FQs given that these are the WT forms for *P. aeruginosa* and *M. tuberculosis,* respectively. For Pro, it is possible that it would distort the protein structure and may result in an inactive enzyme. Other possible mutations that are not commonly observed are Trp, Cys, Asn, and Glu. While the reason for this is not known, they may result in too high of a fitness cost.

1.2.4 Summary

Antibiotic resistance is one of the major challenges facing modern medicine. Novel antibiotics capable of treating these resistant bacteria are greatly needed. While the development of antibiotics with novel mechanisms is a worthwhile goal, eventually resistance will develop to these antibiotics resulting in the constant need for new antibiotics. One potential way of overcoming this challenge is to develop antibiotics that specifically target the cause of antibiotic resistance. While this strategy has previously been explored for two mechanisms of resistance (i.e. decreased permeability and inactivation of antibiotics by β-lactamases), developing compounds to inhibit the modified targets which cause antibiotic resistance is not well investigated. We hypothesize that inhibiting these modified targets may be a highly effective way both to kill the antibiotic resistant bacteria and to prevent novel mechanisms of resistance by pressuring the bacteria to revert to the wild type phenotype. In Chapter 3, we provide evidence to support this hypothesis by exploring the compound DNM and its ability to inhibit mutant DNA gyrase responsible for fluoroquinolone resistance.

1.3 Discovering novel anticancer agents from cell-based phenotypic screens

The discovery of novel anticancer agents from cell-based phenotypic screens has been described previously in great detail.[181] Described herein are (1) the importance of factors other than potency in choosing lead compounds, and (2) the induction of endoplasmic reticulum (ER) stress as an anticancer strategy.

1.3.1 The importance of the shape of the dose-response curve on anticancer efficacy

Phenotypic screening of compound libraries, especially cell-based screening for cytotoxicity, has led to the discovery of promising antitumor agents.[182-183] Prioritization of lead anticancer compounds identified in high throughput screens is often based on potency and

selectivity, but recent reports have highlighted the importance of other parameters in evaluating candidate molecules.[184] Specifically, drug efficacy is related to the slope of the dose-response curve (Hill slope) and the fraction of the population killed at high compound concentrations (E_{max}). Steep slopes (e.g., Hill slope > 1) reflect a lower degree of variation in response to compound within a given population, whereas high E_{max} values (e.g., E_{max} of 100 = 100% death) indicate efficient induction of cell death at concentrations above the IC_{50}.[184]

A steep Hill slope indicates that reduced amounts of compound above the IC_{50} are needed to efficiently kill a population of cells. For example, a compound with an E_{max} of 100, an IC_{50} of 1 µM, and a Hill slope of 1 will require a 100 µM concentration to kill 99% of the cells. In contrast, for a compound with a Hill slope of 2 and identical values for E_{max} and IC_{50} as above, only a 10 µM concentration is required to achieve 99% cell death (Figure 1.10).[184] The full potential of anticancer compounds with steep Hill slopes and high E_{max} values remains to be determined; however, it is reasonable to believe that such compounds are more likely to be maximally active in vivo at lower doses (based on the steep Hill slope), and the quantitative cell death (100% E_{max}) could help prevent or delay the development of resistance.

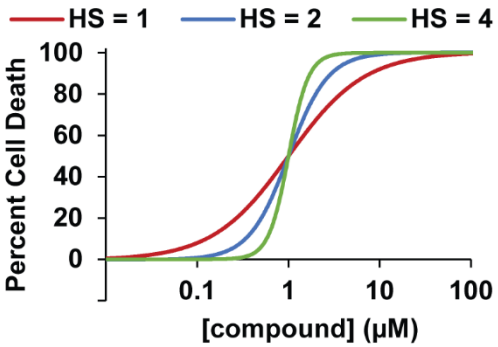

Figure 1.10. General cytotoxicity dose-response curve with different Hill slope values. HS = Hill slope.

The importance of Hill slope and E_{max} is well established in the context of anti-retroviral therapy. Anti-retroviral agents with steep Hill slopes have greater antiviral activity at clinically relevant concentrations and are key components of the most effective drug combinations.[185]

Further, mutations associated with clinical resistance to anti-retrovirals such as the protease inhibitor atazanavir can cause minimal changes in IC_{50} but significantly reduce the Hill slope.[186] Recently, the importance of Hill slope and E_{max} for anticancer therapy was thoroughly examined.[184] Among anticancer agents, HDAC inhibitors and proteasome inhibitors had significantly higher Hill slopes than the other classes of drugs (average Hill slope ~1.5 to 2.6). The highest average Hill slope observed for clinically used anticancer agents were 2.9 ± 0.8 for the Bcr-Abl inhibitor imatinib and 2.8 ± 1.0 for the receptor tyrosine kinase inhibitor sunitinib.[184] These parameters have significant clinical implications, as illustrated by the much steeper Hill slope of imatinib against cancer cells expressing wild type Bcr-Abl compared to cells with mutant Bcr-Abl proteins. This change in Hill slope upon mutation of Bcr-Abl correlates with the poor efficacy of imatinib in cancer patients with these mutations.[187]

1.3.2 Induction of endoplasmic reticulum stress as an anticancer strategy

The ER is responsible for Ca^{2+} storage and for the folding and maturation of many secreted and transmembrane proteins.[188] ER stress is defined as any disturbance in normal ER function that activates the unfolded protein response (UPR).[189] It can be caused by a variety of events including improper redox regulation, glucose deprivation, Ca^{2+} misregulation, energy fluctuations, DNA damage, and viral infections.[189-191]

ER stress is signaled by the activation of any one of three transmembrane proteins within the ER: IRE1α, PERK, and ATF6 (Figure 1.11). Activation of IRE1α causes dimerization, autophosphorylation, and splicing of XPB1 mRNA, which leads to the expression of a subset of UPR genes that promote ER-associated degradation of misfolded proteins and ER biogenesis (Figure 1.11A).[192-193] Phosphorylation of IRE1α is commonly used as a biochemical marker of IRE1α activation,[194] although downstream markers of IREα activation such as XPB1 splicing can be observed more easily.[188]

ER stress also induces dimerization and autophosphorylation of PERK, as well as

phosphorylation of eIF2α by PERK.[189] Phosphorylation of eIF2α leads to a reduction in translation of most genes, as well as activation of AT4, which induces expression of UPR genes such as amino acid transporters and the transcription factor CHOP (Figure 1.11B).[193] CHOP subsequently activates transcription of GADD34, a regulatory subunit of the phosphatase PP1 that dephosphorylates phospho-eIF2α (p-eIF2α). Levels of p-eIF2α are commonly used to measure PERK activation.[188,194]

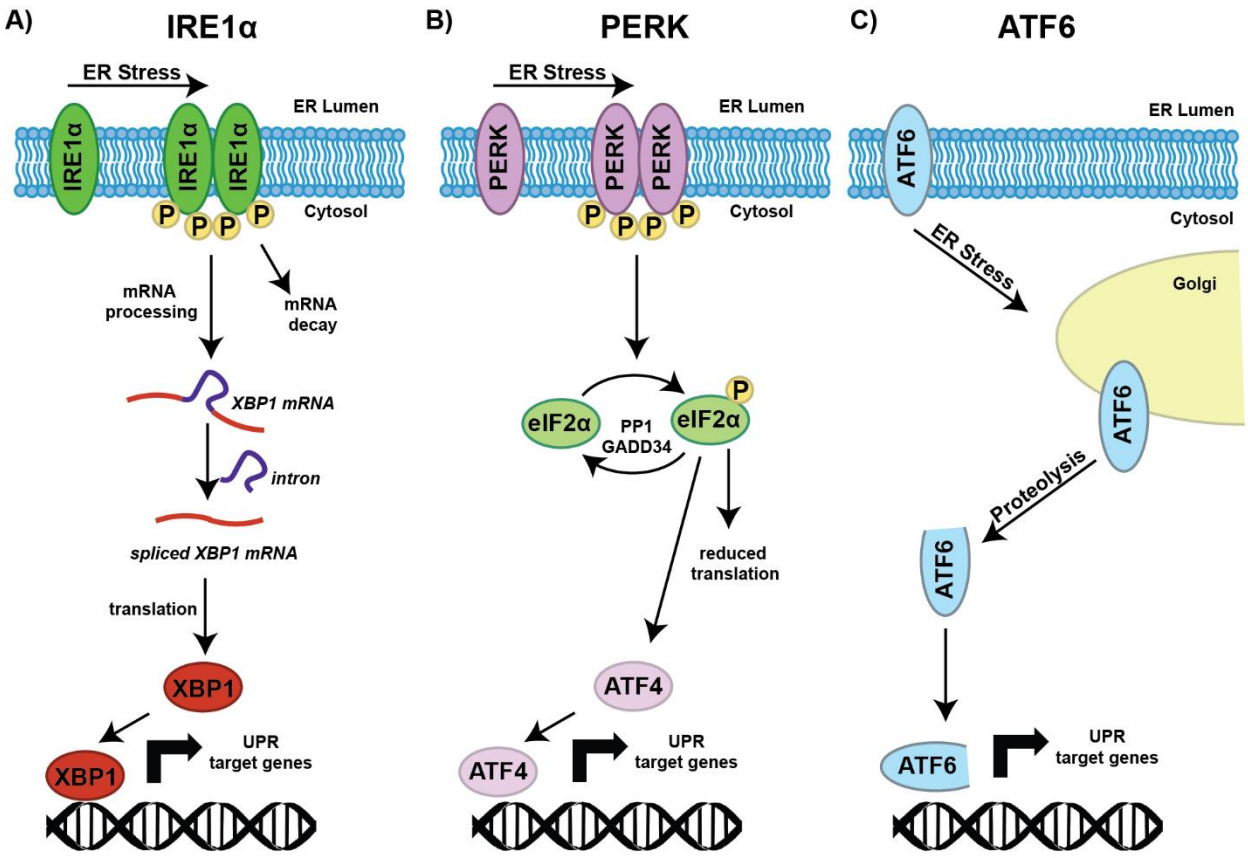

Figure 1.11. The three families of signal transducers for ER stress: (**A**) IRE1α, (**B**) PERK, and (**C**) ATF6. This figure is adapted from figures found in two recent reviews.[195-196]

ATF6 is activated in a different manner than IRE1α and PERK are activated. Upon ER stress, ATF6 translocates to the Golgi, where it is cleaved by proteases.[189] This cleavage allows the transcription factor to migrate to the nucleus, where it induces the expression of UPR genes such as *XBP1* (Figure 1.11C).[193] As with IRE1α and PERK, it is generally challenging to

monitor the proteolysis of ATF6 directly.[188] Instead, activation of ATF6 is more reliably determined by examining mRNA levels of its target genes, including *GRP78*[197] and *HRD1*.[188]

While mild ER stress promotes a pro-survival response, acute ER stress results in pro-death signaling that leads to cell death through a variety of pathways.[189,195,198-199] Due to the nutrient deprivation and dysregulation of protein synthesis in cancer cells, ER stress is often more common in tumor cells than in associated healthy tissues.[190-191] Increased expression of XBP1, ATF6, CHOP, and ER chaperone BIP (also known as GRP78) have been detected in breast cancer, hepatocellular carcinomas, gastric tumors, and esophageal adenocarcinomas.[191] Because of the high secretory nature of rare mucinous and secretory breast cancers and myelomas, including Burkitt's lymphoma and multiple myeloma, they are particularly prone to elevated levels of ER stress compared to associated normal tissues.[190]

Due to increased ER stress in cancer cells, over-activation of ER stress has been recognized as a possible targeted anticancer strategy.[191] ER stress-inducing compounds can selectively activate ER stress pathways in cancer cells, both in cell culture and in vivo, to induce cell death, while inducing minimal ER stress in normal cells.[200-202] Both the FDA-approved agent bortezomib (a proteasome inhibitor) and the investigational compound 17-AAG (an Hsp90 inhibitor) induce cancer cell death via ER stress.[203-204] In addition, other compounds that induce ER stress in the laboratory are now under investigation as potential anticancer agents. The two most common chemical tools for the study of ER stress and its downstream effects are thapsigargin, a sarco/endoplasmic reticulum Ca^{2+}-ATPase (SERCA) inhibitor,[205] and tunicamycin, a heterogeneous natural product mixture that inhibits N-glycosylation.[206] Tunicamycin has recently been shown to potentiate the effects of cisplatin in murine models of hepatocellular carcinoma.[207] An antigen-targeted prodrug of thapsigargin, G-202, is currently in Phase 2 clinical trials for liver, brain, and prostate cancers (clinicaltrials.gov, NCT01777594 and NCT02067156).

1.3.3 Summary

Phenotypic screens have led to the discovery of many anticancer agents with unique characteristics and modes of action. While lead compounds are traditionally chosen based on potency of the compound, many other factors, including the shape of the dose-response curve, are also important to consider before advancement of a given compound. Further evaluation of hit compounds with steep Hill slopes and high E_{max} values may aid in the discovery of anticancer agents with slower rates of resistance development. Additionally, investigation of anticancer leads that act through traditionally underrepresented modes of action such as induction of ER stress is advantageous due to the potential for these compounds to show improved activity against certain cancers (e.g. those with high secretory rates).

1.4 References

(1) Siegel, R. L.; Miller, K. D.; Jemal, A. Cancer statistics, 2015. *CA Cancer J Clin* **2015**, *65*, 5-29.

(2) Pavet, V.; Portal, M. M.; Moulin, J. C.; Herbrecht, R.; Gronemeyer, H. Towards novel paradigms for cancer therapy. *Oncogene* **2011**, *30*, 1-20.

(3) Papadopoulos, N.; Kinzler, K. W.; Vogelstein, B. The role of companion diagnostics in the development and use of mutation-targeted cancer therapies. *Nat Biotechnol* **2006**, *24*, 985-995.

(4) Siegel, D.; Yan, C.; Ross, D. NAD(P)H:quinone oxidoreductase 1 (NQO1) in the sensitivity and resistance to antitumor quinones. *Biochem Pharmacol* **2012**, *83*, 1033-1040.

(5) Schlager, J. J.; Powis, G. Cytosolic NAD(P)H:(quinone-acceptor)oxidoreductase in human normal and tumor tissue: effects of cigarette smoking and alcohol. *Int J Cancer* **1990**, *45*, 403-409.

(6) Malkinson, A. M.; Siegel, D.; Forrest, G. L.; Gazdar, A. F.; Oie, H. K.; Chan, D. C.; Bunn, P. A.; Mabry, M.; Dykes, D. J.; Harrison, S. D.; et al. Elevated DT-diaphorase activity and messenger RNA content in human non-small cell lung carcinoma: relationship to the response of lung tumor xenografts to mitomycin Cl. *Cancer Res* **1992**, *52*, 4752-4757.

(7) Smitskamp-Wilms, E.; Giaccone, G.; Pinedo, H. M.; van der Laan, B. F.; Peters, G. J. DT-diaphorase activity in normal and neoplastic human tissues; an indicator for sensitivity to bioreductive agents? *Br J Cancer* **1995**, *72*, 917-921.

(8) Marin, A.; Lopez de Cerain, A.; Hamilton, E.; Lewis, A. D.; Martinez-Penuela, J. M.; Idoate, M. A.; Bello, J. DT-diaphorase and cytochrome B5 reductase in human lung and breast tumours. *Br J Cancer* **1997**, *76*, 923-929.

(9) Siegel, D.; Ross, D. Immunodetection of NAD(P)H:quinone oxidoreductase 1 (NQO1) in human tissues. *Free Radic Biol Med* **2000**, *29*, 246-253.

(10) Kolesar, J. M.; Pritchard, S. C.; Kerr, K. M.; Kim, K.; Nicolson, M. C.; McLeod, H. Evaluation of NQO1 gene expression and variant allele in human NSCLC tumors and matched normal lung tissue. *Int J Oncol* **2002**, *21*, 1119-1124.

(11) Bey, E. A.; Bentle, M. S.; Reinicke, K. E.; Dong, Y.; Yang, C. R.; Girard, L.; Minna, J. D.; Bornmann, W. G.; Gao, J.; Boothman, D. A. An NQO1- and PARP-1-mediated cell death pathway induced in non-small-cell lung cancer cells by beta-lapachone. *Proc Natl Acad Sci U S A* **2007**, *104*, 11832-11837.

(12) Yilmaz, A.; Mohamed, N.; Patterson, K. A.; Tang, Y.; Shilo, K.; Villalona-Calero, M. A.; Davis, M. E.; Zhou, X.; Frankel, W.; Otterson, G. A.; Beall, H. D.; Zhao, W. Increased NQO1 but not c-MET and survivin expression in non-small cell lung carcinoma with KRAS mutations. *Int J Environ Res Public Health* **2014**, *11*, 9491-9502.

(13) Li, Z.; Zhang, Y.; Jin, T.; Men, J.; Lin, Z.; Qi, P.; Piao, Y.; Yan, G. NQO1 protein expression predicts poor prognosis of non-small cell lung cancers. *BMC Cancer* **2015**, *15*, 207.

(14) Yang, Y.; Zhang, Y.; Wu, Q.; Cui, X.; Lin, Z.; Liu, S.; Chen, L. Clinical implications of high NQO1 expression in breast cancers. *J Exp Clin Cancer Res* **2014**, *33*, 14.

(15) Mikami, K.; Naito, M.; Ishiguro, T.; Yano, H.; Tomida, A.; Yamada, T.; Tanaka, N.; Shirakusa, T.; Tsuruo, T. Immunological quantitation of DT-diaphorase in carcinoma cell lines and clinical colon cancers: advanced tumors express greater levels of DT-diaphorase. *Jpn J Cancer Res* **1998**, *89*, 910-915.

(16) Ji, L.; Wei, Y.; Jiang, T.; Wang, S. Correlation of Nrf2, NQO1, MRP1, cmyc and p53 in colorectal cancer and their relationships to clinicopathologic features and survival. *Int J Clin Exp Pathol* **2014**, *7*, 1124-1131.

(17) Logsdon, C. D.; Simeone, D. M.; Binkley, C.; Arumugam, T.; Greenson, J. K.; Giordano, T. J.; Misek, D. E.; Kuick, R.; Hanash, S. Molecular profiling of pancreatic adenocarcinoma and chronic pancreatitis identifies multiple genes differentially regulated in pancreatic cancer. *Cancer Res* **2003**, *63*, 2649-2657.

(18) Lewis, A. M.; Ough, M.; Hinkhouse, M. M.; Tsao, M. S.; Oberley, L. W.; Cullen, J. J. Targeting NAD(P)H:quinone oxidoreductase (NQO1) in pancreatic cancer. *Mol Carcinog* **2005**, *43*, 215-224.

(19) Lyn-Cook, B. D.; Yan-Sanders, Y.; Moore, S.; Taylor, S.; Word, B.; Hammons, G. J. Increased levels of NAD(P)H: quinone oxidoreductase 1 (NQO1) in pancreatic tissues from smokers and pancreatic adenocarcinomas: A potential biomarker of early damage in the pancreas. *Cell Biol Toxicol* **2006**, *22*, 73-80.

(20) Awadallah, N. S.; Dehn, D.; Shah, R. J.; Russell Nash, S.; Chen, Y. K.; Ross, D.; Bentz, J. S.; Shroyer, K. R. NQO1 expression in pancreatic cancer and its potential use as a biomarker. *Appl Immunohistochem Mol Morphol* **2008**, *16*, 24-31.

(21) Cui, X.; Li, L.; Yan, G.; Meng, K.; Lin, Z.; Nan, Y.; Jin, G.; Li, C. High expression of NQO1 is associated with poor prognosis in serous ovarian carcinoma. *BMC Cancer* **2015**, *15*, 244.

(22) Lin, L.; Qin, Y.; Jin, T.; Liu, S.; Zhang, S.; Shen, X.; Lin, Z. Significance of NQO1 overexpression for prognostic evaluation of gastric adenocarcinoma. *Exp Mol Pathol* **2014**, *96*, 200-205.

(23) Ma, Y.; Kong, J.; Yan, G.; Ren, X.; Jin, D.; Jin, T.; Lin, L.; Lin, Z. NQO1 overexpression is associated with poor prognosis in squamous cell carcinoma of the uterine cervix. *BMC Cancer* **2014**, *14*, 414.

(24) Cheng, Y.; Li, J.; Martinka, M.; Li, G. The expression of NAD(P)H:quinone oxidoreductase 1 is increased along with NF-kappaB p105/p50 in human cutaneous melanomas. *Oncol Rep* **2010**, *23*, 973-979.

(25) Leinonen, H. M.; Kansanen, E.; Polonen, P.; Heinaniemi, M.; Levonen, A. L. Role of the Keap1-Nrf2 pathway in cancer. *Adv Cancer Res* **2014**, *122*, 281-320.

(26) Hayes, J. D.; McMahon, M. NRF2 and KEAP1 mutations: permanent activation of an adaptive response in cancer. *Trends Biochem Sci* **2009**, *34*, 176-188.

(27) Solis, L. M.; Behrens, C.; Dong, W.; Suraokar, M.; Ozburn, N. C.; Moran, C. A.; Corvalan, A. H.; Biswal, S.; Swisher, S. G.; Bekele, B. N.; Minna, J. D.; Stewart, D. J.; Wistuba, II Nrf2 and Keap1 abnormalities in non-small cell lung carcinoma and association with clinicopathologic features. *Clin Cancer Res* **2010**, *16*, 3743-3753.

(28) CancerGenomeAtlasNetwork. Comprehensive genomic characterization of squamous cell lung cancers. *Nature* **2012**, *489*, 519-525.

(29) Onodera, Y.; Motohashi, H.; Takagi, K.; Miki, Y.; Shibahara, Y.; Watanabe, M.; Ishida, T.; Hirakawa, H.; Sasano, H.; Yamamoto, M.; Suzuki, T. NRF2 immunolocalization in human breast cancer patients as a prognostic factor. *Endocr Relat Cancer* **2014**, *21*, 241-252.

(30) Konstantinopoulos, P. A.; Spentzos, D.; Fountzilas, E.; Francoeur, N.; Sanisetty, S.; Grammatikos, A. P.; Hecht, J. L.; Cannistra, S. A. Keap1 mutations and Nrf2 pathway activation in epithelial ovarian cancer. *Cancer Res* **2011**, *71*, 5081-5089.

(31) Schulze, K.; Imbeaud, S.; Letouze, E.; Alexandrov, L. B.; Calderaro, J.; Rebouissou, S.; Couchy, G.; Meiller, C.; Shinde, J.; Soysouvanh, F.; Calatayud, A. L.; Pinyol, R.; Pelletier, L.; Balabaud, C.; Laurent, A.; Blanc, J. F.; Mazzaferro, V.; Calvo, F.; Villanueva, A.; Nault, J. C.; Bioulac-Sage, P.; Stratton, M. R.; Llovet, J. M.; Zucman-Rossi, J. Exome sequencing of hepatocellular carcinomas identifies new mutational signatures and potential therapeutic targets. *Nat Genet* **2015**, *47*, 505-511.

(32) Kovac, M.; Navas, C.; Horswell, S.; Salm, M.; Bardella, C.; Rowan, A.; Stares, M.; Castro-Giner, F.; Fisher, R.; de Bruin, E. C.; Kovacova, M.; Gorman, M.; Makino, S.; Williams, J.; Jaeger, E.; Jones, A.; Howarth, K.; Larkin, J.; Pickering, L.; Gore, M.; Nicol, D. L.; Hazell, S.; Stamp, G.;

O'Brien, T.; Challacombe, B.; Matthews, N.; Phillimore, B.; Begum, S.; Rabinowitz, A.; Varela, I.; Chandra, A.; Horsfield, C.; Polson, A.; Tran, M.; Bhatt, R.; Terracciano, L.; Eppenberger-Castori, S.; Protheroe, A.; Maher, E.; El Bahrawy, M.; Fleming, S.; Ratcliffe, P.; Heinimann, K.; Swanton, C.; Tomlinson, I. Recurrent chromosomal gains and heterogeneous driver mutations characterise papillary renal cancer evolution. *Nat Commun* **2015**, *6*, 6336.

(33) Cullen, J. J.; Hinkhouse, M. M.; Grady, M.; Gaut, A. W.; Liu, J.; Zhang, Y. P.; Weydert, C. J.; Domann, F. E.; Oberley, L. W. Dicumarol inhibition of NADPH:quinone oxidoreductase induces growth inhibition of pancreatic cancer via a superoxide-mediated mechanism. *Cancer Res* **2003**, *63*, 5513-5520.

(34) Winski, S. L.; Faig, M.; Bianchet, M. A.; Siegel, D.; Swann, E.; Fung, K.; Duncan, M. W.; Moody, C. J.; Amzel, L. M.; Ross, D. Characterization of a mechanism-based inhibitor of NAD(P)H:quinone oxidoreductase 1 by biochemical, X-ray crystallographic, and mass spectrometric approaches. *Biochemistry* **2001**, *40*, 15135-15142.

(35) Reigan, P.; Colucci, M. A.; Siegel, D.; Chilloux, A.; Moody, C. J.; Ross, D. Development of indolequinone mechanism-based inhibitors of NAD(P)H:quinone oxidoreductase 1 (NQO1): NQO1 inhibition and growth inhibitory activity in human pancreatic MIA PaCa-2 cancer cells. *Biochemistry* **2007**, *46*, 5941-5950.

(36) Danson, S.; Ward, T. H.; Butler, J.; Ranson, M. DT-diaphorase: a target for new anticancer drugs. *Cancer Treat Rev* **2004**, *30*, 437-449.

(37) Lou, Y.; Li, R.; Xiong, L.; Gu, A.; Shi, C.; Chu, T.; Zhang, X.; Gu, P.; Zhong, H.; Wen, S.; Han, B. NAD(P)H: quinone oxidoreductase 1 (NQO1) C609T polymorphism and lung cancer risk: a meta-analysis. *Tumour Biol* **2013**, *34*, 3967-3979.

(38) Peng, Q.; Lu, Y.; Lao, X.; Chen, Z.; Li, R.; Sui, J.; Qin, X.; Li, S. The NQO1 Pro187Ser polymorphism and breast cancer susceptibility: evidence from an updated meta-analysis. *Diagn Pathol* **2014**, *9*, 100.

(39) Kelsey, K. T.; Ross, D.; Traver, R. D.; Christiani, D. C.; Zuo, Z. F.; Spitz, M. R.; Wang, M.; Xu, X.; Lee, B. K.; Schwartz, B. S.; Wiencke, J. K. Ethnic variation in the prevalence of a common NAD(P)H quinone oxidoreductase polymorphism and its implications for anti-cancer chemotherapy. *Br. J. Cancer* **1997**, *76*, 852-854.

(40) Dinkova-Kostova, A. T.; Talalay, P. NAD(P)H:quinone acceptor oxidoreductase 1 (NQO1), a multifunctional antioxidant enzyme and exceptionally versatile cytoprotector. *Arch Biochem Biophys* **2010**, *501*, 116-123.

(41) Ross, D.; Kepa, J. K.; Winski, S. L.; Beall, H. D.; Anwar, A.; Siegel, D. NAD(P)H:quinone oxidoreductase 1 (NQO1): chemoprotection, bioactivation, gene regulation and genetic polymorphisms. *Chem Biol Interact* **2000**, *129*, 77-97.

(42) Deller, S.; Macheroux, P.; Sollner, S. Flavin-dependent quinone reductases. *Cell Mol Life Sci* **2008**, *65*, 141-160.

(43) Siegel, D.; Beall, H.; Senekowitsch, C.; Kasai, M.; Arai, H.; Gibson, N. W.; Ross, D. Bioreductive activation of mitomycin C by DT-diaphorase. *Biochemistry* **1992**, *31*, 7879-7885.

(44) Fitzsimmons, S. A.; Workman, P.; Grever, M.; Paull, K.; Camalier, R.; Lewis, A. D. Reductase enzyme expression across the National Cancer Institute Tumor cell line panel: correlation with sensitivity to mitomycin C and EO9. *J Natl Cancer Inst* **1996**, *88*, 259-269.

(45) Nemeikaite-Ceniene, A.; Sarlauskas, J.; Anusevicius, Z.; Nivinskas, H.; Cenas, N. Cytotoxicity of RH1 and related aziridinylbenzoquinones: involvement of activation by NAD(P)H:quinone oxidoreductase (NQO1) and oxidative stress. *Arch Biochem Biophys* **2003**, *416*, 110-118.

(46) Ross, D.; Beall, H. D.; Siegel, D.; Traver, R. D.; Gustafson, D. L. Enzymology of bioreductive drug activation. *Br. J. Cancer Suppl.* **1996**, *27*, S1-8.

(47) Colucci, M. A.; Moody, C. J.; Couch, G. D. Natural and synthetic quinones and their reduction by the quinone reductase enzyme NQO1: from synthetic organic chemistry to compounds with anticancer potential. *Org. Biomol. Chem.* **2008**, *6*, 637-656.

(48) Beall, H. D.; Winski, S. I. Mechanisms of action of quinone-containing alkylating agents. I: NQO1-directed drug development. *Front Biosci* **2000**, *5*, D639-648.

(49) Parkinson, E. I.; Bair, J. S.; Cismesia, M.; Hergenrother, P. J. Efficient NQO1 Substrates are Potent and Selective Anticancer Agents. *ACS Chem Biol* **2013**, *8*, 2173-2183.

(50) Guo, W.; Reigan, P.; Siegel, D.; Zirrolli, J.; Gustafson, D.; Ross, D. Formation of 17-allylamino-demethoxygeldanamycin (17-AAG) hydroquinone by NAD(P)H:quinone oxidoreductase 1: role of 17-AAG hydroquinone in heat shock protein 90 inhibition. *Cancer Res* **2005**, *65*, 10006-10015.

(51) Gaspar, N.; Sharp, S. Y.; Pacey, S.; Jones, C.; Walton, M.; Vassal, G.; Eccles, S.; Pearson, A.; Workman, P. Acquired resistance to 17-allylamino-17-demethoxygeldanamycin (17-AAG, tanespimycin) in glioblastoma cells. *Cancer Res* **2009**, *69*, 1966-1975.

(52) Douglas, M.; Lim, A. R.; Porter, J. R.; West, K.; Pink, M. M.; Ge, J.; Wylie, A. A.; Tibbits, T. T.; Biggs, K.; Curtis, M.; Palombella, V. J.; Adams, J.; Fritz, C. C.; Normant, E. The antiproliferative activity of the heat shock protein 90 inhibitor IPI-504 is not dependent on NAD(P)H:quinone oxidoreductase 1 activity in vivo. *Mol Cancer Ther* **2009**, *8*, 3369-3378.

(53) Huang, X.; Dong, Y.; Bey, E. A.; Kilgore, J. A.; Bair, J. S.; Li, L. S.; Patel, M.; Parkinson, E. I.; Wang, Y.; Williams, N. S.; Gao, J.; Hergenrother, P. J.; Boothman, D. A. An NQO1 Substrate with Potent Antitumor Activity That Selectively Kills by PARP1-Induced Programmed Necrosis. *Cancer Res* **2012**, *72*, 3038-3047.

(54) Beall, H. D.; Mulcahy, R. T.; Siegel, D.; Traver, R. D.; Gibson, N. W.; Ross, D. Metabolism of bioreductive antitumor compounds by purified rat and human DT-diaphorases. *Cancer Res* **1994**, *54*, 3196-3201.

(55) Yee, S. B.; Pritsos, C. A. Comparison of oxygen radical generation from the reductive activation of doxorubicin, streptonigrin, and menadione by xanthine oxidase and xanthine dehydrogenase. *Arch Biochem Biophys* **1997**, *347*, 235-241.

(56) Smith, G. M.; Gordon, J. A.; Sewell, I. A.; Ellis, H. A trial of streptonigrin in the treatment of advanced malignant disease. *Brit J Cancer* **1967**, *21*, 295-301.

(57) Pink, J. J.; Planchon, S. M.; Tagliarino, C.; Varnes, M. E.; Siegel, D.; Boothman, D. A. NAD(P)H:Quinone oxidoreductase activity is the principal determinant of beta-lapachone cytotoxicity. *J. Biol. Chem.* **2000**, *275*, 5416-5424.

(58) Bey, E. A.; Bentle, M. S.; Reinicke, K. E.; Dong, Y.; Yang, C. R.; Girard, L.; Minna, J. D.; Bornmann, W. G.; Gao, J.; Boothman, D. A. An NQO1- and PARP-1-mediated cell death pathway induced in non-small-cell lung cancer cells by beta-lapachone. *Proc. Natl. Acad. Sci. U. S. A.* **2007**, *104*, 11832-11837.

(59) Planchon, S. M.; Pink, J. J.; Tagliarino, C.; Bornmann, W. G.; Varnes, M. E.; Boothman, D. A. beta-Lapachone-induced apoptosis in human prostate cancer cells: involvement of NQO1/xip3. *Exp Cell Res* **2001**, *267*, 95-106.

(60) Ough, M.; Lewis, A.; Bey, E. A.; Gao, J.; Ritchie, J. M.; Bornmann, W.; Boothman, D. A.; Oberley, L. W.; Cullen, J. J. Efficacy of beta-lapachone in pancreatic cancer treatment: exploiting the novel, therapeutic target NQO1. *Cancer Biol. Ther.* **2005**, *4*, 95-102.

(61) Li, L. S.; Bey, E. A.; Dong, Y.; Meng, J.; Patra, B.; Yan, J.; Xie, X. J.; Brekken, R. A.; Barnett, C. C.; Bornmann, W. G.; Gao, J.; Boothman, D. A. Modulating endogenous NQO1 levels identifies key regulatory mechanisms of action of beta-lapachone for pancreatic cancer therapy. *Clin Cancer Res* **2011**, *17*, 275-285.

(62) Park, E. J.; Min, K. J.; Lee, T. J.; Yoo, Y. H.; Kim, Y. S.; Kwon, T. K. beta-Lapachone induces programmed necrosis through the RIP1-PARP-AIF-dependent pathway in human hepatocellular carcinoma SK-Hep1 cells. *Cell Death Dis* **2014**, *5*, e1230.

(63) Bey, E. A.; Reinicke, K. E.; Srougi, M. C.; Varnes, M.; Anderson, V. E.; Pink, J. J.; Li, L. S.; Patel, M.; Cao, L.; Moore, Z.; Rommel, A.; Boatman, M.; Lewis, C.; Euhus, D. M.; Bornmann, W. G.; Buchsbaum, D. J.; Spitz, D. R.; Gao, J.; Boothman, D. A. Catalase abrogates beta-lapachone-induced PARP1 hyperactivation-directed programmed necrosis in NQO1-positive breast cancers. *Mol Cancer Ther* **2013**, *12*, 2110-2120.

(64) Gerber, D.; Arriaga, Y.; Beg, M. S.; Dowell, J. E.; Schiller, J. H.; Frankel, A. E.; Leff, R.; Meek, C.; Bolluyt, J.; Fatunde, O.; Martinez, R. T.; Vo, P.; Fattah, F.; Sarode, V.; Zhou, Y.; Xie, Y.; McLeod, M.; Schwartz, B.; Boothman, D. A. Phase I Correlative Studies of ARQ761, a Beta-Lapachone analogue that promotes NQO1-mediated programmed cancer cell necrosis. *Eur J Cancer* **2014**, *50*, 84-85.

(65) Scott, K. A.; Barnes, J.; Whitehead, R. C.; Stratford, I. J.; Nolan, K. A. Inhibitors of NQO1: identification of compounds more potent than dicoumarol without associated off-target effects. *Biochem Pharmacol* **2011**, *81*, 355-363.

(66) Asher, G.; Dym, O.; Tsvetkov, P.; Adler, J.; Shaul, Y. The crystal structure of NAD(P)H quinone oxidoreductase 1 in complex with its potent inhibitor dicoumarol. *Biochemistry* **2006**, *45*, 6372-6378.

(67) Yan, C.; Shieh, B.; Reigan, P.; Zhang, Z.; Colucci, M. A.; Chilloux, A.; Newsome, J. J.; Siegel, D.; Chan, D.; Moody, C. J.; Ross, D. Potent activity of indolequinones against human pancreatic cancer: identification of thioredoxin reductase as a potential target. *Mol Pharmacol* **2009**, *76*, 163-172.

(68) Gonzalez-Aragon, D.; Alcain, F. J.; Ariza, J.; Jodar, L.; Barbarroja, N.; Lopez-Pedrera, C.; Villalba, J. M. ES936 stimulates DNA synthesis in HeLa cells independently on NAD(P)H:quinone oxidoreductase 1 inhibition, through a mechanism involving p38 MAPK. *Chem Biol Interact* **2010**, *186*, 174-183.

(69) Keyes, S. R.; Rockwell, S.; Sartorelli, A. C. Modification of the metabolism and cytotoxicity of bioreductive alkylating agents by dicoumarol in aerobic and hypoxic murine tumor cells. *Cancer Res* **1989**, *49*, 3310-3313.

(70) Dehn, D. L.; Siegel, D.; Swann, E.; Moody, C. J.; Ross, D. Biochemical, cytotoxic, and genotoxic effects of ES936, a mechanism-based inhibitor of NAD(P)H:quinone oxidoreductase 1, in cellular systems. *Mol Pharmacol* **2003**, *64*, 714-720.

(71) Hosoda, S.; Nakamura, W.; Hayashi, K. Properties and reaction mechanism of DT diaphorase from rat liver. *J Biol Chem* **1974**, *249*, 6416-6423.

(72) De Haan, L. H.; Boerboom, A. M.; Rietjens, I. M.; van Capelle, D.; De Ruijter, A. J.; Jaiswal, A. K.; Aarts, J. M. A physiological threshold for protection against menadione toxicity by human NAD(P)H:quinone oxidoreductase (NQO1) in Chinese hamster ovary (CHO) cells. *Biochem Pharmacol* **2002**, *64*, 1597-1603.

(73) Sharp, S. Y.; Kelland, L. R.; Valenti, M. R.; Brunton, L. A.; Hobbs, S.; Workman, P. Establishment of an isogenic human colon tumor model for NQO1 gene expression: application to investigate the role of DT-diaphorase in bioreductive drug activation in vitro and in vivo. *Mol Pharmacol* **2000**, *58*, 1146-1155.

(74) Dehn, D. L.; Winski, S. L.; Ross, D. Development of a new isogenic cell-xenograft system for evaluation of NAD(P)H:quinone oxidoreductase-directed antitumor quinones: evaluation of the activity of RH1. *Clin Cancer Res* **2004**, *10*, 3147-3155.

(75) Rinehart, K. L.; Renfroe, H. B. The Structure of Nybomycin. *J. Am. Chem. Soc.* **1961**, *83*, 3729-3731.

(76) Li, S.; Tian, X.; Niu, S.; Zhang, W.; Chen, Y.; Zhang, H.; Yang, X.; Li, W.; Zhang, S.; Ju, J.; Zhang, C. Pseudonocardians A-C, new diazaanthraquinone derivatives from a deap-sea actinomycete Pseudonocardia sp. SCSIO 01299. *Marine drugs* **2011**, *9*, 1428-1439.

(77) Tian, X. P.; Long, L. J.; Li, S. M.; Zhang, J.; Xu, Y.; He, J.; Li, J.; Wang, F. Z.; Li, W. J.; Zhang, C. S.; Zhang, S. Pseudonocardia antitumoralis sp. nov., a deoxynyboquinone-producing actinomycete isolated from a deep-sea sediment. *Int J Syst Evol Microbiol* **2013**, *63*, 893-899.

(78) Putt, K. S. The Modulation of Life and Death: Small Molecule Activators and Inhibitors of Necrotic and Apoptotic Pathways, University of Illinois at Urbana-Champaign, 2006.

(79) Tudor, G.; Gutierrez, P.; Aguilera-Gutierrez, A.; Sausville, E. A. Cytotoxicity and apoptosis of benzoquinones: redox cycling, cytochrome c release, and BAD protein expression. *Biochem. Pharmacol.* **2003**, *65*, 1061-1075.

(80) Forbis, R. M.; Rinehart, K. L. Nybomycin .4. Total Synthesis of Deoxynybomycin. *J. Am. Chem. Soc.* **1970**, *92*, 6995-&.

(81) Forbis, R. M.; Rinehart, K. L. Nybomycin .7. Preparative Routes to Nybomycin and Deoxynybomycin. *J. Am. Chem. Soc.* **1973**, *95*, 5003-5013.

(82) Bair, J. S.; Palchaudhuri, R.; Hergenrother, P. J. Chemistry and biology of deoxynyboquinone, a potent inducer of cancer cell death. *J Am Chem Soc* **2010**, *132*, 5469-5478.

(83) Parkinson, E. I.; Bair, J. S.; Nakamura, B. A.; Lee, H. Y.; Kuttab, H. I.; Southgate, E. H.; Lezmi, S.; Lau, G. W.; Hergenrother, P. J. Deoxynybomycins inhibit mutant DNA gyrase and rescue mice infected with fluoroquinolone-resistant bacteria. *Nat Commun* **2015**, *6*, 6947.

(84) Bair, J. S. The Development of Deoxynyboquinone as a Personalized Anticancer Compound, University of Illinois at Urbana-Champaign, 2012.

(85) Gutierrez, P. L. The metabolism of quinone-containing alkylating agents: free radical production and measurement. *Front Biosci* **2000**, *5*, D629-638.

(86) Fleming, A. In *Nobel Lecture*; The Nobel Foundation: Amsterdam, 1945; Vol. 2015.

(87) McClure, N. S.; Day, T. A theoretical examination of the relative importance of evolution management and drug development for managing resistance. *Proc Biol Sci* **2014**, *281*.

(88) CDC: Atlanta, GA, 2013.

(89) Friedman, T.; Skinner, T.; Bell, M.; Centers for Disease Control and Prevention: Atlanta, GA, 2013; Vol. 2015.

(90) Allen, H. K.; Donato, J.; Wang, H. H.; Cloud-Hansen, K. A.; Davies, J.; Handelsman, J. Call of the wild: antibiotic resistance genes in natural environments. *Nat Rev Microbiol* **2010**, *8*, 251-259.

(91) Penchovsky, R.; Traykovska, M. Designing drugs that overcome antibacterial resistance: where do we stand and what should we do? *Expert Opin Drug Discov* **2015**, *10*, 631-650.

(92) Lorenzetti, L. In *Fortune*; Time Inc., 2015.

(93) Ling, L. L.; Schneider, T.; Peoples, A. J.; Spoering, A. L.; Engels, I.; Conlon, B. P.; Mueller, A.; Schaberle, T. F.; Hughes, D. E.; Epstein, S.; Jones, M.; Lazarides, L.; Steadman, V. A.; Cohen, D. R.; Felix, C. R.; Fetterman, K. A.; Millett, W. P.; Nitti, A. G.; Zullo, A. M.; Chen, C.; Lewis, K. A new antibiotic kills pathogens without detectable resistance. *Nature* **2015**, *517*, 455-459.

(94) Brooks, B. D.; Brooks, A. E. Therapeutic strategies to combat antibiotic resistance. *Adv Drug Deliv Rev* **2014**, *78*, 14-27.

(95) Clatworthy, A. E.; Pierson, E.; Hung, D. T. Targeting virulence: a new paradigm for antimicrobial therapy. *Nat Chem Biol* **2007**, *3*, 541-548.

(96) Blair, J. M.; Webber, M. A.; Baylay, A. J.; Ogbolu, D. O.; Piddock, L. J. Molecular mechanisms of antibiotic resistance. *Nat Rev Microbiol* **2015**, *13*, 42-51.

(97) *Basic & Clinical Pharmacology, 13th Edition*; 13 ed.; Katzung, B.; Trevor, A., Eds.; McGraw-Hill Education, 2015.

(98) Redgrave, L. S.; Sutton, S. B.; Webber, M. A.; Piddock, L. J. Fluoroquinolone resistance: mechanisms, impact on bacteria, and role in evolutionary success. *Trends Microbiol* **2014**, *22*, 438-445.

(99) Davies, J.; Davies, D. Origins and evolution of antibiotic resistance. *Microbiol Mol Biol Rev* **2010**, *74*, 417-433.

(100) Meka, V. G.; Gold, H. S. Antimicrobial resistance to linezolid. *Clin Infect Dis* **2004**, *39*, 1010-1015.

(101) Gordon, N. C.; Png, K.; Wareham, D. W. Potent synergy and sustained bactericidal activity of a vancomycin-colistin combination versus multidrug-resistant strains of Acinetobacter baumannii. *Antimicrob Agents Chemother* **2010**, *54*, 5316-5322.

(102) Vidaillac, C.; Benichou, L.; Duval, R. E. In vitro synergy of colistin combinations against colistin-resistant Acinetobacter baumannii, Pseudomonas aeruginosa, and Klebsiella pneumoniae isolates. *Antimicrob Agents Chemother* **2012**, *56*, 4856-4861.

(103) Opperman, T. J.; Nguyen, S. T. Recent advances toward a molecular mechanism of efflux pump inhibition. *Front Microbiol* **2015**, *6*, 421.

(104) Boucher, H. W.; Talbot, G. H.; Bradley, J. S.; Edwards, J. E.; Gilbert, D.; Rice, L. B.; Scheld, M.; Spellberg, B.; Bartlett, J. Bad bugs, no drugs: no ESKAPE! An update from the Infectious Diseases Society of America. *Clin Infect Dis* **2009**, *48*, 1-12.

(105) Garber, K. A beta-lactamase inhibitor revival provides new hope for old antibiotics. *Nat Rev Drug Discov* **2015**, *14*, 445-447.

(106) Skold, O. Sulfonamide resistance: mechanisms and trends. *Drug Resist Updat* **2000**, *3*, 155-160.

(107) Taitt, C. R.; Leski, T. A.; Stockelman, M. G.; Craft, D. W.; Zurawski, D. V.; Kirkup, B. C.; Vora, G. J. Antimicrobial resistance determinants in Acinetobacter baumannii isolates taken from military treatment facilities. *Antimicrob Agents Chemother* **2014**, *58*, 767-781.

(108) Shin, H. W.; Lim, J.; Kim, S.; Kim, J.; Kwon, G. C.; Koo, S. H. Characterization of trimethoprim-sulfamethoxazole resistance genes and their relatedness to class 1 integron and insertion sequence common region in gram-negative bacilli. *J Microbiol Biotechnol* **2015**, *25*, 137-142.

(109) Frey, K. M.; Lombardo, M. N.; Wright, D. L.; Anderson, A. C. Towards the understanding of resistance mechanisms in clinically isolated trimethoprim-resistant, methicillin-resistant Staphylococcus aureus dihydrofolate reductase. *J Struct Biol* **2010**, *170*, 93-97.

(110) Dale, G. E.; Broger, C.; D'Arcy, A.; Hartman, P. G.; DeHoogt, R.; Jolidon, S.; Kompis, I.; Labhardt, A. M.; Langen, H.; Locher, H.; Page, M. G.; Stuber, D.; Then, R. L.; Wipf, B.; Oefner, C. A single amino acid substitution in Staphylococcus aureus dihydrofolate reductase determines trimethoprim resistance. *J Mol Biol* **1997**, *266*, 23-30.

(111) Lee, J.; Yennawar, N. H.; Gam, J.; Benkovic, S. J. Kinetic and structural characterization of dihydrofolate reductase from Streptococcus pneumoniae. *Biochemistry* **2010**, *49*, 195-206.

(112) Watson, M.; Liu, J. W.; Ollis, D. Directed evolution of trimethoprim resistance in Escherichia coli. *FEBS J* **2007**, *274*, 2661-2671.

(113) Toprak, E.; Veres, A.; Michel, J. B.; Chait, R.; Hartl, D. L.; Kishony, R. Evolutionary paths to antibiotic resistance under dynamically sustained drug selection. *Nat Genet* **2012**, *44*, 101-105.

(114) Skold, O. Resistance to trimethoprim and sulfonamides. *Vet Res* **2001**, *32*, 261-273.

(115) Peacock, S. J.; Paterson, G. K. Mechanisms of Methicillin Resistance in Staphylococcus aureus. *Annu Rev Biochem* **2015**, *84*, 577-601.

(116) Zapun, A.; Contreras-Martel, C.; Vernet, T. Penicillin-binding proteins and beta-lactam resistance. *FEMS Microbiol Rev* **2008**, *32*, 361-385.

(117) Kahne, D.; Leimkuhler, C.; Lu, W.; Walsh, C. Glycopeptide and lipoglycopeptide antibiotics. *Chem Rev* **2005**, *105*, 425-448.

(118) Okano, A.; Nakayama, A.; Schammel, A. W.; Boger, D. L. Total synthesis of [Psi[C(horizontal lineNH)NH]Tpg(4)]vancomycin and its (4-chlorobiphenyl)methyl derivative: impact of peripheral modifications on vancomycin analogues redesigned for dual D-Ala-D-Ala and D-Ala-D-Lac binding. *J Am Chem Soc* **2014**, *136*, 13522-13525.

(119) Courvalin, P. Vancomycin resistance in gram-positive cocci. *Clin Infect Dis* **2006**, *42 Suppl 1*, S25-34.

(120) Marshall, C. G.; Broadhead, G.; Leskiw, B. K.; Wright, G. D. D-Ala-D-Ala ligases from glycopeptide antibiotic-producing organisms are highly homologous to the enterococcal vancomycin-resistance ligases VanA and VanB. *Proc Natl Acad Sci U S A* **1997**, *94*, 6480-6483.

(121) Gaupp, R.; Lei, S.; Reed, J. M.; Peisker, H.; Boyle-Vavra, S.; Bayer, A. S.; Bischoff, M.; Herrmann, M.; Daum, R. S.; Powers, R.; Somerville, G. A. Staphylococcus aureus Metabolic Adaptations during the Transition from a Daptomycin Susceptibility Phenotype to a Daptomycin Nonsusceptibility Phenotype. *Antimicrob Agents Chemother* **2015**, *59*, 4226-4238.

(122) Kotra, L. P.; Haddad, J.; Mobashery, S. Aminoglycosides: perspectives on mechanisms of action and resistance and strategies to counter resistance. *Antimicrob Agents Chemother* **2000**, *44*, 3249-3256.

(123) Doi, Y.; Arakawa, Y. 16S ribosomal RNA methylation: emerging resistance mechanism against aminoglycosides. *Clin Infect Dis* **2007**, *45*, 88-94.

(124) Wachino, J.; Arakawa, Y. Exogenously acquired 16S rRNA methyltransferases found in aminoglycoside-resistant pathogenic Gram-negative bacteria: an update. *Drug Resist Updat* **2012**, *15*, 133-148.

(125) Wilson, D. N. Ribosome-targeting antibiotics and mechanisms of bacterial resistance. *Nat Rev Microbiol* **2014**, *12*, 35-48.

(126) Connell, S. R.; Tracz, D. M.; Nierhaus, K. H.; Taylor, D. E. Ribosomal protection proteins and their mechanism of tetracycline resistance. *Antimicrob Agents Chemother* **2003**, *47*, 3675-3681.

(127) Li, W.; Atkinson, G. C.; Thakor, N. S.; Allas, U.; Lu, C. C.; Chan, K. Y.; Tenson, T.; Schulten, K.; Wilson, K. S.; Hauryliuk, V.; Frank, J. Mechanism of tetracycline resistance by ribosomal protection protein Tet(O). *Nat Commun* **2013**, *4*, 1477.

(128) Wilson, D. N. The A-Z of bacterial translation inhibitors. *Crit Rev Biochem Mol Biol* **2009**, *44*, 393-433.

(129) Billal, D. S.; Feng, J.; Leprohon, P.; Legare, D.; Ouellette, M. Whole genome analysis of linezolid resistance in Streptococcus pneumoniae reveals resistance and compensatory mutations. *BMC Genomics* **2011**, *12*, 512.

(130) Floss, H. G.; Yu, T. W. Rifamycin-mode of action, resistance, and biosynthesis. *Chem Rev* **2005**, *105*, 621-632.

(131) Chen, S. H.; Chan, N. L.; Hsieh, T. S. New mechanistic and functional insights into DNA topoisomerases. *Annu Rev Biochem* **2013**, *82*, 139-170.

(132) Pommier, Y. Drugging topoisomerases: lessons and challenges. *ACS Chem Biol* **2013**, *8*, 82-95.

(133) Bax, B. D.; Chan, P. F.; Eggleston, D. S.; Fosberry, A.; Gentry, D. R.; Gorrec, F.; Giordano, I.; Hann, M. M.; Hennessy, A.; Hibbs, M.; Huang, J.; Jones, E.; Jones, J.; Brown, K. K.; Lewis, C. J.; May, E. W.; Saunders, M. R.; Singh, O.; Spitzfaden, C. E.; Shen, C.; Shillings, A.; Theobald, A. J.; Wohlkonig, A.; Pearson, N. D.; Gwynn, M. N. Type IIA topoisomerase inhibition by a new class of antibacterial agents. *Nature* **2010**, *466*, 935-940.

(134) Fisher, L. M.; Pan, X. S. Methods to assay inhibitors of DNA gyrase and topoisomerase IV activities. *Methods Mol Med* **2008**, *142*, 11-23.

(135) Kampranis, S. C.; Maxwell, A. The DNA gyrase-quinolone complex. ATP hydrolysis and the mechanism of DNA cleavage. *J Biol Chem* **1998**, *273*, 22615-22626.

(136) Hiramatsu, K.; Igarashi, M.; Morimoto, Y.; Baba, T.; Umekita, M.; Akamatsu, Y. Curing bacteria of antibiotic resistance: reverse antibiotics, a novel class of antibiotics in nature. *Int J Antimicrob Agents* **2012**, *39*, 478-485.

(137) Hooper, D. C. Fluoroquinolone resistance among Gram-positive cocci. *Lancet Infect Dis* **2002**, *2*, 530-538.

(138) Imamovic, L.; Sommer, M. O. Use of collateral sensitivity networks to design drug cycling protocols that avoid resistance development. *Sci Transl Med* **2013**, *5*, 204ra132.

(139) Brock, T. D.; Sokolski, W. T. Biological studies on the antibiotic, nybomycin. *Antibiot Chemother (Northfield Ill)* **1958**, *8*, 631-636.

(140) Strelitz, F.; Flon, H.; Asheshov, I. N. Nybomycin, A New Antibiotic with Antiphage and Antibacterial Properties. *Proc. Natl. Acad. Sci. U. S. A.* **1955**, *41*, 620-624.

(141) Naganawa, H. W., T.; Yagi, A.; Kondo, S.; Takita, T.; Hamada, M.; Maeda, K.; Umezawa, H. Deoxynybomycin from a Streptomyces. *J. Antibiot.* **1970**, *23*, 365-378.

(142) Kwak, Y. G.; Truong-Bolduc, Q. C.; Bin Kim, H.; Song, K. H.; Kim, E. S.; Hooper, D. C. Association of norB overexpression and fluoroquinolone resistance in clinical isolates of Staphylococcus aureus from Korea. *J Antimicrob Chemother* **2013**, *68*, 2766-2772.

(143) Wang, S.; Wang, Y.; Shen, J.; Wu, Y.; Wu, C. Polymorphic mutation frequencies in clinical isolates of Staphylococcus aureus: the role of weak mutators in the development of fluoroquinolone resistance. *FEMS Microbiol Lett* **2013**, *341*, 13-17.

(144) Baba, K.; Ishihara, K.; Ozawa, M.; Usui, M.; Hiki, M.; Tamura, Y.; Asai, T. Prevalence and mechanism of antimicrobial resistance in Staphylococcus aureus isolates from diseased cattle, swine and chickens in Japan. *J Vet Med Sci* **2012**, *74*, 561-565.

(145) Costa, S. S.; Falcao, C.; Viveiros, M.; Machado, D.; Martins, M.; Melo-Cristino, J.; Amaral, L.; Couto, I. Exploring the contribution of efflux on the resistance to fluoroquinolones in clinical isolates of Staphylococcus aureus. *BMC Microbiol* **2011**, *11*, 241.

(146) Sanfilippo, C. M.; Hesje, C. K.; Haas, W.; Morris, T. W. Topoisomerase mutations that are associated with high-level resistance to earlier fluoroquinolones in Staphylococcus aureus have less effect on the antibacterial activity of besifloxacin. *Chemotherapy* **2011**, *57*, 363-371.

(147) Aligholi, M.; Mirsalehian, A.; Halimi, S.; Imaneini, H.; Taherikalani, M.; Jabalameli, F.; Asadollahi, P.; Mohajer, B.; Abdollahi, A.; Emaneini, M. Phenotypic and genotypic evaluation of fluoroquinolone resistance in clinical isolates of Staphylococcus aureus in Tehran. *Med Sci Monit* **2011**, *17*, PH71-74.

(148) Yoon, E. J.; Lee, C. Y.; Shim, M. J.; Min, Y. H.; Kwon, A. R.; Lee, J.; Choi, E. C. Extended spectrum of quinolone resistance, even to a potential latter third-generation agent, as a result of a minimum of two GrlA and two GyrA alterations in quinolone-resistant Staphylococcus aureus. *Chemotherapy* **2010**, *56*, 153-157.

(149) Coskun-Ari, F. F.; Bosgelmez-Tinaz, G. grlA and gyrA mutations and antimicrobial susceptibility in clinical isolates of ciprofloxacin- methicillin-resistant Staphylococcus aureus. *Eur J Med Res* **2008**, *13*, 366-370.

(150) Price, L. B.; Vogler, A.; Pearson, T.; Busch, J. D.; Schupp, J. M.; Keim, P. In vitro selection and characterization of Bacillus anthracis mutants with high-level resistance to ciprofloxacin. *Antimicrob Agents Chemother* **2003**, *47*, 2362-2365.

(151) Vila, J.; Ruiz, J.; Marco, F.; Barcelo, A.; Goni, P.; Giralt, E.; Jimenez de Anta, T. Association between double mutation in gyrA gene of ciprofloxacin-resistant clinical isolates of Escherichia coli and MICs. *Antimicrob Agents Chemother* **1994**, *38*, 2477-2479.

(152) Hirose, K.; Terajima, J.; Izumiya, H.; Tamura, K.; Arakawa, E.; Takai, N.; Watanabe, H. Antimicrobial susceptibility of Shigella sonnei isolates in Japan and molecular analysis of S.

sonnei isolates with reduced susceptibility to fluoroquinolones. *Antimicrob Agents Chemother* **2005**, *49*, 1203-1205.

(153) Mensa, L.; Marco, F.; Vila, J.; Gascon, J.; Ruiz, J. Quinolone resistance among Shigella spp. isolated from travellers returning from India. *Clin Microbiol Infect* **2008**, *14*, 279-281.

(154) Vila, J.; Ruiz, J.; Goni, P.; Marcos, A.; Jimenez de Anta, T. Mutation in the gyrA gene of quinolone-resistant clinical isolates of Acinetobacter baumannii. *Antimicrob Agents Chemother* **1995**, *39*, 1201-1203.

(155) Werner, G.; Fleige, C.; Ewert, B.; Laverde-Gomez, J. A.; Klare, I.; Witte, W. High-level ciprofloxacin resistance among hospital-adapted Enterococcus faecium (CC17). *Int J Antimicrob Agents* **2010**, *35*, 119-125.

(156) Bast, D. J.; Low, D. E.; Duncan, C. L.; Kilburn, L.; Mandell, L. A.; Davidson, R. J.; de Azavedo, J. C. Fluoroquinolone resistance in clinical isolates of Streptococcus pneumoniae: contributions of type II topoisomerase mutations and efflux to levels of resistance. *Antimicrob Agents Chemother* **2000**, *44*, 3049-3054.

(157) Deguchi, T.; Fukuoka, A.; Yasuda, M.; Nakano, M.; Ozeki, S.; Kanematsu, E.; Nishino, Y.; Ishihara, S.; Ban, Y.; Kawada, Y. Alterations in the GyrA subunit of DNA gyrase and the ParC subunit of topoisomerase IV in quinolone-resistant clinical isolates of Klebsiella pneumoniae. *Antimicrob Agents Chemother* **1997**, *41*, 699-701.

(158) Vernel-Pauillac, F.; Hogan, T. R.; Tapsall, J. W.; Goarant, C. Quinolone resistance in Neisseria gonorrhoeae: rapid genotyping of quinolone resistance-determining regions in gyrA and parC genes by melting curve analysis predicts susceptibility. *Antimicrob Agents Chemother* **2009**, *53*, 1264-1267.

(159) Sadowy, E.; Sienko, A.; Gawryszewska, I.; Bojarska, A.; Malinowska, K.; Hryniewicz, W. High abundance and diversity of antimicrobial resistance determinants among early vancomycin-resistant Enterococcus faecium in Poland. *Eur J Clin Microbiol Infect Dis* **2013**, *32*, 1193-1203.

(160) Grohs, P.; Houssaye, S.; Aubert, A.; Gutmann, L.; Varon, E. In vitro activities of garenoxacin (BMS-284756) against Streptococcus pneumoniae, viridans group streptococci, and Enterococcus faecalis compared to those of six other quinolones. *Antimicrob Agents Chemother* **2003**, *47*, 3542-3547.

(161) Tremblay, C. L.; Charlebois, A.; Masson, L.; Archambault, M. Characterization of hospital-associated lineages of ampicillin-resistant Enterococcus faecium from clinical cases in dogs and humans. *Front Microbiol* **2013**, *4*, 245.

(162) Rathnayake, I. U.; Hargreaves, M.; Huygens, F. Antibiotic resistance and virulence traits in clinical and environmental Enterococcus faecalis and Enterococcus faecium isolates. *Syst Appl Microbiol* **2012**, *35*, 326-333.

(163) Yonezawa, M.; Takahata, M.; Matsubara, N.; Watanabe, Y.; Narita, H. DNA gyrase gyrA mutations in quinolone-resistant clinical isolates of Pseudomonas aeruginosa. *Antimicrob Agents Chemother* **1995**, *39*, 1970-1972.

(164) Ferreira, M. L.; Dantas, R. C.; Faria, A. L.; Goncalves, I. R.; Silveira de Brito, C.; Queiroz, L. L.; Gontijo-Filho, P. P.; Ribas, R. M. Molecular epidemiological survey of the quinolone- and carbapenem-resistant genotype and its association with the type III secretion system in Pseudomonas aeruginosa. *J Med Microbiol* **2015**, *64*, 262-271.

(165) Yang, X.; Xing, B.; Liang, C.; Ye, Z.; Zhang, Y. Prevalence and fluoroquinolone resistance of pseudomonas aeruginosa in a hospital of South China. *Int J Clin Exp Med* **2015**, *8*, 1386-1390.

(166) Pasca, M. R.; Dalla Valle, C.; De Jesus Lopes Ribeiro, A. L.; Buroni, S.; Papaleo, M. C.; Bazzini, S.; Udine, C.; Incandela, M. L.; Daffara, S.; Fani, R.; Riccardi, G.; Marone, P. Evaluation of fluoroquinolone resistance mechanisms in Pseudomonas aeruginosa multidrug resistance clinical isolates. *Microb Drug Resist* **2012**, *18*, 23-32.

(167) Avalos, E.; Catanzaro, D.; Catanzaro, A.; Ganiats, T.; Brodine, S.; Alcaraz, J.; Rodwell, T. Frequency and geographic distribution of gyrA and gyrB mutations associated with fluoroquinolone resistance in clinical Mycobacterium tuberculosis isolates: a systematic review. *PLoS One* **2015**, *10*, e0120470.

(168) Tanaka, M.; Wang, T.; Onodera, Y.; Uchida, Y.; Sato, K. Mechanism of quinolone resistance in Staphylococcus aureus. *J Infect Chemother* **2000**, *6*, 131-139.

(169) Maleki, M. H.; Jalilian, F. A.; Khayat, H.; Mohammadi, M.; Pourahmad, F.; Asadollahi, K.; Pakzad, I.; Sadeghifard, N.; Soroush, S.; Emaneini, M.; Taherikalani, M. Detection of highly ciprofloxacin resistance acinetobacter baumannii isolated from patients with burn wound infections in presence and absence of efflux pump inhibitor. *Maedica (Buchar)* **2014**, *9*, 162-167.

(170) Sun, C.; Hao, J.; Dou, M.; Gong, Y. Mutant prevention concentrations of levofloxacin, pazufloxacin and ciprofloxacin for A. baumannii and mutations in gyrA and parC genes. *J Antibiot (Tokyo)* **2015**, *68*, 313-317.

(171) Lopes, B. S.; Amyes, S. G. Insertion sequence disruption of adeR and ciprofloxacin resistance caused by efflux pumps and gyrA and parC mutations in Acinetobacter baumannii. *Int J Antimicrob Agents* **2013**, *41*, 117-121.

(172) Golanbar, G. D.; Lam, C. K.; Chu, Y. M.; Cueva, C.; Tan, S. W.; Silva, I.; Xu, H. H. Phenotypic and molecular characterization of Acinetobacter clinical isolates obtained from inmates of California correctional facilities. *J Clin Microbiol* **2011**, *49*, 2121-2131.

(173) Hu, L. F.; Li, J. B.; Ye, Y.; Li, X. Mutations in the GyrA subunit of DNA gyrase and the ParC subunit of topoisomerase IV in clinical strains of fluoroquinolone-resistant Shigella in Anhui, China. *J Microbiol* **2007**, *45*, 168-170.

(174) Folster, J. P.; Pecic, G.; Bowen, A.; Rickert, R.; Carattoli, A.; Whichard, J. M. Decreased susceptibility to ciprofloxacin among Shigella isolates in the United States, 2006 to 2009. *Antimicrob Agents Chemother* **2011**, *55*, 1758-1760.

(175) Kumari, N.; Subramaniam, G.; Navaratnam, P.; Sekaran, S. D. Molecular characterization of genes encoding the quinolone resistance determining regions of Malaysian Streptococcus pneumoniae strains. *Indian J Med Microbiol* **2008**, *26*, 148-150.

(176) Pan, X. S.; Ambler, J.; Mehtar, S.; Fisher, L. M. Involvement of topoisomerase IV and DNA gyrase as ciprofloxacin targets in Streptococcus pneumoniae. *Antimicrob Agents Chemother* **1996**, *40*, 2321-2326.

(177) Piekarska, K.; Wolkowicz, T.; Zacharczuk, K.; Rzeczkowska, M.; Chrost, A.; Bareja, E.; Olak, M.; Gierczynski, R. Co-existence of plasmid-mediated quinolone resistance determinants and mutations in gyrA and parC among fluoroquinolone-resistant clinical Enterobacteriaceae isolated in a tertiary hospital in Warsaw, Poland. *Int J Antimicrob Agents* **2015**, *45*, 238-243.

(178) Nagasaka, Y.; Kimura, K.; Yamada, K.; Wachino, J.; Jin, W.; Notake, S.; Yanagisawa, H.; Arakawa, Y. Genetic profiles of fluoroquinolone-nonsusceptible Klebsiella pneumoniae among cephalosporin-resistant K. pneumoniae. *Microb Drug Resist* **2015**, *21*, 224-233.

(179) Chen, F. J.; Lauderdale, T. L.; Ho, M.; Lo, H. J. The roles of mutations in gyrA, parC, and ompK35 in fluoroquinolone resistance in Klebsiella pneumoniae. *Microb Drug Resist* **2003**, *9*, 265-271.

(180) Li, J.; Gao, X.; Luo, T.; Wu, J.; Sun, G.; Liu, Q.; Jiang, Y.; Zhang, Y.; Mei, J.; Gao, Q. Association of gyrA/B mutations and resistance levels to fluoroquinolones in clinical isolates of Mycobacterium tuberculosis. *Emerg Microbes Infect* **2014**, *3*, e19.

(181) Knezevic, C. E. Development of Poly(ADP-Ribose) Glycohydrolase Inhibitors and Tetracyclic Indoles as Anticancer Compounds, University of Illinois at Urbana-Champaign, 2014.

(182) Zheng, W.; Thorne, N.; McKew, J. C. Phenotypic screens as a renewed approach for drug discovery. *Drug Discov Today* **2013**, *18*, 1067-1073.

(183) Moffat, J. G.; Rudolph, J.; Bailey, D. Phenotypic screening in cancer drug discovery - past, present and future. *Nat Rev Drug Discov* **2014**, *13*, 588-602.

(184) Fallahi-Sichani, M.; Honarnejad, S.; Heiser, L. M.; Gray, J. W.; Sorger, P. K. Metrics other than potency reveal systematic variation in responses to cancer drugs. *Nat Chem Biol* **2013**, *9*, 708-714.

(185) Shen, L.; Peterson, S.; Sedaghat, A. R.; McMahon, M. A.; Callender, M.; Zhang, H.; Zhou, Y.; Pitt, E.; Anderson, K. S.; Acosta, E. P.; Siliciano, R. F. Dose-response curve slope sets class-specific limits on inhibitory potential of anti-HIV drugs. *Nat Med* **2008**, *14*, 762-766.

(186) Sampah, M. E.; Shen, L.; Jilek, B. L.; Siliciano, R. F. Dose-response curve slope is a missing dimension in the analysis of HIV-1 drug resistance. *Proc Natl Acad Sci U S A* **2011**, *108*, 7613-7618.

(187) Vainstein, V.; Eide, C. A.; O'Hare, T.; Shukron, O.; Druker, B. J. Integrating in vitro sensitivity and dose-response slope is predictive of clinical response to ABL kinase inhibitors in chronic myeloid leukemia. *Blood* **2013**, *122*, 3331-3334.

(188) Samali, A.; Fitzgerald, U.; Deegan, S.; Gupta, S. Methods for monitoring endoplasmic reticulum stress and the unfolded protein response. *Int J Cell Biol* **2010**, *2010*, 830307.

(189) Xu, C.; Bailly-Maitre, B.; Reed, J. C. Endoplasmic reticulum stress: cell life and death decisions. *J Clin Invest* **2005**, *115*, 2656-2664.

(190) Clarke, H. J.; Chambers, J. E.; Liniker, E.; Marciniak, S. J. Endoplasmic reticulum stress in malignancy. *Cancer Cell* **2014**, *25*, 563-573.

(191) Wang, G.; Yang, Z. Q.; Zhang, K. Endoplasmic reticulum stress response in cancer: molecular mechanism and therapeutic potential. *Am J Transl Res* **2010**, *2*, 65-74.

(192) Bertolotti, A.; Zhang, Y.; Hendershot, L. M.; Harding, H. P.; Ron, D. Dynamic interaction of BiP and ER stress transducers in the unfolded-protein response. *Nat. Cell Biol.* **2000**, *2*, 326-332.

(193) Ron, D.; Walter, P. Signal integration in the endoplasmic reticulum unfolded protein response. *Nat Rev Mol Cell Biol* **2007**, *8*, 519-529.

(194) Oslowski, C. M.; Urano, F. Measuring ER stress and the unfolded protein response using mammalian tissue culture system. *Methods Enzymol* **2011**, *490*, 71-92.

(195) Hetz, C. The unfolded protein response: controlling cell fate decisions under ER stress and beyond. *Nat Rev Mol Cell Biol* **2012**, *13*, 89-102.

(196) Walter, P.; Ron, D. The unfolded protein response: from stress pathway to homeostatic regulation. *Science* **2011**, *334*, 1081-1086.

(197) Ye, J.; Rawson, R. B.; Komuro, R.; Chen, X.; Dave, U. P.; Prywes, R.; Brown, M. S.; Goldstein, J. L. ER stress induces cleavage of membrane-bound ATF6 by the same proteases that process SREBPs. *Mol Cell* **2000**, *6*, 1355-1364.

(198) Ron, D.; Walter, P. Signal integration in the endoplasmic reticulum unfolded protein response. *Nat. Rev. Mol. Cell Bio.* **2007**, *8*, 519-529.

(199) Hetz, C. The unfolded protein response: controlling cell fate decisions under ER stress and beyond. *Nat. Rev. Mol. Cell Bio.* **2012**, *13*, 89-102.

(200) Thomas, S.; Sharma, N.; Golden, E. B.; Cho, H.; Agarwal, P.; Gaffney, K. J.; Petasis, N. A.; Chen, T. C.; Hofman, F. M.; Louie, S. G.; Schonthal, A. H. Preferential killing of triple-negative breast cancer cells in vitro and in vivo when pharmacological aggravators of endoplasmic reticulum stress are combined with autophagy inhibitors. *Cancer Lett* **2012**, *325*, 63-71.

(201) Kardosh, A.; Golden, E. B.; Pyrko, P.; Uddin, J.; Hofman, F. M.; Chen, T. C.; Louie, S. G.; Petasis, N. A.; Schonthal, A. H. Aggravated endoplasmic reticulum stress as a basis for enhanced glioblastoma cell killing by bortezomib in combination with celecoxib or its non-coxib analogue, 2,5-dimethyl-celecoxib. *Cancer Res* **2008**, *68*, 843-851.

(202) Pyrko, P.; Kardosh, A.; Wang, W.; Xiong, W.; Schonthal, A. H.; Chen, T. C. HIV-1 protease inhibitors nelfinavir and atazanavir induce malignant glioma death by triggering endoplasmic reticulum stress. *Cancer Res* **2007**, *67*, 10920-10928.

(203) Taiyab, A.; Sreedhar, A. S.; Rao Ch, M. Hsp90 inhibitors, GA and 17AAG, lead to ER stress-induced apoptosis in rat histiocytoma. *Biochem Pharmacol* **2009**, *78*, 142-152.

(204) Fels, D. R.; Ye, J.; Segan, A. T.; Kridel, S. J.; Spiotto, M.; Olson, M.; Koong, A. C.; Koumenis, C. Preferential cytotoxicity of bortezomib toward hypoxic tumor cells via overactivation of endoplasmic reticulum stress pathways. *Cancer Res* **2008**, *68*, 9323-9330.

(205) Wictome, M.; Henderson, I.; Lee, A. G.; East, J. M. Mechanism of inhibition of the calcium pump of sarcoplasmic reticulum by thapsigargin. *Biochem J* **1992**, *283 (Pt 2)*, 525-529.

(206) Duksin, D.; Mahoney, W. C. Relationship of the structure and biological activity of the natural homologues of tunicamycin. *J Biol Chem* **1982**, *257*, 3105-3109.

(207) Hou, H.; Sun, H.; Lu, P.; Ge, C.; Zhang, L.; Li, H.; Zhao, F.; Tian, H.; Chen, T.; Yao, M.; Li, J. Tunicamycin potentiates cisplatin anticancer efficacy through the DPAGT1/Akt/ABCG2 pathway in mouse Xenograft models of human hepatocellular carcinoma. *Mol Cancer Ther* **2013**, *12*, 2874-2884.

Chapter 2. Deoxynyboquinones as NQO1-targeted anticancer agents

Portions of this Chapter are reprinted with permission from Huang, X.; Dong, Y.; Bey, E. A.; Kilgore, J. A.; Bair, J. S.; Li, L.-S.; Patel, M.; Parkinson, E. I.; Wang, Y.; Williams, N. S.; Gao, J.; Hergenrother, P. J.; Boothman, D. A. "An NQO1 Substrate with Potent Anti-Tumor Activity that Selectively Kills by PARP-1-Induced Programmed Necrosis" *Cancer Res*. **2012**, *72*, 3038-3047 and Parkinson, E. I.; Bair, J. S.; Cismesia, M.; Hergenrother, P. J. "Efficient NQO1 Substrates are Potent and Selective Anticancer Agents" *ACS Chem. Biol*. **2013**, *8*, 2173-2183., and Parkinson, E.I.; Hergenrother, P.J. "Deoxynyboquinones as Personalized Anticancer Therapeutics" *Acc. Chem. Res.* Submitted **2015**. Copyright 2012 American Association of Cancer Research and Copyright 2013 American Chemical Society. Contributions of others are noted when applicable.

2.1 Deoxynyboquinone (DNQ) is an NQO1-activated anticancer agent with activity *in vivo*

As discussed in Chapter 1.1.5, DNQ is an anticancer agent that causes reactive oxygen species (ROS) dependent cell death. However when this work was started, the mechanism by which DNQ induces ROS had not been elucidated. In collaboration with the Prof. David Boothman (UT-Southwestern) and his laboratory, we discovered that DNQ is an NQO1-activated anticancer agent with potent activity *in vitro* and *in vivo*. Additionally, we directly compared DNQ to the other putative NQO1 substrates reported in the literature and found that DNQ and derivatives appear to be the most promising NQO1-activated anticancer drugs.

2.1.1 Mechanisms by which quinones cause reactive oxygen species formation

For quinones, two major pathways for ROS generation exist: 1) 2-electron reduction by NQO1 followed by reduction-oxidation (redox) cycling of the unstable hydroquinone as previously discussed in Chapter 1.1.2 or 2) 1-electron reduction by one of the various 1-electron reductases to an unstable semiquinone that then redox cycles (Scheme 2.1).[1-2] We chose to first investigate

the NQO1-dependence of the DNQ due to the overexpression of NQO1 in many cancer types (see Chapter 1.1.1 for a further discussion of NQO1-overexpression in cancer).

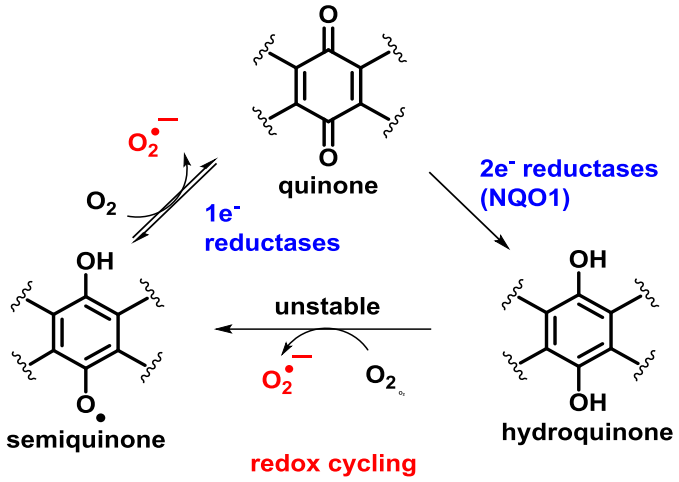

Scheme 2.1. Reduction pathways and subsequent redox cycling of quinones.

2.1.2 *In vitro* Activation of DNQ by NQO1[3]

In order to elucidate the mechanism by which DNQ causes ROS formation, we first investigated the ability of NQO1 to reduce DNQ along with other putative NQO1 substrates (β-Lap, STN, RH1 and MMC) *in vitro* (Figure 2.1A). In this assay, the quinone is co-incubated with both NQO1 as well as an excess of NADH, and oxidation of NADH is followed by the decrease in absorbance at 340 nm. DNQ, β-Lap, and STN were all substrates for NQO1 and each utilized greater than one equivalent of NADH over the course of the assay, demonstrating the ability of these quinones to redox cycle (Figure 2.1B-D). From these data Michaelis-Menten curves were generated, and apparent catalytic efficiencies were calculated (apparent because they also reflect the kinetics of redox cycling for each compound). As shown in Figure 2.1A, DNQ is a highly efficient substrate and redox cycler, with an apparent catalytic efficiency that approaches the diffusion controlled limit (k_{cat}/K_M = 6.2 x 10^7 $M^{-1}s^{-1}$). DNQ is processed over 9 times faster than the next best compound, β-Lap (k_{cat}/K_M = 0.67 x 10^7 $M^{-1}s^{-1}$), and 24 times faster than STN (k_{cat}/K_M

= 0.26 x 10^7 $M^{-1}s^{-1}$). RH1 and MMC are extremely poor substrates for NQO1 in this assay with observed activity less than 100 µmol/min/µmol of enzyme.

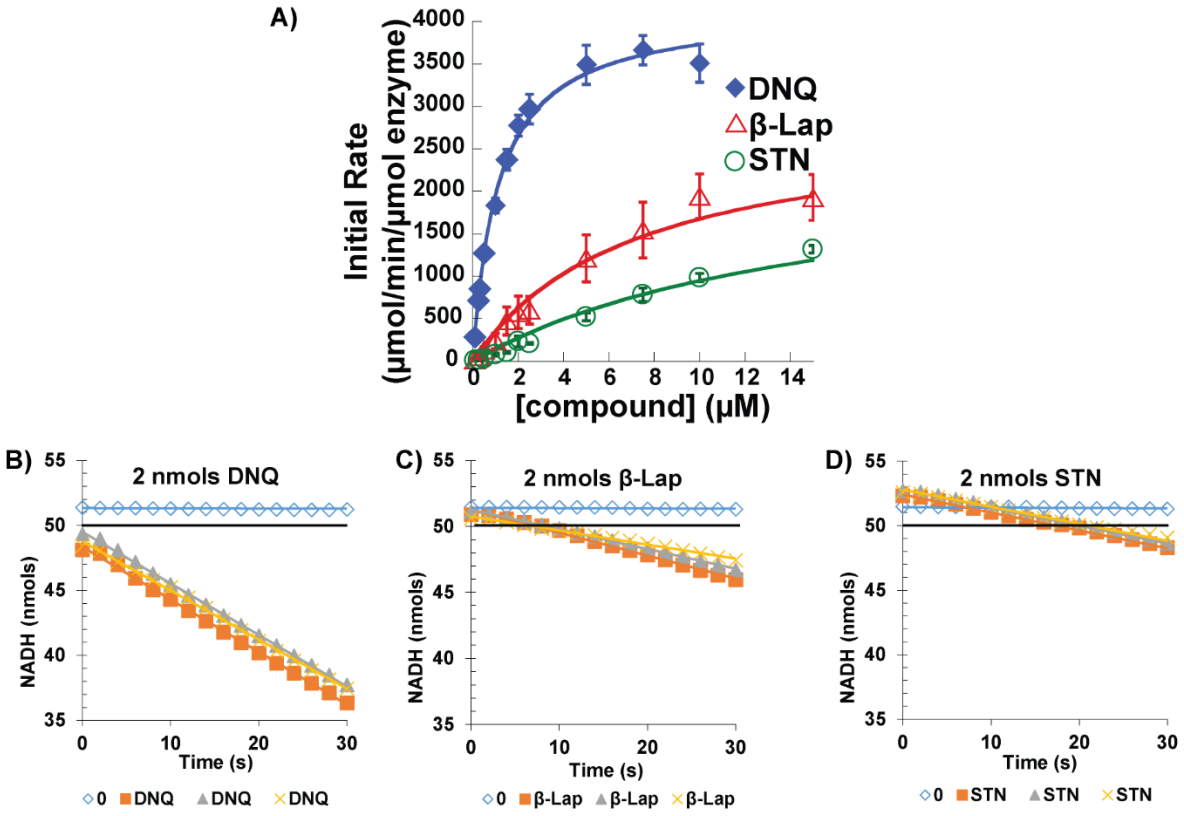

Figure 2.1. (**A**) Michaelis-Menten curves for DNQ, β-Lapachone (β-Lap), and streptonigrin (STN) with NQO1. Virtually no activity (<100 µmol/min/µmol) is observed with RH1 and mitomycin C (MMC) at these concentrations (data not shown). (**B**) Analysis of number of moles NADH used after coincubation with 2 nmol DNQ and NQO1. Blue = DMSO control, Orange, grey, and yellow = representative technical replicates. Black line represents the stoichiometric amount of NADH compared to DNQ. (**C**) Same as B but with β-Lap. (**D**) Same as B but with STN.

2.1.3 DNQ kills cancer cells in an NQO1-dependent manner[3-4]

After determining that DNQ is a highly efficient NQO1 substrate, the correlation between NQO1 activity *in vitro* and anticancer potency in cell culture was investigated.

2.1.3.1 NQO1 inhibitors protect high NQO1-expressing cell lines from DNQ[3]

DNQ, β-Lap, STN, RH1, and MMC were investigated for their potency against cancer cells that overexpress NQO1. The lung adenocarcinoma cell line A549 and the breast cancer cell line MCF-7 both have robust expression of NQO1,[4] and we measured the NQO1 activity in the cell

lysates at 2700 nmol/min/µg protein and 1900 nmol/min/µg protein, respectively (compared to <10 nmol/min/µg for cells that do not express NQO1,[4] see section 2.5.1 for details). A549 and MCF-7 cells were exposed to each of the five quinones for 2 hours, and cell death was assessed at 72 hours. As shown by the logistical dose response curves (Figures 2.2A-D), the five quinones show considerably different potency in their ability to induce cell death, with DNQ, STN and RH1 being the most potent (See Figure 2.2E for the IC_{50} of each compound).

The quinones were also tested against A549 and MCF-7 cells in the presence of the NQO1 inhibitor dicoumarol (DIC, 25 µM, Figure 2.2). Details of this inhibitor are described in Chapter 1.1.3. As shown in Figure 2.2A-B, co-incubation with DIC dramatically protects A549 and MCF-7 cells from DNQ-mediated cell death, shifting the IC_{50} 53-fold and 8-fold respectively (the fold is the ratio of the IC_{50} of co-treatment with quinone and inhibitor to the IC_{50} of treatment with only quinone, and a higher ratio indicates greater protection and greater NQO1 selectivity). DIC also significantly protect cells from β-Lap-induced cell death, shifting the IC_{50} 10-fold and 2-fold for A549 and MCF-7 cells, respectively (Figure 2.2C-E). DIC has little-to-no effect on STN, MMC, or RH1-induced cell death, suggesting that only DNQ and β-Lap kill in this assay by an NQO1-dependent mechanism.

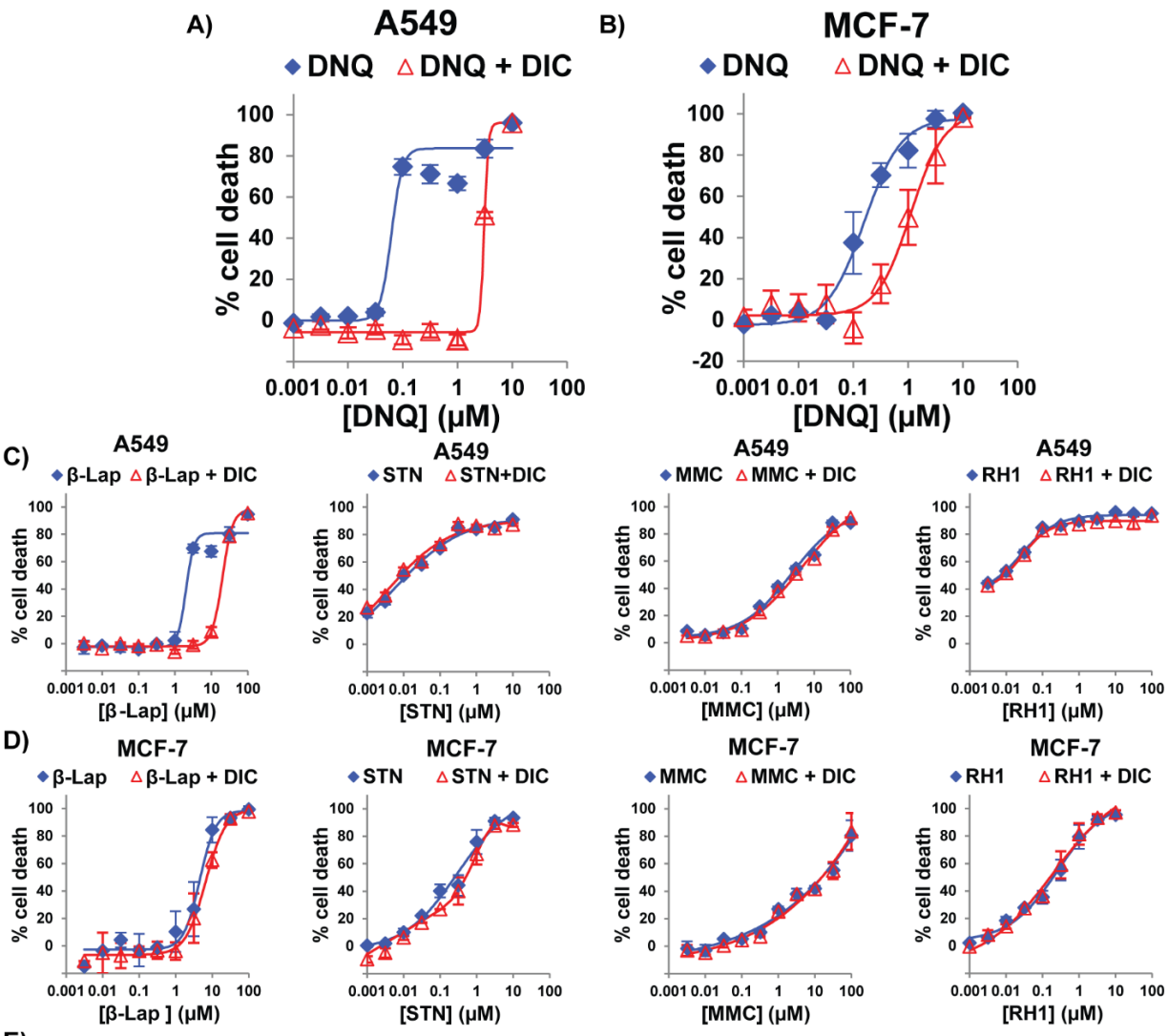

E)

Compound	A549			MCF-7		
	A549 IC_{50} (μM)	A549 + DIC IC_{50} (μM)	Fold Change	MCF-7 IC_{50} (μM)	MCF-7 + DIC IC_{50} (μM)	Fold Change
DNQ	0.06 ± 0.01	3.16** ± 0.01	53 ± 9	0.19 ± 0.07	1.5* ± 0.7	7.6 ± 1.4
β-Lap	2.0 ± 0.4	19** ± 2	10 ± 3	3.7 ± 1.5	7.9* ± 1.3	2.4 ± 0.6
STN	0.013 ± 0.003	0.010 ± 0.03	0.8 ± 0.4	0.31 ± 0.13	0.47 ± 0.42	1.4 ± 0.5
MMC	2.3 ± 0.7	4.7** ± 0.2	2.0 ± 0.7	14 ± 1	15 ± 3	1.0 ± 0.1
RH1	0.026 ± 0.005	0.025 ± 0.003	1.0 ± 0.3	0.21 ± 0.09	0.18 ± 0.05	0.9 ± 0.1

Figure 2.2. (**A**) Cell death curves of A549 cells treated for 2h with DNQ in the presence (red)

Figure 2.2. (cont.) and absence (blue) of the NQO1 inhibitor dicoumarol (DIC, 25 μM) (**B**) Same as A only with MCF-7 breast cancer cells. (**C**) Same as A but for β-Lap, streptonigrin (STN), mitomycin C (MMC), and RH1. (**D**) Same as B but for β-Lap, STN, MMC, and RH1. (E) Table of IC_{50} values and fold protections (Fold Change) for each treatment with standard error (n ≥ 3). The fold change is $\left(\frac{IC_{50}\ of\ DNQ\ or\ derivative\ with\ inhibitor}{IC_{50} of\ DNQ\ or\ derivative\ alone}\right)$. *p < 0.05, **p < 0.01, ***p < 0.001, paired t-tests on the IC_{50} values comparing treatments with or without inhibitor.

Similar studies were also performed with A549 cells and the NQO1 inhibitor ES936 (100 nM, Figure 2.3) discussed further in Chapter 1.1.3. As shown in Figure 2.3A, co-incubation with ES936 also dramatically protects A549 cells from DNQ-mediated cell death, shifting the IC_{50} >170-fold. ES936 also protect cells from β-Lap-induced cell death, shifting the IC_{50} 6-fold (Figure 2.3B-C). A small but not statistically significant difference in IC_{50} values was observed for STN, RH1, and MMC with ES936.

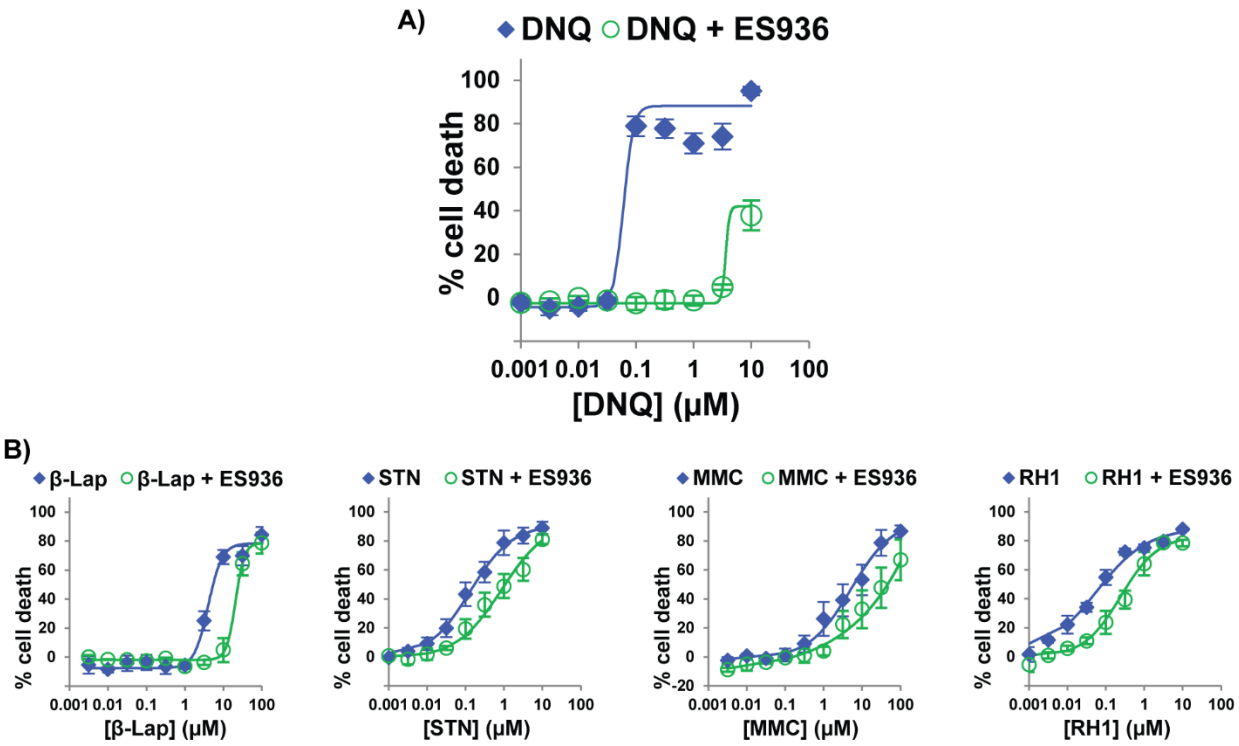

C)

Compound	A549 IC_{50} (μM)	A549 + ES936 IC_{50} (μM)	Fold Change
DNQ	0.06 ± 0.01	>10***	>170
β-Lap	4.0 ± 0.5	23* ± 4	6 ± 2
STN	0.13 ± 0.02	0.9 ± 0.5	7 ± 5
MMC	5 ± 2	52 ± 27	9 ± 8
RH1	0.05 ± 0.02	0.25 ± 0.07	5 ± 3

Figure 2.3. (**A**) Cell death curves of A549 cells treated for 2h with DNQ in the presence (green) and absence (blue) of the NQO1 inhibitor ES936 (100 nM) (**B**) Same as A but for β-Lap, STN, MMC, and RH1. (**C**) Table of IC_{50} values and fold protections (Fold change) for each treatment with standard error (n ≥ 3). The fold change is $\left(\frac{IC_{50}\ of\ DNQ\ or\ derivative\ with\ inhibitor}{IC_{50} of\ DNQ\ or\ derivative\ alone}\right)$. *p < 0.05, **p < 0.01, ***p < 0.001, paired t-tests on the IC_{50} values comparing treatments with or without inhibitor.

2.1.3.2 Activity of DNQ depends on presence of active NQO1[3-4]

After demonstrating the NQO1 dependence of DNQ and β-Lap utilizing high NQO1 expressing cell lines and the NQO1 inhibitors DIC and ES936, we chose to confirm this activity utilizing isogenic cell lines expressing different levels of NQO1. First, the pancreatic cell line MIA PaCa-2 was investigated. MIA PaCa-2 cells naturally express high levels of active NQO1 (NQO1 activity = 1130 nmol/min/μg protein, Figure 2.4A).[3] The Boothman laboratory previously generated isogenic MIA PaCa-2 cell lines which express low levels of active NQO1 using shRNA against NQO1[5] (NQO1 activity = 87 nmol/min/μg protein, Figure 2.4A).[3] DNQ shows good activity against MIA PaCa-2 transformed with a nonsense shRNA (MIA PaCa-2 NS, IC_{50} = 0.31 μM) and significantly less potent activity against the MIA PaCa-2 cells transformed with shRNA against the gene for NQO1 (MIA PaCa-2 shNQO1, IC_{50} = 1.6 μM, Figure 2.4B). The difference in potency against the shRNA provides further evidence that the activity of DNQ is NQO1 dependent. The fact that DNQ still has a small amount of activity against NQO1-knockdown cells is not surprising because the knockdown is not complete. β-Lap, STN, MMC, and RH1 also all showed potent activity against MIA PaCa-2 NS cells (Figure 2.4C-D). β-Lap showed a slight decrease in sensitivity to the MIA PaCa-2 shNQO1 cells, but the difference was not statistically significant. This is in agreement with a previously published paper which showed that β-Lap needed ~90 U of NQO1 (the approximate amount that the MIA PaCa-2 shNQO1 has) to show full activity.[5] STN showed no change in activity against MIA PaCa-2 cells in response to the change in NQO1 levels consistent with the lack of protection provided by NQO1 inhibitors seen in Figure 2.2. There was slight protection against MMC in the shNQO1 cells but the difference was not statistically significant. Interestingly, RH1 appears to be sensitized to MIA PaCa-2 upon knockdown of NQO1. Previously, RH1 activity has been shown to be dependent upon NQO2 expression.[6] It is possible that knocking down NQO1 causes changes in NQO2 expression and thus sensitivity to RH1 although this is not confirmed.

A)

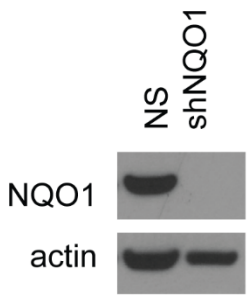

NQO1 Activity for MIA PaCa2:
NS = 1130 ± 80 nmol/min/µg
shNQO1 = 87 ± 3 nmol/min/µg

B)

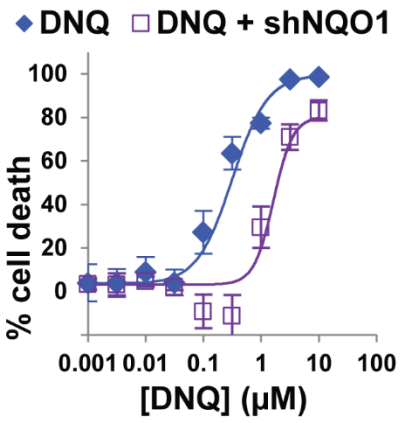

C)

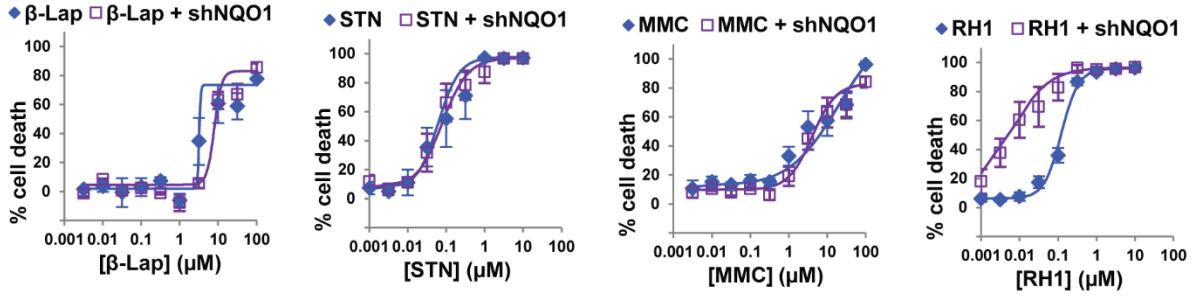

D)

Compound	MIA PaCa-2 +NS IC_{50} (µM)	MIA PaCa-2 +shNQO1 IC_{50} (µM)	Fold Change
DNQ	0.31 ± 0.08	1.6* ± 0.3	5 ± 2
β-Lap	3.2 ± 1.8	7.9 ± 5.3	2 ± 2
STN	0.06 ± 0.01	0.08 ± 0.02	1.3 ± 0.3
MMC	4 ± 1	15 ± 12	4 ± 4
RH1	0.12 ± 0.01	0.005* ± 0.002	0.04 ± 0.02

Figure 2.4. (**A**) NQO1 expression and activity of the isogenic pancreatic cell lines MIA PaCa-2 NS (nonsense shRNA) and shNQO1 (shRNA against NQO1). (**B**) Cell death curves of DNQ against the cell lines in A. (**C**) Same as B but for β-Lap, STN, MMC, and RH1. (**D**) Table of IC_{50} values and fold protections (Fold Change) for each treatment with standard error (n ≥ 3). The fold change is $\left(\frac{IC_{50}\ of\ DNQ\ against\ MIA\ PaCa{-}2\ shNQO1}{IC_{50} of\ DNQ\ against\ MIA\ PaCa{-}2\ NS}\right)$. *p < 0.05, paired t-tests on the IC_{50} values comparing NS with shNQO1 cell lines.

The Boothman laboratory performed a similar analysis using the human prostrate cancer cell line PC-3.[4] The WT cell line has high NQO1 levels (200 ± 5 nmol/min/μg protein) and is very sensitive to DNQ (IC_{50} = 0.07 μM) and β-Lap (IC_{50} = 3.2 μM).[4] When the cell line has NQO1 knocked down using shNQO1, the NQO1 activity is decreased significantly (26 ± 10 nmol/min/μg protein) and shows much lower sensitivity to DNQ (IC_{50} > 1 μM, >14 fold change) and β-Lap (IC_{50} > 20 μM, >6 fold change). This data is consistent with the MIA PaCa-2 data for DNQ, further confirming its dependence on NQO1. The Boothman laboratory did not analyze STN, MMC or RH1 in these cell lines so no conclusions can be made about these compounds.

As mentioned in Chapter 1.1.1, some humans have a polymorphism in NQO1 (oftentimes NQO1*2) which results in degradation of the enzyme. Cell lines derived from these individuals do not express active NQO1 and thus serve as a perfect backdrop to assess the effect of this enzyme on the potency of DNQ (and the other quinones). First, the breast cancer cell line MDA-MB-231 (which is known to contain the NQO1*2 polymorphism[4]) was explored. The Boothman laboratory has generated isogenic cell line pairs which have been transformed with plasmids containing either empty vector (231-) or the *nqo1* gene (231+).[4] 231- has very low NQO1 expression and activity (13 nmol/min/μg protein) consistent with having this polymorphism while the 231+ has greatly increased activity (1500 nmol/min/μg protein, Figure 2.5A).[3] Unsurprisingly, DNQ has very little activity against 231- (IC_{50} > 10 μM, Figure 2.5B) and is significantly sensitized to 231+ (IC_{50} = 1.1 μM, >9 fold change). The Boothman laboratory saw even greater sensitization in their viability assay with this cell line (231- IC_{50} > 1 μM and 231+ IC_{50} = 0.06 μM; fold > 17). While the reason for this difference in sensitization is not clear, it may relate to the different viability readouts used in these assays (protein content by sulforhodamine B staining[7] vs. DNA content by Hoechst 33258 staining[8]). β-Lap was also not particularly sensitive to 231- (IC_{50} = 36 μM, Figure 2.5C). However, we observed no significant sensitization to β-Lap the 231+ cells (IC_{50} = 39 μM).

A)

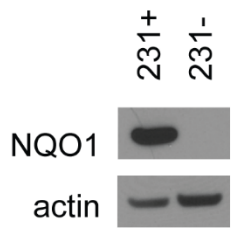

NQO1 Activity for MDA-MB-231:

231+ = 1500 ± 60 nmol/min/µg

231- = 13 ± 3 nmol/min/µg

B)

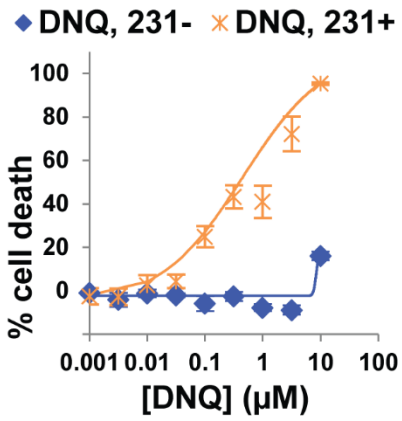

C)

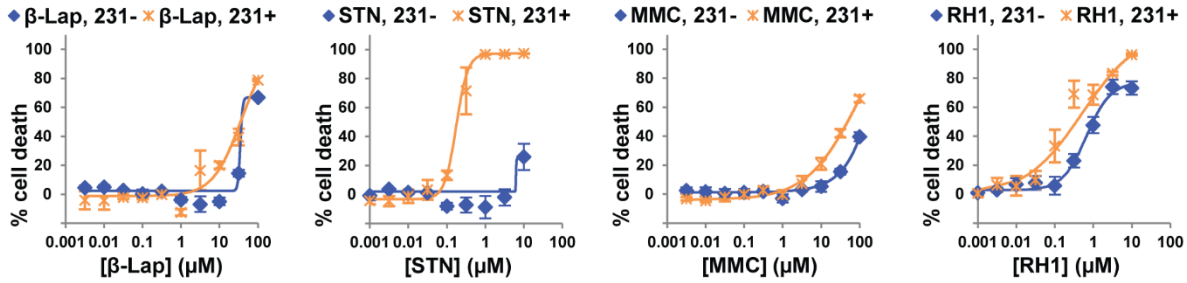

D)

Compound	MDA-MB-231- IC_{50} (µM)	MDA-MB-231+ IC_{50} (µM)	Fold Change
DNQ	>10	1.1*** ± 0.4	>9
β-Lap	36 ± 2	39 ± 4	0.9 ± 0.1
STN	>10	0.24*** ± 0.07	>42
MMC	>100	46*** ± 5	>2
RH1	1.0 ± 0.2	0.3 ± 0.1	5 ± 1

Figure 2.5. (**A**) NQO1 expression and activity of the isogenic breast cancer cell lines MDA-MB-231 transfected with empty vector (231-) and the gene for NQO1 (231+). (**B**) Cell death curves of DNQ against the cell lines in A. (**C**) Same as B but for β-Lap, STN, MMC, and RH1. (**D**) Table of IC_{50} values and fold protections (Fold Change) for each treatment with standard error (n ≥ 3). The fold change is $\left(\frac{IC_{50}\ of\ DNQ\ against\ 231-}{IC_{50} of\ DNQ\ against\ 231+}\right)$. *p < 0.05, **p < 0.01, ***p < 0.001, paired t-tests on the IC_{50} values comparing 231- and 231+.

This is in contrast to previous publications that showed a modest increase of approximately 2 fold in sensitivity.[4] As with DNQ, slight differences in the assay might explain these incongruities. Interestingly, STN is significantly sensitized to MDA-MD-231 upon introduction of NQO1 (Figure 2.5C). This data is consistent with the modest protection observed for A549 cells co-treated with STN and the inhibitor ES936 and the *in vitro* data showing that STN is a moderate substrate for NQO1. Together these data suggest that STN can be activated by NQO1. MMC is also more sensitive to 231+ than to 231-. However, the effect is small. This is consistent with data showing that MMC can be activated by NQO1 but that this is likely not the clinically relevant mode of action.[9-10] RH1 is also slightly more sensitive to 231+ than to 231-. Similar to MMC, RH1 has been shown to be activated by NQO1 but this activation is likely not the primary mechanism of action.[6]

The sensitivity of the lung cancer cell line H596, which also has the NQO1*2 polymorphism, to DNQ was then also explored. The Boothman laboratory also generated paired isogenic cells with either empty vector (H596-) or the *nqo1* gene (H596+). Similar results were observed as with the MDA-MB-231 paired cell lines. Unsurprisingly, H596- had very low NQO1 activity (30 nmol/min/µg protein), and H596+ had greatly increased NQO1 activity (1740 nmol/min/µg protein, Figure 2.6A). DNQ had little to no activity against H596- (IC_{50} > 10 µM) and increased activity against H596+ (IC_{50} = 3.5 µM, >3 fold change, Figure 2.6B). Similar to the MDA-MB-231 cell lines, the Boothman laboratory saw even greater sensization (H596- IC_{50} >1 µM, H596+ IC_{50} = 0.1 µM, >10 fold change). Little sensitization was seen with β-Lap upon expression of NQO1 (Figure 2.6C). However, the Boothman laboratory saw sensitization to β-Lap with increase in NQO1 expression (H596- IC_{50} > 20 µM, H596+ IC_{50} = 3.8 µM, >5 fold change). STN, MMC, and RH1 all had higher activities against H596+ than H596- similar to what was observed in MDA-MB-236.

A)

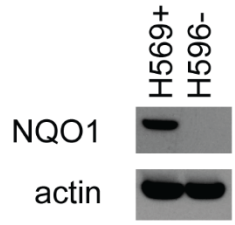

NQO1 Activity for H596:

H596+ = 1740 ± 70 nmol/min/μg

H596- = 30 ± 20 nmol/min/μg

B)

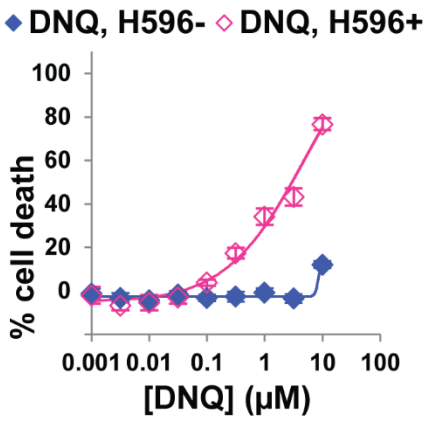

C)

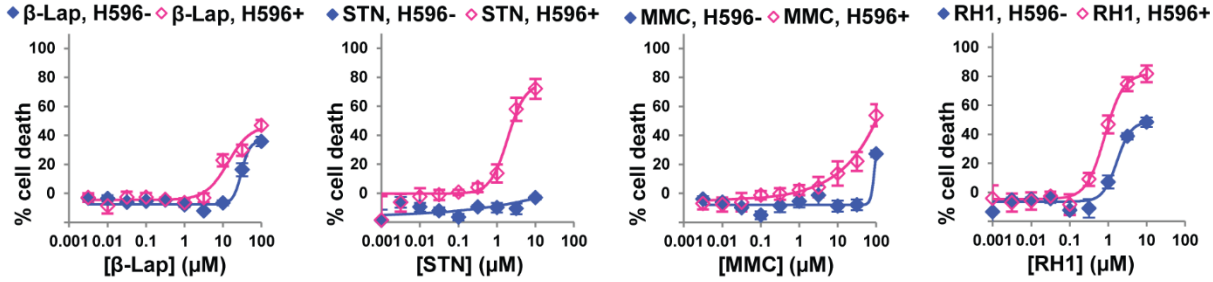

D)

Compound	H596- IC_{50} (μM)	H596+ IC_{50} (μM)	Fold Change
DNQ	>10	3.5*** ± 0.7	>3
β-Lap	>100	~100	>1
STN	>10	3.0** ± 1.0	>3
MMC	>100	83 ± 11	>1
RH1	8.5 ± 1.5	1.1** ± 0.4	8 ± 2

Figure 2.6. (**A**) NQO1 expression and activity of the isogenic lung cancer cell lines H596 transfected with empty vector (H596-) and the gene for NQO1 (H596+). (**B**) Cell death curves of DNQ against the cell lines described in A. (**C**) Same as B but for β-Lap, STN, MMC, and RH1. (**D**) Table of IC_{50} values and fold protections (Fold Change) for each treatment with standard error (n ≥ 3). The fold protection is $\left(\frac{IC_{50}\ of\ DNQ\ against\ H596-}{IC_{50} of\ DNQ\ against\ H596+}\right)$. *p < 0.05, **p < 0.01, ***p < 0.001, paired t-tests on the IC_{50} values comparing H596- and H596+.

Overall, the results from the chemical and genetic inhibition studies demonstrate that the anticancer activity of DNQ is dependent on the expression of high levels of active NQO1. Similar results, although to a less impressive degree, were observed with β-Lap. STN, MMC, and RH1 are inconsistent in their response to decreased NQO1 levels. Generally, it seems that they might be activated by NQO1 to a small degree but that this is not the primary mechanism of their activity.

It should be noted that extended treatment times reduces the selectivity of DNQ for NQO1-expressing cell lines (Figure 2.7). In these studies performed by the Boothman, A549 cells were treated with DNQ alone or with DNQ and DIC for the indicated times. At 2 and 8 h exposures, the selectivity for cells treated with DNQ alone is clear (Figure 2.7A-B). However, at longer treatment times (e.g. 24 and 48 h), the DIC treated cells also begin to die (Figure 2.7C-D). A similar phenomenon was observed for the isogenic H596+/- cells (Figure 2.7E-F). Additionally, the Hergenrother laboratory has observed that it is possible to kill low NQO1-expressing cell lines (e.g. U937) by extended treatment times.[1] The effect seen at the longer treatment times is likely due to activation by other reductases such as one electron reductases (e.g. cytochrome P450 reductase and cytochrome b5 reductase). Studies with purified one-electron reductases need to be performed to confirm this. This is not expected to be a problem *in vivo* given the pharmacokinetics of the compound (see Chapter 2.1.4.2). However, one future direction of this work is to develop a prodrug that would mask the quinone and thus prevent any toxicity due to one-electron reductases. An alternative future direction is the development of DNQ derivatives which are worse substrates for one-electron reductases than DNQ. This would allow for an increased therapeutic window.

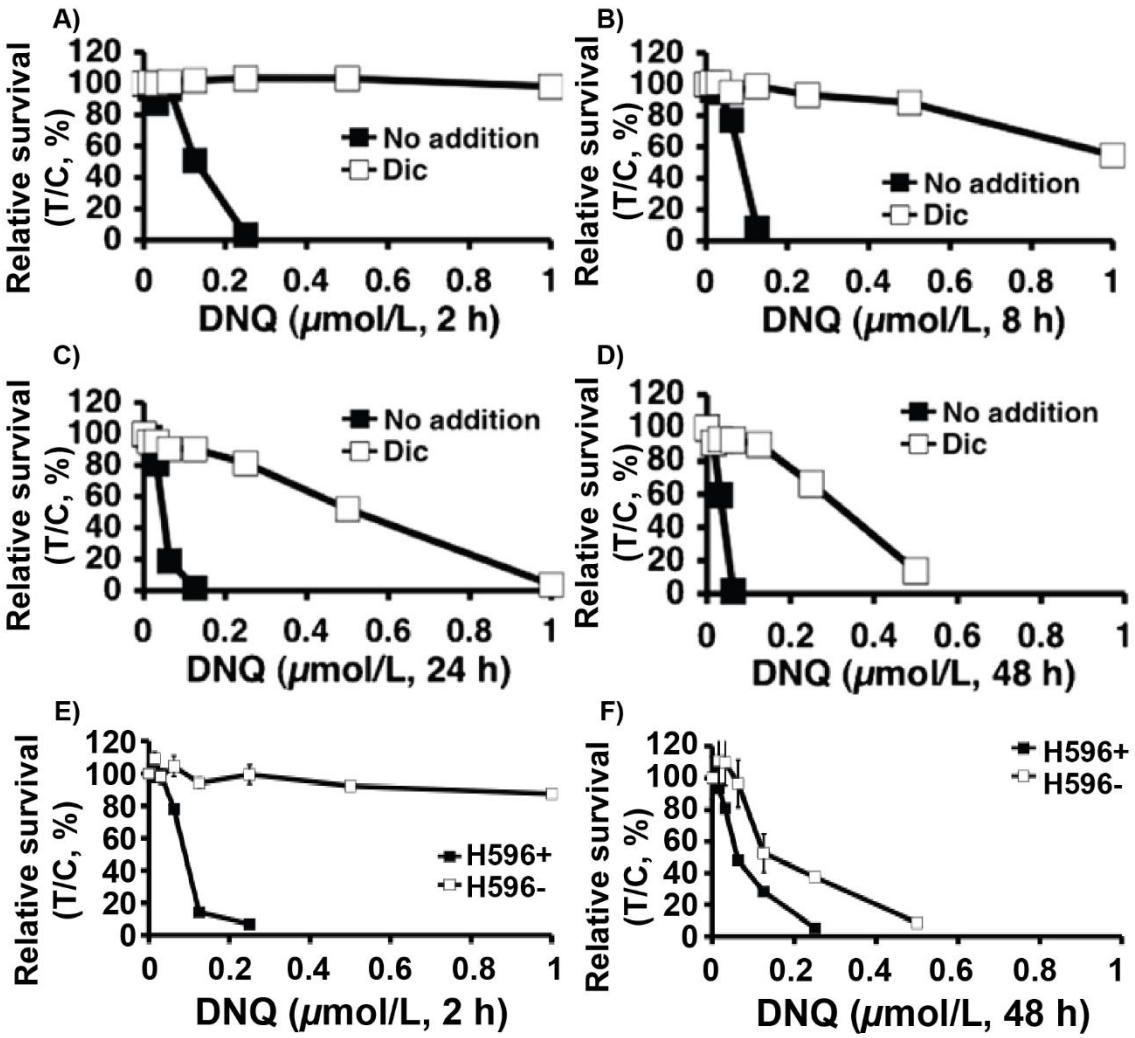

Figure 2.7. DNQ shows a broad NQO1-dependent therapeutic window. Relative survival was monitored in A549 cells treated with various DNQ concentrations (μM) ± dicoumarol (Dic, 40 μM) for (**A**) 2 hours, (**B**) 8 hours, (**C**) 24 hours, or (**D**) 48 hours. Graphed are means, ± SE of duplicate experiments, repeated in sextuplets. (**E**) Same as A only with H596+ and H596- cells instead of A549 cells ± Dic. (**F**) Same as D only with H596+ and H596- cells instead of A549 cells ± Dic. Graphed are means, ± SE of sextuplets from a representative experiment. T/C = treated compared to control.

2.1.4 DNQ causes NQO1-dependent ROS formation, DNA damage, and parthanatos[4]

Previously, the Hergenrother laboratory had determined that DNQ kills cancer cells in a ROS-dependent mechanism.[1] In collaboration with the Boothman laboratory, we have established that DNQ causes ROS generation in an NQO1-dependent manner, that this ROS generation is

catalytic in DNQ, and that ROS causes DNA damage which leads to parthanatos (i.e. PARP-1 dependent cell death). In the following paragraphs are the experiments that the Boothman laboratory performed to confirm this.

First, the oxygen consumption rates (OCR) of A549 cells treated with either β-Lap or DNQ were determined (Figure 2.8A-D). Both compounds cause a rapid increase in the OCR with DNQ doing so at 20-fold lower concentration. This rapid increase in oxygen consumption is consistent with the redox cycling that was discussed earlier (see Chapter 1.1.1 and Scheme 2.1). Importantly, for DNQ the oxygen consumption at 0.25 μM was completely prevented by the NQO1 inhibitor DIC suggesting that the oxygen consumption is dependent upon reduction of DNQ by NQO1. β-Lap still has a small level of oxygen consumption in the presence of DIC suggesting that it is partly reduced by one-electron reductases. Similar results were observed for the isogenic cell line pair with H596+ showing large increases in oxygen consumption upon treatment with DNQ and H596- showing little to no change in oxygen consumption over the blank control. The high OCRs of both β-Lap and DNQ-treated cells suggest that both compounds likely redox cycle after reduction by NQO1. The *in vitro* studies performed with compound, NADH, and NQO1 further support this since each mole of compound results in the oxidation of more than one mole of NADH (Figure 2.1B-C), suggesting that the compounds are reduced more than once during the course of the experiment.

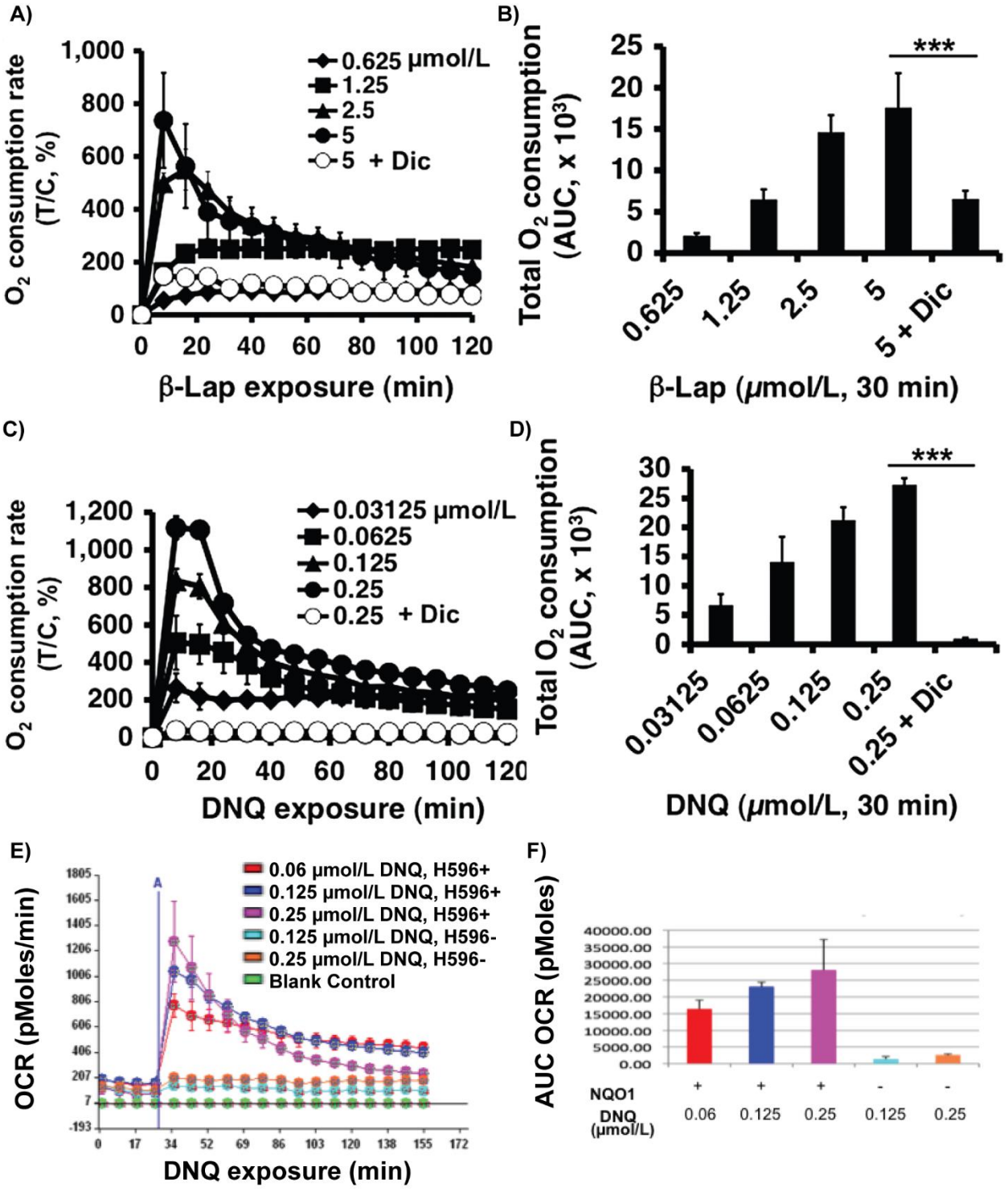

Figure 2.8. Elevated oxygen consumption in DNQ treated cells. (**A**) Oxygen consumption rates (OCR) in A549 cells treated with β-Lap ± dicoumarol (Dic, 40 µM). OCR was monitored every 8 minutes for 2 h. Data are means ± SEM normalized to untreated controls. n = 3. (**B**) Quantitative data of A after 30 minutes. (**C**) Same as A but with DNQ instead of β-Lap. (**D**) Same as B but for DNQ. (**E**) Same as C but with H596+ and H596- cells. (**F**) Same as D but for H596+ and H596- cells. ***P ≤ 0.001, comparing ± Dic treatments.

After confirming oxygen consumption, the ability of these compounds to produce ROS was explored. As discussed earlier in Chapter 1.1.4, the Hergenrother laboratory had previously shown that DNQ results in ROS formation and that DNQ-induced cell death is dependent upon ROS formation.[1] The Boothman laboratory confirmed that A549 cells treated with DNQ have increased levels of superoxide and that this increase is NQO1 dependent (Figure 2.9A). Additionally, they confirmed that ROS is necessary for DNQ-induced cancer cell death by showing that A549 cells are protected from DNQ upon co-treatment with catalase (CAT, an enzyme responsible for catalyzing the conversion of hydrogen peroxide to water and oxygen, Figure 2.9B)

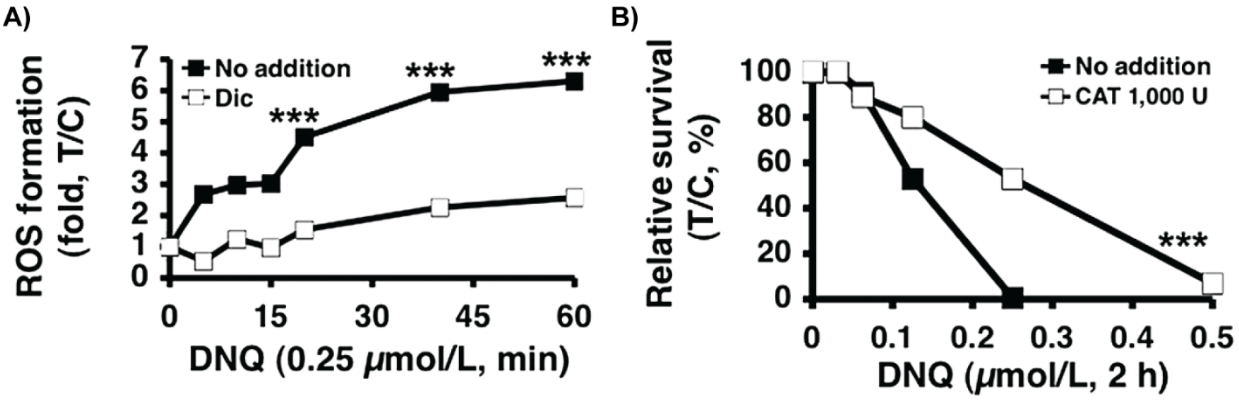

Figure 2.9. Elevated ROS formation in NQO1-overexpressing cell lines upon treatment with DNQ. (**A**) A549 cells were cells were treated with or without DNQ (0.25 µM) ± dicoumarol (Dic, 40 µM). ROS formation was assessed by dihydroethidium (DHE) staining. Results are means, ± SE of arbitrary units measured by staining intensity from 100 cells using NIH Image J. (**B**) DNQ (µM, 2 hours) -exposed A549 cells were cotreated with ± catalase (CAT, 1,000 U) and clonogenic survival was monitored. ***, P ≤ 0.001, comparing DNQ-treated A549 cells ± CAT cotreatment.

After confirming that DNQ causes ROS-dependent cell death, the Boothman laboratory investigated the type of cell death induced by DNQ. ROS is known to cause DNA damage, especially DNA base and single stranded break lesions.[4] Poly(ADP-ribose) polymerase 1 (PARP-1) is typically recruited to these breaks where it synthesizes poly(ADP-ribose) polymers (PAR) that recruit DNA repair proteins.[11] In cases of extensive DNA damage, PARP-1 can be overactivated resulting in PARP-1-dependent cell death called parthanatos.[11-12] Within five minutes of treating the NQO1-overexpressing cancer cell line A549 with DNQ, significant PAR

formation is observed (Figure 2.10A-B).[4] This PAR formation is inhibited by co-incubation with the NQO1 inhibitor DIC suggesting that this formation is dependent upon DNQ activation by NQO1. Additionally, in the same cell line, there is a significant reduction in both NAD^+ and ATP levels after treatment with DNQ that is concentration, time and NQO1 dependent (Figure 2.10C-F), consistent with overactivation of PARP-1 and parthanatos.[4] A similar result was seen with the paired isogenic cell line H596 with the NQO1 expressing cell line (H596+) showing significant ATP loss and the cell line lacking active NQO1 (H596-) showing very little reduction in ATP levels (Figure 2.10G). Additionally, the ATP reduction observed in H596+ cells was prevented by co-treatment with DIC (Figure 2.10H).

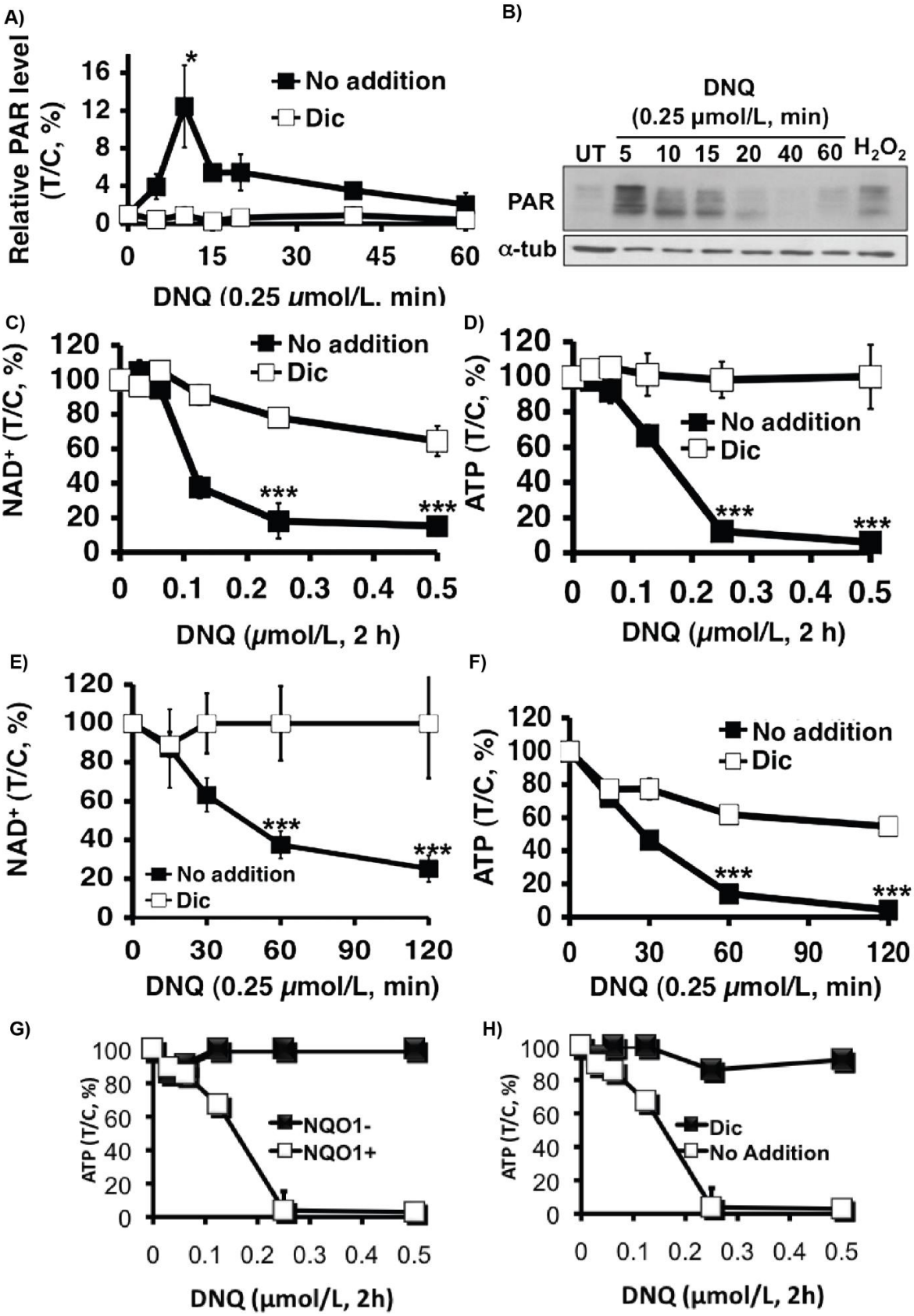

Figure 2.10. DNQ induces NQO1-dependent PARP-1 hyperactivation and nucleotide depletion.

Figure 2.10. (cont.) (**A**) PARP-1 hyperactivation, monitored by poly(ADP)-ribosylated protein (PAR) formation using an ELISA method, was detected in A549 cells treated with DNQ ± dicoumarol (Dic, 40 μM). Data are means, ± SEM from 3 independent experiments. (**B**) Western blot assays confirmed PAR formation (PAR-PARP-1, ~120 kDa) in A549 cells treated with or without 0.25 μM DNQ at indicated times (minutes). Cells were treated with H_2O_2 (1 mM, 15 minutes) as a positive control for PAR formation. Loading was controlled by α-tubulin (α-tub) levels. Dose-dependent NAD^+ (**C**) and ATP (**D**) loss in A549 cells after various DNQ doses ± Dic (40 μM). NAD^+ (**E**) and ATP (**F**) depletion was analyzed at indicated times, with or without DNQ (0.25 μM) ± Dic (40 μM). (**G**) Dose-dependent ATP loss in H596+ and H596- cells after DNQ treatment . (**H**) Same as D only for H596+ cells. Data are means, ± SEM from 3 independent experiments. *, $P \leq 0.05$; ***, $P \leq 0.001$.

To further demonstrate that DNQ induces NQO1-dependent parthanatos, the effects of DNQ on a PARP-1 knockdown cell line was explored. A549 cells were transfected with siRNA against PARP-1 resulting in a transient knockdown of PARP-1 (Figure 2.11A). Transient knockdown of PARP-1 decreased cell death following exposure to DNQ as evidenced by both micrographs and the TUNEL assay (Figure 2.11B-C).[4] Additionally, knockdown of PARP-1 significantly decreased NAD+ and ATP loss (Figure 2.11 D-E). Together these data strongly implicate parthanatos as the major form of DNQ-induced cell death.

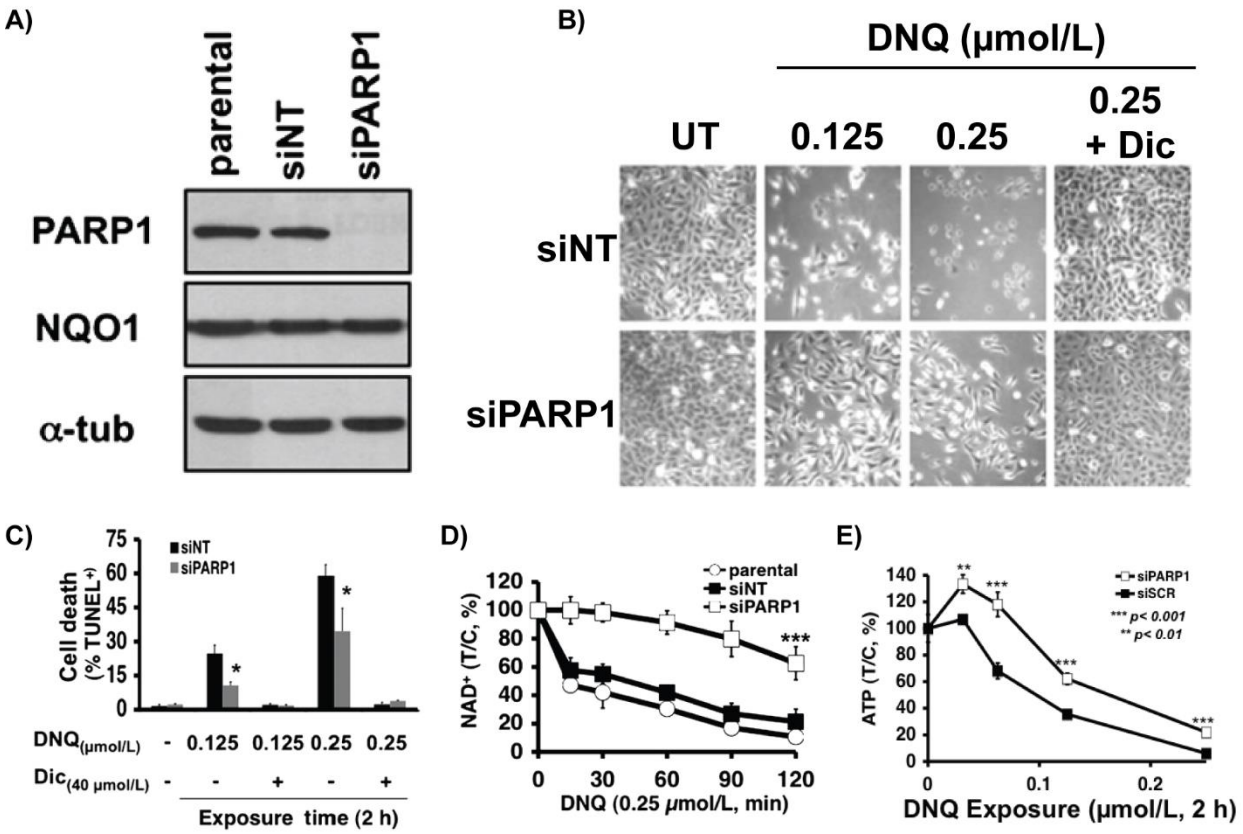

Figure 2.11. DNQ induces NQO1-dependent parthanatos. (**A**) Steady-state PARP-1,NQO1, and α-tubulin (α-tub) levels were assessed by Western blots in mock-transfected (parental), nontargeted siRNA (siNT), or transiently PARP-1 knockdown (siPARP-1) A549 cells 48 hours posttransfection. Loading was monitored by α-tub. (**B**) Micrographs of DNQ-treated nontargeted (siNT) or PARP-1-specific (siPARP-1) siRNA knockdown A549 cells at 24 hours posttreatment with LD_{50} (0.125 μM) or lethal doses (0.25 μM), ± dicoumarol (Dic, 40 μM). (**C**) PARP-1 knockdown significantly protects A549 cells from DNQ-induced programmed necrosis (%TUNEL+ cells). Treatment conditions were as in B. (**D**) PARP-1 is essential for NAD^+ loss at the indicated times (minutes) in DNQ-treated (0.25 μM) A549 cells. P values compare NAD^+ levels in PARP-1 knockdown versus parental or siNT A549 cells. *P ≤ 0.05; ***P≤ 0.001 (**E**) ATP levels in DNQ-treated A549 cells transfected with either non-silencing siRNA (siSCR) or siRNA specific for PARP-1 (siPARP-1). Data are means, ± SEM from three independent experiments. **P ≤ 0.01; ***P≤ 0.001

2.1.5 DNQ has *in vivo* anticancer efficacy

2.1.5.1 *In vitro* toxicity to normal cells

Before investigating the *in vivo* activity of DNQ, its effect on normal cells was assessed. First, the lung fibroblast cell line IMR90 which expresses no detectable NQO1 (Figure 2.12A,

insert) was examined. This cell line has low-to-no sensitivity to DNQ (IC_{50} > 10 µM) as one would expect based on its NQO1 expression.

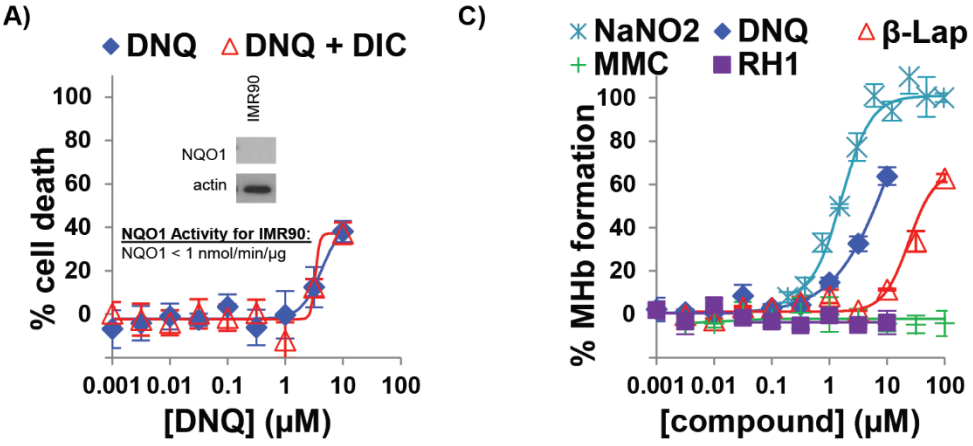

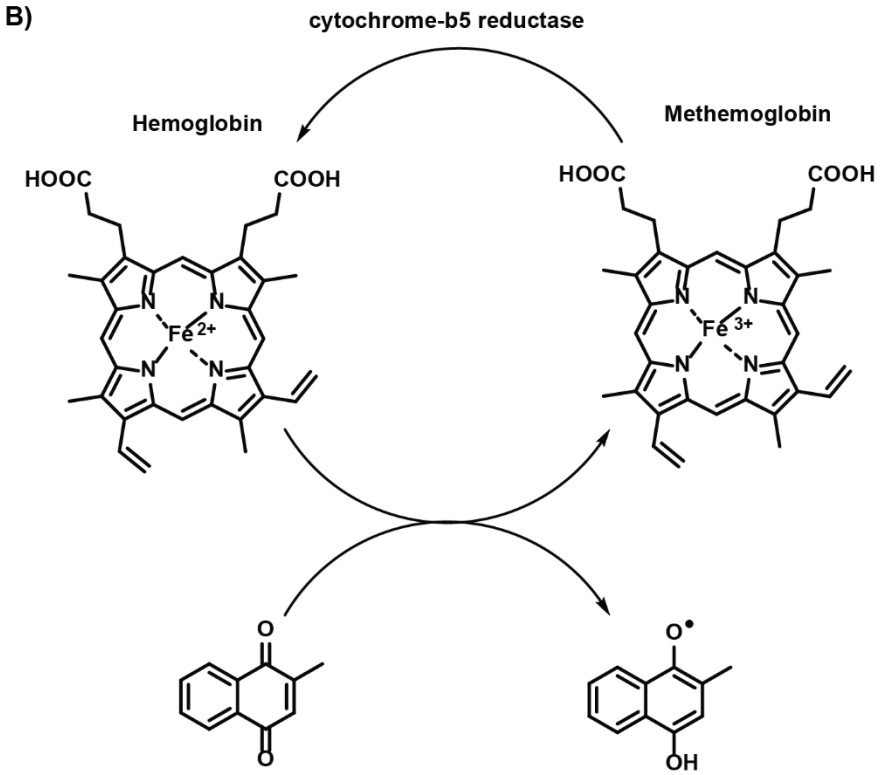

Figure 2.12. (**A**) Cell death curves of IMR90 cells treated for 2h with DNQ in the presence (red) and absence (blue) of the NQO1 inhibitor dicoumarol (DIC, 25 µM) (**B**) Proposed oxidation of hemoglobin to methemoglobin by menadione.[13-18] Methemoglobin is converted back to hemoglobin by the enzymes cytochrome-b5 reductase and NADPH methemoglobin reductase.[19] (**C**) Dose-response curves of methemoglobin (MHb) formation induced in human erythrocytes by sodium nitrite (NaNO2), DNQ, β-Lap, MMC, and RH1 after 1 h shaking at 37 °C. Percent MHb calculated by dividing amount of MHb by total heme.

The effect of DNQ on red blood cells (RBCs) was then assessed. While DNQ does not induce hemolysis (data not shown), it does cause the RBC pellet to turn dark brown/black. This change in color was concerning since this is often indicative of methemoglobin formation.[20] Methemoglobin is formed when the iron in hemoglobin (Fe^{2+}) is oxidized to Fe^{3+} resulting in the hemoglobin having a higher affinity for oxygen and thus decreasing the amount of oxygen released into the body. While small amounts of methemoglobin (1-2% of total hemoglobin) are normal, higher levels can result in toxicities such as cyanosis (10-20%), headaches, dyspnea, and anxiety (~20-50%), coma, seizures, and acidosis (50-70%) and death (>70%).[21] Methemoglobin formation is most often due to exposure to oxidizing agents.[22] Many chemicals are known to cause methemoglobin formation including the antimalarial chloroquine, some sulfonamide antibiotics, and local anesthetics such as benzocaine.[20,22] Quinones such as menadione are known to oxidize hemoglobin to methemoglobin and it has been proposed that this is via direct oxidation (see Figure 2.12B).[13-18] Alternatively, some propose that the methemoglobin is formed indirectly: reduction of the quinone to the semiquinone which redox cycles to form superoxide which causes the oxidation of the heme iron.[13-18] There is also evidence to suggest that quinones such as menadione are capable of reducing methemoglobin back to hemoglobin under certain conditions likely by acting as an electron shuttle in the NADPH-depedent methemoglobin reductase system.[23-24]

We investigated the ability of DNQ, β-Lap, MMC, and RH1 to induce methemoglobin formation via a modified version of the method developed by Evelyn and Malloy[25] with sodium nitrite used as a positive control. For the sodium nitrite control, potent methemoglobin formation is observed (IC_{50} = 2.0 ± 0.2 μM). Methemoglobin formation was also observed for DNQ (IC_{50} = 4.2 ± 1.0 μM) and β-Lap (IC_{50} = 49 ± 10 μM). No methemoglobin formation was observed for either MMC or RH1. While methemoglobin formation is an undesirable attribute of DNQ, IV administration of methylene blue is an effective treatment for most mild-to-moderate cases of

methemoglobin.[20,22] It could be used as a co-treatment with DNQ if methemoglobin proves to be a significant problem *in vivo*. Another alternative is to develop derivatives or prodrugs with decreased methemoglobin formation. This is an ongoing area of research in the laboratory.

2.1.5.2 *In vivo* toxicity and pharmacokinetics

While methemoglobin formation does occur, the anticancer activity is approximately 70-fold more potent that the methemoglobin formation. We hypothesized that this would likely provide us with a reasonable therapeutic window, and thus we chose to go forward with animal studies. We found that DNQ has a maximum tolerated dose (MTD) of 10 mg/kg when treated every other day either i.v.[4] or 5 mg/kg when treated every day by i.p injection. Mice that received five doses of this treatment showed no long term pathological effects in the liver (Figure 2.13A), lung, bone marrow, spleen, or thymus.[4] The Boothman laboratory reported observing methemoglobin formation *in vivo* after a 10 mg/kg dose, [4] but we were never able to observe it (see section 2.2.6). With the establishment of the MTD, both the Boothman laboratory and Prof. Tim Fan (UIUC) determined pharmacokinetic parameters for DNQ. The Boothman laboratory found that DNQ has a markedly longer half-life, higher C_{max}, and higher AUC compared to β-Lap (Figure 2.13B-C). Additionally, Prof. Fan found that DNQ has good oral bioavailability (Figure 2.13D).

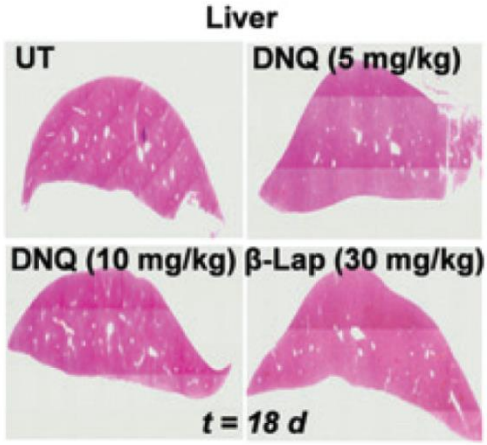

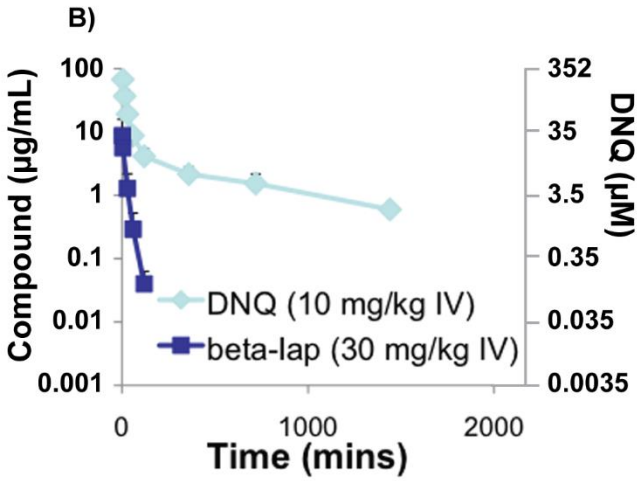

C)

In vivo pharmacokinetic parameters		
	β-Lap 30 mg/kg IV	**DNQ 10 mg/kg IV**
Terminal $t_{1/2}$ (min)	18.4	576
C_{max} (ng/mL)	8720 (36 µM)	67,000 (236 µM)
AUC (min*ng/mL)	165,838 (685 min*µM)	4,423,818 (15,562 min*µM)
Vz (mL/kg)	4760	1688
Cl (mL/min/kg)	179.7	2.03

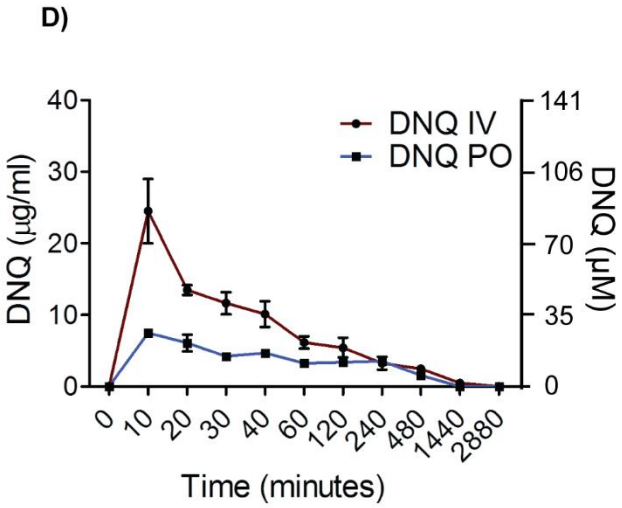

Figure 2.13. (**A**) Female athymic nude mice bearing visible tumors were treated once every other day for 5 IV injections. Normal tissues were assessed with no long-term pathologic injury noted; shown here is H&E-stained livers (**B**) Mice were dosed IV with either 30 mg/kg of β-Lap or 10 mg/kg DNQ formulated with hydroxypropyl-β-cyclodextrin (HPβCD). At varying times after dosing, the mice were sacrificed and plasma samples taken out to 120 mins for β-Lap and 1440 mins for DNQ. Plasma levels were monitored by LC/MS/MS after extraction of the compounds from the plasma matrix by solid phase extraction (β–Lap) or simple removal of plasma proteins by precipitation with acetonitrile (DNQ). Recoveries of both compounds were near 100% for both methods (**C**) Calculated noncompartmental pharmacokinetic parameters for B. $t_{1/2}$ = half life, C_{max} = maximal concentration, AUC = area under the concentration-time curve, Vz = volume of distribution, Cl = clearance. (**D**) Mice were dose either IV or orally (PO) with 9 mg/kg DNQ formulated with HPβCD. At At varying times after dosing, the mice were sacrificed and plasma samples were obtained. Plasma levels were monitored by LC/MS/MS.

2.1.5.3 *In vivo* activity

Based on the promising *in vivo* toxicity and pharmacokinetics data, an extremely aggressive orthotopic Lewis Lung Carcinoma (LLC) model in athymic mice was performed to examine the antitumor efficacy of DNQ. Mice were treated every other day for a total of 5 injections with either HPβCD alone, DNQ (2.5, 5, or 10 mg/kg) or β-Lap (30 mg/kg). After 18 days, lungs were removed, weighed, and visually scored for tumor nodules (Figure 2.14A and B). DNQ (5 and 10 mg/kg) and β-Lap treated mice showed significant tumor growth reductions, confirmed by decreases in tumor nodule formation and histology (Figure 2.14A-B). Overall survival confirmed significant antitumor efficacy of DNQ (5 mg/kg; $P \leq 0.04$), at a 6-fold lower dose than β-Lap (30 mg/kg; Figure 2.14C). Finally, PAR formation and energy (ATP) losses in LLC tumors after DNQ or β-Lap exposures confirmed that the mechanism of cell death *in vivo* is consistent with the one observed *in vitro* (Figure 2.14D-E); tumor-specific ATP losses were confirmed by LC/MS/MS analyses. In contrast, associated normal lung tissue was unaffected, showing no PARP-1 hyperactivation or ATP loss (Figure 2.14D-E).

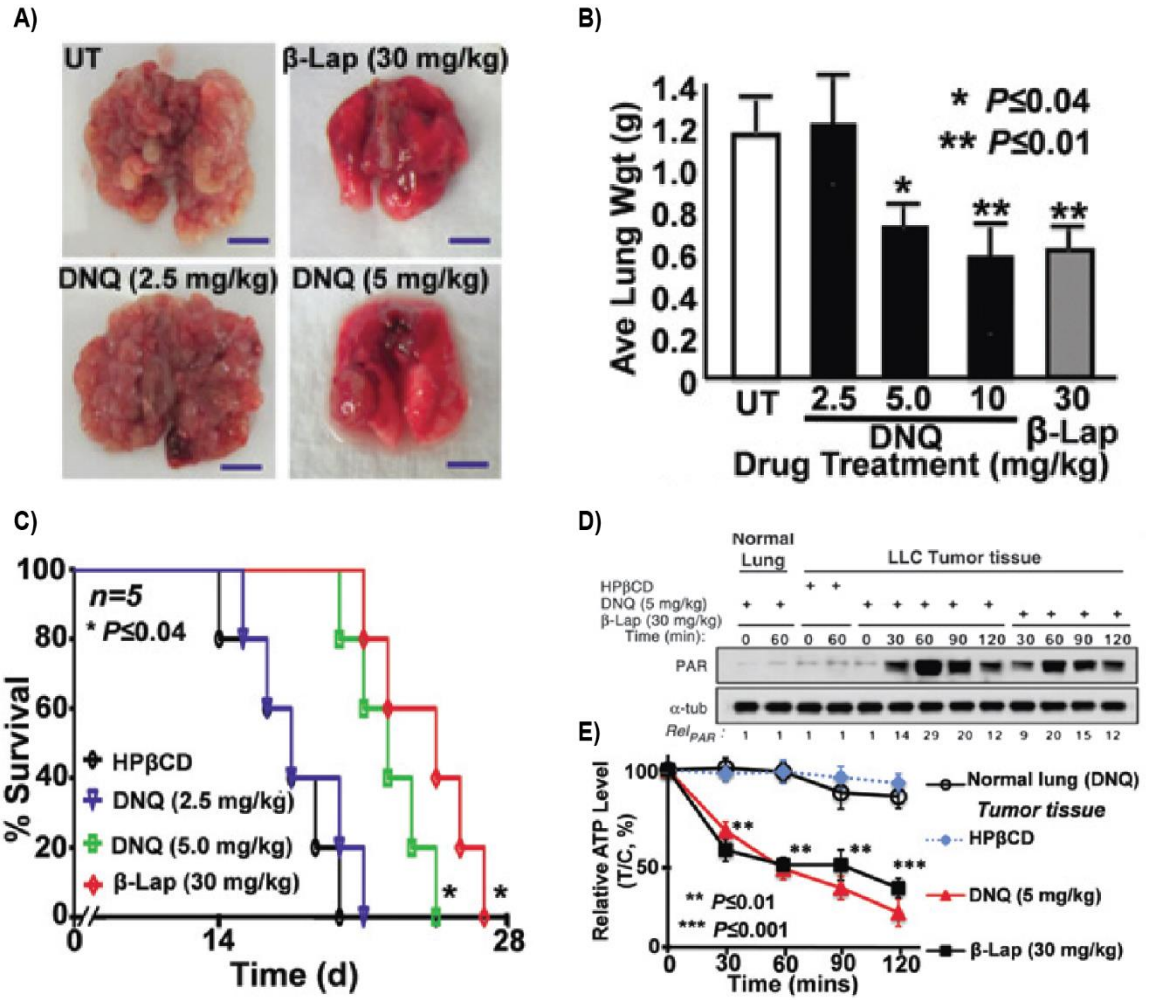

Figure 2.14. (**A**) Female athymic nude mice bearing visible tumors were treated once every other day for 5 injections. On day 18, mice were sacrified and tumor nodules were confirmed visually and histologically (data not shown). 5 mice per group. (**B**) Average wet weights from A. UT = vehicle (HPβCD) treated control. *P ≤ 0.04, **P ≤ 0.01. (**C**) Kaplan-Meier survival curves showing significant (P ≤ 0.04) survival advantage of DNQ (5 mg/kg) or β-Lap (30 mg/kg) groups. Treatment groups were HPβCD alone (1,000 mg/kg), DNQ (2.5 and 5.0 mg/kg), and β-Lap (30 mg/kg). 5 mice per group. *P ≤ 0.04. (**D**) PAR formation and (**E**) ATP loss were observed in LLC tumors where animals were treated with 3 doses of either vehicle (HPβCD), DNQ, or β-Lap and sacrified 24 h later. Lungs were removed and tumor and normal tissues were analyzed. **P ≤ 0.01, ***P ≤ 0.001. α-tub = α-tubulin (loading control).

2.2 Design, synthesis, and activity of DNQ derivatives

As DNQ is processed by NQO1 near the diffusion controlled limit, it would be unlikely to find a derivative that is a better NQO1 substrate. However, derivatives were sought to determine

what makes an excellent NQO1 substrate and to find compounds with improved solubility and tolerability profiles.

2.2.1 *In silico* design of DNQ derivatives

A suite of compounds that are structurally related, but processed by NQO1 at different rates, would be valuable toward establishing the relationship between *in vitro* NQO1 processing and anticancer activity. Thus, due to the remarkable processing of DNQ by NQO1, and the clear NQO1-dependent activity of DNQ against cancer cells in culture, derivatives of this compound were designed.

The NQO1-mediated bioreduction of quinones initially involves a hydride transfer from NAD(P)H to the associated FAD cofactor, which subsequently transfers the hydride to the substrate.[26] Crystallographic data with known substrates such as duroquinone show that NQO1 substrates typically π-stack with the isoalloxazine ring of the FAD.[26-28] Additionally, depending on the substrate, the quinone oxygens can hydrogen bond with Tyr-126, Tyr-128, or His-161. Therefore we hypothesized that DNQ and its active derivatives would π-stack and hydrogen bond similarly to these known substrates.

To address this hypothesis computationally, DNQ and its derivatives were docked into the active site of NQO1 (PDB 1DXO)[27] using the Molecular Operating Environment.[29] Previously, a correlation was observed between NQO1 catalytic efficiency and the docked distance between the substrate (carbon α to quinone carbonyl) and the FAD co-factor (nitrogen which transfers the hydride), with compounds that have a shorter predicted “hydride donor-acceptor distance” being better NQO1 substrates.[30] Therefore, we analyzed this key distance parameter for DNQ and representative derivatives.

DNQ was found to form π-stacking interactions with the isoalloxazine ring of the associated FAD co-factor and hydrogen bonds with Tyr 126 and 128 (Figure 2.15A), very similar to duroquinone.[27] Additionally, the hydride donor-acceptor distance for DNQ was found to be 3.88 Å (Figure 2.15B). Many DNQ derivatives, depending on the position of substitution, fit well

into the active site. For example, compounds with bulky substitutions in place of the *N*-methyl such as isobutyl-DNQ (IB-DNQ, compound **2**) still fit deep into the active site and maintain π-stacking with FAD and hydrogen bonding with Tyr-126 and Tyr-128 (Figure 2.15C, hydride donor-acceptor distance of 4.41 Å), suggesting they would be excellent substrates for NQO1. Alternatively, compounds with multiple substitutions (e.g. **3**) did not fit deeply into the active site and thus did not π-stack or make the appropriate hydrogen bonds (Figure 2.15D, hydride donor-acceptor distance of 5.65 Å), suggesting that these compounds would be poorer substrates for NQO1.

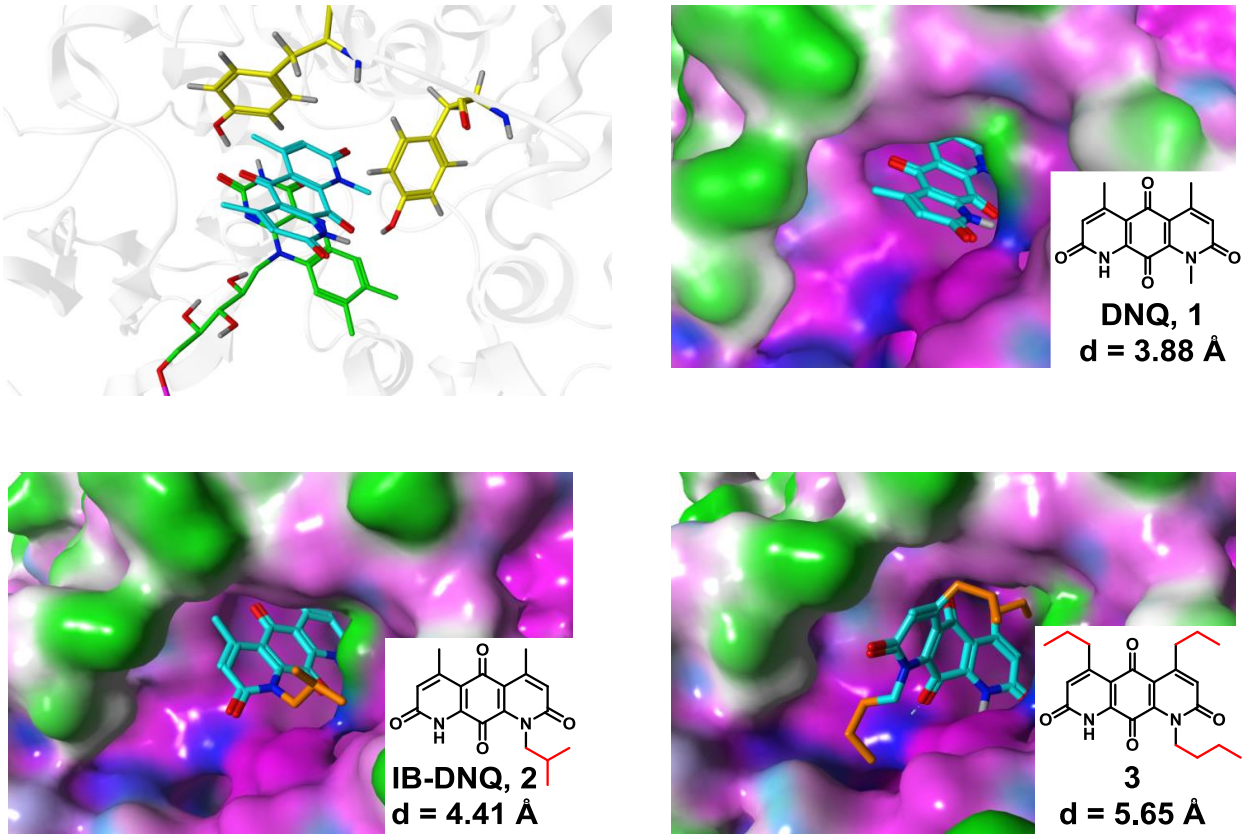

Figure 2.15. Modeling of DNQ and derivatives in the NQO1 active site. (**A**) The π-stacking and hydrogen bonding interactions between DNQ (blue), the cofactor FAD (green), and Tyr-126 and 128 (yellow) with NQO1. (**B**) DNQ fits deeply into the active site pocket (d = hydride donor-acceptor distance). (**C**) Derivative IB-DNQ (compound 2, difference from DNQ highlighted in red) also fits deeply into the active site. (**D**) Derivative 3 does not fit as deeply into the active site and has a longer hydride donor-acceptor distance.

Overall, these computational results were encouraging, with many derivatives fully entering the NQO1 active site, and others being at least partially occluded. A collection of DNQ derivatives was therefore synthesized to provide structurally related compounds predicted to be differentially processed by NQO1.

2.2.2 Synthesis of DNQ derivatives

With the modeling data in hand, a diverse set of 25 DNQ derivatives (compounds **2-26**, Figure 2.16A) that were expected to have a range of NQO1 activities were synthesized. This was accomplished using a modified version of the original DNQ synthesis (Scheme 2.2). Compounds **2-19**, and **21-23** were synthesized via the four step protocol outlined in Scheme 2.2, with isolated yields comparing favorably to those from the original synthesis (average yield over 4 steps = 12%, see Section 2.5.2 for complete characterization).[1]

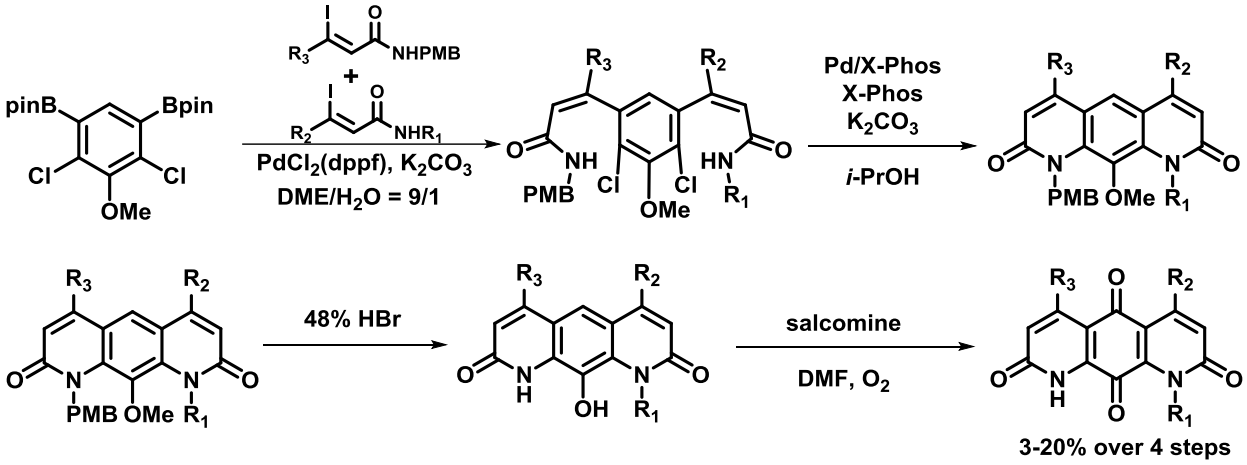

Scheme 2.2. General synthesis used for the construction of DNQ derivatives 2-19, 21-23. These compounds were prepared in an average yield of 12% from the aryl bispinacol borane.

Although some of the amides bore very bulky substituents, we were pleased to find that the Suzuki-Miyaura cross-couplings and Buchwald-Hartwig amidations all proceeded uniformly well. However, a handful of intermediates, specifically those en route to the isopropyl (**20**), cyclopropyl (**24**), cyclooctyl (**25**), and alcohol (**26**) derivatives, were not amenable to deprotection under the harsh hydrobromic acid conditions. In these cases, an alternative deprotection strategy was utilized via treatment with trifluoroacetic acid followed by BBr_3 to provide the penultimate phenols; these compounds were subsequently oxidized under standard conditions (salcomine and O_2) to give the desired products (Scheme 2.3).

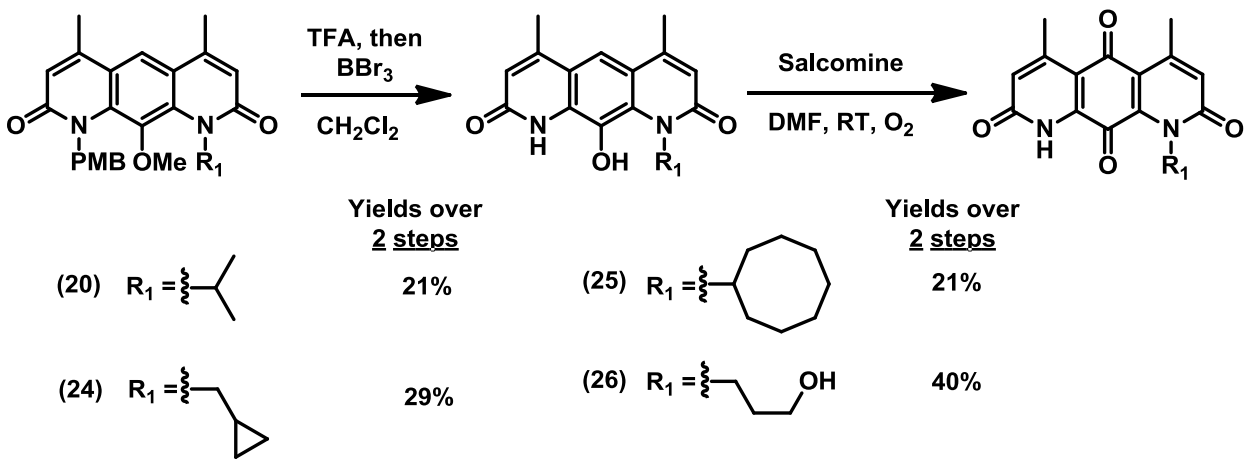

Scheme 2.3. Alternative deprotection conditions used for preparation DNQ derivatives **20**, **24**-**26**.

2.2.3 Evaluation of DNQ derivatives as NQO1 substrates.

In order to compare the newly constructed derivatives to DNQ, the *in vitro* catalytic efficiency of NQO1 with these derivatives as substrates was first assessed as described in section 2.1.2. All compounds were found to be substrates of NQO1, with a range of catalytic efficiencies, consistent with the *in silico* modeling; the structure of the DNQ derivatives together with their catalytic efficiencies with NQO1 are listed in Figure 2.16A. Derivatives with multiple substitutions, such as **3**, **5**, and **6**, are less efficient substrates, processed 30, 11, and 15 times less efficiently than DNQ, respectively. In contrast, substitution of the *N*-methyl (R_1 in Scheme 2.2) with alkyl groups has little effect on the catalytic efficiency, with even bulky compounds such as **21**-**24** being processed very efficiently by NQO1. The computational modeling suggests that extensions at this position project out of the active site while still allowing the quinone core access to the deep pocket (for example, Figure 2.15C). However, extremely bulky or lengthy substitution at R_1 (such as **13** or **25**) were less efficient NQO1 substrates.

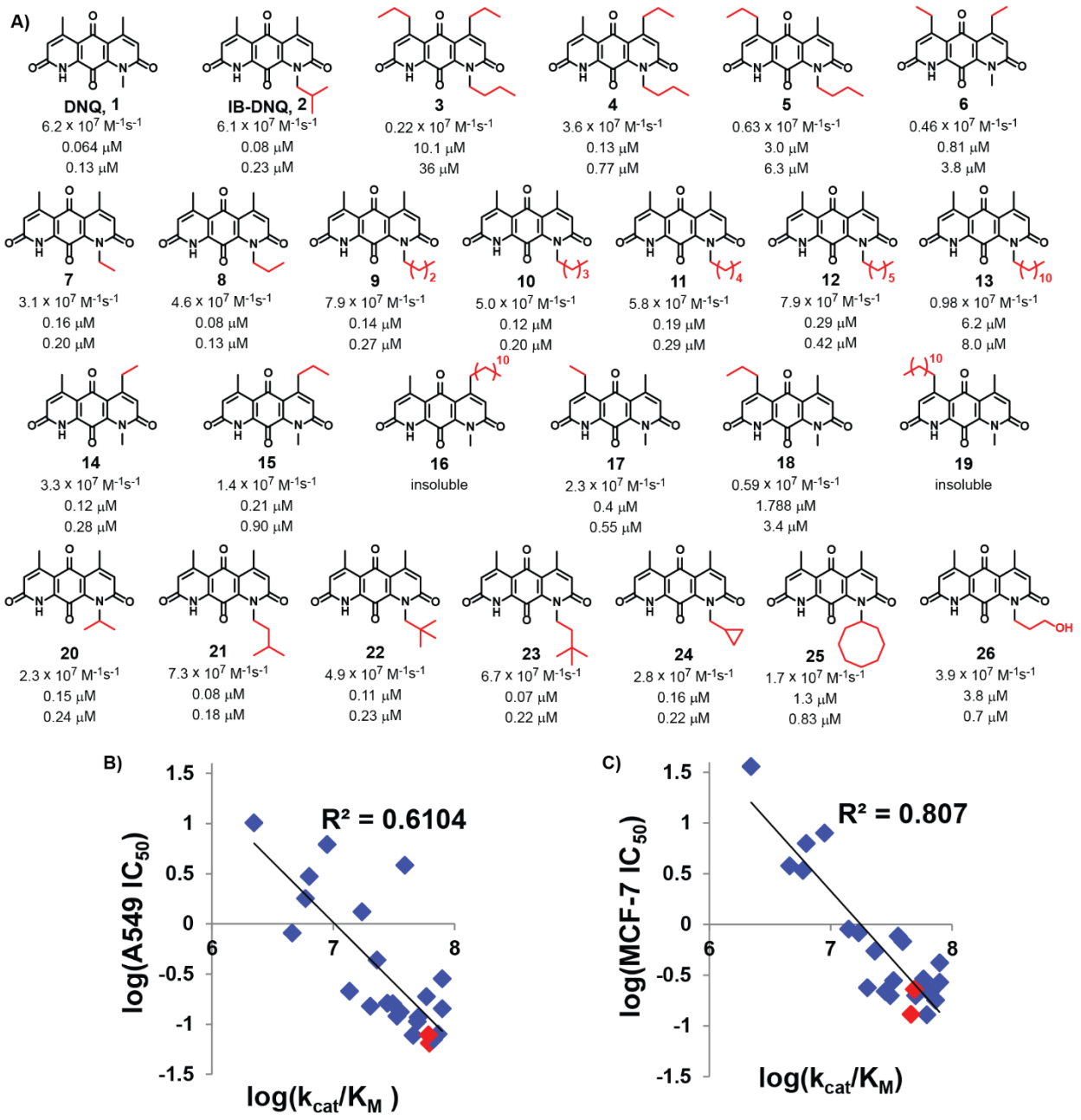

Figure 2.16. (**A**) DNQ derivatives. Below each structure is the catalytic efficiency (k_{cat}/K_M) with NQO1 and IC_{50} against A549 cells (first value) and MCF-7 cells (second value) in culture. Correlation between *in vitro* processing of DNQ analogues by NQO1 (k_{cat}/K_M in $M^{-1}s^{-1}$) with their ability to induce death (IC_{50} in μM) in (**B**) A549 cells and (**C**) MCF-7 cells. Red points are DNQ and IB-DNQ.

2.2.4 Evaluation of DNQ derivatives versus cancer cells in culture

In an effort to probe the relationship of NQO1 processing with the ability to induce death of NQO1-expressing cancer cells, the collection of DNQ analogues was assessed versus A549 and MCF-7 cancer cells in culture (Figure 2.16A). Each derivative was assessed as before: cells were incubated with compound for 2 hr followed by analysis of cell death at 72 hr and IC_{50} values were calculated from logistical dose response curves. Graphing the NQO1 catalytic efficiency versus the IC_{50} value for A549 cells (Figure 2.16B) and MCF-7 cells (Figure 2.16C) reveals a clear trend: compounds that are efficient NQO1 substrates are also potent cancer cell death inducers.

To confirm this correlation, we performed the same experiments that were initially performed with DNQ (see Section 2.1.3) on compounds that were good NQO1 substrates (e.g. IB-DNQ and **23**) and less efficient NQO1 substrates (e.g. **3** and **13**). First, the ability of the NQO1 inhibitor DIC to protect from compound-induced cell death was explored. Co-treatment with DIC (Figure 2.17) significantly protects A549 and MCF-7 cells from compounds that were good NQO1 substrates (e.g. **2** and **23**) while having little to no effect on compounds that were poor substrates (e.g. **3** and **13**). This is seen most clearly in the fold protection. As would be expected, cell death induced by compounds that are better substrates for NQO1 (higher k_{cat}/K_m) is prevented to a greater extent by DIC (higher fold protection) (Figure 2.18A-B).

A)

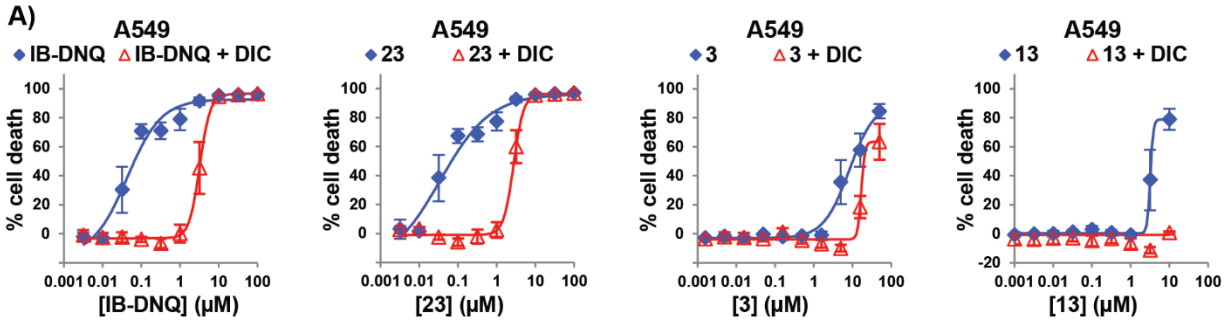

B)

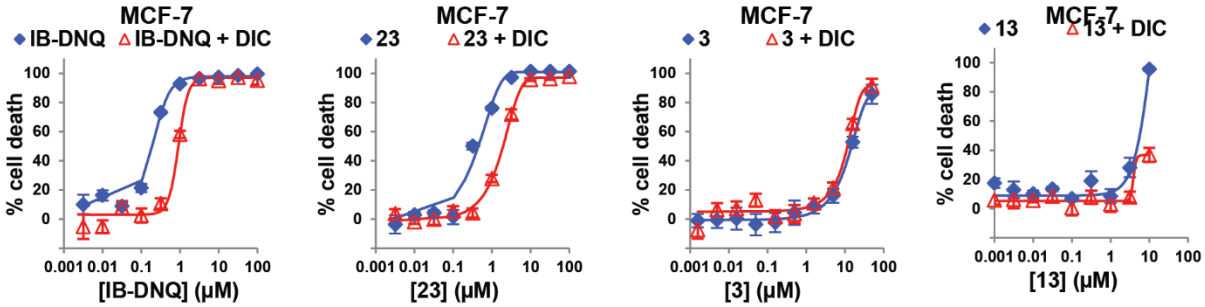

C)

Compound	A549			MCF-7		
	A549 IC_{50} (μM)	A549 + DIC IC_{50} (μM)	Fold Change	MCF-7 IC_{50} (μM)	MCF-7 + DIC IC_{50} (μM)	Fold Change
DNQ	0.06 ± 0.01	3.16** ± 0.01	53 ± 9	0.19 ± 0.07	1.5* ± 0.7	7.6 ± 1.4
IB-DNQ	0.08 ± 0.2	3.8* ± 1.3	49 ± 31	0.23 ± 0.02	0.88*** ± 0.03	3.9 ± 0.4
23	0.07 ± 0.02	2.8** ± 0.4	39 ± 17	0.42 ± 0.02	2.0*** ± 0.1	4.8 ± 0.3
3	10 ± 3	20 ± 2	2.0 ± 0.8	15 ± 2	12 ± 1	0.8 ± 0.1
13	6 ± 2	>10	>1.7	4.2 ± 0.6	>10***	>2.5

Figure 2.17. (**A**) Cell death curves of A549 cells treated for 2h with DNQ derivatives that are good NQO1 substrates (IB-DNQ and **23**) and less efficient NQO1 substrates (**3** and **13**) in the presence (red) and absence (blue) of the NQO1 inhibitor dicoumarol (DIC, 25 μM) (**B**) Same as A only with MCF-7 breast cancer cells. (**C**) Table of IC_{50} values and fold protections (Fold Change) for each treatment with standard error (n ≥ 3). DNQ values from Figure 2.2 are included for comparison. The fold protection is $\left(\frac{IC_{50}\ of\ DNQ\ or\ derivative\ with\ inhibitor}{IC_{50} of\ DNQ\ or\ derivative\ alone}\right)$. *p < 0.05, **p < 0.01, ***p < 0.001, paired t-tests on the IC_{50} values comparing treatments with or without inhibitor.

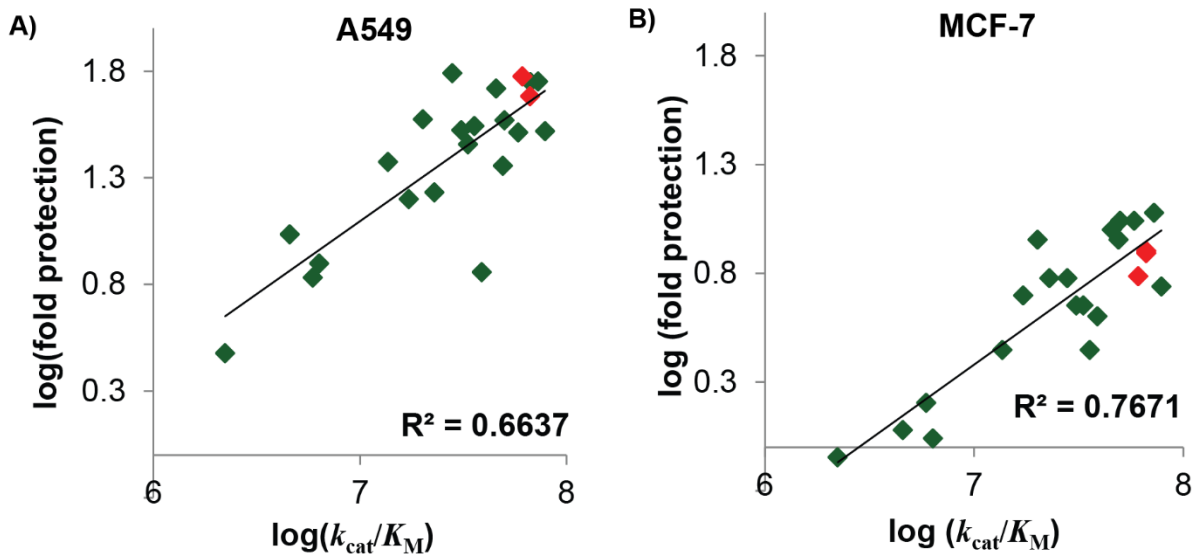

Figure 2.18. Correlation of catalytic efficiency with the fold protection by DIC in (A) A549 cells and (B) MCF-7 cells. Red points are DNQ and IB-DNQ.

Similar to the results with DIC, the NQO1 inhibitor ES936 significantly protects A549 cells from IB-DNQ and **23** while having little effect on **3** and **13** (Figure 2.19).

A)

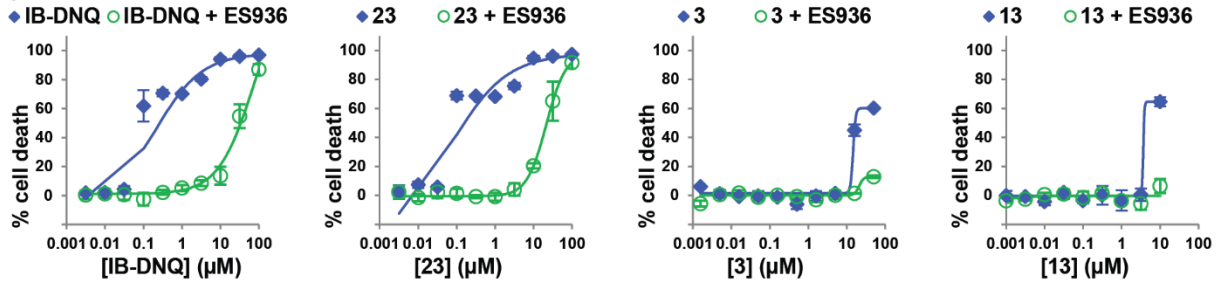

B)

Compound	A549 IC_{50} (μM)	A549 + ES936 IC_{50} (μM)	Fold Change
DNQ	0.06 ± 0.01	>10***	>170
IB-DNQ	0.09 ± 0.1	27** ± 4	300 ± 80
23	0.08 ± 0.01	25* ± 8	300 ± 100
3	16.6 ± 0.3	>50	>3
13	7 ± 1	>10	>1

Figure 2.19. (**A**) Cell death curves of A549 cells treated for 2h with DNQ derivatives in the presence (green) and absence (blue) of the NQO1 inhibitor ES936 (100nM) (**B**) Table of IC_{50} values and fold protections (Fold) for each treatment with standard error (n ≥ 3). The fold protection is $\left(\frac{IC_{50}\ of\ DNQ\ or\ derivative\ with\ inhibitor}{IC_{50} of\ DNQ\ or\ derivative\ alone}\right)$. *p < 0.05, **p < 0.01, ***p < 0.001, paired t-tests on the IC_{50} values comparing treatments with or without inhibitor.

This specificity was further confirmed by analysis of select derivatives with the isogenic cell line pairs described earlier (MDA-MB-231+/−, H596+/−, and MIA PaCa-2 NS and shNQO1, Figure 2.20). The isogenic cell lines showed a similar pattern to that observed with the chemical inhibitors. DNQ derivatives IB-DNQ and **23** were significantly more potent against cell lines that expressed active NQO1 than those with that did not (compare 231+/- and H596+/-, Figure 2.20A-B). Additionally, shRNA knockdown of NQO1 caused these compound to be less sensitive (Figure 2.20C). As expected, derivative **3** and **13** were not sensitized to cell lines upon introduction of NQO1 or desensitized to cell lines upon knockdown of NQO1 (Figure 2.20A-C). This data is

summarized in Figure 2.20D. The Boothman laboratory is currently performing further mechanistic investigations to confirm that IB-DNQ is acting in the same way as DNQ.

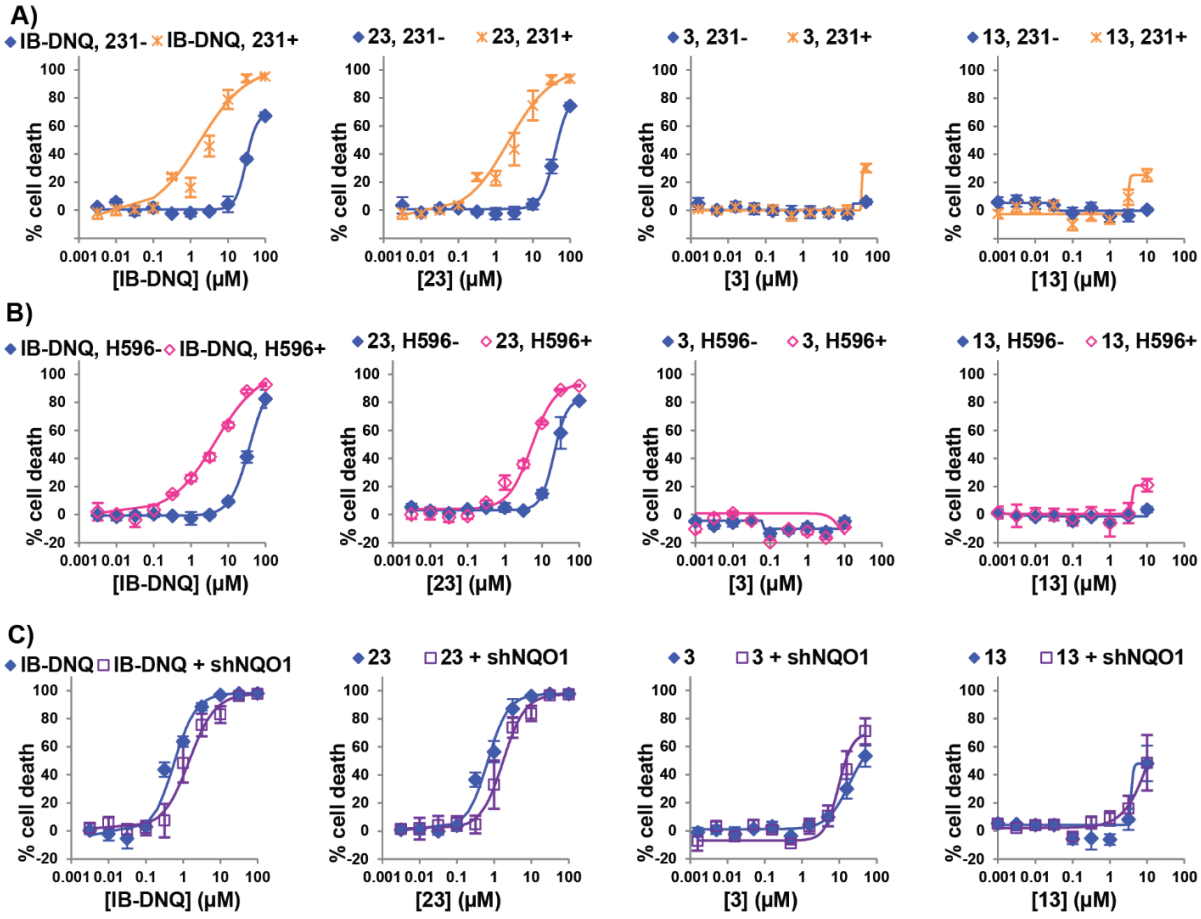

D)

Cmpd	231+ IC_{50} (μM)	231- IC_{50} (μM)	Fold Δ	H596+ IC_{50} (μM)	H596- IC_{50} (μM)	Fold Δ	MP +NS IC_{50} (μM)	MP +shNQ IC_{50} (μM)	Fold Δ
DNQ	1.1 ± 0.4	>10***	>9	3.5 ± 0.7	>10***	>3	0.31 ± 0.08	1.6* ± 0.3	5 ± 2
IB-DNQ	1.8 ± 0.9	31*** ± 3	17 ± 10	4.0 ± 1.0	37** ± 5	9 ± 3	0.56 ± 0.09	1.4 ± 0.3	3 ± 1
23	2.2 ± 1.1	39*** ± 10	18 ± 14	5.3 ± 0.8	21 ± 5	4 ± 2	0.66 ± 0.10	1.7 ± 0.3	3 ± 1
3	>50	>50	ND	>10	>10	ND	14 ± 3	17 ± 7	1.2 ± 0.6
13	>10	>10	ND	>10	>10	ND	>10	>10	ND

Figure 2.20. (**A**) Cell death curves of DNQ derivatives against the isogenic breast cell lines MDA-MB-231 transfected with empty vector (231-) and the gene for NQO1 (231+). (**B**) Cell death curves

Figure 2.20. (cont.) of DNQ derivatives against the isogenic breast cell lines H596 transfected with empty vector (H596-) and the gene for NQO1 (H596+). (**C**) Cell death curves of DNQ against the isogenic pancreatic cell lines MiaPaCa-2 NS (nonsense shRNA) and shNQO1 (shRNA against NQO1). (**D**) Table of IC_{50} values and fold protections (Fold Δ) for each treatment with standard error (n ≥ 3). The fold protection are the same as described previously. *p < 0.05, **p < 0.01, ***p < 0.001, paired t-tests on the IC_{50} values comparing treatments with or without alteration of NQO1 levels. MP = MIA PaCa-2.

2.2.5 Solubility of DNQ derivatives[31]

It has previously been noted that DNQ has poor solubility in aqueous media (PBS solubility = 115 μM).[31] While utilization of the adjuvant HPβCD does increase its solubility to a usable range for *in vivo* studies (20% HPβCD solubility = 3.3 mM), discovery of more soluble derivatives make dosing simpler and thus is advantageous. Previously, Dr. Joseph Bair found that several DNQ derivatives have increased solubility in either PBS or HPβCD compared to DNQ (Table 2.1).[31] The low solubility of DNQ is likely due to its ability to π-stack with itself, as was observed in its crystal structure.[32] The addition of alkyl chains likely interferes with the π-stacking, allowing for better aqueous and organic solubility; a similar phenomenon is observed for DNM and its derivatives (see Chapter 3.2).[33] The solubilities of these derivatives are promising for application *in vivo*.

Table 2.1. Solubility data for DNQ and its derivatives

Cmpd	PBS (μM)	Fold Δ	HPβCD (mM)	Fold Δ
DNQ	115	1	3.3	1
7	319	2.8	5.7	1.7
14	439	3.8	4.4	1.3
IB-DNQ	115	1	13	3.9
23	7	0.06	19	5.8

Solubility was assessed by LC-MS. Fold Δ = fold change from DNQ solubility

2.2.6 Tolerability of DNQ derivatives

Before investigating the *in vivo* activity of DNQ derivatives, the effect of each on the lung fibroblast cell line IMR90 was determined. IMR90 cells showed low sensitivity to both IB-DNQ (IC_{50} = 20 µM, Figure 2.21A) and **23** (IC_{50} = 30 µM, Figure 2.21B). Additionally, no protection was observed upon co-treatment with the NQO1 inhibitor DIC as one would expect based on the very low expression of NQO1 by this cell line (see Figure 2.12).

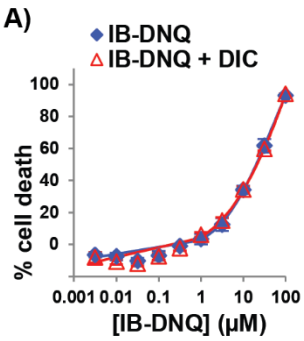

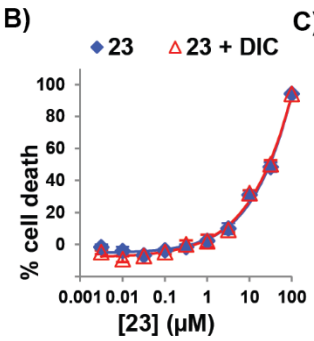

C)

Cmpd	IMR90 IC_{50} (µM)	IMR90 + DIC IC_{50} (µM)	Fold Δ
DNQ	>10	>10	ND
IB-DNQ	20 ± 3	21 ± 1	1.0 ± 0.2
23	30 ± 3	28 ± 2	0.9 ± 0.2

Figure 2.21. (**A**) Cell death curves of IB-DNQ against the lung fibroblast cell line IMR-90 treated with or without the NQO1 inhibitor DIC (25 µM). (**B**) Same as A but for derivative **23**. (**C**) Table of IC_{50} values and fold protections (Fold Δ) for each treatment with standard error (n ≥ 3). The fold protection is $\left(\frac{IC_{50}\ of\ DNQ\ or\ derivative\ with\ inhibitor}{IC_{50} of\ DNQ\ or\ derivative\ alone}\right)$. *p < 0.05, **p < 0.01, ***p < 0.001, paired t-tests on the IC_{50} values comparing treatments with or without alteration of NQO1 levels.

The ability of derivatives to induce methemoglobin formation was also explored. Both active derivatives and inactive derivatives (defined as having an IC_{50} > 1 µM in A549) were explored. All of the derivatives appear to cause less methemoglobin formation compared to DNQ (Table 2.2) suggesting that they may be better tolerated *in vivo*.

Maximum tolerated dose (MTD) studies were then performed with some of the most active derivatives. All compounds were better tolerated than DNQ (Table 2.2). Interestingly, tolerability did not track with methemoglobin formation suggesting either the toxicity that is observed *in vivo* is not due to methemoglobin formation or that the assay does not accurately predict methemoglobin formation *in vivo*. While the Boothman laboratory reports having seen methemoglobin after treatment with DNQ *in vivo*, our attempts to detect methemoglobin after

administration of compound to mice were unsuccessful (Figure 2.22). This could be either because methemoglobin formation does not occur or because mice have high levels of cytochrome b5 reductase and are thus able to rapidly convert methemoglobin back to hemoglobin.[19] An alternative explanation for the toxicity is that cytochrome b5 reductase is known to reduce certain quinones to toxic semiquinones.[34] If DNQ is a even a modest substrate for this reductase, the high levels of cytochrome b5 reductase in mice might explain the toxicity of DNQ and could mean that humans would see less toxicity due to the lower levels of this enzyme. Studies examining the ability of DNQ to be reduced by this one-electron reductase along with others would be valuable in accessing the major mode of toxicity (i.e. is it methemoglobin formation or conversion to the semiquinone by one-electron reductases).

Table 2.2. Potency, methemoglobin formation, and MTD of DNQ derivatives

Compound	A549 IC_{50} (μM)	MHb IC_{50} (μM)	MTD	
			mg/kg	μg/kg
$NaNO_2$	ND	2.0 ± 0.2	ND	ND
DNQ	0.06	4.2 ± 1.0	10*	36*
23	0.07	7.1 ± 1.7	22	62
IB-DNQ	0.08	7.6 ± 1.0	14	44
8	0.08	7.8 ± 3.3	17	53
14	0.12	9.9 ± 3.4	<13	<44
4	0.13	>100	ND	ND
7	0.16	7.5 ± 1.3	<13	<44
17	0.4	9.9 ± 3.4	ND	ND
18	1.8	20 ± 7	ND	ND
13	6.2	>10	ND	ND

A549 potencies are from Figure 2.16A. Methemoglobin (MHb) formation is reported as the concentration needed to cause 50% of the hemoglobin to be converted to MHb. For maximum tolerated dose (MTD) studies, compounds were formulated in HPβCD. They were administered i.p. daily into C57BL/6 mice for 5 days unless otherwise noted. *DNQ was administered every other day. DNQ MTD is 5 mg/kg daily if administered i.p.

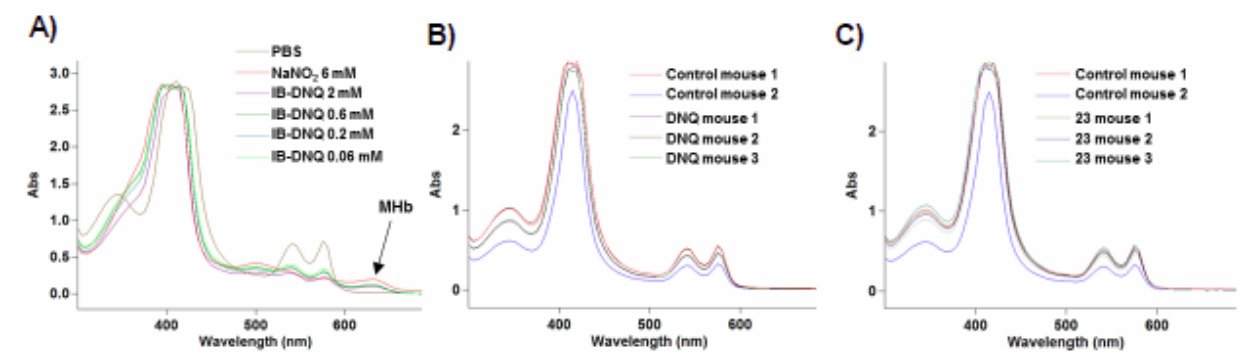

Figure 2.22. (**A**) *In vitro* methemoglobin (MHb) formation is observed for human blood treated with $NaNO_2$ (red) and IB-DNQ but not the PBS control (gray) as evidenced by the increase in absorption at 635 nm (noted with arrow). (B) *In vivo* MHb formation was not observed after treatment with DNQ. Mice received 5 treatments of either HPβCD vehicle (control) or DNQ (5 mg/kg every day). On the day of the last treatment, mice were treated and sacrificed after 1 hr. Blood was collected and analyzed for MHb formation. No increase in OD_{635} was observed. (**C**) Same as B but with 22 mg/kg of **23**.

2.2.7 *In vivo* activity of DNQ derivatives

After determining that compound **23** was the most well tolerated compound, we chose to perform an *in vivo* efficacy study. For the study, 10 million A549 lung cancer cells were injected subcutaneously into right flank of female athymic nude mice. Treatment began when the tumor volume reached 80 mm^3. Mice were treated with either vehicle (HPβCD), DNQ (5 mg/kg), or **23** (22 mg/kg) daily for 5 days followed by 5 days off for a total of 19 treatments. DNQ showed some activity but it was not statistically significant (Figure 2.23). Derivative **23** showed no activity. The reason for the difference in activity of **23** and DNQ is unclear. Also, the poor activity of DNQ in this model is slightly concerning given the fact that A549 cells express very high levels of NQO1. It is possible that a subcutaneous model is not a good model for these compounds because the subcutaneous tumor is likely able to develop a hypoxic center which would limit the ability of DNQ and its derivatives to redox cycle. Alternatively, the tumors could have been implanted too shallowly resulting in poor vasculature and thus poor exposure to compound. The poor vasculature would also explain why the tumors were very slow to establish and grow.

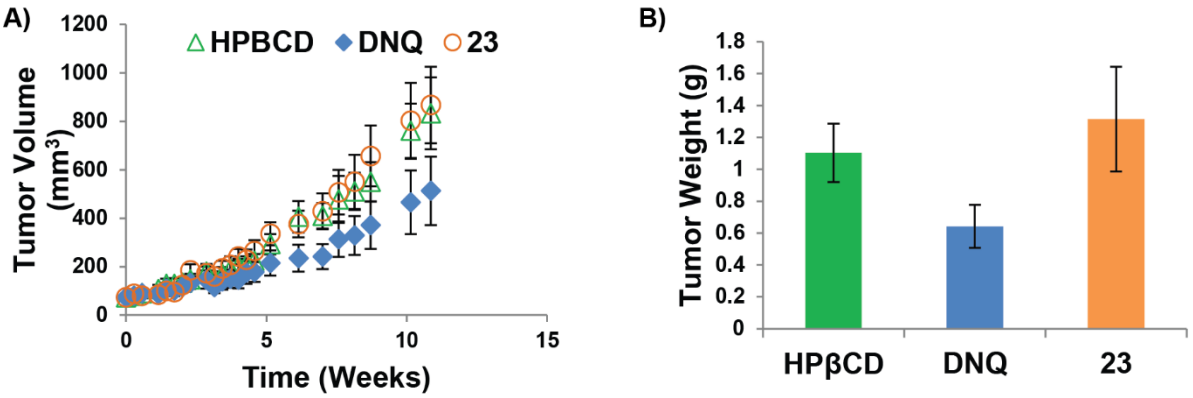

Figure 2.23. A549 mouse model. 10 million A549 cells were injected into right flank of female athymic nude mice. When the tumors reached 80 mm^3, the mice were split into treatment groups including vehicle (950 mg/kg HPβCD), DNQ (5 mg/kg formulated in HPβCD), and 23 (22 mg/kg formulated in HPβCD). Each group contained 10 mice. Mice received a total of 19 treatments (Days 2-6, 12-16, 22-26, 32-35) all injected i.p. Tumors were measured and volumes calculated using the formula $V = 0.5LW^2$ where V = volume, L = length, and W = width. Mice were sacrificed on day 80. (**A**) Tumor growth curves. Mean ± SEM. (**B**) Tumor mass from day 80. Mean ± SEM.

The Boothman laboratory is performing *in vivo* studies with IB-DNQ in different mouse models. A preliminary survival study from a collaboration between the Boothman and Gao laboratories at UT-Southwestern showed promising results with IB-DNQ significantly extending the survival of mice inoculated subcutaneously with 4T1 cells (murine breast cancer, Figure 2.24). Future work with a larger number of mice is needed to confirm this result.

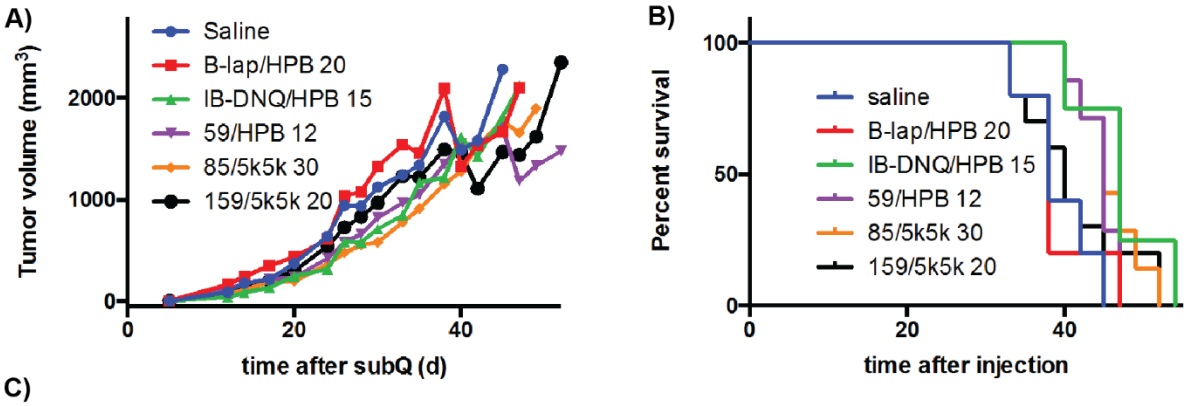

C)

	saline	β-lap 20 mg/kg	GB-059 12 mg/kg	IB-DNQ 15 mg/kg	GB-085 30 mg/kg	GB-159 20 mg/kg
# of mice	5	5	8	3	7	10
Median survival (days)	38	38	45	47	45	40
P-value	1	0.8	0.04	0.03	0.02	0.5

Figure 2.24. 4T1 mouse model. 100,000 4T1 cells were injected into right flank of Balb/c mice. Mice were then treated with either β-Lap (20 mg/kg), IB-DNQ (15 mg/kg), or a β-Lap ester prodrug in micelles (GB-085, 30 mg/kg). Each treatment was given i.v. every 4 days for a total of 4 treatments. (**A**) Tumor growth curves. (**B**) Kaplan-Meier survival curves. (**C**) Table with more details of the study.

2.3 Exploring the scope of the deoxynyboquinones as anticancer agents

In the previous sections, we have shown that DNQ and its derivatives show potent activity against the NQO1-overexpressing lung cancer cell line A549 and breast cancer cell line MCF-7. In order to demonstrate the generality of this approach, the activity of DNQ and its derivatives against other cancer cell lines was explored.

2.3.1 Breast Cancer

The first type of cancer that we explored was breast cancer. Breast cancer is the most commonly diagnosed cancer in women with 231,840 estimated new cases (29% of cancer diagnoses in women) and 40,290 predicted deaths (15% of cancer deaths in women) in the United

States in 2015.[35] Differences in aggressiveness and response to chemotherapeutics along with genetic profiling demonstrate that breast cancer is quite heterogeneous, with at least five molecular subtypes (Luminal A, Luminal B, Her2, Triple Negative (TNBC), and normal breast–like cancers).[36-38] Each subtype responds differently to chemotherapeutic agents with luminal and HER2 subtypes being generally responsive to targeted therapies (tamoxifen and Herceptin, respectively).[39] TNBC treatment, however, continues to rely on traditional cytotoxic agents such as anthracyclines, taxanes, and alkylating agents.[39-41] Initially, TNBC responds well to these agents with high rates of pathologic complete response (27% for TNBC compared to 7% for luminal, $P < 0.0001$).[41-42] Despite this initial response, patients with TNBC have worse overall prognoses compared to all other types of breast cancers with increased risk of relapse (33.9% versus 20.4%, $P < 0.0001$) and likelihood of death (42.2% versus 28%, $P < 0.0001$) in the first five years.[41-42] For this reason, novel targeted therapeutics for TNBC with enhanced efficacy are needed. TNBC clinical trials of targeted therapies such as PARP-1 inhibitors and VEGF ligands have been performed, but thus far have had mixed results, with subsets of patients showing increased response.[43-44] These mixed results are likely due to the heterogeneity of TNBC.[43,45] As such, identification and validation of multiple targets and corresponding therapeutics are needed for TNBC. Additionally, effective therapies for the other subtypes would also be useful given the observation of tamoxifen[46] and herceptin[47] resistant tumors.

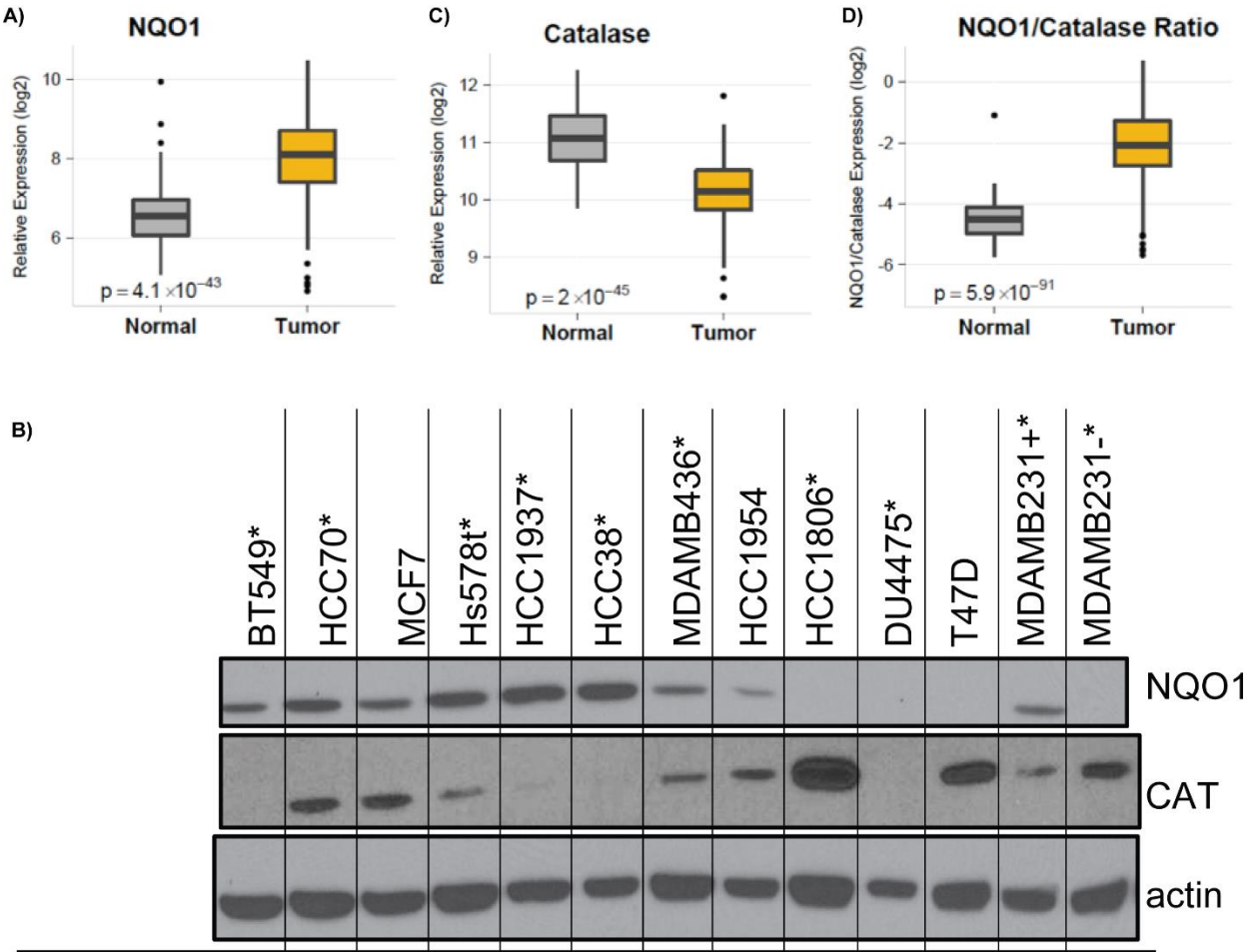

NQO1 activity (nmol/min/mg protein)	2400 (200)	2100 (100)	1900 (100)	1900 (100)	1600 (50)	1500 (60)	1050 (50)	570 (90)	180 (30)	100 (2)	8 (4)	1500 (60)	13 (3)
Catalase activity (Units activity /mg)	ND	ND	35 (3)	ND	ND	ND	ND	131 (5)	200 (20)	ND	108 (5)	ND	ND
DNQ IC_{50} (μM)	0.084 (0.008)	0.036 (0.001)	0.19 (0.07)	0.33 (0.04)	0.036 (0.005)	0.23 (0.05)	1.4 (0.2)	0.35 (0.01)	1.9 (0.2)	2.4 (0.5)	>10	1.1 (0.4)	>10
Protect (25 μM DIC)	15	28	8	5	31	17	5	5	2	2	ND	ND	ND
iB-DNQ IC_{50} (μM)	0.112 (0.006)	0.083 (0.007)	0.25 (0.05)	0.39 (0.04)	0.068 (0.001)	0.106 (0.004)	1.69 (0.04)	1.12 (0.03)	2.5 (0.1)	1.1 (0.3)	61 (6)	1.8 (0.9)	31 (3)
Protect (25 μM DIC)	8	14	5	8	12	22	4	3	2	1	1	ND	ND
23 IC_{50} (μM)	0.081 (0.006)	0.15 (0.01)	0.19	0.50 (0.02)	0.14 (0.03)	0.21 (0.02)	2.2 (0.3)	0.86	2.2 (0.5)	ND	ND	2.2 (1.1)	39 (10)
Protect (25 μM DIC)	10	8	8	3	16	7	3	4	2	ND	ND	ND	ND

Figure 2.25. (**A**) NQO1 mRNA expression in normal vs. breast cancer tissue. Data are from tumor and associated normal tissue. y-axis is NQO1 expression levels, log2. P = 4.1 X 10^{-43} (B) Western blot for NQO1, catalase (CAT), and actin as the loading control in the breast cancer cell lines indicated. *Triple negative breast cancer cell line. Below the western is the NQO1 activity and catalase activity of each cell line along with IC_{50} values and fold protections (Protect) for each treatment with standard error (n ≥ 3). The fold protection is $\left(\frac{IC_{50}\ of\ DNQ\ or\ derivative\ with\ inhibitor}{IC_{50} of\ DNQ\ or\ derivative\ alone}\right)$. ND = not determined. (**C**) Catalase mRNA expression in normal vs. breast cancer tissue. Data are from tumor and associated normal tissue from the same patients as in A. y-axis is catalase

Figure 2.25. (cont.) expression levels, log2. P = 2 X 10^{-45} (**D**) Ratio of NQO1 to catalase mRNA expression in matched tumor and normal tissues.

As discussed previously in Chapter 1.1.1, NQO1 is often overexpressed in breast cancer. The Boothman laboratory confirmed this by analyzing NQO1 mRNA expression of breast cancer and the associated normal tissue (Figure 2.25A). They found that the NQO1 transcript is significantly elevated (~4 fold) in breast cancers compared to healthy tissue ($p<0.0001$, Figure 2.25A). A similar study has been performed with just TNBC and analogous results were found (data not shown). After confirming the clinical relevance of NQO1 expression, I evaluated 13 breast cancer cell lines (10 of which were TNBC) cell lines for NQO1 expression (Figure 2.25B). Many of the breast cancer cell lines showed strong NQO1 expression with the exception of HCC1806, DU4475, T47D and MDA-MB-231. It is known that MDA-MB-231 contains a known polymorphism (NQO1*2) resulting in an unstable NQO1 protein,[48] and it is possible that the other low-expressing cell lines do as well. Enzyme activity in lysates of each cell line was determined and matched the Western blot data (Figure 2.25B). After determining that many breast cancer cell lines overexpress NQO1, the sensitivity of breast cancer cell lines to DNQ, IB-DNQ, and **23** was determined. IB-DNQ and compound **23** were chosen because each has potent activity in other cancer cell lines and favorable solubility and toxicity profiles. Cell lines with NQO1 activity over a certain threshold (~500 nmol/min/mg protein) were sensitive to DNQ, IB-DNQ, and **23** (IC_{50} < 1 μM). Additionally, cell lines were significantly protected by co-treatment with the NQO1 inhibitor DIC, confirming NQO1 as the primary determinant of activity in TNBC (Figure 2.25B).

As we were performing these studies, we noticed that the potency of the DNQ and its derivatives did not always correlate with increased NQO1 activity. For example, MDA-MB-436 has good NQO1 activity (1050 nmol/min/mg protein) but is not very sensitive to DNQ. Also, Hs578t and HCC1937 have similar NQO1 activities but the sensitivity to DNQ differs by approximately 10-fold. While there are many possible explanations for this, one is that these cell lines express

different amounts of enzymes that help the cancer cell deal with oxidative stress. One such enzyme is catalase (CAT), which catalyzes the conversion of hydrogen peroxide to water and oxygen. Recently, it was observed that higher levels of catalase decrease sensitivity to β-Lap.[49] It may be that higher catalase levels also decrease sensitivity to the deoxynyboquinones. This appears to be true in both MDA-MB-436 and Hs578t which have high levels of CAT expression compared to HCC1937. While the ratio of NQO1 to CAT levels do not explain all the differences that are observed here (Figure 2.25B), there are many other enzymes (e.g. superoxide dismutase and glutathione peroxidase) that also help the cell to cope with higher oxidative stress levels. It is likely that these cancer cell lines express varied levels of these enzymes which may help to explain the variation in sensitivity to DNQ. Intriguingly, the Boothman laboratory has also recently found that CAT levels are generally lower in cancer cells compared to normal cells (Figure 2.25C-D) suggesting that the deoxynyboquinones have an even higher chance of success.

2.3.2 Lung Cancer

The second type of cancer that was explored was lung cancer. Lung cancer is the second most commonly diagnosed cancer in both men and women with 115,610 (14%) and 105,590 (13%) estimated new cases, respectively, in the United States in 2015.[35] Additionally, lung cancer causes the most deaths of any type of cancer in both men and women with 86,380 (28%) and 71,660 (26%) estimated deaths, respectively, in the United States in 2015.[35] This high numbers of death makes lung cancer an especially important disease to try to target. Given the high incidence of NQO1 overexpression in lung cancer samples from patients (discussed more extensively in Chapter 1.1.1), we expected that DNQ and its derivatives would have potent activity against lung cancer cell lines.

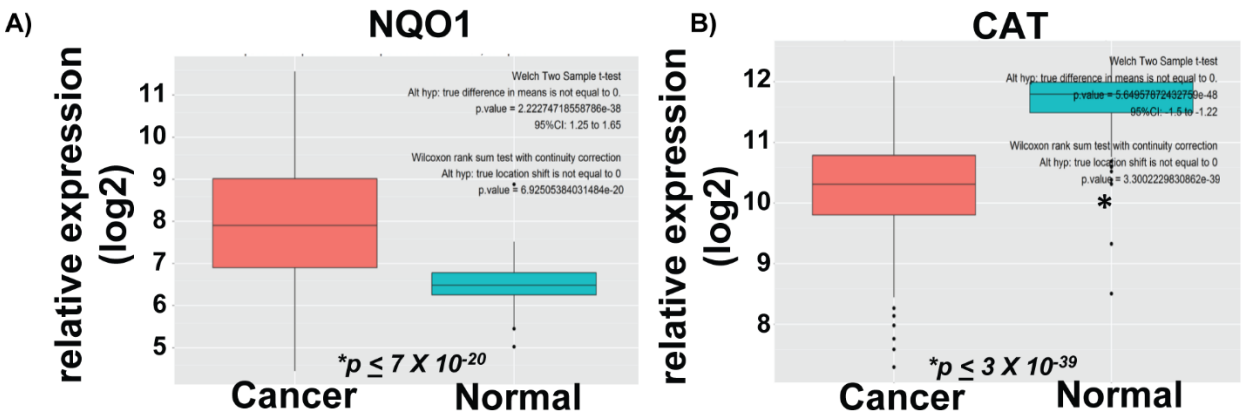

C)

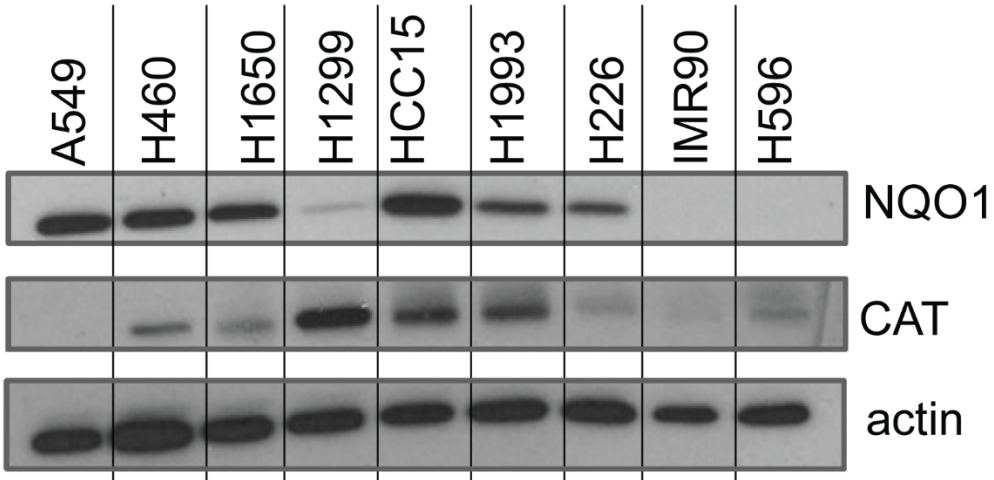

NQO1 activity (nmol/min/mg protein)	2600 (100)	3000 (500)	1100 (100)	170 (20)	2800 (300)	1170 (30)	700 (100)	<1	30 (20)
DNQ IC_{50} (μM)	0.064 (0.006)	0.16 (0.01)	0.12 (0.03)	0.36 (0.01)	0.46 (0.02)	1.5 (0.4)	1.74 (0.01)	>10	>10
Protect (25 μM DIC)	56	66	14	5	7	4	2	ND	ND
IB-DNQ IC_{50} (μM)	ND	0.11 (0.01)	0.17 (0.03)	ND	ND	ND	ND	20 (3)	37 (5)
Protect (25 μM DIC)	ND	42	9	ND	ND	ND	ND	1	ND
23 IC_{50} (μM)	ND	0.14 (0.01)	0.36 (0.07)	ND	ND	ND	ND	30 (3)	21 (5)
Protect (25 μM DIC)	ND	33	6	ND	ND	ND	ND	0.9	ND
3 IC_{50} (μM)	ND	11 (1)	21 (1)	ND	ND	ND	ND	>50	>10
Protect (25 μM DIC)	ND	1.4	1.9	ND	ND	ND	ND	ND	ND

Figure 2.26. (**A**) NQO1 mRNA expression in normal vs lung cancer tissue. Samples are from 432 patients and consist of tumor and associated normal tissue. y-axis is NQO1 expression levels, log2. (**B**) Same as A but for catalase (CAT) mRNA expression. (**C**) Western blot for NQO1, CAT, and actin as the loading control in the lung cancer cell lines indicated. * Below the western is the

Figure 2.26. (cont.) NQO1 activity of each cell line along with IC_{50} values and fold protections (Protect) for each treatment with standard error (n ≥ 3). The fold protection is $\left(\frac{IC_{50}\ of\ DNQ\ or\ derivative\ with\ inhibitor}{IC_{50} of\ DNQ\ or\ derivative\ alone}\right)$. ND = not determined.

The Boothman laboratory confirmed NQO1-overexpression in lung cancer by analyzing NQO1 mRNA expression of lung cancer and the associated normal tissue (Figure 2.26A). At the same time, they also analyzed CAT mRNA expression of the same samples (Figure 2.26B). The lung cancer samples had a similar pattern to that of the breast cancer samples (Figure 2.25A and C) with significantly overexpressed NQO1 and decreased CAT mRNA. I evaluated 8 lung cancer cell lines and 1 lung fibroblast cell line (IMR90). Many of the lung cancer cell lines showed strong NQO1 activity with the exception of H596 which is known to contain a polymorphism (NQO1*2) resulting in the inactivation of the enzyme. IMR90 also expressed low levels as would be expected in a non-cancerous cell line. The sensitivity of these cell lines to DNQ, IB-DNQ, **23**, and the inactive DNQ derivative **3** was determined. Generally, DNQ is very active against lung cancer cell lines that express high levels of NQO1. An exception to this was H1993. H1993 expresses high levels of CAT which could explain this low sensitivity. Another anomaly was H1299 which had relatively low NQO1 levels and high CAT expression but still was sensitive to DNQ (IC_{50} = 0.36 μM). This result is perplexing, but it is possible that this cell line already has very high levels of oxidative stress compared to the other cell lines and is thus sensitized to DNQ.

2.4 Conclusions and future directions

NQO1 Activation of Quinones: NQO1-mediated activation of an anticancer agent is an excellent targeted strategy as NQO1 is often dramatically overexpressed in cancer cells compared to normal cells. Many quinones have been touted as being activated by NQO1 and thus have been proposed as potential targeted anticancer agents. In this Chapter, we have described a set of experiments which can be utilized to determine whether a quinone is in fact bioactivated by NQO1 and whether this mechanism is responsible for its anticancer activity: 1) *In vitro* reduction by

NQO1, 2) Protection of NQO1-overexpressing cell lines by small molecule inhibitors of NQO1 or shRNA knockdown of NQO1, and 3) Sensitization to NQO1*2 cell lines upon transfection with WT cDNA for NQO1. Utilizing these techniques, we have found that while many of these quinones (specifically MMC, RH1, and STN) are activated by NQO1 to some extent, their primary modes of activation are via other reductases. β-Lap and DNQ, on the other hand, do appear to be primarily dependent upon NQO1 for their anticancer activities. However, based on the data set presented here, DNQ is the most promising NQO1-activated anticancer drug. Discussed below is a summary of the findings (both previous literature reports and our findings reported in this Chapter) which support these conclusions.

Mitomycin C. It is well accepted that MMC must first be bioreduced before it can alkylate DNA and ultimately cause cancer death. [50] However, the enzyme responsible for the reduction remains controversial. One way of determining which enzyme is responsible for the bioactivation of MMC (as well as other quinones) is to determine what enzymes can reduce MMC *in vitro*. While MMC previously has been shown to be an *in vitro* substrate for NQO1, its processing is pH dependent with increasing amounts of metabolism being observed as pH is decreased from 7.8 to 5.8.[9] Little-to-no reduction of MMC was previously observed at physiological pH (i.e. pH 7.4).[9] These results are consistent with our *in vitro* assay (run at pH 7.4) during which we saw no detectable reduction of MMC by NQO1.[3] Additionally, others have found that MMC actually inhibits NQO1 at this pH,[51] suggesting that NQO1 likely does not activate MMC *in vivo.* MMC is an excellent substrate for other reductases such as NADPH cytochrome P450 reductase[52] or xanthine oxidase[53], and one of these enzymes is likely responsible for bioactivation of MMC.

As discussed in Chapter 1.1.3 and this Chapter, another way to determine whether NQO1 is responsible for bioactivation of MMC (or other quinones) is to examine the ability of NQO1 inhibitors to protect NQO1-overexpressing cell lines from the compound. When the mouse breast cancer EMT6 was co-treated with DIC in normoxia, a slight decrease in toxicity of MMC was

observed.[54] This differs from our results where we saw no protection of human lung (A549) or breast (MCF-7) cancer cell lines (Figure 2.2). However, these studies used a higher amount of DIC (100 μM versus 25 μM) and examined a different cell line which may explain the small difference. Another interesting finding of this study was that dicoumarol actually increases toxicity of MMC in hypoxia suggesting that MMC, at least in a hypoxic environment, is not dependent upon NQO1 activation and is instead detoxified by it. To the best of our knowledge, no previous studies examining the effect of ES936 on the potency of MMC have been reported. However, our results with this NQO1 inhibitor were similar to those previously reported for DIC with slight protection occurring in normoxia (Figure 2.3).[3,54]

A final way of examining the enzymes responsible for bioactivation of MMC (or other quinones) is to examine cell lines with different levels of enzyme and correlate the enzyme levels with compound activity. Fitzsimmons and co-workers analyzed sensitivities of the NCI 60 and found that aerobic sensitivity to MMC was highly correlated with NQO1 activity but not to the one electron reductases NADPH cytochrome P450 reductase and cytochrome b5 reductase.[10] Additionally, another study showed that transfection of a non-NQO1 expressing cell with the cDNA for NQO1 results in a slight increase in sensitivity to MMC.[55] A different study with an NQO1*2 cell line, however, found no change in sensitivity of MMC upon expression of NQO1.[52] Overall, these results are consistent with our results with the NQO1+/- cell lines (MDA-MB-231+/- and H596+/-) which saw modest (although not statistically significant) sensitization to MMC upon expression of NQO1 (Figure 2.5 and 2.6).[3] Additionally, they are consistent with the modest protection we observed for A549 cells co-treated with the NQO1 inhibitor ES936. While MMC can be activated by NQO1 in normoxia, it does not require NQO1 for bioactivation and is also activated by other reductases.

RH1. While RH1 has previously been found to be a substrate for NQO1 *in vitro*,[56] we did not observe activation upon incubation with NQO1 in our assay.[3] Assay conditions did differ slightly

(they utilized NADPH and observed at absorbance at 370 nm whereas we utilized NADH and observed at absorbance at 340 nm) and absorption of RH1 at the wavelengths used may explain the difference in results.[56] RH1 is also an *in vitro* substrate for NADPH cytochrome P450 reductase, xanthine oxidase/xanthine dehydrogenase, and NQO2.[6,56]

Previous literature on co-treatment of RH1 with the NQO1 inhibitor DIC is contradictory. Some studies report good protection,[56-57] but both of these studies used cell lines with very low NQO1 activity (e.g. T47D) which complicates the interpretation of these results. A study that examined the effect of DIC on NQO1-overexpressing cell lines (e.g. H460 and MCF-7) saw no protection from RH1[58] consistent with our results with both A549 and MCF-7 cells (Figure 2.2).[3] Previous reports investigating co-treatment of RH1 with the NQO1 inhibitor ES936 have shown modest protection,[59-60] consistent with our results (Figure 2.3).[3] These findings suggest that RH1 is activated by NQO1 but likely has other modes of activation. The difference in the DIC and ES936 protection likely results from different modes of inhibition of NQO1 with ES936 being a more efficient inhibitor.

Similar to MMC, previous work had shown that transfecting a cell line with an NQO1*2 polymorphism (e.g. MDA-MB-468 and BE) sensitizes cells to treatment with RH1.[6,60-62] This is in agreement with our data where both MDA-MB-231 and H596 cells were modestly sensitized to RH1 upon expression of active NQO1 suggesting that RH1 is activated by NQO1 (Figure 2.5 and 2.6).[3] However, studies analyzing the NCI 60 suggest that there is no correlation between the NQO1 activity of a cell line and the anticancer activity of RH1.[58] Additionally, similar to studies with MMC,[63] cells treated with RH1 in hypoxia are unaffected by overexpression of NQO1 with the NQO1*2 cell lines having approximately equal sensitivity to those transfected with WT NQO1 gene.[64] This suggests that while NQO1 may activate RH1, other enzymes are also important (probably more important) for its activation. The effect of different concentrations of NADPH cytochrome P450 reductase and cytochrome b5 reductase was explored but no correlations were

found.[6] However, it was found that the cell lines could be greatly sensitized to RH1 by overexpression of NQO2.[6] The importance of NQO2 in RH1 activation was further demonstrated in an analysis of cell lines of pediatric tumors. Several of the tumors expressed no detectable NQO1 (but moderate to high levels of NQO2) and were sensitive to RH1.[65] Overall, previous literature reports combined with the data presented here suggest that RH1 can be activated by NQO1 but is also activated by other reductases.

Streptonigrin. STN has previously been shown to be a good substrate for NQO1[66] but is also known to be processed by other reductases such as xanthine oxidase and xanthine dehydrogenase.[67] In agreement with these previous studies, we found that STN is a good NQO1 substrate (much more efficiently processed than either MMC or RH1, Figure 2.1).[3] STN was previously found to have activity against cell lines that do not express NQO1 (e.g. the human colon cell line BE[62] and the breast cancer cell line MDA-MB-468[61] which both have the NQO1*2 polymorphism). However, it is greatly sensitized to both of these cell lines upon expression of NQO1. In fact, STN consistently has a more potent sensitization upon expression of NQO1 compared to both MMC and RH1.[61-62] Consistent with the literature reports mentioned above, we found that induction of expression of NQO1 in NQO1-deficient cell lines (MDA-MB-231+/- and H596+/-) greatly sensitizes cells to STN (and to a greater degree than for MMC or RH1, Figure 2.5 and 2.6).[3] Previous reports also found that both DIC[68] and ES936[69] protect NQO1-overexpressing cells from STN. While we did not observe protection with DIC (Figure 2.2), we saw similar protection with ES936 (Figure 3.3).[3] Overall, these studies suggest that the anticancer activity of STN is more NQO1-dependent than that of MMC or RH1. However, as will be discussed next, β-Lap and DNQ appear to have even greater selectivity.

DNQ versus β-Lap. Previous studies[5,49,70-72] along with the studies presented in this chapter[3-4] strongly suggest that β-Lap is activated by NQO1. It is a very efficient substrate for NQO1 *in vitro* (Figure 2.1),[3] is significantly protected by both DIC and ES936 (Figure 2.2 and 2.3),[3-4] and has

been shown to be sensitized to NQO1*2 cell lines upon transfection with the WT gene for NQO1 (Figure 2.5 and 2.6).[4] DNQ shows a similar profile, but it has several advantages over β-Lap. First, it is more potent than β-Lap. In cell culture, it consistently has an approximately 20-fold more potent IC_{50} than β-Lap. It is also more potent *in vivo,* showing similar activity in a murine lung cancer model at approximately 3 to 6-fold lower concentrations (Figure 2.14). This is advantageous because it allows for lower compound use.

Second, DNQ appears to have a wider therapeutic window than β-Lap, at least in cell culture. When cell lines that overexpress NQO1 are co-treated with either DIC or ES936, the fold protection for treatment with DNQ is consistently higher than that observed for β-Lap (3 to 5 fold higher for DIC and >28 fold higher for ES936, Figure 2.2 and 2.3).[3] Additionally, NQO1*2 that are transfected with WT NQO1 cDNA are sensitized to a greater extent with DNQ than they are with β-Lap (Figure 2.5 and 2.6).[3-4] This is further supported by oxygen consumption studies. When DNQ is co-treated with DIC, no observable increase in oxygen consumption occurs (Figure 2.8C-D).[4] This is in contrast to β-Lap which still has a slight increase in oxygen consumption (Figure 2.8A-B).[4] Together, these results suggest that DNQ might be more selective for activation by NQO1 compared to β-Lap. Specifically, β-Lap might be processed by one electron reductases to a greater extent than DNQ. Studies examining the ability of other reductases to process both β-Lap and DNQ should be performed in order to confirm this.

A third advantage that DNQ has over β-Lap is its pharmacokinetic properties. The half-life of DNQ is over 30-times longer than that of β- Lap (Figure 2.13).[4] Additionally, the DNQ C_{max} is 7-times higher and the AUC is 27-times higher allowing for longer exposure to the tumor *in vivo*. The greater compound exposure combined with the better potency of DNQ compared to β-Lap strongly suggest that DNQ is the more promising compound going forward.

DNQ induces DNA damage and death by parthanatos: After determining that DNQ is the most promising NQO1-activated anticancer agent of the previously reported NQO1 substrates, the mechanism of its cell death was determined. In agreement with previous studies,[1,31] DNQ was found to induce ROS formation that causes DNA damage.[4] At concentrations of DNQ above the IC_{50}, extensive DNA damage occurs resulting in PARP-1 hyperactivation, depletion of NAD^+, and ultimately PARP-1 dependent cell death (a.k.a. parthanatos).[4] These events could be prevented by inhibition of NQO1 further demonstrating the NQO1 dependence of DNQ activation. Additionally, cell death was prevented by transient knockdown of PARP-1. With this extensive mechanistic investigation in hand, one future direction would be investigation of synergistic combinations. In the clinic, nearly all cancers are treated with combination therapy.[73] These combinations are advantageous both because they often allow for lower amounts of compound to be used[73-74] and often result in decreased resistance development.[74] Below are a few compound classes that have the potential to synergize with DNQ and would likely be fruitful to explore.

PARP-1 inhibitors. PARP-1 is a DNA damage repair enzyme which activates the base-excision repair process upon single stranded breaks.[11] PARP-1 inhibition has been extensively explored as an anticancer therapy, specifically with a focus on treating BRCA-deficient cancers due to the potential for synthetic lethality.[75] Recently, the PARP-1 inhibitor olaparib was approved by the FDA for the treatment of BRCA-deficient ovarian cancers.[76] In addition to their single-agent use, PARP-1 inhibitors have also been investigated in combination studies with DNA damaging agents. Cell cultures studies showed good synergy with DNA methylating agents (e.g. temozolomide and dacarbazine), topoisomerase inhibitors (e.g. camptothecin), and platinum alkylating agents (e.g. cisplatin and carboplatin),[77] likely due to the decreased ability of the cells to repair damaged DNA. However, clinical trials of combinations of PARP-1 inhibitors with cisplatin, gemcitabine, dacarbazine, and temozolomide all showed significantly higher toxicity

than initially expected, even at relatively low doses.[78] This toxicity is likely due to the untargeted nature of the DNA damaging agents described above. Utilization of a targeted DNA damaging agent could decrease the toxicity while demonstrating a similar synergy with PARP-1 inhibitors.

Initial studies with DNQ suggest that it should not synergize with PARP-1 inhibitors. Specifically, transient knockdown of PARP-1 actually de-sensitized cell lines to DNQ.[4] However, these experiments were performed with relatively high levels of DNQ (greater than or equal to the IC_{50}) which result in extensive DNA damage causing the cell to undergo PARP-1 dependent cell death (parthanatos). It is likely that if sub-lethal doses of DNQ were used, this would cause activation of PARP-1 dependent DNA damage repair instead of PARP-1 dependent cell death. Concurrent inhibition of PARP-1 with olaparib or one of the other PARP-1 inhibitors would prevent repair of the single stranded breaks caused by DNQ. Upon replication the single stranded breaks would become double stranded breaks, and these double stranded breaks would ultimately kill the cell.[79] This technique holds especially great promise for tumors that already have mutations that disrupt other DNA repair pathways (e.g. BRCA deficient breast and ovarian cancer, see below for a further discussion of this).

NAD^+ synthesis inhibitors. NAD^+ is essential to many cellular processes including anabolic metabolism and proliferation in cancer cells as well as cell signaling such as the buildup of PAR polymers on PARP-1 in response to DNA damage.[80] An emerging anticancer technique is the inhibition of NAD^+ synthesis via inhibition of the enzyme nicotinamide phosphoribosyltransferase (NAMPT) which catalyzes the rate-limiting step in this process.[81] The NAMPT inhibitor FK866 has been tested in clinical trials as a single agent, but its efficacy has generally been very low.[81] NAMPT inhibitors FK866 and GMX1778 have been shown to synergize with ROS generating compounds likely due to the ability of ROS to deplete NAD^+ levels via PARP-1 activation (discussed further in the next section).[80] Recently, FK866 was found to potently synergize with β-

Lap in NQO1 over-expressing cell lines.[80] It is expected that similar synergy would be observed for DNQ.

Lactate dehydrogenase A inhibitors. In 1956, Otto Warburg observed that cancer cells have high rates of aerobic glycolysis.[82] Lactate dehydrogenase A (LDH-A) is a key enzyme in glycolysis, catalyzing the conversion of pyruvate to lactate and in the process regenerating NAD^+ from NADH, which is necessary for the continued ATP production in the absence of aerobic oxidation of NADH.[83] Since this discovery, inhibition of LDH-A has been proposed as a promising anticancer strategy. Genetic alteration of LDH-A levels results in reduced viability and tumorigenicity of cancer cells.[83] The Hergenrother laboratory in collaboration with the Minutolo laboratory (University of Pisa) has discovered a novel class of LDH-A inhibitors, the N-hydroxyindole (NHI) LDH-A inhibitors, which show promising activity in cell culture.[84]

Recently, Dr. Hyang Yeon Lee has found that NHI-Glc-2 (a glucose linked NHI)[83] potently synergizes with DNQ against lung cancer cell lines that over-express NQO1 (data not shown). A veterinary medicine student Andrew Lee saw similar results in breast cancer cell lines that over-express NQO1 (data not shown). While the mechanism of this synergy is not known, it is possibly due to the change in NADH/NAD^+ ratio upon inhibition of LDH-A. NQO1 uses NADH to reduce DNQ initiating the redox cycle that kills the cancer cell. Increased levels of NADH upon inhibition of LDH-A may allow for faster or longer cycling of DNQ. Alternatively, the synergy may be due to the decrease in NAD^+ levels. Some suggest that PARP-1 dependent cell death is due to energy depletion (i.e. the rapid decreases in NAD^+ which occurs when NAD^+ is used to build PAR chains in response to DNA damage).[80] Further decrease of NAD^+ due to inhibition of LDH-A may excacerbate this mode of cell death. A final potential mechanism of synergy is that both DNQ and inhibition of LDH-A result in increased ROS production. Transient knockdown of LDH-A as well as inhibition of LDH-A with the small molecule FX-11 have been shown to lead to increased oxygen consumption and ROS production that can be prevented by co-treatment with the

antioxidant NAC.[85] Dr. Hyang Yeon Lee has seen a similar ROS production with NHI-Glc-2 (data not shown). The dual mechanisms of ROS production may result in synergistic cancer cell death. Further studies are needed to confirm which of these mechanisms is responsible for this synergy. Regardless of the mechanism, additional investigations into the therapeutic potential of this combination should be performed.

Predictability of DNQ activity in cell culture: After determining the mechanism of cell death induced by DNQ, we then explored the scope of cancers which are amenable to this cancer-targeted strategy. Both breast cancer (including the especially the difficult to treat TNBC) and lung cancer show good response to both DNQ and its most active derivatives. Additionally, the work presented in this chapter shows that NQO1 is required for the anticancer activity of DNQ against these cell lines. Testing DNQ against panels of other cancer types that commonly overexpress NQO1 such as colon and pancreatic cancer would be useful to further probe its potential scope. Recently, a veterinary medicine student Gosia Pajak found that DNQ has activity against feline squamous cell carcinoma cell lines which over express NQO1. Our collaborator Prof. Tim Fan will be performing further evaluation of these head and neck cancers both in mice and in cats. If successful, this would strongly support the use of DNQ for human head and neck cancers which have been shown to be very similar to those of cats.[86]

While the anticancer activity of DNQ depends on activation by NQO1, the potency of DNQ against different cell lines does not always correlate with the NQO1 activities of these cell lines. Studies performed by Boothman and co-workers with β-Lap suggest that a threshold of NQO1 activity is necessary for activity.[5] Specifically, utilizing isogenic pancreatic cell lines expressing different levels of NQO1, they found that if the cell lines have NQO1 activities over 90 nmol/min/μg protein, they have similar sensitivities to β-Lap. However, studies presented in this Chapter of non-isogenic cancers from the same tissue of origin suggest that sensitivity to NQO1-activated anticancer agents is more complicated than a simple threshold effect. For example the breast

cancer cell lines Hs578t and HCC1937 have similar NQO1 activities (1900 and 1600 nmol/min/µg protein, respectively), but the potency of DNQ is approximately 10-fold lower for Hs578t compared to HCC1937 (IC_{50} = 0.33 and 0.036 µM, respectively, Figure 2.25). Analagous results were seen for lung cancer cell lines A549 and HCC15 that have similar NQO1 activities (2600 and 2800 nmol/min/µg protein, respectively) but drastically different sensitivities to DNQ (IC_{50} = 0.064 and 0.46 µM, respectively, Figure 2.26).

Oxidative Stress Enzymes. One explanation for the difference in potency is that the less sensitive cell lines (i.e. Hs578t and HCC15) express higher levels of enzymes capable of dealing with oxidative stress (e.g. catalase, superoxide dismutase, glutathione-S-transferase, glutathione peroxidase, peroxiredoxin, thioredoxin, and thioredoxin reductase).[87-88] compared to the sensitive cell lines (e.g. HCC1937 and A549). This would ultimately result in these cell lines having reduced amounts of ROS and thus lower levels of DNA damage after treatment with DNQ. Previously, addition of exogenous catalase has been shown to decrease sensitivity to both DNQ and β-Lap in NQO1-overexpressing cell lines.[4,49] Similar results were observed for treatment with β-Lap in combination with either addition of exogeneous superoxide dismutase or forced overexpression of catalase in NQO1 over-expressing cell lines.[49] Analysis of the level of catalase in the breast and lung cancer cell lines investigated here (Figure 2.25 and 2.26) suggest that this does affect sensitivity of the cell line. The less DNQ-sensitive cell lines (Hs578t and HCC15) express higher levels of catalase than more sensitive cell lines (HCC1937 and A549). However, this is not a complete explanation because some sensitive cell lines such as HCC70 and H460 express levels of catalase similar to the less sensitive cell lines. Further investigation into the levels of the other oxidative stress enzymes in these cell lines is needed. If one or several of these enzymes is found to be predictive of response, a diagnostic that examines their level of expression could be developed in order to choose patients that best respond to DNQ. ELISA assays for determination

of catalase,[89] superoxide dismutase,[89] and peroxiredoxin[90] levels in patient tumor samples already exist and could be easily applied for this purpose.

DNA Repair Pathways. Another potential explanation for the difference in sensitivity to DNQ is differences in the DNA repair pathways of these cell lines. The Boothman laboratory has demonstrated that IB-DNQ causes extensive DNA base lesions and single-strand breaks that are converted to lethal double-strand breaks (DSB) during replication (data not shown). In order to avoid death due to these breaks, cancer cells must repair their DNA. A variety of DNA repair pathways exist including mismatch repair (MMR), base-excision repair (BER), nucleotide-excision repair (NER), translesion synthesis (TLS), nonhomologous end joining (NHEJ), and homologous recombination (HR).[91] BER is the primary mode of repairing single-stranded breaks and involves activation of PARP-1 which recruits BER factors such as XRCC1 to the site of injury. HR is the primary mode of repairing double-stranded breaks and unlike NHEJ is known as an "error-free" repair pathway. HR repair depends on multiple enzymes including ATM, CHK2, BRCA1, BRCA2, and PALB2. Many cancers commonly have defects in these DNA repair pathways.[91] One of the most common examples is BRCA1/2 mutations in ovarian and breast cancer. It has been shown that cell lines with these mutations are more sensitive to DNA-damaging agents such as platinum agents compared to cell lines with WT BRCA1/2.[92]

It is possible that the highly DNQ-sensitive cell lines have mutations in DNA damage repair machinery. In agreement with this, the DNQ-sensitive breast cancer cell line HCC1937 is known to have a BRCA1 mutation whereas the less sensitive breast cancer cell line Hs578t has WT BRCA1.[93] However, this is also not a full explanation because the sensitive cell line BT549 is WT in BRCA1 and the less sensitive cell line MDA-MB-436 has a BRCA1 mutation. Further investigations of the sensitivity of BRCA1/2 mutant cell lines is needed before conclusions can be made. Also, other cancer types are known to have mutations in repair pathways (e.g. colorectal cancers have mutations in MMR and HR pathways and prostate cancers have impaired HR and

NER pathways).[91] If BRCA mutations (or mutations in other DNA repair pathways) do turn out to be important predictors for cancer cell sensitivity to DNQ, genetic testing for such mutations is already a commonly performed procedure[94] and could be used to identify patients that would respond to DNQ.

Optimization of DNQ: In order to further explore NQO1-activation as a mechanism to induce cancer cell death, DNQ derivatives were designed that were expected to have different efficiencies as substrates for NQO1. Through a modified version of the synthesis of DNQ, we were able to synthesize these derivatives. Testing of these molecules both *in vitro* and using the previously described cell culture experiments, we were able to identify many derivatives with similar activity and better solubility properties. Additionally, some of the derivatives appear to be much better tolerated by mice than DNQ (e.g. IB-DNQ and 23, Table 2.2). Further exploration of these compounds *in vivo* will more fully elucidate their promise as an anticancer agents. One question that also needs to be addressed is the cause of the dose-limiting toxicity. Discussed below are the two most likely possibilities.

Methemoglobin formation. As noted in this Chapter, DNQ results in methemoglobin formation *in vitro.* Many of the derivatives also cause methemoglobin formation *in vitro*, but all derivatives cause less methemoglobin formation than the parent. Interestingly, we were never able to detect methemoglobin formation *in vivo* in mice although the Boothman laboratory reports having seen it. Additionally, the maximum tolerated dose of the derivatives does not correlate with the *in vitro* methemoglobin formation. Little data exists on how well the *in vitro* assay predicts methemoglobin formation *in vivo.* However, a similar technique is used to detect methemoglobinemia in hospital settings. Specifically, a co-oximeter is used to measure the absorbance of blood at several wavelengths and is capable of accurately calculating the levels of methemoglobin.[95] The similarity in the assay techniques suggests that DNQ likely does cause methemoglobin formation *in vivo*, but methemoglobin formation may not be the main cause of toxicity. Further investigations using

a different assay such as an ELISA assay against methemoglobin or utilizing the co-oximeter used in hospital settings will hopefully aid in elucidating its role in the toxicity of DNQ. If methemoglobin is the dose limiting toxicity of DNQ and a derivative cannot be designed that does not induce methemoglobinemia, the toxicity can likely be controlled. Mild methemoglobinemia is typically treated by supplemental oxygen therapy whereas moderate to severe methemoglobinemia is often handled by treatment with methylene blue.[96] Either of these procedures could be performed along with administration of DNQ to reduce this toxicity.

Reduction by other reductases followed by redox cycling. Cell culture experiments demonstrate that DNQ has selectivity for cancer cell lines that overexpress NQO1. However, if treatment times are extended, DNQ and its derivatives are capable of killing cells that have no active NQO1 (e.g. cell lines with the NQO1*2 polymorphism). While there are many possibilities for how DNQ is killing, it is likely that it is being processed by one electron reductases such as NADPH cytochrome P450 reductase or cytochrome b5 reductase and subsequently redox cycling to produce ROS. Because both of these enzymes are typically expressed in all mammalian cells,[97] reduction of DNQ by these enzymes would result in ROS formation in a variety of tissues, not just cancer tissues, and could explain the toxicity that is observed. Future directions should include determining if DNQ is an *in vitro* substrate for these enzymes. If DNQ is a moderate-to-good substrate for these one electron reductases, derivatives that are poor substrates for the one electron reductases should be investigated. If this is not possible, development of a DNQ prodrug similar to the ester protected quinone that has been developed with β-Lap[98] could decrease the toxicity of the compound by decreasing the amount of free quinone that comes into contact with the one electron reductases.

Overall, the studies described in this Chapter demonstrate the cancer cell selectivity, potency, and outstanding *in vivo* properties of DNQ and its derivatives. This work suggests the great potential of the deoxynyboquinones as a new class of personalized anticancer therapy.

2.5 Materials and methods

2.5.1 Biology materials and methods

Chemicals, reagents, and antibodies. Deoxynyboquinone was synthesized as described.[1] β-Lapachone and dicoumarol were obtained from Prof. David Boothman (UT Southwestern). Streptonigrin, mitomycin C, menadione, Hoechst 33258, hydrogen peroxide (H_2O_2), cytochrome c, propidium iodide, and Sulforhodamine B, resazurin, and ES936 were purchased from Sigma-Aldrich. All quinones and were dissolved in dimethyl sulfoxide (DMSO). Dihydroethidium (DHE, 5 mmol/L in DMSO) was purchased from Invitrogen Life Technologies. RH1 was provided by Prof. David Boothman who obtained it from Dr. David Ross (University of Colorado Health Science Center, Denver, CO). α-NQO1 (A180, Cell Signaling) α-PAR (BD Pharmingen), which detects poly (ADP-ribosyl)ated (PAR) proteins (typically ADP-ribosylated PARP1), and α-PARP1 (sc-8007, Santa Cruz Biotechnology) antibodies were used at 1:4,000 and 1:2,000 dilutions, respectively. Either α-tubulin or α-actin (13E5, Cell signaling) was monitored for loading.

In vitro NQO1 Assay. Deoxynyboquinone, β-Lapachone, and other quinones (0.1 – 100 μM) were monitored as NQO1 substrates using an NADH recycling assay[99] and recombinant NQO1 (Sigma, St. Louis, MO), in which NADH oxidation to NAD^+ was monitored by absorbance (A_{340} nm) on a SpectraMax Plus 384 (Molecular Devices, Sunnyvale, CA). Compounds in DMSO stock (2 μL of 10X stock per well) were added to a 96 well plate. NADH (400 μM) and NQO1 (1.4 μg/mL) in 50 mM potassium phosphate buffer (pH = 7.4) was added to each well (198 μL). Data was recorded at 2 second intervals for 5 minutes. Changes in absorbance were converted to changes in NADH concentration using a calibration curve for NADH. NADH oxidation rates were compared with reactions lacking compound or containing dicoumarol (10 μM). Initial velocities were calculated and data expressed as dicoumarol-inhibited relative units (μmol NADH oxidized/min/μmol protein). Initial velocities were calculated for a variety of concentrations and

Michaelis-Menten curves were generated using KaleidaGraph4 (Syngergy Software, Reading, PA).

Cell Lines and Culture. Cell lines were obtained from either ATCC, the Boothman lab (UT Southwestern), or the Bey lab (WVU). A549, BT549, HCC70, HCC1937, HCC38, HCC1954, HCC1806, DU4475, T47D, H460, H1650, H1299, HCC15, H1993, and H226 cells were grown in RPMI 1640 medium with 10% fetal bovine serum, 100 U/mL penicillin, and 100 µg/mL streptomycin. MCF-7 and IMR90 cells were grown in EMEM with 10% fetal bovine serum, 100 U/mL penicillin, and 100 µg/mL streptomycin. Hs578t and MDA-MB-436 cells were grown in DMEM with 10% fetal bovine serum, 100 U/mL penicillin, and 100 µg/mL streptomycin. MDA-MB-231 cells were grown in RPMI 1640 medium with 10% fetal bovine serum, 100 U/mL penicillin, and 100 µg/mL streptomycin, and 1 µg/mL puromycin to select for transfected cells. H596 and MIA Paca-2 cells were grown in DMEM with 10% fetal bovine serum, 100 U/mL penicillin, and 100 µg/mL streptomycin, and 1 µg/mL puromycin to select for transfected cells. Cells were cultured at 37 °C in a 5% CO_2-95% air humidified atmosphere.

Cytotoxicity Assays. Cells were seeded at 2000 (A549, IMR90, MDA-MB-231, H596, MIA PaCa-2, H460, HCC15, H1299, H1993, H1650), 5000 (MCF-7, HCC70, HCC1806, HCC38, HCC1937, HCC1954, Hs578t, H226, BT549, T47D, MDA-MB-436), or 15,000 (DU4475) cells per well in 96 well plates and allowed to attach overnight. Cells were then treated with various concentrations of compound (0.3 nM to 100 µM unless solubility prevented this; for less soluble compounds 0.03 nM to 10 µM was used). When investigating the effect of dicoumarol, cells were co-treated with vehicle or 25 µM dicoumarol and the compound of interest for 2h with at least five technical replicates. When determining the effect of ES936, cells were pre-treated for 1 h with 100 nM ES936 and then co-treated with 100 nM ES936 and compound of interest for 2h with at least five technical replicates. In either case, drug-free medium was then added and cells were allowed to grow for 48 to 72 hours until control cells reached ~100% confluence. Viability was assessed

using the sulforhodamine B (SRB) assay for the adherent cell lines (all but DU4475).[100] Briefly, cells were fixed with 3% trichloroacetic acid for 1h and then dyed with 0.057% SRB in 1% acetic acid. The dye was solubilized in 10 mM Tris base pH 10.4 and absorption (A_{510} nm) was read on a SpectraMax Plus 384 (Molecular Devices, Sunnyvale, CA). For DU4475, viability was assessed using Alamar blue. Briefly, after 48-72 h 20 µL of Alamary blue (440 µM resazurin in sterile PBS) was added and plates were allowed to incubate for 4-8 h at 37 °C (or until live control were purple/pink and dead control were still blue). Fluorescence was read on an Analyst HT (or or a Molecular Devices SpectraMax 3 (excitation = 555 nm, emission = 585 nm, emission cutoff = 570 nm). Percent death was calculated by subtracting background from all wells and setting 0% death to DMSO-treated controls. Percent death was plotted against concentration and this data was fitted to a Logistic dose response curve $\left(y = \frac{A_1 - A_2}{1+(\frac{x}{x_o})^p} + A_2 \; where \; A_1 = initial \; value, A_2 = final \; value, x_o = center, p = power\right)$ using Origin 9.0.0 (Northampton, MA). Statistical significance was determined using a paired t-test to compare the IC_{50} values. All data are averages of at least 3 independent replicates.

Cytotoxicity Assays performed in the Boothman laboratory. Relative survival assays were assessed as described[8] and correlated well with colony forming assays.[101] Results were reported as means, SE from sextuplate repeats. Experiments were independently repeated 3 times.

Western Blot Analysis. Cells were grown to 70-90% confluency at which point they were trypsinized and harvested. After centrifugation and washing, the cells were lysed with RIPA lysis buffer containing protease inhibitor and cell debris was removed by centrifugation (16000 x *g* for 5 min). Protein concentration was determined by the Pierce BCA Assay (Thermo Scientific, Rockford, IL) and whole cell lysate (20-40 µg) was resolved by 4-20% SDS-PAGE gel electrophoresis at 120 V for 90 min after which proteins were transferred onto nitrocellulose membranes (45 V for 2 h) and blocked in 5% milk TBST overnight at 4 ºC. The membranes were

blotted for molecules of interest with anti-NQO1 (1:2000 in 2% milk TBST), and anti-actin (1:1000 in 2% milk TBST) overnight at 4 ºC. The bound primary antibodies were detected using appropriate secondary HRP conjugated antibodies (1:20000 for NQO1 and 1:10000 for actin in TBST) for 1 hr at room temperature and visualized by ECL autoradiography. The membranes were stripped in acidic methanol and re-probed as necessary.

NQO1 Activity Assay. Cells were grown to 70-90% confluency in T-75 flasks and harvested by trypsinization. Supernatants were prepared as previously described.[99] Cells were washed twice in ice-cold PBS and resuspended in 500 µL of PBS, pH 7.4 containing 10 µg/µL aprotinin. Cell suspensions were sonicated on ice four times using 3 second pulses and then centrifuged at 14000 x *g* for 20 min. Protein concentration was determined using the Pierce BCA Assay (Thermo Scientific, Rockford, IL). The NQO1 activity assay was then performed as previously described.[99,102] Samples containing 0, 10, 25, and 50 µg protein were analyzed. Supernatant was added to a 1-mL quartz cuvette. To this was added the reaction medium containing 77 µM cytochrome c (Sigma), 0.14% bovine serum albumin, 200 µM NADH as the electron donor, and 10 µM menadione as the intermediate electron acceptor in Tris-HCl buffer (50 mM, pH 7.5). The initial rate of change of absorbance (A_{550} nm) was read on a SpectraMax Plus 384 (Molecular Devices, Sunnyvale, CA) and the extinction coefficient for cytochrome c (21.1 $mM^{-1}cm^{-1}$) was used to determine the change in concentration. These experiments were repeated in the presence of 25 µM dicoumarol. NQO1 activity was calculated as the dicoumarol inhibited oxidoreductase activity. At least three independent replicates were performed.

Oxygen consumption rates. Assays were carried out using Seahorse 24-well dishes in conjunction with an XF24 sensor cartridge and a XF24 Extracellular Flux Analyzer (Seahorse Biosciences) as per the manufacturer's instructions. Briefly, 30,000 cells per well were seeded using a 2-step process, and cells grown as above with unseeded background correction wells. O_2 consumption rates (OCR) and proton production rates were measured using the XF24 Analyzer

and Assay Wizard software. Data represent means, %treated/control (T/C,%) SE from quadruplet assessments.

ROS formation. ROS (superoxide) formation was monitored by DHE staining and microscopy. Quantitative data were analyzed using NIH ImageJ software, in which data are means, SE of 100 cells and duplicate experiments conducted in triplicate.

PAR formation. PAR formation in vivo was assessed by Western blotting controlled for α-tubulin. Chemiluminescence ELISA assays, to quantify PAR formation, were carried out by HT PARP in vivo Pharmacodynamic II Assays (Trevigen, Inc.). Untreated or treated cells were incubated with α-PAR antibody, then with goat α-rabbit IgG-horseradish peroxidase. Chemiluminescence by PeroxyGlow assays were expressed as means, SE from 3 independent experiments.

Nucleotide analyses. Changes in intracellular NAD^+ pools were measured using Fluorescent NAD/NADH Detection Kits (Cell Technology, Inc.[103]). NAD^+/NADH levels were graphed as means, SE from at least 3 independent experiments carried out in sextuplets each. Changes in ATP in vivo were measured as described previously[8,71,103] and using a colorimetric/fluorometric assay (BioVision).

PARP1 siRNA knockdown. siRNA specific to the open reading frame of PARP1, 50-CCAAAGGAATTCCGAGAAA-30 (Thermo Fisher Scientific) was transiently transfected into cancer cells. PARP1 knockdown was confirmed using Western blot assays. Results were confirmed using the ON-TARGETplus PARP1 SMARTpool.

TUNEL assays. Terminal deoxynucleotidyl transferase dUTP nick endlabeling (TUNEL) assays were carried out by FC-500 flow cytometry (Beckman Coulter Electronics[70]), and data were means, SE from 3 independent experiments, carried out in triplicate.

Methemoglobin formation.

In vitro Dose Response. 100 µL of human blood (Bioreclamation) was centrifuged at 300 rpm for 5 min. The pellet was washed 3X with 100 µL of PBS and resuspended in 1 mL of PBS. 1 µL of

compound stock was then added to an 0.5 mL eppendorf tube. 99 µL of blood suspension is added to each sample and the solution is gently pipetted up and down to mix. It is then placed in a 37 °C incubator for 1 h. The suspension was then centrifuged at 300 rpm for 5 min. The supernatant was removed and the pellet was washed with 100 µL PBS. The cells were then lysed by resuspending the pellet in 100 µL of PBS with 1% Triton X-100. 10 µL of this solution was added to a well of a 96 well plate and 90 µL of PBS was added. Absorbance was then read at 635 nm. After documenting these absorbances, 4 µL of a 20% potassium ferricyanide was added and allowed to sit for ~5 minutes. Potassium ferricyanide converts all hemoglobin to methemoglobin. Absorbance was then read again at 635 nm.

In vivo Full Spectrum. received 5 treatments of either HPβCD vehicle (control) or DNQ (5 mg/kg every day). On the day of the last treatment, mice were treated and sacrificed after 1 hr. Blood was collected from the posterior vena cava. The blood was then centrifuged for 2 min at 16,000 X g. Plasma and supernatant was removed. The pellet was resuspended in 50 µL of PBS with 1% Triton X-100 and vortexed to lyse. After 30 min sitting on ice, lysis was complete. 1 mL of PBS was added and the samples were centrifuged for 5 min at 16,000 X g. Diluted 1:10 in PBS and read on a UV-Vis for MHb formation (scan of 300 – 700 nm).

Pharmacokinetic assessments. Mice were dosed IV with either 30 mg/kg of β-Lap or 10 mg/kg DNQ formulated with hydroxypropyl-β-cyclodextrin as described previously.[72] At varying times after dosing, the mice were sacrificed and whole blood isolated with an ACD (acidified sodium citrate-dextrose) coated syringe and needle. Samples were taken out to 120 mins for β-Lap and 1440 mins for DNQ. Plasma was isolated from whole blood by centrifugation at 4ºC for 10 mins at 9,300xg. For β-Lap: 100 µL of plasma was mixed with 200 µL of acetonitrile. Samples were vortexed 15 s and set at room temperature for 10 mins. 700 µL of ddH2O was added and the samples were vortexed. Samples were spun for 5 mins at 16,100xg. The supernatant was collected and 1 mL of ddH2O was added. The supernatant solution was then loaded onto an

Oasis HLB 3cc extraction column (Waters) that had been previously washed with 2 mL MeOH and equilibrated with 2 mL dH2O. The sample column was then washed twice with 2 mL of 5% MeOH/95% dH2O. The sample was eluted with 2 mL of 100% MeOH. 2 mL of ddH2O and 0.2% formic acid were added to the sample and then analyzed by HPLC/MS/MS using an Applied Biosystems/MDS Sciex 3200-QTRAP coupled to a Shimadzu Prominence LC. Chromatography conditions were as follows. Buffer A consisted of 25% Isopropanol/75% HPLC grade H2O + 0.1% formic acid. Buffer B consisted of 25% Isopropanol/75% Methanol + 0.1% formic acid. The column flow rate was 0.5 ml/min using a Phenomenex Synergi Fusion RP 75 X 2 mM, 4 micron packing column. The gradient conditions were: 0-2 min 100% A, 2-3 min gradient to 100% B, 3-7 min 100% B, 7-7.5 min gradient to 100% A, 7.5-8.5 min 100%A. β-Lap was detected in MRM mode following the 243.1 to 187.2 transition. Back-calculation of standard curve and quality control samples were accurate to within 25% for 74% of these samples at concentrations ranging from 5 to 10000 ng/ml. For DNQ, 100 µl of plasma was mixed with 400 µl of acetonitrile containing 0.5% formic acid and 10 ng/ml tolbutamide (internal standard, Sigma-Aldrich). Samples were vortexed 15 s and set at room temperature for 10 mins. Samples were spun for 5 mins at 16,100xg. The supernatant (480 µL) was removed and spun a second time for 5 mins at 16,100xg. The supernatant was then analyzed by HPLC/MS/MS again using an Applied Biosystems/MDS Sciex 3200-QTRAP coupled to a Shimadzu Prominence LC. Chromatography conditions were as follows. Buffer A consisted of HPLC grade dH2O + 0.1% formic acid and Buffer B consisted of MeOH + 0.1% formic acid. The column flow rate was 0.5 ml/min using a Phenomenex Synergi Fusion RP 75 X 2 mM, 4 micron packing column. The gradient conditions were as for β-Lap. Both DNQ and tolbutamide were monitored in MRM mode following the 283.0 to 255.0 transition for DNQ and the 269.1 to 169.9 transition for tolbutamide. Back-calculation of standard curve and quality control samples were accurate to within 20% for 75% of these samples at concentrations ranging from 1 ng/ml to 10,000 ng/ml.

LLC Murine Model.

Antitumor efficacy. LLC cells (0.5 X 10^6) were intravenously injected into the tail veins of female (~22 g) athymic nude mice. Two days later, randomized groups of mice (5 per group) were treated intravenously with hydroxypropyl-β-cyclodextrin (HPβCD) vehicle alone, or β-Lapachone (30 mg/kg) or deoxynyboquinone (2.5–10 mg/kg) dissolved in HPbCD,[72] every other day for 5 injections; mice treated with HPβCD (600 or 1,000 mg/kg for β-Lapachone or deoxynyboquinone, respectively) did not influence tumor growth or survival. Later (18 days posttumor inoculation), mice were euthanized, lungs removed, and average lung wet weights of tumor-bearing minus control nontumor-bearing animals calculated. Lungs were visually examined to confirm LLC nodules. Tumors and associated normal lung tissue were also assessed for PARP1 hyperactivation (PAR formation) and ATP loss. Experiments were carried out twice and average lung wet weights graphed/group.

Survival. LLC-bearing mice were treated with HPβCD alone, β-Lap-HPbCD (30 mg/kg), or DNQ-HPbCD (5 mg/kg) as above and monitored for changes in weight and survival, and Kaplan-Meier curves generated. P values were reported with asterisks. All animal protocols have Institutional Animal Care and Use Committee approval (#2008-1080, UT Southwestern).

Molecular Modeling of DNQ in NQO1. DNQ (or derivative) was built and a 10 Å water layer was built around the molecule. The DNQ structure was then energy minimized using MOE[29] with a MMFF94x forcefield using gas phase calculations and a cutoff of 0.01. Charges were then fixed using an MMFF94 forcefield. The NQO1 structure was downloaded from the PDB (1DXO).[27] One of the homodimers was extracted and protonated. DNQ was then modeled into the protein active site, using the site of duroquinone to identify the active site. It was docked using the Dock program in MOE which uses Triangle Matching for the placement of the small molecule and London dG for rescoring of the placement of the small molecule. Using LigX, the top configuration was protonated and energy minimized.

Maximum Tolerated Dose Studies for DNQ derivatives.

Compound Preparation. First, compounds were dissolved in the excipient HPβCD. It had previously been noted that DNQ and its derivatives have much higher solubility in basic solutions[31] so basic HPβCD is initially used. Briefly, 60 mM HPβCD is made basic by the addition of 1-2 drops of 10 M NaOH (final pH ~11 to 12). Solid DNQ or a derivative is weighed into a vial and HPβCD is added to the appropriate concentration. The slurry is then vortexed and sonicated until all solid dissolves. The solution is then brought back to pH 7.5 to 8.5 with 1 M HCl. Note: if the solution is made more acidic than pH 7.5, the compound will fall out of solution.

Compound administration. Maximum tolerated dose (MTD) was tested in 6-8 week old female C57BL/6 mice (Charles River). Briefly, a dose of compound was administered to three mice via intraperitoneal injection (i.p.) using insulin syringes. The mice were then monitored for toxicity for at 1, 4, 8, 12, and 24 h. Criteria used to judge toxicity will include excess weight loss (>20% of aged match control), unhealthy appearance (for example, ruffled coat, hunched posture, distended abdomen), prolonged diarrhea and diuresis, and respiratory diseases. If life-limiting toxicity (defined above) was during the first 24 hours, the animals were removed from the study and humanely euthanized. Also, this dose was established as the MTD. If no clinical signs were observed in the mice 24 hours after the first compound administration, the next dose was be administered and observations were made in the same manner as described previously. If at any point during the 5 days of treatment life-limiting toxicity is observed, the mice were humanely euthanized and this dose will be established as the MTD. If the 5 continuous days of treatment of the lowest dose did not result in any significant toxicity, this same procedure was followed for the next dose with three naïve mice. As long as no toxicity was observed, this process was repeated with three naïve mice for each increasing dose. All animal protocols have Institutional Animal Care and Use Committee approval (#11178, UIUC).

A548 Murine Model. Ten million A549 cells were prepared in HBSS and injected subcutaneously on the right flank of sedated (ketamine/xylazine) female athymic nude mice (NCI Frederick). By three hours postinjection the injection bleb was no longer evident. By day 30, tumors that were

~80 mm^3 had formed and thus treatment began on that day. Mice were randomized into three treatment groups of 10 mice each: vehicle (950 mg/kg HPβCD), DNQ (5 mg/kg formulated in HPβCD), and **23** (22 mg/kg formulated in HPβCD). Mice received a total of 19 treatments (Days 2-6, 12-16, 22-26, 32-35) all injected i.p. Tumors were measured and volumes calculated using the formula $V = 0.5LW^2$ where V = volume, L = length, and W = width. Mice were sacrificed on day 80 and tumors were excised and weighed. All animal protocols have Institutional Animal Care and Use Committee approval (#11178, UIUC).

4T1 Murine Model. 100,000 4T1 cells were injected into right flank of Balb/c mice. Mice were then treated with either β-Lap (20 mg/kg), IB-DNQ (15 mg/kg), or a β-Lap ester prodrug in micelles (GB-085, 30 mg/kg). Each treatment was given i.v. every 4 days for a total of 4 treatments. This was all the information which Prof. Gao provided. All animal protocols have Institutional Animal Care and Use Committee approval (UT Southwestern).

Catalase Activity Assay. This assay was performed by Jessica White (an undergraduate at UIUC). The assay was performed using the Invitrogen Amplex Red Catalase Assay kit according to its instructions.

2.5.2 Chemistry materials and methods

General chemical reagents were purchased from Sigma Aldrich. Metal catalysts and ligands were purchased from Strem Chemicals Inc. (Newburyport, MA). Alkynes were purchased from GFS Chemicals (Powell, OH) and bis-pinacolboronate was purchased from Frontier Scientific (Logan, UT). All reagents were used without further purification unless otherwise noted. Solvents were dried by passage through columns packed with activated alumina (THF, CH_2Cl_2, diethyl ether) or activated molecular sieves (DMSO). Amines were freshly distilled over CaH_2 under a nitrogen atmosphere. Reactions involving n-BuLi were performed using standard Schlenk techniques under argon

^{1}H-NMR and ^{13}C-NMR spectra were recorded on Varian Unity spectrometers at 500 MHz and 125 MHz, respectively. Spectra generated from a solution of $CDCl_3$ were referenced to residual chloroform (^{1}H: δ 7.26 ppm, ^{13}C: δ 77.16 ppm). Spectra generated in mixtures of $CDCl_3$ and CD_3OD were referenced to CD_3OD (^{1}H: δ 3.31 ppm, ^{13}C: δ 49.0 ppm). Spectra generated from d-TFA were referenced to residual H (^{1}H: δ 11.50 ppm) or F_3CCO_2D (^{13}C: δ 164.2 ppm).

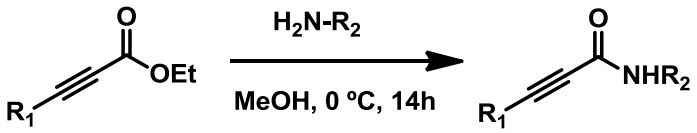

General protocol A: Amidation of ester

To a solution of alkynyl ester (1 equiv.) in methanol (1 M), chilled in an ice-water bath was added alkyl amine (1.2 equiv.). The reaction was stirred at 0 ºC for 14h. The solvent was evaporated directly from the flask and the residue was separated by silica gel chromatography (9:1 hexanes:ethyl acetate to 1:1 hexanes:ethylacetate) to yield the desired alkynyl amide as a mixture of rotamers.

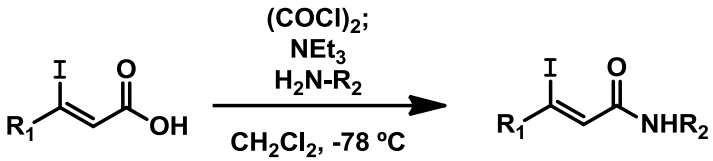

General protocol B: Amidation of acid chloride

To an oven-dried Schlenk flask with a stirbar was added the iodoacid and the flask was evacuated and backfilled with argon. Dry CH_2Cl_2 (0.4 M iodoacid) was added and the solution was chilled on an ice-water bath. Oxalyl chloride (3 equiv.) was added by syringe and the cold bath was removed. After 5h at room temperature the volatile components were evaporated directly from the flask. Dry CH_2Cl_2 (0.5 M) was added to the residual oil and the vial was chilled on a dry ice/isopropanol bath. Freshly distilled p-methoxybenzyl amine (1.1 equiv.) was added dropwise by syringe followed by NEt_3 (1.2 equiv.). The mixture was stirred for 10 minutes then was allowed to warm to RT. 1 M HCl (1.5 mL per mmol) was added and the solution was poured into a separatory funnel with CH_2Cl_2 (1.5 mL per mmol), shaken and separated. The aqueous fraction was extracted with CH_2Cl_2 (0.8 mL per mmol, 3 times) then dried over $MgSO_4$ and evaporated. The residue was purified by silica gel chromatography.

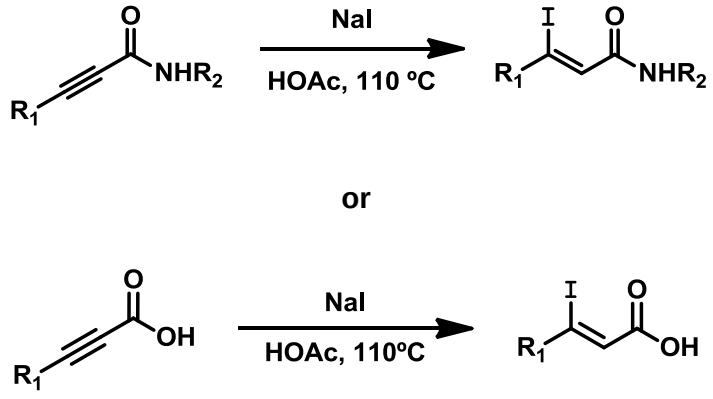

General protocol C: Hydroiodination

Alkynyl amide (1 equiv.), NaI (2 equiv.), and acetic acid (10 equiv.) were combined and heated to 110 ºC for 8h. Reaction completion was determined by removing aliquots for ^{1}H-NMR analysis.

The deep red reaction mixture was diluted with water (1-2 mL per mmol alkyne) and CH_2Cl_2 (3-4 mL per mmol alkyne), treated with $NaHSO_3$ until colorless, and carefully neutralized with a saturated aqueous solution of $NaHCO_3$. This mixture was poured into a separatory funnel with CH_2Cl_2, shaken and separated. The aqueous fraction was extracted with CH_2Cl_2 (4-5 mL per mmol alkyne, 2 times). The combined organic fractions were washed with brine, dried over $MgSO_4$, and evaporated to yield the desired iodoamide.

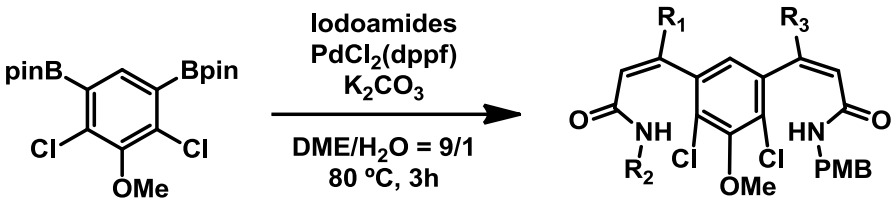

General protocol D: Suzuki cross-coupling

To a Schlenk flask with a stir bar was added pure (recrystallized) 2,6-dichloro-3,5-bis(pinacolboronato)anisole (**70**)[1] (1 equiv.), $PdCl_2$(dppf) (20 mol%), K_2CO_3 (6 equiv.), and both desired iodoamides (1.3 equiv. of amide bearing PMB, 1.5 equiv. of *N*-alkyl amide) and the flask was evacuated and backfilled with argon three times. Water (1 mL per mmol bispinacolboronate) and DME (9 mL per mmol bispinacolboronate) were added by syringe after degassing the solvents by bubbling with argon for 45 minutes. The flask was plunged into an oil bath at 80 ºC for 3h. The mixture was poured into a separatory funnel and diluted with water (12-13 mL per mmol bispinacolboronate). The mixture was extracted with EtOAc (12-13 mL per mmol bispinacolboronate, 2 times). The combined organic extracts were dried over $MgSO_4$, filtered and evaporated to a deep red oil. The crude product was dissolved in CH_2Cl_2 and separated by silica gel chromatography (100:0 to 70:30 to 30:70 to 0:100 hexanes:ethyl acetate). The purity of the diamide product was highly variable and the product was subjected to intramolecular amidation without further purification.

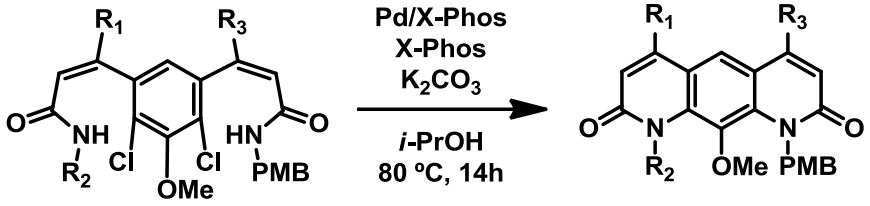

General protocol E: Intramolecular aryl amidation

In a Schlenk flask or a vial with a Teflon-lined cap were combined the diamide starting material, K_2CO_3 (6 equiv.), Pd/X-Phos (10 mol%), and X-Phos (10 mol%). The flask was cycled between vacuum and argon three times and argon-sparged *i*-PrOH (20-30 mL per mmol diamide) was added by syringe. The mixture was heated to 80 ºC with stirring for 14h. Insoluble materials were removed by filtration through Celite and rinsed with CH_2Cl_2. The filtrate was evaporated and the residue was used directly in the next step.

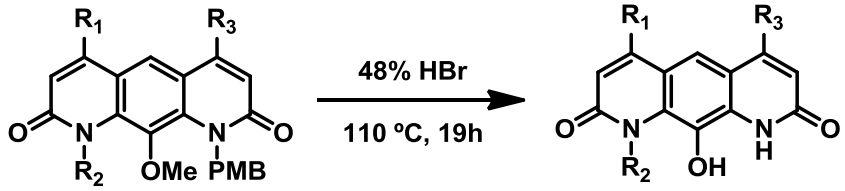

General protocol F: HBr deprotection

The crude diazaanthracene was dissolved in 48% HBr (12-13 mL per mmol diazaanthracene) and heated to 110 ºC. After 19 hours the reaction was removed from heat. The mixture was cooled on an ice bath and was carefully rendered basic by adding 10 M NaOH. The residual solid was removed by filtration through hardened filter paper and discarded. The filtrate was rendered acidic with 1 M HCl, whereupon a colloidal precipitate formed. The mixture was then centrifuged (3220 x g for 5 minutes). The resulting semi-compact gelatinous solid was collected by filtration through

hardened filter paper and dried to a constant mass under vacuum to yield the desired diazaanthracenol in frequently high purity as assessed by NMR.

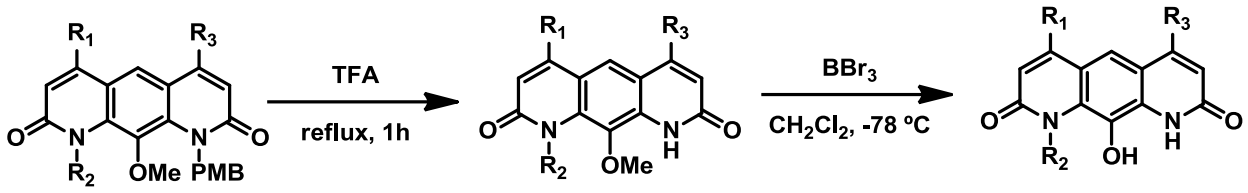

General protocol G: TFA and BBr_3 deprotection

For substrates that proved sensitive to global deprotection by HBr, the following protocol was employed.

The product of intramolecular amidation (General Protocol E) was dissolved in TFA (15-20 mL per mmol) and heated to reflux for 1h. The solvent was then evaporated and the residue was purified by silica gel chromatography (DCM, 0-5% MeOH).

In a Schlenk flask containing the PMB-deprotected material under Ar was added DCM (70 mL per mmol) and the solution was cooled in a dry ice/isopropanol bath. BBr_3 (6 equiv.) was added by syringe and the solution was stirred until starting material was consumed as shown by TLC. Residual BBr_3 was quenched by the addition of conc. $NaHCO_3$ solution until pH neutral. The solvents were evaporated. The residue was taken directly to oxidation (General Protocol H) without further purification.

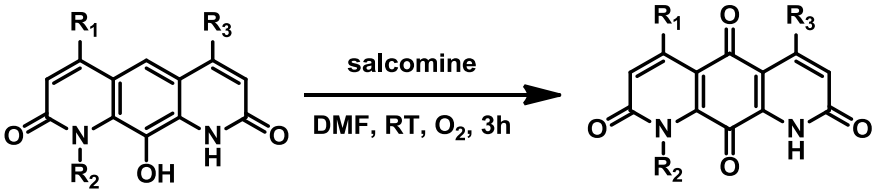

General protocol H: Oxidation

To a flask containing the diazaanthracenol starting material was added salcomine (10 mol%) and DMF (~0.02 to 0.04 mL per mg of impure diazaanthracenol). A balloon containing O_2 was fitted over the mouth of the flask and the slurry was stirred at room temperature. The solid dissolved after about 30 minutes. After 3h stirring, the mixture was diluted with one volume each of DCM and hexanes and loaded directly onto a chromatography column consisting of a layer of basic alumina (5 cm) under a layer of silica gel (5 cm) prepared in DCM. The column was flushed with increasing amounts of methanol (0-2%) in DCM until the red product band entered the alumina layer which retained the product, allowing coeluting impurities to be removed. The product was then released from the basic alumina by adding 1% HOAc to the mobile phase. The red fractions were evaporated and purified by chromatography through silica gel (0-5% MeOH in DCM) to yield the desired DNQ derivative as an orange, red, or red-pink solid.

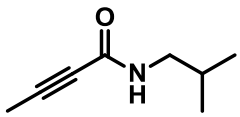

27

Synthesized from ethyl-2-butynoate and isobutylamine by General Protocol A. 50% yield. Compound is a light yellow oil at rt.

^{1}H-NMR ($CDCl_3$, 500 MHz): δ 5.78 (bs, 1H, major rotamer, N*H*), 3.21 (t, 2H, *J* = 6.5 Hz, minor rotamer, NCH_2), 3.10 (t, 2H, *J* = 6.5 Hz, major rotamer, NCH_2), 2.01 (s, 3H, minor rotamer, allylic CH_3), 1.93 (s, 3H, major rotamer, allylic CH_3), 1.78 (sept, 1H, *J* = 6.5 Hz, major rotamer, C*H*), 0.94 (d, 6H, *J* = 7.0 Hz, minor rotamer CH(CH_3)$_2$), 0.91 (d, 6H, *J* = 6.5 Hz, major rotamer, CH(CH_3)$_2$)

^{13}C-NMR ($CDCl_3$, 125 MHz) δ 153.68 (major), 83.17 (major), 75.11 (major), 50.90 (minor), 47.15 (major), 29.56 (minor), 28.50 (major), 20.16 (major), 19.96 (minor), 4.13 (minor), 3.80 (major)

HRMS (ESI) calcd for $C_8H_{14}NO$ $(M+H)^+$: 140.1075, found: 140.1070.

Melting Point Not determined (oil).

IR (cm^{-1}, thin film in CCl_4): 3450 (w), 3292 (b, m), 3062 (b, w), 2962 (m), 2254 (m), 1654 (s), 1544 (s), 1468 (m) 1275 (m), 1006 (w).

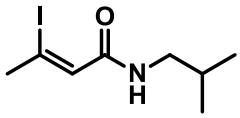

28

Synthesized from **27** by General Protocol C. 95% yield. Compound is a yellow/orange solid.

^{1}H-NMR ($CDCl_3$, 500 MHz): δ 6.25 (q, 1H, *J* = 1.0 Hz, vinyl C*H*), 5.75 (bs, 1H, N*H*), 3.17 (t, 2H, *J* = 6.5 Hz, NCH_2), 2.66 (d, 3H, *J* = 1.5 Hz, allylic CH_3), 1.85 (sept, 1H, *J* = 6.5 Hz, C*H*), 0.95 (d, 6H, *J* = 6.5 Hz, CH(CH_3)$_2$)

^{13}C-NMR ($CDCl_3$, 125 MHz) δ 165.00, 129.73, 105.42, 46.97, 35.78, 28.50, 20.37.

HRMS (ESI-TOF) calcd for $C_8H_{15}NOI$ $(M+H)^+$: 268.0198, found: 268.0197.

Melting Point: 49.3-51.2 °C

IR (cm^{-1}, thin film in $CHCl_3$): 3450 (m), 3280 (b, m), 3060 (b, w), 2962 (m), 1650 (s), 1620 (m), 1430 (w), 1410 (w), 1370 (w), 1330 (w), 1230 (w), 1160 (m).

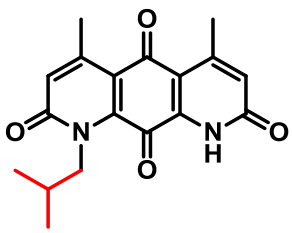

2

Synthesized from **70**,[1] (Z)-3-iodo-N-(4-methoxybenzyl)but-2-enamide,[1] and **28** by General Protocols D, E, F, and H. 9% yield over 4 steps. Compound is an orange/red solid at rt.

^{1}H-NMR ($CDCl_3$ 500 MHz): δ 6.78 (d, 1H, *J* = 1.0 Hz, vinyl C*H*), 6.67 (d, 1H, *J* = 1.5 Hz, vinyl C*H*), 4.64 (d, 2H), 2.62 (d, 3H, *J* = 1.0 Hz, allylic CH_3), 2.60 (d, 3H, *J* = 1.0 Hz, allylic CH_3), 1.88 (sept, 1H, *J* = 7.0 Hz, C*H*), 0.93 (d, 6H, *J* = 6.5 Hz, CH(CH_3)$_2$).

^{13}C-NMR ($CDCl_3$, 125 MHz): δ 181.71, 175.38, 161.47, 160.73, 151.21, 149.01, 138.99, 137.93, 128.64, 128.35, 120.11, 114.49, 50.58, 29.83, 23.49, 22.33, 20.07.

HRMS (ESI-TOF) calcd for $C_{18}H_{19}N_2O_4$ $(M+H)^+$: 327.1345, found: 327.1347.

Melting Point >250 °C.

IR (cm^{-1}, thin film in $CDCl_3$): 1676 (m), 1653 (b, s), 1607 (m), 1592 (m), 1467 (w), 1401 (w), 1376 (m), 1350 (w), 1290 (m), 1203 (w), 1101 (w).

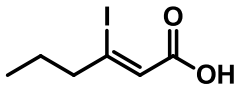

29

Synthesized from 2-hexynoic acid by General Protocol C. 83% yield. Compound is an off-white solid at rt.

^{1}H-NMR ($CDCl_3$, 500 MHz): δ 6.40 (t, 1H, *J* = 1.2 Hz, vinyl C*H*), 2.71 (dt, 2H, *J* = 1.2 Hz, 7.2 Hz, allylic CH_2), 1.65 (sext, 2H, *J* = 7.2 Hz, CH_2CH_2), 0.93 (t, 3H, *J* = 7.2 Hz, CH_2CH_3)

^{13}C-NMR ($CDCl_3$, 125 MHz): δ 169.78, 125.11, 124.62, 50.35, 22.69, 12.83.

HRMS (ESI-TOF) calcd for $C_6H_{11}NOI$ $(M+Na)^+$: 262.9545, found: 262.9555.

Melting Point: 55.2-55.8 °C.

IR (cm^{-1}, thin film in $CDCl_3$): 2964 (b, s), 2709 (m), 2596 (m), 1704 (s), 1616 (s), 1464 (m), 1405 (s), 1311 (s), 1240 (s), 1212 (s).

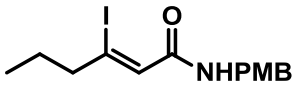

30

Synthesized from **29** and 4-methoxybenzylamine by General Protocol B. 99% yield. Compound is an off-white solid.

^{1}H-NMR ($CDCl_3$, 400 MHz): δ 7.23 (d, 2H, *J* = 8.8 Hz, aryl C*H*), 6.84 (d, 2H, *J* = 8.8 Hz, aryl C*H*), 6.26 (s, 1H, vinylic C*H*), 5.96 (bs, 1H, N*H*), 4.42 (d, 2H, *J* = 5.6 Hz, NCH_2), 3.77 (s, 3H, OCH_3), 2.54 (t, 2H, *J* = 7.2 Hz, allylic CH_2), 1.57 (sext, 2H, *J* = 7.2 Hz), 0.88 (t, 3H, *J* = 7.2 Hz)

^{13}C-NMR ($CDCl_3$, 125 MHz): δ 164.85, 159.10, 129.96, 129.49, 128.40, 114.42, 114.10, 55.36, 49.06, 43.15, 22.49, 12.84.

HRMS (ESI-TOF) calcd for $C_{14}H_{19}NO_2I$ $(M+H)^+$: 360.0461, found: 360.0471.

Melting Point: 57.2-59.2 °C.

IR (cm^{-1}, thin film in $CDCl_3$): 3421 (b, s), 3262 (s), 3033 (m), 2959 (s), 2835 (w), 1618 (s), 1514 (s), 1460 (m), 1303 (w), 1237 (m), 1177 (w), 1038 (w).

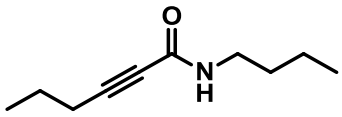

31

Synthesized by from ethyl-2-hexynoate and butylamine by General Protocol A. 68% yield. Compound is a pale yellow oil.

^{1}H-NMR ($CDCl_3$, 500 MHz): δ 6.07 (s, 1H, minor rotamer, N*H*), 5.95 (s, 1H, major rotamer, N*H*), 3.35 (dq, 2H, minor rotamer, *J* = 7.0 Hz, 2.0 Hz, NCH_2), 3.24 (dq, 2H, major rotamer, *J* = 7.0 Hz, 2.0 Hz, NCH_2), 2.22 (dt, 2H, *J* = 7.0 Hz, 2.0 Hz, allylic CH_2), 1.54 (dq, 2H, *J* = 7.0 Hz, 2.0 Hz), 1.46 (quint, 2H, *J* = 7.0 Hz), 1.32 (sext, 2H, *J* = 7.5 Hz), 0.96 (dt, 3H, *J* = 7.0 Hz, 2.0 Hz), 0.88 (dt, 3H, *J* = 7.5 Hz, 2.0 Hz)

^{13}C-NMR ($CDCl_3$, 125 MHz): δ 153.68 (major), 93.69 (minor), 86.89 (major), 75.87 (major), 73.56 (minor), 43.14 (minor), 39.59 (major), 32.71 (minor), 31.45 (major), 21.37 (major), 20.60 (major), 20.08 (major), 19.76 (minor), 13.73 (major), 13.56 (major).

HRMS (ESI) calcd for $C_{10}H_{15}NO$ $(M+H)^+$: 168.1388, found: 168.1382.

Melting Point Not determined (oil).

IR (cm^{-1}, thin film in CCl_4): 3588 (m), 3294 (b, m), 3060 (b, w), 2964 (m), 2247 (m), 2221 (m), 1637 (s), 1515 (s), 1460 (m), 1278 (m), 1095 (w).

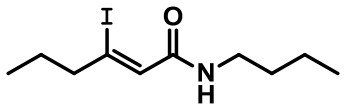

32

Synthesized from **31** by General Protocol C. 98% yield. Compound is a yellow/brown oil.

^{1}H-NMR ($CDCl_3$, 500 MHz): δ 6.26 (s, 1H, vinyl C*H*), 3.25 (q, 2H, *J* = 7.0 Hz), 2.51 (t, 2H, *J* = 7.5 Hz), 1.54 (sext, 2H, *J* = 7.5 Hz), 1.48 (pent, 2H, *J* = 7.5 Hz), 1.32 (sext, 2H, *J* = 8.0 Hz), 0.86 (t, 3H, *J* = 7.0 Hz), 0.85 (t, 3H, *J* = 7.5 Hz).

^{13}C-NMR ($CDCl_3$, 125 MHz): δ 165.13, 128.87, 113.51, 49.01, 39.36, 31.54, 22.51, 20.27, 13.81, 12.83.

HRMS (ESI-TOF) calcd for $C_{10}H_{19}NOI$ $(M+H)^+$: 296.0511, found: 296.0503.

Melting Point Not determined (oil).

IR (cm^{-1}, thin film in $CHCl_3$): 3439 (m), 3324 (b, m), 3073 (w), 2965 (m), 1655 (s), 1621 (m), 1467 (m), 1335(w), 1283 (w), 1239 (w), 1204 (w), 1087 (w).

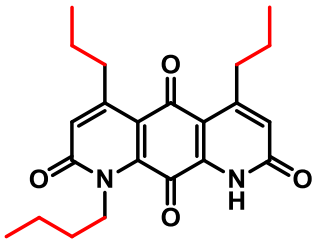

3

Synthesized from **70**, **30**, and **32** by General Protocols D, E, F, and H. 13% yield over 4 steps. Compound is a red/pink solid.

^{1}H-NMR ($CDCl_3$, 500 MHz): δ 9.67 (s, 1H, N*H*), 6.77 (s, 1H, vinyl C*H*), 6.68 (s, 1H, vinyl C*H*), 4.49 (m, 2H), 2.98 (t, 2H, *J* = 7.0 Hz, allylic CH_2), 2.95 (t, 2H, *J* = 7.0 Hz, allylic CH_3), 1.69 (pent, 2H, *J* = 8.5 Hz, C*H*), 1.72-1.65 (m, 2H), 1.65-1.55 (m, 4H), 1.47 (sext, 2H, *J* = 7.5 Hz), 1.03 (t, 3H, *J* = 7.0 Hz), 1.03 (t, 3H, *J* = 7.5 Hz), 1.00 (t, 3H, *J* = 7.5 Hz, CH_3).

^{13}C-NMR ($CDCl_3$, 125 MHz): δ 181.70, 175.33, 161.47, 160.79, 155.34, 153.19, 139.15, 138.01, 127.93, 127.62, 120.10, 114.69, 46.31, 37.09, 36.23, 31.41, 23.25, 22.98, 20.40, 14.28, 14.14, 13.93.

HRMS (ESI-TOF) calcd for $C_{22}H_{27}N_2O_4$ $(M+H)^+$: 383.1971, found: 383.1969.

Melting Point: >200 °C.

IR (cm^{-1}, thin film in $CHCl_3$): 2940 (b, w), 1649 (b, s), 1587 (w), 1382 (w), 1299 (w), 1281 (w), 1254 (w).

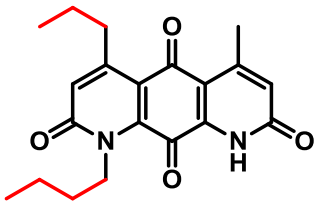

4

Synthesized from **70**, (Z)-3-iodo-N-(4-methoxybenzyl)but-2-enamide, and **32** by General Protocols D, E, F, and H. 6.3% yield over 4 steps. Compound is a pink/red solid at rt.

^{1}H-NMR ($CDCl_3$, 500 MHz): δ 9.46 (s, 1H, N*H*), 6.77 (s, 1H, vinyl C*H*), 6.67 (d, 1H, *J* = 1.0 Hz, vinyl C*H*), 4.50 (m, 2H), 2.97 (t, 2H, *J* = 7.5 Hz, allylic CH_2), 2.61 (d, 3H, *J* = 1.0 Hz, allylic CH_3), 1.69 (pent, 2H, *J* = 8.0 Hz), 1.60 (sext, 2H, *J* = 7.5 Hz), 1.47 (sext, 2H, *J* = 8.0 Hz), 1.03 (t, 3H, *J* = 7.5 Hz, CH_3), 0.99 (t, 3H, *J* = 7.5 Hz, CH_3).

^{13}C-NMR ($CDCl_3$, 125 MHz): δ 181.73, 175.37, 161.47, 160.91, 153.23, 151.31, 139.49, 137.78, 128.40, 127.82, 119.67, 114.98, 46.35, 39.15, 31.40, 23.14, 22.40, 20.40, 14.28, 13.93.

HRMS (ESI-TOF) calcd for $C_{20}H_{23}N_2O_4$ $(M+H)^+$: 355.1658, found: 355.1655.

Melting Point: >270 °C.

IR (cm^{-1}, thin film in $CDCl_3$): 1680 (m), 1651 (s), 1608 (m), 1535 (w), 1458 (w), 1396 (w), 1368 (w), 1281 (w), 1153 (w), 1108 (w).

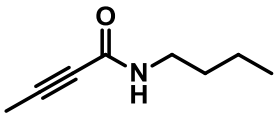

33

Synthesized from ethyl-2-butynoate and butylamine by General Protocol A. 78% yield. Compound is a clear, colorless oil at rt.

^{1}H-NMR ($CDCl_3$, 500 MHz): δ 6.01 (bs, 1H), 3.34 (q, 2H, *J* = 7.0 Hz, minor rotamer NC*H*$_2$), 3.23 (q, 2H, *J* = 6.0 Hz, major rotamer NC*H*$_2$), 1.98 (s, 3H, minor rotamer allylic C*H*$_3$), 1.89 (s, 3H, major rotamer allylic C*H*$_3$), 1.46 (pent, 2H, *J* = 7.0 Hz), 1.31 (sext, 2H *J* = 7.5 Hz), 0.88 (t, 3H, *J* = 7.5 Hz).

^{13}C-NMR ($CDCl_3$, 125 MHz): δ 153.71 (major), 89.96 (major), 75.13 (major), 45.15 (minor), 41.57 (major), 23.92 (minor), 22.69 (major), 11.39 (major), 11.18 (minor), 3.69 (major).

HRMS (ESI-TOF) calcd for $C_8H_{14}NO$ $(M+H)^+$: 140.1075, found: 140.1071.

Melting Point Not determined (oil).

IR (cm^{-1}, thin film, neat): 3512 (b, w), 3271 (m), 3066 (w), 2954 (m), 2878 (m), 2257 (m), 2216 (w), 1651 (s), 1538 (s), 1285 (m), 1226 (w), 1150 (w).

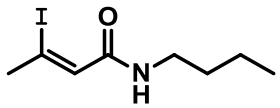

34

Synthesized from **33** by General Protocol C. 97% yield. Compound is a light yellow/brown oil.

^{1}H-NMR ($CDCl_3$, 500 MHz): δ 6.23 (d, 1H. *J* = 1.5 Hz, vinyl C*H*), 3.26 (q, 2H, *J* = 7.0 Hz, NC*H*$_2$), 2.59 (d, 3H, *J* = 1.5 Hz, allylic C*H*$_3$), 1.48 (p, 2H, *J* = 7.5 Hz), 1.32 (sext, 2H, *J* = 7.5 Hz), 0.87 (t, 3H, *J* = 7.5 Hz).

^{13}C-NMR ($CDCl_3$, 125 MHz): δ 164.93, 129.47, 105.41, 39.35, 35.75, 31.55, 20.26, 13.83.

HRMS (ESI-TOF) calcd for $C_8H_{15}NOI$ $(M+H)^+$: 268.0198, found: 268.0197.

Melting Point Not determined (oil).

IR (cm^{-1}, thin film in $CHCl_3$): 3441 (m), 3324 (b,m), 3073 (b, w), 2965 (m), 1653 (s), 1628 (s), 1515 (s), 1435 (m), 1331 (w), 1269 (w), 1232 (m), 1154 (w), 1080 (w).

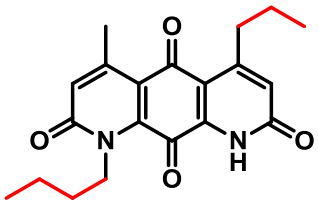

5

Synthesized from **70**, **30**, and **34** by General Protocols D, E, F, and H. 6.7% yield over 4 steps. Compound is a pink/red solid at rt.

^{1}H-NMR ($CDCl_3$, 500 MHz): δ 9.52 (s, 1H, N*H*), 6.77 (d, 1H, *J* = 1.0 Hz, vinyl C*H*), 6.68 (s, 1H, vinyl C*H*), 4.52-4.49 (m, 2H), 2.99 (t, 2H, *J* = 7.5 Hz, allylic CH_2), 2.59 (d, 3H, *J* = 1.0 Hz, allylic CH_3), 1.68 (pent, 2H, *J* = 7.5 Hz), 1.61 (sext, 2H, *J* = 8.0 Hz, $CH_2CH_2CH_3$), 1.47 (sext, 2H, *J* = 8.0 Hz, $CH_2CH_2CH_3$), 1.04 (t, 3H, *J* = 7.5 Hz, CH_3), 1.00 (t, 3H, *J* = 7.5 Hz, CH_3).

^{13}C-NMR ($CDCl_3$, 125 MHz): δ 181.67, 175.28, 161.28, 160.96, 155.41, 149.27, 138.84, 138.25, 128.69, 127.59, 120.12, 114.40, 46.20, 36.30, 31.40, 23.53, 22.88, 20.39, 14.13, 13.92.

HRMS (ESI-TOF) calcd for $C_{20}H_{23}N_2O_4$ $(M+H)^+$: 355.1658, found: 355.1658.

Melting Point: >270 °C.

IR (cm^{-1}, thin film in $CHCl_3$): 1677 (w), 1651 (b, s), 1604 (w), 1555(w), 1455 (w), 1399 (w), 1306 (w), 1285 (w), 1212 (w), 1108 (w).

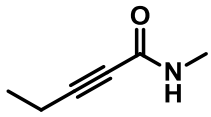

35

Synthesized from ethyl-2-pentynoate and methylamine by General Protocol A. 78% yield. Compound is a yellow oil at rt.

^{1}H-NMR ($CDCl_3$, 500 MHz): δ 5.95 (bs, 1H), 2.99 (d, 3H, *J* = 5.0 Hz, minor rotamer), 2.82 (d, 3H, *J* = 5.0 Hz, major rotamer), 2.37 (t, 2H, *J* = 7.0 Hz, minor rotamer), 2.27 (t, 2H, *J* = 7.0 Hz, major rotamer), 1.20 (t, 3H, *J* = 7.5 Hz, minor rotamer), 1.15 (t, 3H, *J* = 7.5 Hz, major rotamer).

^{13}C-NMR ($CDCl_3$, 125 MHz): δ 157.11 (minor), 154.40 (major), 95.38 (minor), 87.96 (major), 74.62 (major), 72.25 (minor), 29.56 (minor), 26.17 (major), 12.66 (minor), 12.58 (major), 12.33 (minor), 12.40.

HRMS (ESI-TOF) calcd for $C_6H_{10}NO$ $(M+H)^+$: 112.0762, found: 112.0765.

Melting Point Not determined (oil).

IR (cm^{-1}, thin film in $CHCl_3$): 3501 (w), 3282 (b, m), 3069 (w), 2981 (m), 2259 (m), 2223 (m), 1629 (s), 1540 (s), 1413 (m), 1317 (m), 1286 (m), 1162 (w).

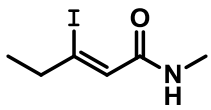

36

Synthesized from **35** by General Protocol C. 92% yield. Compound is a yellow/brown oil.

^{1}H-NMR ($CDCl_3$, 500 MHz): δ 6.28 (q, 1H. *J* = 1.5 Hz, vinyl C*H*), 5.9 (bs, 1H, N*H*), 2.88 (d, 3H, *J* = 5.0 Hz, NCH_3), 2.62 (dq, 2H, *J* = 1.5 Hz, 7.5 Hz, allylic CH_2), 1.11 (t, 3H, *J* = 7.5 Hz, -CH_3).

^{13}C-NMR ($CDCl_3$, 125 MHz): δ 166.14, 127.91, 115.56, 40.94, 26.39, 14.67.

HRMS (ESI-TOF) calcd for $C_6H_{11}NOI$ $(M+H)^+$: 239.9885, found: 239.9885.

Melting Point Not determined (oil).

IR (cm^{-1}, thin film in $CHCl_3$): 3455 (m), 3323 (b, m), 3082 (b, w), 2978 (m), 1653 (s), 1626 (m), 1524 (m), 1411 (w), 1342 (w), 1292 (w), 1220 (m), 1161 (w), 1069 (w).

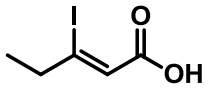

37

Synthesized from 2-pentynoic acid by General Protocol C. 91% yield. Compound is an off-white solid.

^{1}H-NMR ($CDCl_3$, 500 MHz): δ 6.40 (t, 1H, *J* = 1.0 Hz, vinyl C*H*), 2.78 (dq, *J* = 7.5 Hz, 1.0 Hz, 2H, allylic CH_2), 1.16 (t, 3H, *J* = 7.5 Hz, CH_2CH_3)

^{13}C-NMR ($CDCl_3$, 125 MHz): δ 169.66, 126.56, 123.62, 42.36, 14.72.

HRMS (ESI-TOF) calcd for C_5H_7NOI $(M+H)^+$: 225.9491, found: 225.9507.

Melting Point: 67.0-67.9 °C.

IR (cm^{-1}, thin film in $CHCl_3$): 3233 (b, m), 2703 (w), 2578 (w), 1694 (s), 1626 (s), 1455 (m), 1418 (w), 1310 (w), 1237 (m), 1077 (w).

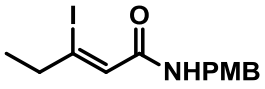

38

Synthesized from **37** and 4-methoxybenzylamine by General Protocol B. 84% yield. Compound is an off-white/light yellow solid.

^{1}H-NMR ($CDCl_3$, 400 MHz): δ 7.23 (d, 2H, *J* = 8.4 Hz, aryl C*H*), 6.83 (d, 2H, *J* = 8.8 Hz, aryl C*H*), 6.26 (s, 1H, vinylic C*H*), 6.01 (bs, 1H, N*H*), 4.42 (d, 2H, *J* = 5.6 Hz, NCH_2), 3.76 (s, 3H, OCH_3), 2.61 (q, 2H, *J* = 7.6 Hz, allylic CH_2), 1.08 (t, 3H, *J* = 7.2 Hz)

^{13}C-NMR ($CDCl_3$, 125 MHz): δ165.00, 159.04, 129.95, 129.44, 127.41, 115.90, 114.06, 55.34, 43.11, 40.91, 14.55.

HRMS (ESI-TOF) calcd for $C_{13}H_{17}NO_2I$ $(M+H)^+$: 346.0304, found: 346.0308.

Melting Point: 60.7-63.3 °C.

IR (cm^{-1}, thin film in $CDCl_3$): 3519 (w), 3283 (b, s), 3059 (m), 2970 (m), 2834 (m), 1651 (s), 1505 (s), 1455 (m), 1250 (m), 1175 (m), 1033 (m).

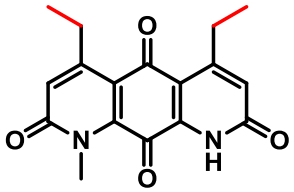

6

Synthesized from **70**, **36**, and **38** by General Protocols D, E, F, and H. 17% yield over 4 steps. Compound is a pink amorphous solid.

^{1}H-NMR ($CDCl_3$, 500 MHz): δ 10.28 (bs, 1H), 6.83 (s, 1H, vinyl C*H*), 6.75 (s, 1H, vinyl C*H*), 3.93 (s, 3H), 3.07 (dq, 2H, *J* = 7.5 Hz, 1.0 Hz), 3.04 (dq, 2H, *J* = 7.5 Hz, 1.0 Hz), 1.25 (t, 3H, *J* = 7.5 Hz), 1.24 (t, 3H, *J* = 7.5 Hz).

^{13}C-NMR (2:1 $CDCl_3$:CD_3OD, 125 MHz): δ 181.29, 175.34, 162.29, 162.15, 157.28, 155.52, 140.00, 138.78, 33.96, 27.90, 27.27, 13.62, 13.34.

HRMS (ESI-TOF) calcd for $C_{17}H_{17}N_2O_4$ $(M+H)^+$: 313.1188, found: 313.1193.

Melting Point: >280 °C.

IR (cm^{-1}, thin film in $CDCl_3$): 1684 (w), 1648 (s), 1604 (w), 1580 (w), 1507 (w), 1406 (w), 1363 (w), 1289 (w), 1153 (w), 1101 (w).

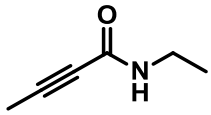

39

Synthesized from ethyl-2-butynoate and ethylamine by General Protocol A. 83% yield. Compound is a pale yellow oil.

^{1}H-NMR ($CDCl_3$, 500 MHz): δ 6.25 (bs, 1H), 3.35 (pent, 2H, *J* = 7.0 Hz, minor rotamer NC*H*$_2$), 3.23 (pent, 2H, *J* = 7.5 Hz, major rotamer), 1.95 (s, 3H, minor rotamer), 1.85 (s, 3H, major rotamer), 1.12 (t, 3H, *J* = 7.5 Hz, minor rotamer), 1.08 (t, 3H, *J* = 7.0 Hz, major rotamer).

^{13}C-NMR ($CDCl_3$, 125 MHz): δ 153.58 (major), 82.80 (major), 75.05 (major), 38.20 (minor), 34.66 (major), 15.91 (minor), 14.51 (major), 3.93 (minor), 3.59 (major).

HRMS (ESI) calcd for $C_6H_{10}NO$ $(M+H)^+$: 112.0762, found: 112.0764.

Melting Point Not determined (oil).

IR (cm^{-1}, neat): 3438 (m), 3291 (b, m), 3066 (b, w), 2983 (m), 2240 (m), 2209 (m), 1641 (s), 1520 (s), 1437 (m), 1379 (w), 1283 (m), 1149 (w).

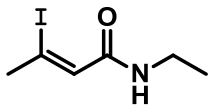

40

Synthesized from **39** by General Protocol C. 98% yield. Compound is a pale yellow/brown oil.

^{1}H-NMR ($CDCl_3$, 500 MHz): δ 6.28 (bs, 1H, N*H*), 6.22 (s, 1H, vinyl C*H*), 3.30 (pent, 2H, *J* = 7.5 Hz, NCH_2), 2.59 (s, 3H, allylic CH_3), 1.12 (s, 3H).

^{13}C-NMR ($CDCl_3$, 125 MHz): δ 164.85, 129.28, 105.58, 35.75, 34.45, 14.74.

HRMS (ESI-TOF) calcd for $C_6H_{11}NOI$ $(M+H)^+$: 139.9885, found: 139.9884.

Melting Point Not determined (oil).

IR (cm^{-1}, thin film in $CHCl_3$): 3441 (m), 3322 (b, m), 3073 (b,w), 2976 (m), 1653 (s), 1626 (m), 1515 (m), 1432 (m), 1375 (w), 1326 (w), 1269 (w), 1211 (m), 1152 (w), 1080 (m).

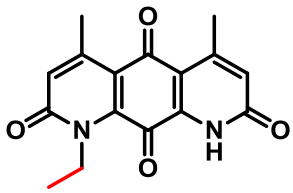

7

Synthesized from **70**, (Z)-3-iodo-N-(4-methoxybenzyl)but-2-enamide, and **40** by General Protocols D, E, F, and H. 13% yield over 4 steps. Compound is a red/orange solid at rt.

^{1}H-NMR (2:1 $CDCl_3$:CD_3OD, 500 MHz): δ 6.76 (d, 1H, *J* = 1.0 Hz, vinyl C*H*), 6.67 (d, 1H, *J* = 1.0 Hz, vinyl C*H*), 4.51 (q, 2H, *J* = 8.0 Hz), 2.36 (m, 6H, allylic C*H*$_3$), 1.45 (t, 3H, *J* = 7.0 Hz).

^{13}C-NMR ($CDCl_3$, 125 MHz): δ 182.06, 175.64, 162.52, 162.29, 152.29, 150.66, 140.21, 139.27, 127.93, 127.71, 119.94, 115.35, 42.97, 23.42, 22.39, 14.36.

HRMS (ESI-TOF) calcd for $C_{16}H_{15}N_2O_4$ $(M+H)^+$: 299.1032, found: 299.1034.

Melting Point: >280 °C.

IR (cm^{-1}, thin film in $CHCl_3$): 1680 (w), 1647 (b, s), 1601 (w), 1580 (w), 1374 (m), 1292 (m), 1161 (m).

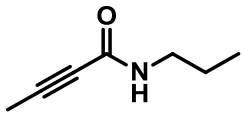

41

Synthesized from ethyl-2-butynoate and propylamine by General Protocol A. 71% yield. Compound is a clear, colorless oil.

^{1}H-NMR ($CDCl_3$, 500 MHz): δ 5.99 (bs, 1H), 3.35 (q, 2H, *J* = 7.0 Hz, minor rotamer NC*H*$_2$), 3.24 (q, 2H, *J* = 7.5 Hz, major rotamer NC*H*$_2$), 2.02 (s, 3H, minor rotamer allylic C*H*$_3$), 1.93 (s, 3H, major rotamer allylic C*H*$_3$), 1.53 (sext, 2H, *J* = 7.5 Hz), 0.93 (t, 3H, *J* = 7.5 Hz).

^{13}C-NMR ($CDCl_3$, 125 MHz): δ 156.60 (minor), 153.62 (major), 89.57 (minor), 82.71 (major), 74.90 (major), 72.54 (minor), 44.97 (minor), 41.34 (major), 23.68 (minor), 22.43 (major), 11.21 (major), 10.98 (minor), 3.83 (minor), 3.50 (major).

HRMS (ESI-TOF) calcd for $C_7H_{12}NO$ $(M+H)^+$: 126.0919, found: 126.0914

Melting Point Not determined (oil).

IR (cm^{-1}, thin film in $CHCl_3$): 3441 (m), 3300 (b, m), 3066 (b, w), 2967 (m), 2249 (s), 2224 (m), 1649 (s), 1517 (s), 1440 (w), 1272 (m), 1162 (w).

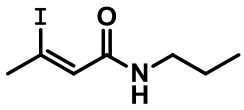

42

Synthesized from **41** by General Protocol C. 98% yield. Compound is a clear, colorless oil.

^{1}H-NMR ($CDCl_3$, 500 MHz): δ 6.23 (d, 1H. *J* = 1.5 Hz, vinyl C*H*), 6.22 (bs, 1H, N*H*), 3.23 (d, 2H, *J* = 7.0 Hz, NCH_2), 2.60 (d, 3H, *J* = 1.5 Hz, allylic CH_3), 1.53 (sext, 2H, *J* = 7.0 Hz), 0.90 (t, 3H, 7.5 Hz).

^{13}C-NMR ($CDCl_3$, 125 MHz): δ 164.98, 129.47, 105.47, 41.34, 35.76, 22.77, 11.61.

HRMS (ESI-TOF) calcd for $C_7H_{13}NOI$ $(M+H)^+$: 254.0042, found: 254.0044.

Melting Point Not determined (oil).

IR (cm^{-1}, thin film in $CHCl_3$): 3437 (m), 3324 (b, m), 3073 (b, w), 2967 (m), 1654 (s), 1628 (m), 1513 (m), 1455 (w), 1428 (w), 1377 (w), 1338 (w), 1283 (w), 1154 (w), 1080 (w).

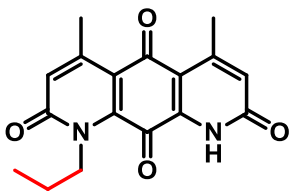

8

Synthesized from **70**, (Z)-3-iodo-N-(4-methoxybenzyl)but-2-enamide, and **42** by General Protocols D, E, F, and H. 13% yield over 4 steps. Compound is a red/orange solid.

^{1}H-NMR ($CDCl_3$, 500 MHz): δ 6.77 (d, 1H, *J* = 1.0 Hz, vinyl C*H*), 6.68 (d, 1H, *J* = 1.5 Hz, vinyl C*H*), 4.60 (m, 2H), 2.62 (d, 3H, *J* = 1.5 Hz, allylic CH_3), 2.60 (d, 3H, *J* = 1.0 Hz, allylic CH_3), 1.73 (sext, 2H, *J* = 8.0 Hz, C*H*), 1.04 (t, 3H, *J* = 7.5 Hz).

^{13}C-NMR ($CDCl_3$, 125 MHz): δ 182.08, 175.69, 162.52, 162.38, 152.31, 150.63, 140.01, 139.25, 127.94, 127.73, 120.05, 115.39, 48.50, 23.45, 22.77, 22.38, 11.29.

HRMS (ESI-TOF) calcd for $C_{17}H_{17}N_2O_4$ $(M+H)^+$: 313.1188, found: 313.1192.

Melting Point: >260 °C.

IR (cm^{-1}, thin film in $CDCl_3$:MeOH, 2:1): 1651 (b, s), 1557 (w), 1535 (w), 1401 (w), 1289 (w), 1153 (w), 1094 (w).

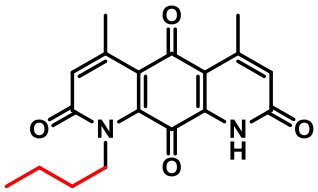

9

Synthesized from **70**, (Z)-3-iodo-N-(4-methoxybenzyl)but-2-enamide, and **34** by General Protocols D, E, F, and H. 9.9% yield over 4 steps. Compound is a red solid.

^{1}H-NMR ($CDCl_3$, 500 MHz): δ 9.54 (bs, 1H), 6.77 (q, 1H, *J* = 1.0 Hz, vinyl C*H*), 6.68 (q, 1H, *J* = 1.0 Hz, vinyl C*H*), 4.53-4.50 (m, 2H), 2.62 (d, 3H, *J* = 1.0 Hz, allylic CH_3), 2.60 (d, 3H, *J* = 1.0 Hz, allylic CH_3), 1.68 (pent, 2H, *J* = 7.5 Hz), 1.47 (sext, 2H, *J* = 7.5 Hz), 1.00 (t, 3H, *J* = 7.5 Hz).

^{13}C-NMR ($CDCl_3$, 125 MHz): δ ^{13}C NMR (126 MHz, CD_3OD) δ 181.79, 175.38, 162.20, 162.06, 152.03, 150.29, 139.65, 138.89, 127.71, 127.50, 119.82, 115.11, 48.76, 31.16, 29.76, 23.20, 22.14, 20.27, 13.61.

HRMS (ESI-TOF) calcd for $C_{18}H_{19}N_2O_4$ $(M+H)^+$: 327.1345, found: 327.1358.

Melting Point: >270 °C.

IR (cm^{-1}, thin film in $CDCl_3$): 1670 (m), 1651 (b, s), 1609 (w), 1587 (w), 1466 (w), 1401 (w), 1375 (w), 1289 (w), 1157 (w), 1100 (w), 1046 (w).

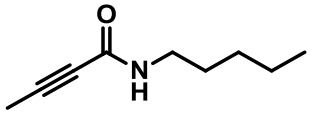

43

Synthesized from ethyl-2-butynoate and pentylamine by General Protocol A. 86% yield. Compound is a clear, colorless oil.

^{1}H-NMR ($CDCl_3$, 500 MHz): δ 5.91 (bs, 1H), 3.35 (q, 2H, minor rotamer, *J* = 6.8 Hz, NC*H*$_2$), 3.24 (q, 2H, major rotamer, *J* = 6.8 Hz, NC*H*$_2$), 1.99 (s, 3H, minor rotamer, allylic C*H*$_3$), 1.90 (s, 3H, major rotamer, allylic C*H*$_3$), 1.48 (quint, 2H, *J* = 7.2 Hz), 1.28 (m, 4H), 0.86 (t, 3H, *J* = 6.8 Hz)

^{13}C-NMR ($CDCl_3$, 125 MHz): δ 156.37 (minor), 153.54 (major), 89.39 (minor), 82.51 (major), 74.86 (major), 72.49 (minor), 43.15 (minor), 39.57 (major), 30.01 (minor), 28.82 (major), 28.74 (major), 28.45 (minor), 22.13 (major), 22.05 (minor), 13.75 (major), 3.71 (minor), 3.39 (major) .

HRMS (ESI) calcd for $C_9H_{16}NO$ $(M+H)^+$: 154.1232, found: 154.1231.

Melting Point: Not determined (oil).

IR (cm^{-1}, thin film in $CDCl_3$): 3498 (m), 3270 (b, s), 3063 (m), 2933 (s), 2861 (m), 2256 (m), 2216 (m), 1651 (s), 1539 (s), 1455 (m), 1373 (m), 1288 (m), 1211 (w), 1149 (w).

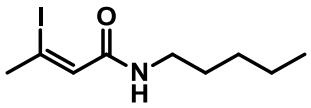

44

Synthesized from **43** by General Protocol C. 81% yield. Compound is a pale yellow/brown oil.

^{1}H-NMR ($CDCl_3$, 500 MHz): δ 6.22 (d, 1H. *J* = 1.5 Hz, vinyl C*H*), 5.77 (bs, 1H, N*H*), 3.32 (q, 2H, *J* = 7.0 Hz, NCH_2), 2.64 (d, 3H, *J* = 1.5 Hz, allylic CH_3), 1.55 (pent, 2H, *J* = 7.0 Hz), 1.35-1.30 (m, 4H), 0.89 (t, 3H, *J* = 7.0 Hz)

^{13}C-NMR ($CDCl_3$, 125 MHz): δ 164.60, 128.78, 105.36, 39.36, 35.62, 29.00, 28.92, 22.19, 13.87.

HRMS (ESI-TOF) calcd for $C_9H_{17}NOI$ $(M+H)^+$: 282.0355, found: 282.0356.

Melting Point: Not determined (oil).

IR (cm^{-1}, thin film in $CDCl_3$): 3498 (m), 3288 (b, s), 3072 (m), 2928 (s), 2859 (s), 1651 (s), 1618 (s), 1557 (s), 1434 (m), 1374 (m), 1337 (m), 1228 (m), 1149 (w), 1087 (m).

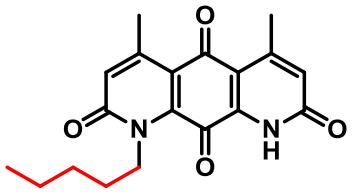

10

Synthesized from **70**, (Z)-3-iodo-N-(4-methoxybenzyl)but-2-enamide, and **44** by General Protocols D, E, F, and H. 11% yield over 4 steps. Compound is a red amorphous solid.

^{1}H-NMR (2:1 $CDCl_3$:CD_3OD, 500 MHz): δ 6.76 (d, 1H, *J* = 1.0 Hz, vinyl C*H*), 6.67 (d, 1H, *J* = 1.5 Hz, vinyl C*H*), 4.48-4.43 (m, 2H), 2.63 (d, 3H, *J* = 1.5 Hz, allylic C*H*$_3$), 2.63 (d, 3H, *J* = 1.0 Hz, allylic C*H*$_3$), 1.77 (pent, 2H, *J* = 7.5 Hz), 1.48-1.40 (m, 4H), 0.95 (t, 3H, *J* = 7.0 Hz).

^{13}C-NMR (2:1 $CDCl_3$:CD_3OD, 125 MHz): δ 181.47, 175.05, 161.83, 161.68, 151.66, 149.89, 139.31, 138.53, 127.40, 127.19, 119.45, 114.75, 28.82, 28.48, 22.87, 22.07, 21.81, 13.58.

HRMS (ESI-TOF) calcd for $C_{19}H_{21}N_2O_4$ $(M+H)^+$: 341.1501, found: 341.1496.

Melting Point: >250 °C.

IR (cm^{-1}, thin film in $CDCl_3$): 1683 (m), 1651 (b, s), 1613 (m), 1591 (w), 1471 (w), 1399, (w), 1368 (w), 1290 (w), 1160 (w), 1053 (w).

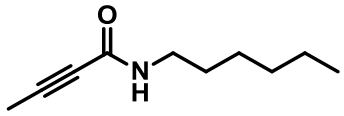

45

Synthesized from ethyl-2-butynoate and hexylamine by General Protocol A. 79% yield. Compound is a white crystalline solid.

^{1}H-NMR ($CDCl_3$, 500 MHz): δ 5.95 (bs, 1H, major rotamer N*H*), 3.34 (q, 2H, *J* = 7.0 Hz, minor rotamer), 3.23 (q, 2H, *J* = 7.0 Hz, major rotamer), 1.98 (s, 3H, minor rotamer), 1.89 (s, 3H, major rotamer), 1.47 (pent, 2H, *J* = 7.0 Hz), 1.33-1.23 (m, 6H), 0.84 (t, 3H, *J* = 7.0 Hz).

^{13}C-NMR ($CDCl_3$, 125 MHz) δ 153.58 (major), 82.92 (major), 75.05 (major), 43.37 (minor), 39.85 (major), 31.49 (major), 30.56 (minor), 29.33 (major), 26.57 (major), 26.22 (minor), 22.59 (major), 14.06 (major), 3.69 (major).

HRMS (ESI) calcd for $C_{10}H_{18}NO$ $(M+H)^+$: 168.1388, found: 168.1391.

Melting Point: 39.0-39.8 °C.

IR (cm^{-1}, thin film in $CHCl_3$): 3540 (b, s), 2957 (m), 2858 (w), 2252 (w), 2222 (w), 1635 (s), 1541 (m), 1458 (w), 1291 (w).

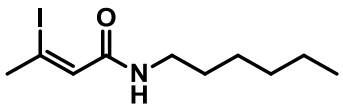

46

Synthesized from **45** by General Protocol C. 98% yield. Compound is a light yellow/brown oil.

^{1}H-NMR ($CDCl_3$, 500 MHz): δ 6.22 (q, 1H. *J* = 1.5 Hz, vinyl C*H*), 5.73 (bs, 1H, N*H*), 3.32 (q, 2H, *J* = 7.0 Hz), 2.64 (d, 3H, *J* = 1.5 Hz, allylic CH_3), 1.55 (pent, 2H, *J* = 7.0 Hz), 1.38-1.27 (m, 6H), 0.88 (t, 3H, *J* = 7.0 Hz).

^{13}C-NMR ($CDCl_3$, 125 MHz) δ 164.51, 128.65, 105.27, 39.35, 35.58, 31.27, 29.14, 26.49, 22.33, 13.83.

HRMS (ESI-TOF) calcd for $C_{10}H_{19}NOI$ $(M+H)^+$: 296.0511, found: 296.0510.

Melting Point Not determined (oil).

IR (cm^{-1}, thin film in $CDCl_3$): 3291 (b, s), 3070 (m), 2954 (s), 2857 (s), 1654 (s), 1625 (m), 1542 (m), 1458 (m), 1437 (m), 1375 (w), 1339 (w), 1226 (m), 1078 (w).

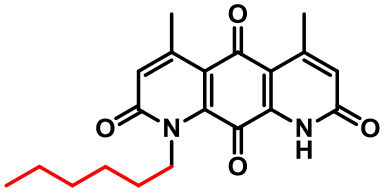

11

Synthesized from **70**, (Z)-3-iodo-N-(4-methoxybenzyl)but-2-enamide, and **46** by General Protocols D, E, F, and H. 12% yield over 4 steps. Compound is a pink/red solid.

^{1}H-NMR (2:1 $CDCl_3$:CD_3OD, 500 MHz): δ 6.76 (s, 1H), 6.67 (s, 1H), 4.45 (m, 2H), 2.63 (d, 3H, *J* = 1.0 Hz, allylic C*H*$_3$), 2.63 (d, 3H, *J* = 1.0 Hz, allylic C*H*$_3$), 1.76 (pent, 2H, *J* = 7.5 Hz), 1.46 (pent, 2H, *J* = 7.0 Hz), 1.40-1.34 (m, 4H), 0.92 (t, 3H, *J* = 7.0 Hz).

^{13}C-NMR (2:1 $CDCl_3$:CD_3OD, 125 MHz): δ181.46, 175.04, 161.82, 161.66, 151.65, 149.88, 139.30, 138.53, 127.40, 127.20, 119.44, 114.74, 46.57, 31.18, 28.76, 26.36, 22.87, 22.35, 21.81, 13.58.

HRMS (ESI-TOF) calcd for $C_{20}H_{23}N_2O_5$ $(M+H)^+$: 355.1658, found: 355.1660.

Melting Point: >250 °C.

IR (cm^{-1}, thin film in $CDCl_3$): 1677 (m), 1651 (b, s), 1613 (m), 1586 (m), 1469 (w), 1434 (w), 1402 (m), 1386 (m), 1328 (w), 1291 (m), 1150 (w), 1102 (m), 1060 (w).

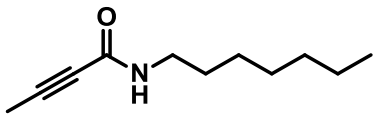

47

Synthesized from ethyl-2-butynoate and heptylamine by General Protocol A. 72% yield. Compound is white crystalline solid.

^{1}H-NMR ($CDCl_3$, 500 MHz): δ 5.95 (bs, 1H, N*H*), 3.34 (q, 2H, *J* = 7.0 Hz, minor rotamer NC*H*$_2$), 3.22 (dt, 2H, *J* = 7.0 Hz, major rotamer), 1.98 (s, 3H, minor rotamer), 1.89 (s, 3H, major rotamer), 1.47 (pent, 2H, *J* = 7.5 Hz), 1.30-1.20 (m, 8H), 0.84 (t, 3H, *J* = 7.0 Hz).

^{13}C-NMR ($CDCl_3$, 125 MHz): δ 156.51 (minor), 153.65 (major), 89.75 (minor), 82.97 (major), 75.14 (major), 72.80 (minor), 43.44 (minor), 39.93, (major), 31.84 (major), 30.67 (minor), 29.44 (major), 29.04 (major), 28.97 (minor), 26.94 (major), 26.59 (minor), 22.69 (major).

HRMS (ESI-TOF) calcd for $C_{11}H_{20}NO$ $(M+H)^+$: 182.1545, found: 182.1550.

Melting Point: 50.1-52.2 °C.

IR (cm^{-1}, thin film in $CHCl_3$): 3449 (b, s), 2960 (m), 2250 (w), 2202 (w), 1636 (s), 1278 (m).

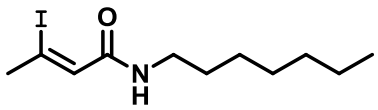

48

Synthesized from **47** by General Protocol C. 86% yield. Compound is a pale yellow oil.

^{1}H-NMR ($CDCl_3$, 500 MHz): δ 6.24 (q, 1H. *J* = 1.5 Hz, vinyl C*H*), 5.73 (bs, 1H, N*H*), 3.33 (q, 2H, *J* = 6.5 Hz), 2.65 (d, 3H, *J* = 1.5 Hz, allylic CH_3), 1.55 (pent, 2H, *J* = 7.0 Hz), 1.38-1.23 (m, 8H), 0.88 (t, 3H, *J* = 7.0 Hz).

^{13}C-NMR ($CDCl_3$, 125 MHz): δ 164.72, 129.06, 105.40, 39.52, 35.68, 31.68, 29.37, 28.92, 26.95, 22.52, 14.02.

HRMS (ESI-TOF) calcd for $C_{11}H_{21}NOI$ $(M+H)^+$: 310.0668, found: 310.0654.

Melting Point Not determined (oil).

IR (cm^{-1}, thin film in $CHCl_3$): 3289 (b, s), 3069 (m), 2926 (s), 2855 (s), 1651 (b, s), 1539 (s), 1435 (m), 1229 (m), 1077 (w).

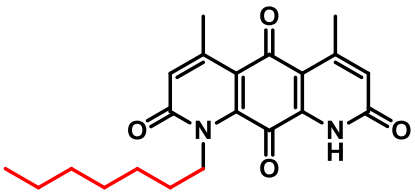

12

Synthesized from **70**, (Z)-3-iodo-N-(4-methoxybenzyl)but-2-enamide, and **48** by General Protocols D, E, F, and H. 10% yield over 4 steps. Compound is an orange solid.

^{1}H-NMR (2:1 $CDCl_3$:CD_3OD, 500 MHz): δ 6.76 (q, 1H, *J* = 1.5 Hz, vinyl C*H*), 6.66 (q, 1H, *J* = 1.0 Hz, vinyl C*H*), 4.47-4.44 (m, 2H), 2.63 (d, 3H, *J* = 1.0 Hz, allylic CH_3), 2.63 (d, 3H, *J* = 1.0 Hz, allylic CH_3), 1.77 (bpent, 2H, *J* = 8.0 Hz), 1.46 (bpent, 2H, *J* = 8.0 Hz), 1.42-1.26 (m, 6H), 0.90 (t, 3H, *J* = 7.0 Hz).

^{13}C-NMR ($CDCl_3$, 125 MHz): δ 182.01, 175.59, 162.40, 162.24, 152.24, 150.46, 139.86, 139.09, 127.95, 127.73, 120.01, 115.32, 47.14, 32.13, 29.39, 29.26, 27.23, 23.43, 22.89, 22.37, 14.20.

HRMS (ESI-TOF) calcd for $C_{21}H_{25}N_2O_4$ $(M+H)^+$: 369.1814, found: 369.1811.

Melting Point: >220 °C.

IR (cm^{-1}, thin film in $CHCl_3$): 1651 (b, s), 1611 (m), 1587 (w), 1397 (w), 1323 (w), 1292 (w), 1177 (w), 1102 (w).

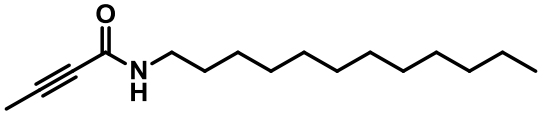

49

Synthesized from ethyl-2-butynoate and dodecylamine by General Protocol A. 72% yield. Compound is a white amorphous solid.

^{1}H-NMR ($CDCl_3$, 500 MHz): δ 5.72 (bs, 1H, major rotamer N*H*), 5.64 (bs, 1H, minor rotamer N*H*), 3.37 (q, 2H, *J* = 7.0 Hz, minor rotamer NCH_2), 3.26 (q, 2H, *J* = 7.0 Hz, major rotamer NCH_2), 2.01 (d, 3H, *J* = 1.0 Hz, minor rotamer allylic CH_3), 1.93 (d, 3H, *J* = 1.0 Hz, major rotamer allylic CH_3), 1.50 (pent, 2H, *J* = 7.0 Hz), 1.34-1.20 (m, 18H), 0.87 (t, 3H, *J* = 7.0 Hz).

^{13}C-NMR ($CDCl_3$, 125 MHz): δ 153.61 (major), 82.73 (major), 75.05 (major), 43.36 (minor), 39.81 (major), 31.92 (major), 30.55 (minor), 29.66 (major), 29.64 (major), 29.61(major), 29.56 (major), 29.37 (major), 29.31 (2C, major), 26.90 (major), 26.53 (minor), 22.69 (major), 14.12 (major), 3.95 (minor), 3.62 (major).

HRMS (ESI-TOF) calcd for $C_{16}H_{30}NO$ $(M+H)^+$: 252.2327, found: 252.2327.

Melting Point: 63.4-64.6 °C.

IR (cm^{-1}, thin film in $CDCl_3$): 3300 (b, w), 3273 (m), 3059 (w), 2956 (w), 2918 (m), 2848 (m), 2258 (w), 2216 (w), 1645 (w), 1615 (s), 1541 (m), 1474 (m), 1296 (w).

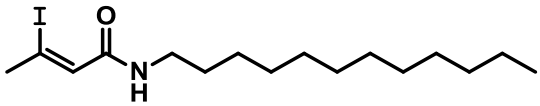

50

Synthesized from **49** by General Protocol C. 98% yield. Compound is an off-white solid.

^{1}H-NMR ($CDCl_3$, 500 MHz): δ 6.22 (q, 1H. *J* = 1.5 Hz, vinyl C*H*), 5.93 (bs, 1H, N*H*), 3.29 (q, 2H, *J* = 6.0 Hz), 2.62 (d, 3H, *J* = 1.5 Hz, NCH_3), 1.52 (pent, 2H, *J* = 7.5 Hz), 1.35-1.20 (m, 18H), 0.85 (t, 3H, *J* = 7.0 Hz).

^{13}C-NMR ($CDCl_3$, 125 MHz): δ 164.97, 129.73, 105.42, 39.74, 35.80, 32.07,29.80, 29.79, 29.74, 29.71, 29.59, 29.50, 29.46, 27.20, 22.84, 14.27.

HRMS (ESI-TOF) calcd for $C_{16}H_{31}NOI$ $(M+H)^+$: 380.1450, found: 380.1452.

Melting Point: 51.9-53.6 °C.

IR (cm^{-1}, thin film in $CDCl_3$): 3512 (b, s), 3308 (s), 3094 (m), 2916 (s), 2850 (s), 1651 (s), 1632 (s), 1557 (s), 1470 (m), 1431 (w), 1372 (w), 1337 (w), 1237 (m), 1157 (w), 1076 (w).

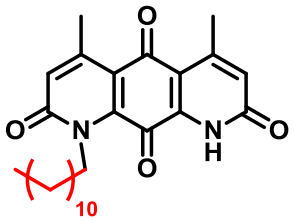

13

Synthesized from **70**, (Z)-3-iodo-N-(4-methoxybenzyl)but-2-enamide, and **50** by General Protocols D, E, F, and H. 15% yield over 4 steps. Compound is an orange solid.

^{1}H-NMR ($CDCl_3$, 500 MHz): δ 10.3 (bs, 1H, N*H*), 6.75 (d, 1H, *J* = 1.0 Hz, vinyl C*H*), 6.68 (s, 1H, vinyl C*H*), 4.48 (t, 2H, *J* = 8.0 Hz, NC*H*$_2$), 2.61 (d, 3H, *J* = 0.5 Hz, allylic C*H*$_3$), 2.59 (d, 3H, *J* = 1.0 Hz, allylic C*H*$_3$), 1.69 (pent, 2H, *J* = 7.5 Hz, NCH_2CH_2-), 1.42 (pent, 2H, *J* = 7.5 Hz, $NCH_2CH_2CH_2$-), 1.38-1.18 (m, 16H), 0.86 (t, 3H, *J* = 7.0 Hz, -CH_2CH_3).

^{13}C-NMR ($CDCl_3$, 125 MHz): δ181.78, 175.27, 161.27, 130.99, 151.38, 149.30, 139.13, 137.98, 128.64, 128.40, 119.69, 114.66, 46.50, 32.12, 29.87, 29.85, 29.81, 29.80, 29.55, 29.44, 29.39, 27.14, 23.55, 22.88, 22.44, 14.32.

HRMS (ESI-TOF) calcd for $C_{26}H_{35}N_2O_4$ $(M+H)^+$: 439.2597, found: 439.2595.

Melting Point: >180 °C.

IR (cm^{-1}, thin film in $CHCl_3$): 2919 (m), 2850 (m), 1680 (m), 1651 (b, s), 1613 (m), 1557 (w), 1470 (w), 1401 (m), 1302 (m), 1157 (w), 1052 (w).

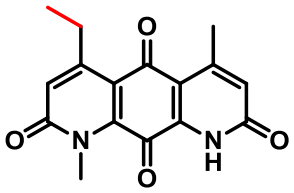

14

Synthesized from **70**, (Z)-3-iodo-N-(4-methoxybenzyl)but-2-enamide, and **36** by General Protocols D, E, F, and H. 7.4% yield over 4 steps. Compound is a red solid.

^{1}H-NMR (2:1 $CDCl_3$:CD_3OD, 500 MHz): δ 6.81 (d, 1H, *J* = 1.0 Hz, vinyl C*H*), 6.67 (d, 1H, *J* = 1.0 Hz, vinyl C*H*), 3.92 (s, 3H), 3.09 (dq, 2H, *J* = 7.0, 0.5 Hz, allylic CH_2), 2.64 (d, 3H, *J* = 1.5 Hz, allylic CH_3), 1.26 (t, 3H, *J* = 7.5 Hz, C*H3*).

^{13}C-NMR ($CDCl_3$, 125 MHz): δ181.33, 175.31, 162.29, 161.90, 155.57, 151.68, 140.24, 138.50, 127.15, 125.27, 118.83, 115.06, 33.98, 27.88, 21.83, 13.55.

HRMS (ESI-TOF) calcd for $C_{16}H_{15}N_2O_4$ $(M+H)^+$: 299.1032, found: 299.1034.

Melting Point: >290 °C.

IR (cm^{-1}, thin film in $CHCl_3$): 3024 (w), 2905 (w), 1684 (m), 1653 (b, s), 1607 (m), 1583 (w), 1458 (w), 1399 (m), 1363 (m), 1291 (m), 1264 (w), 1165 (w), 1035 (w).

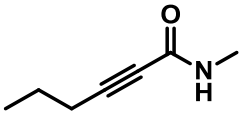

51

Synthesized from ethyl-2-hexynoate and methylamine by General Protocol A. 92% yield. Compound is a pale yellow oil.

^{1}H-NMR ($CDCl_3$, 500 MHz): δ 6.04 (bs, 1H, major rotamer N*H*), 5.89 (bs, 1H, minor rotamer), 2.99 (d, 3H, *J* = 5.0 Hz, minor rotamer), 2.81 (d, 3H, *J* = 5.0 Hz, major rotamer), 2.33 (t, 2H, *J* = 7.0 Hz, minor rotamer), 2.22 (t, 2H, *J* = 7.0 Hz, major rotamer), 1.59 (sext, 2H, *J* = 7.0 Hz, minor rotamer), 1.54 (sext, 2H, *J* = 7.0 Hz, major rotamer), 0.99 (t, 3H, *J* = 7.5 Hz, minor rotamer), 0.96 (t, 3H, *J* = 7.5 Hz, major rotamer).

^{13}C-NMR ($CDCl_3$, 125 MHz): δ 54.47 (major), 87.18 (major), 75.76 (major), 29.87 (minor), 26.58 (major), 21.43 (major), 20.97 (minor), 20.65 (major), 13.60 (major).

HRMS (ESI) calcd for $C_7H_{12}NO$ $(M+H)^+$: 126.0919, found: 126.0920.

Melting Point Not determined (oil).

IR (cm^{-1}, thin film in $CHCl_3$): 3455 (m), 3307 (b, m), 3070 (b, w), 2967 (m), 2251 (m), 2217 (m), 1649 (s), 1520 (m), 1411 (w), 1267 (m), 1163 (w).

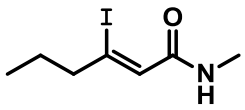

52

Synthesized from **51** by General Protocol C. 96% yield. Compound is a yellow/brown oil.

^{1}H-NMR ($CDCl_3$, 500 MHz): δ 6.40 (bs, 1H, N*H*), 6.30 (s, 1H, vinyl C*H*), 2.82 (d, 3H, *J* = 5.0 Hz, NCH_3), 2.53 (t, 2H, *J* = 7.0 Hz, allylic CH_2), 1.54 (sext, 2H, *J* = 7.5 Hz), 0.86 (t, 3H, *J* = 7.5 Hz).

^{13}C-NMR ($CDCl_3$, 125 MHz): δ 165.86, 128.49, 114.01, 49.03, 26.30, 22.52, 12.82.

HRMS (ESI-TOF) calcd for $C_7H_{13}NOI$ $(M+H)^+$: 254.0042, found: 254.0045.

Melting Point Not determined (oil).

IR (cm^{-1}, thin film in $CHCl_3$): 3455 (m), 3328 (b, m), 3080 (b, w), 2965 (m), 1658 (s), 1624 (m), 1524 (m), 1414 (m), 1333 (w), 1285 (w), 1237 (w), 1165 (w), 1087 (w).

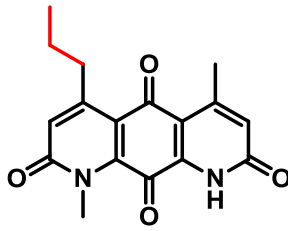

15

Synthesized from **70**, (Z)-3-iodo-N-(4-methoxybenzyl)but-2-enamide, and **52** by General Protocols D, E, F, and H. 3.4% yield over 4 steps. Compound is a red/orange solid.

^{1}H-NMR ($CDCl_3$, 500 MHz): δ 6.80 (s, 1H, vinyl C*H*), 6.68 (d, 1H, *J* = 1.0 Hz, vinyl C*H*), 3.93 (s, 3H), 2.98 (t, 2H, *J* = 7.5 Hz, allylic CH_2), 2.62 (d, 3H, *J* = 1.0 Hz, allylic CH_3), 1.61 (q, 2H, *J* = 7.5 Hz), 1.03 (t, 3H, *J* = 7.5 Hz, CH(CH_3)$_2$).

HRMS (ESI-TOF) calcd for $C_{17}H_{17}N_2O_4$ $(M+H)^+$: 313.1188, found: 313.1189.

Melting Point: >220°C.

IR (cm^{-1}, thin film in $CDCl_3$): 2954 (w), 2912 (w), 2850 (w), 1651 (b, s), 1542 (s), 1632 (m), 1557 (w), 1538 (w), 1505 (w), 1455 (w), 1399 (w), 1288 (m), 1163 (w).

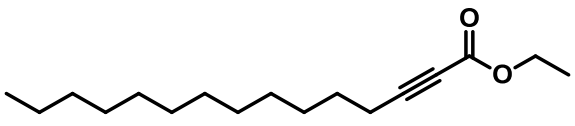

53

To an oven-dried Schlenk flask was added 1-tetradecyne (0.748 g, 3.85 mmol) and THF (10 mL). Chilled to -78 ºC. Added n-BuLi (2.7 mL, 4.32 mmol) dropwise then stirred for 10 minutes. Added ethyl chloroformate (0.56 mL, 5.86 mmol) then allowed the reaction to warm to RT. The solvent was evaporated and the residue was purified by silica gel chromatography. Product was collected as a colorless oil (1.01 g, 3.79 mmol, 98.5% yield). Compound is a clear, colorless oil.

^{1}H-NMR ($CDCl_3$, 500 MHz): δ 4.19 (q, 2H, *J* = 7.5 Hz), 2.30 (t, 2H, *J* = 7.5 Hz), 1.56 (pent, 2H, *J* = 7.5 Hz), 1.37 (bpent, 2H, *J* = 8.0 Hz), 1.29 (t, 3H, *J* = 7.5 Hz), 1.28-1.21 (m, 16H), 0.86 (t, 3H, *J* = 7.0 Hz).

^{13}C-NMR ($CDCl_3$, 125 MHz): δ 154.06, 89.66, 73.33, 61.91, 32.10, 29.82, 29.81, 29.77, 29.60, 29.53, 29.21, 29.04, 27.73, 22.87, 14.29, 14.21.

HRMS (ESI-TOF) calcd for $C_{17}H_{31}O_2$ $(M+H)^+$: 267.2324, found: 267.2327.

Melting Point Not determined (oil).

IR (cm^{-1}, thin film, neat): 2952 (s), 2855 (s), 2320 (w), 2235 (s), 1714 (b, s), 1464 (m), 1366 (m), 1248 (s), 1073 (s).

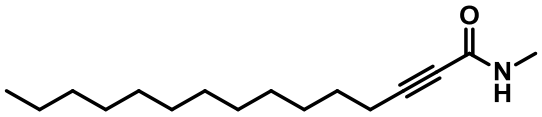

54

Synthesized from **53** and methylamine by General Protocol A. 66% yield. Compound is a white amorphous solid.

^{1}H-NMR ($CDCl_3$, 500 MHz): δ 6.42 (bs, 1H, major rotamer N*H*), 6.24 (bs, 1H, minor rotamer N*H*), 2.93 (d, 3H, *J* = 5.0 Hz, minor rotamer NCH_3), 2.75 (d, 3H, *J* = 5.0 Hz, major rotamer NCH_3), 2.29 (t, 2H, *J* = 7.0 Hz, minor rotamer allylic CH_2), 2.18 (t, 2H, *J* = 7.0 Hz, *J* = 7.0 Hz, major rotamer

allylic C*H*$_2$), 1.50 (pent, 2H, *J* = 7.0 Hz, minor rotamer), 1.45 (pent, 2H, *J* = 7.5 Hz, major rotamer), 1.29 (bpent, 2H, *J* = 7.5 Hz, major rotamer), 1.25-1.13 (m, 16H), 0.79 (t, 3H, *J* = 7.0 Hz).

^{13}C-NMR ($CDCl_3$, 125 MHz): δ 157.35 (minor), 154.47 (major), 94.59 (minor), 87.17 (major), 75.50 (major), 73.14 (minor), 31.92 (major), 29.66 (major), 29.64 (2C, major), 29.48 (major), 29.36 (major), 29.10 (major), 28.90 (major), 27.83 (major), 26.43 (major), 22.69 (major), 18.57 (major), 14.11 (major).

HRMS (ESI-TOF) calcd for $C_{16}H_{30}NO$ $(M+H)^+$: 252.2327, found: 252.2327.

Melting Point: 49.2-50.2 °C.

IR (cm^{-1}, thin film in $CDCl_3$): 3428 (b, m), 3290 (s), 2958 (m), 2920 (s), 2849 (m), 2250 (w), 2221 (w), 1625 (s), 1557 (m), 1469 (m), 1414 (w), 1292 (w), 1160 (w).

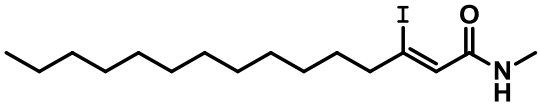

55

Synthesized from **54** by General Protocol C. 100% yield. Compound is a yellow solid.

^{1}H-NMR ($CDCl_3$, 500 MHz): δ 6.27 (s, 1H, vinyl C*H*), 5.74 (bs, 1H, N*H*), 2.89 (d, 3H, *J* = 4.5 Hz), 2.59 (t, 2H, *J* = 7.5 Hz), 1.56 (bt, 2H, *J* = 7.0), 1.33-1.22 (m, 18H), 0.88 (t, 3H, *J* = 7.0 Hz).

^{13}C-NMR ($CDCl_3$, 125 MHz): δ 165.96, 128.50, 114.45, 47.23, 32.07, 29.81, 29.80, 29.77, 29.66, 29.51, 29.50, 29.36, 28.44, 26.36, 22.84, 14.29.

HRMS (ESI-TOF) calcd for $C_{16}H_{31}NOI$ $(M+H)^+$: 380.1450, found: 380.1451.

Melting Point: 45.1-48.8 °C.

IR (cm^{-1}, thin film in $CDCl_3$): 3470 (b, w), 3291 (m), 3080 (w), 2924 (s), 2853 (s), 1651 (s), 1618 (m), 1557 (m), 1464 (w), 1410 (w), 1350 (w), 1234 (w), 1161 (w), 1091 (w).

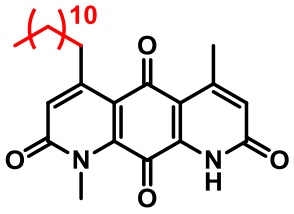

16

Synthesized from **70**, (Z)-3-iodo-N-(4-methoxybenzyl)but-2-enamide, and **55** by General Protocols D, E, F, and H. 7.0% yield over 4 steps. Compound is a peach solid.

^{1}H-NMR (2:1 $CDCl_3$:CD_3OD, 500 MHz): δ 6.78 (s, vinyl C*H*), 6.67 (d, 1H, *J* = 1.0 Hz, vinyl C*H*), 3.91 (s, 3H), 3.03 (t, *J* = 8.0 Hz), 2.64 (d, 3H, *J* = 1.0 Hz, allylic CH_3), 1.58 (p, 2H, *J* = 7.5 Hz), 1.44 (p, 2H, *J* = 7.5 Hz), 1.27-1.4 (m, 16H), 0.89 (t, 3H, *J* = 7.5 Hz).

^{13}C-NMR (d-TFA, 125 MHz): δ182.13, 176.16, 166.58 (bs), 163.92 (bs), 160.66, 141.89, 139.75, 128.19 (bs), 126.92, 125.93, 120.93, 38.25, 37.45, 33.96, 32.05, 31.63 (2C), 31.57, 31.52, 31.41, 31.36, 31.15, 24.53, 23.41, 14.85.

HRMS (ESI-TOF) calcd for $C_{26}H_{35}N_2O_4$ $(M+H)^+$: 439.2597, found: 439.2600.

Melting Point: >220 °C.

IR (cm^{-1}, thin film in $CHCl_3$): 3066 (w), 2916 (m), 2849 (m), 1662 (b, s), 1612 (w), 1583 (w), 1469 (w), 1399 (m), 1297 (m), 1257 (w), 1163 (w), 1095 (w).

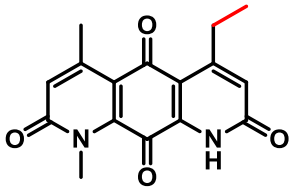

17

Synthesized from **70**, (Z)-3-iodo-N-methylbut-2-enamide,[1] and **38** by General Protocols D, E, F, and H. 6.2% yield over 4 steps. Compound is a red solid at rt.

^{1}H-NMR (2:1 $CDCl_3$:CD_3OD, 500 MHz): δ 6.78 (d, 1H, *J* = 1.0 Hz, vinyl C*H*), 6.70 (s, 1H, vinyl C*H*), 3.92 (s, 3H), 3.09 (qd, 2H, *J* = 7.5, 1.0 Hz), 2.64 (d, 3H, *J* = 1.0 Hz, allylic CH_3), 1.26 (t, 3H, *J* = 7.5 Hz, CH(CH_3)$_2$).

^{13}C-NMR (2:1 $CDCl_3$:CD_3OD, 125 MHz): δ 181.96, 175.93, 162.89, 162.72, 158.05, 150.81, 140.47, 139.74, 127.48, 125.97, 119.98, 115.12, 34.49, 27.94, 23.36, 13.93.

HRMS (ESI-TOF) calcd for $C_{16}H_{15}N_2O_4$ $(M+H)^+$: 299.1032, found: 299.1041.

Melting Point: >290 °C.

IR (cm^{-1}, thin film in $CHCl_3$): 3036 (w), 2968 (w), 2926 (w), 1680 (m), 1651 (b, s), 1601 (m), 1583 (m), 1397 (w), 1375 (w), 1348 (m), 1287 (w), 1156 (w), 1100 (w).

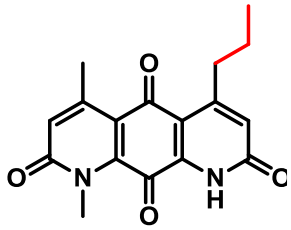

18

Synthesized from **70**, (Z)-3-iodo-N-methylbut-2-enamide, and **30** by General Protocols D, E, F, and H. 11% yield over 4 steps. Compound is an orange solid.

^{1}H-NMR ($CDCl_3$, 500 MHz): δ 9.48 (bs, 1H, N*H*), 6.79 (d, 1H, *J* = 1.5 Hz, vinyl C*H*), 6.69 (s, 1H, vinyl C*H*), 3.93 (s, 3H), 3.00 (t, 2H, *J* = 7.5 Hz) 2.61 (d, 3H, *J* = 1.0 Hz, allylic CH_3), 1.62 (sext, 2H, *J* = 7.5 Hz), 1.04 (t, 3H, *J* = 7.5 Hz).

^{13}C-NMR ($CDCl_3$, 125 MHz): δ 181.55, 175.57, 162.35, 156.13, 150.44, 140.04, 139.38, 127.23, 126.62, 119.70, 114.83, 36.32, 34.18, 23.08, 22.95, 13.83.

HRMS (ESI-TOF) calcd for $C_{17}H_{17}N_2O_4$ $(M+H)^+$: 313.1188, found: 313.1187.

Melting Point: >280 °C.

IR (cm^{-1}, thin film in $CDCl_3$): 3031 (w), 2961 (w), 2912 (w), 1680 (m), 1651 (b, s), 1604 (w), 1583 (w), 1455 (w), 1398 (w), 1350 (m), 1289 (m), 1261 (w), 1160 (w), 1105 (w).

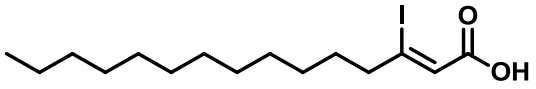

56

To an oven-dried Schlenk flask was added 1-tetradecyne (0.748 g, 3.85 mmol) and THF (10 mL). Chilled to -78 ºC. Added n-BuLi (2.7 mL, 4.32 mmol) dropwise then stirred for 10 minutes. Added a large excess of solid carbon dioxide then allowed the reaction to warm to RT. The solvent was evaporated and the residue was purified by silica gel chromatography. Product was collected as a colorless oil (1.01 g, 3.79 mmol, 88% yield). Followed by General Protocol C, 71% yield.

^{1}H-NMR ($CDCl_3$, 500 MHz): δ 6.39 (s, 1H, vinyl C*H*), 2.72 (t, 2H, *J* = 7 Hz), 1.60 (bp, 2H, *J* = 7.0), 1.33-1.22 (m, 18H), 0.88 (t, 3H, *J* = 7.0 Hz).

^{13}C-NMR ($CDCl_3$, 125 MHz): δ 168.90, 125.50, 124.24, 48.54, 32.07, 29.79, 29.78, 29.74, 29.61, 29.50, 29.46, 29.44, 28.39, 22.85, 14.29.

HRMS (ESI-TOF) calcd for $C_{17}H_{17}N_2O_4$ $(M+Na)^+$: 389.0954, found: 389.0950.

Melting Point Not determined (oil).

IR (cm^{-1}, thin film in $CHCl_3$): 3533 (b, s), 3295 (s), 3080 (m), 2954 (m), 2864 (m), 1651 (s), 1633 (m), 1557 (s), 1538 (m), 1431 (w), 1365 (w), 1330 (w), 1228 (w), 1208 (w).

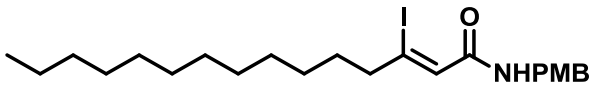

57

Synthesized from **56** and 4-methoxybenzylamine by General Protocol B. 90% yield. Compound is an off-white solid.

^{1}H-NMR ($CDCl_3$, 500 MHz): δ 7.11 (d, 2H, *J* = 8.5 Hz, aryl C*H*), 6.72 (d, 2H, *J* = 8.5 Hz, aryl C*H*), 6.31 (s, 1H, vinylic C*H*), 4.251 (d, 2H, *J* = 5.5 Hz, NCH_2), 3.66 (s, 3H, OCH_3), 2.49 (t, 2H, *J* = 7 Hz), 1.47 (bp, 2H, *J* = 7.0), 1.33-1.22 (m, 18H), 0.83 (t, 3H, *J* = 7.0 Hz).

^{13}C-NMR ($CDCl_3$, 125 MHz): δ 164.88, 159.12, 129.96, 129.50, 128.16, 114.77, 114.11, 55.41, 55.37, 55.32, 55.28, 47.25, 43.18, 31.99, 29.70, 29.56, 29.42, 29.30, 28.38, 22.77, 14.22.

HRMS (ESI-TOF) calcd for $C_{17}H_{17}N_2O_4$ $(M+H)^+$: 486.1869, found: 486.1862.

Melting Point: 50.2-55.0 °C

IR (cm^{-1}, thin film in $CHCl_3$): 3417 (b, s), 3303 (s), 3066 (m), 2925 (s), 2853 (m), 1651 (s), 1621 (s), 1540 (m), 1513 (s), 1464 (m), 1337 (w), 1302 (2), 1248 (m), 1175 (m), 1084 (w).

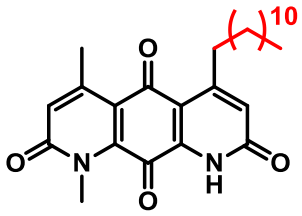

19

Synthesized from **70**, (Z)-3-iodo-N-methylbut-2-enamide, and **57** by General Protocols D, E, F, and H. 20% yield over 4 steps. Compound is an orange solid.

^{1}H-NMR (2:1 $CDCl_3$:CD_3OD, 500 MHz): δ 6.78 (s, vinyl C*H*), 6.67 (s, 1H), 3.92 (s, 3H), 3.03 (t, *J* = 7.5 Hz), 2.64 (d, 3H, *J* = 1.0 Hz, allylic C*H*$_3$), 1.58 (p, 2H, *J* = 7.5 Hz), 1.44 (p, 2H, *J* = 7.5 Hz), 1.27-1.4 (m, 16H), 0.89 (t, 3H, *J* = 7.5 Hz).

^{13}C-NMR (d-TFA, 125 MHz): δ182.21, 176.18, 166.64, 166.55, 165.56, 158.87, 141.347, 140.27, 128.14, 127.13, 126.09, 120.54, 37.93, 36.73, 33.95, 31.84, 31.61 (2H), 31.54, 31.42, 31.38, 31.34, 31.13, 24.50 24.37, 14.79.

HRMS (ESI-TOF) calcd for $C_{26}H_{35}N_2O_4$ $(M+H)^+$: 439.2597, found: 439.2590.

Melting Point: >230 °C.

IR (cm^{-1}, thin film in $CHCl_3$): 2954 (w), 2918 (m), 2850 (m), 1677 (s), 1651 (s), 1639 (s), 1587 (w), 1505 (w), 1408 (w), 1352 (w), 1290 (w), 1254 (w), 1160 (w), 1087 (w).

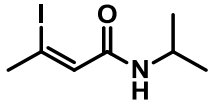

58

Synthesized from (Z)-3-iodobut-2-enoic acid[1] and isopropylamine by General Protocols B. 74% yield over 4 steps. Compound is a off-white solid.

^{1}H-NMR ($CDCl_3$, 500 MHz): δ 6.19 (d, 1H. *J* = 1.5 Hz, vinyl C*H*), 5.52 (bs, 1H, N*H*), 4.18 (sextet, 1H, *J* = 7.5 Hz), 2.64 (d, 3H, *J* = 1.5 Hz, allylic C*H*$_3$), 1.20 (d, 6H, *J* = 7.5 Hz).

^{13}C-NMR ($CDCl_3$, 125 MHz): δ 164.85, 129.28, 105.58, 35.75, 34.45, 14.74. 25Oct11_8-167-1_VXR500

HRMS (ESI-TOF) calcd for $C_7H_{13}NOI$ $(M+H)^+$: 254.0042, found: 254.0043.

Melting Point: 68.8-71.3 °C.

IR (cm^{-1}, thin film in $CHCl_3$): 3248 (m), 3060 (w), 2965 (m), 1642 (m), 1628 (s), 1557 (s), 1466 (w), 1347 (w), 1333 (w), 1240 (m), 1163 (w), 1073 (w).

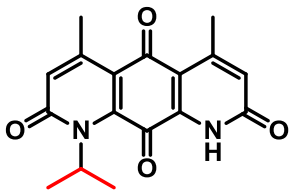

20

Synthesized from **70**, (Z)-3-iodo-N-(4-methoxybenzyl)but-2-enamide, and **58** by General Protocols D, E, G, and H. 20% yield over 4 steps. Compound is a yellow/orange oily solid.

^{1}H-NMR ($CDCl_3$, 500 MHz): δ 9.74 (bs, 1H, N*H*), 6.67 (d, 1H, *J* = 1.0 Hz, vinyl C*H*), 6.62 (d, 1H, *J* = 1.0 Hz, vinyl C*H*), 5.00 (sept, 1H, J = 7.0 Hz), 2.61 (d, 3H, *J* = 1.0 Hz, allylic CH_3), 2.56 (d, 3H, *J* = 1.0 Hz, allylic CH_3), 1.67 (d, 6H, *J* = 7.0 Hz, CH(CH_3)$_2$).

^{13}C-NMR (2:1 $CDCl_3$:CD_3OD, 125 MHz): δ 181.83, 176.18, 163.26, 162.57, 152.34, 149.75, 143.05, 139.79, 129.12, 127.42, 120.40, 115.16, 55.91, 23.01, 22.32, 20.29.

HRMS (ESI-TOF) calcd for $C_{17}H_{17}N_2O_4$ $(M+H)^+$: 313.1188, found: 313.1197.

Melting Point: >280 °C.

IR (cm^{-1}, thin film in $CHCl_3$): 2982 (b, w), 1677 (w), 1647 (b, s), 1611 (m), 1587 (w), 1396 (w), 1344 (w), 1288 (w).

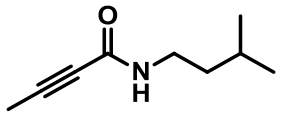

59

Synthesized from ethyl-2-butynoate and isoamylamine by General Protocol A. 73% yield. Compound is a white crystalline solid.

^{1}H-NMR ($CDCl_3$, 500 MHz): δ 5.84 (bs, 1H, major rotamer, N*H*), 3.37 (q, 2H, *J* = 7.0 Hz, minor rotamer, NC*H*$_2$), 3.27 (q, 2H, *J* = 7.0 Hz, major rotamer, NC*H*$_2$), 1.99 (d, 3H, *J* = 1.5 Hz, minor rotamer, allylic C*H*$_3$), 1.90 (d, 3H, *J* = 1.5 Hz, major rotamer, allylic C*H*$_3$), 1.59 (sept, 1H, *J* = 6.5 Hz, major rotamer, C*H*), 1.38 (q, 2H, *J* = 7.5 Hz, major rotamer CH_2CH_2CH), 0.91 (d, 6H, *J* = 6.5 Hz, minor rotamer $CH(CH_3)_2$), 0.88 (d, 6H, *J* = 6.5 Hz, major rotamer, $CH(CH_3)_2$)

^{13}C-NMR ($CDCl_3$, 125 MHz) δ 156.19 (minor), 153.45 (major), 89.12 (minor), 82.24 (major), 74.74 (major), 72.37 (minor), 41.28 (minor), 39.12 (minor), 37.70 (major), 37.63 (major), 25.40 (major), 25.05 (minor), 22.02 (major), 3.50 (minor), 3.22 (major).

HRMS (ESI) calcd for $C_9H_{16}NO$ $(M+H)^+$: 154.1232, found: 154.1233.

Melting Point: 42.2-43.3 °C.

IR (cm^{-1}, thin film in $CHCl_3$): 3626 (b, s), 3303 (s), 3073 (m), 2955 (m), 2871 (w), 2256 (w), 2219 (w), 1651 (s), 1557 (m), 1470 (w), 1455 (w), 1368 (w), 1299 (w), 1230 (w), 1158 (w).

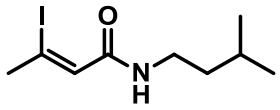

60

Synthesized from **59** by General Protocol C. 95% yield. Compound is a light gold oil.

^{1}H-NMR ($CDCl_3$, 500 MHz): δ 6.22 (q, 1H, *J* = 1.5 Hz, vinyl C*H*), 5.82 (bs, 1H, N*H*), 3.33 (dq, 2H, *J* = 7.5, 1.0 Hz), 2.63 (d, 3H, *J* = 1.5 Hz, allylic CH_3), 1.64 (sept, 1H, *J* = 6.5 Hz), 1.43 (q, 2H, *J* = 7.0 Hz), 0.91 (d, 6H, *J* = 6.5 Hz).

^{13}C-NMR ($CDCl_3$, 125 MHz) δ 165.02, 129.91, 105.08, 50.64, 35.74, 31.98, 27.43, 27.20.

HRMS (ESI-TOF) calcd for $C_9H_{17}NOI$ $(M+H)^+$: 282.0355, found: 282.0351.

Melting Point Not determined (oil).

IR (cm^{-1}, thin film in $CDCl_3$): 3519 (b, w), 3307 (s), 3074 (m), 2957 (s), 1651 (s), 1633 (s), 1538 (s), 1470 (m), 1455 (m), 1434 (w), 1367 (w), 1231 (w), 1090 (w).

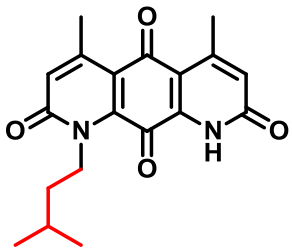

21

Synthesized from **70**, (Z)-3-iodo-N-(4-methoxybenzyl)but-2-enamide, and **60** by General Protocols D, E, F, and H. 12% yield over 4 steps. Compound is a red solid.

^{1}H-NMR (2:1 $CDCl_3$:CD_3OD, 500 MHz): δ 6.76 (q, 1H, *J* = 1.0 Hz, vinyl C*H*), 6.67 (q, 1H, *J* = 1.5 Hz, vinyl C*H*), 4.52-4.49 (m, 2H), 2.64 (d, 3H, *J* = 1.0 Hz, allylic CH_3), 2.63 (d, 3H, *J* = 1.0 Hz,

allylic C*H*$_3$), 1.81 (sept, 1H, *J* = 7.0 Hz, C*H*), 1.68-1.63 (m, 2H, CH$_2$C*H*$_2$CH), 1.03 (d, 6H, *J* = 6.5 Hz, CH(C*H*$_3$)$_2$).

^{13}C-NMR (2:1 $CDCl_3$:CD_3OD, 125 MHz): δ 181.48, 175.02, 161.83, 161.65, 151.69, 149.89, 139.30, 138.50, 127.42, 127.23, 119.52, 114.77, 45.45, 37.28, 26.49, 22.89, 22.02, 21.83.

HRMS (ESI-TOF) calcd for $C_{19}H_{21}N_2O_4$ $(M+H)^+$: 341.1501, found: 341.1507.

Melting Point: >280 °C.

IR (cm^{-1}, thin film in $CDCl_3$): 1684 (m), 1651 (b, s), 1611 (m), 1590 (m), 1469 (w), 1402 (w), 1290 (w), 1261 (w), 1157 (w), 1056 (w).

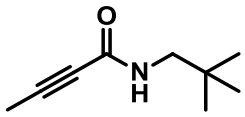

61

Synthesized from ethyl-2-butynoate and neopentylamine by General Protocol A. 38% yield. Compound is a white crystalline solid.

^{1}H-NMR ($CDCl_3$, 500 MHz): δ 5.75 (bs, 1H, major rotamer N*H*), 3.17 (d, 2H, *J* = 7.0 Hz, minor rotamer NC*H*$_2$), 3.09 (d, 2H, *J* = 6.5 Hz, major rotamer NC*H*$_2$), 2.01 (s, 3H, minor rotamer allylic C*H*$_3$), 1.94 (s, 3H, major rotamer allylic C*H*$_3$), 0.93 (s, 9H, minor rotamer), 0.92 (s, 9H, major rotamer).

^{13}C-NMR ($CDCl_3$, 125 MHz): δ 156.81, 153.77, 89.95, 83.20, 75.08, 72.77, 55.08, 50.77, 32.22, 31.99, 27.19, 27.07, 4.01, 3.72.

HRMS (ESI) calcd for $C_9H_{16}NO$ $(M+H)^+$: 154.1232, found: 154.1233.

Melting Point: 76.5-78.5 °C.

IR (cm^{-1}, thin film in $CDCl_3$): 3310 (b, s), 1961 (m), 2248 (m), 2213 (m), 1651 (s), 1574 (m), 1434 (w), 1366 (w), 1281 (m), 1211 (w).

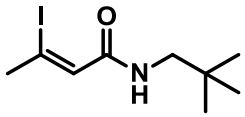

62

Synthesized from **61** by General Protocol C. 96% yield. Compound is white amorphous powder.

^{1}H-NMR ($CDCl_3$, 500 MHz): δ 6.29 (q, 1H. *J* = 1.5 Hz, vinyl C*H*), 5.78 (bs, 1H, N*H*), 3.16 (d, 2H, *J* = 6.0 Hz), 2.66 (d, 3H, *J* = 1.0 Hz), 0.96 (s, 9H).

^{13}C-NMR ($CDCl_3$, 125 MHz): δ 165.02, 129.91, 105.08, 50.64, 35.74, 31.98, 27.43, 27.20.

HRMS (ESI-TOF) calcd for $C_9H_{17}NOI$ $(M+H)^+$: 282.0355, found: 282.0354.

Melting Point: 92.3-94.5 °C.

IR (cm^{-1}, thin film in $CDCl_3$): 3442 (b, m), 3298 (s), 3080 (w), 2956 (m), 1652 (s), 1633 (s), 1557 (m), 1463 (w), 1428 (w), 1365 (w), 1228 (m), 1208 (m), 1063 (w).

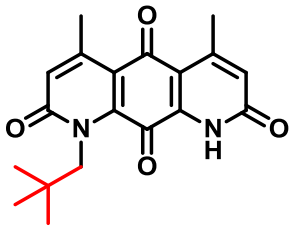

22

Synthesized from **70**, (Z)-3-iodo-N-(4-methoxybenzyl)but-2-enamide, and **62** by General Protocols D, E, F, and H. 10% yield over 4 steps. Compound is a red solid.

^{1}H-NMR (2:1 $CDCl_3$:CD_3OD, 500 MHz): δ 6.75 (d, 1H, *J* = 1.0 Hz, vinyl C*H*), 6.67 (d, 1H, *J* = 1.0 Hz, vinyl C*H*), 4.95 (bs, 1H), 4.86 (bs, 1H), 2.64 (s, 6H, allylic CH_3), 0.87 (s, 9H, (CH_3)$_3$).

^{13}C-NMR ($CDCl_3$, 125 MHz): δ181.20, 176.32, 162.40, 149.55, 141.41, 139.05, 127.31, 127.19, 119.33, 114.87, 51.10, 34.31, 27.58, 22.80, 21.67.

HRMS (ESI-TOF) calcd for $C_{19}H_{21}N_2O_4$ $(M+H)^+$: 341.1501, found: 341.1498.

Melting Point: >270 °C.

IR (cm^{-1}, thin film in $CHCl_3$): 1663 (s), 1651 (s), 1628 (s), 1462 (w), 1396 (w), 1367 (w), 1301 (w), 1106 (w), 1073 (w).

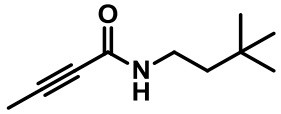

63

Synthesized ethyl-2-butynoate and 3,3-dimethylbutan-1-amine by General Protocol A. 76% yield. Compound is a white amorphous solid.

^{1}H-NMR ($CDCl_3$, 500 MHz): δ 6.00 (bs, 1H, minor rotamer N*H*), 5.60 (bs, 1H, major rotamer N*H*), 3.39 (m, 2H, minor rotamer NCH_2), 3.29 (m, 2H, major rotamer NCH_2), 2.02 (s, 3H, minor rotamer allylic CH_3), 1.93 (s, 3H, major rotamer allylic CH_3), 1.46 (m, 2H, minor rotamer), 1.42 (m, 2H, major rotamer), 0.94 (s, 9H, minor rotamer), 0.92 (s, 9H, major rotamer).

^{13}C-NMR ($CDCl_3$, 125 MHz): δ 153.56, 82.97, 75.14, 43.10, 36.64, 30.04, 29.49, 3.78.

HRMS (ESI) calcd for $C_{10}H_{18}NO$ $(M+H)^+$: 168.1388, found: 168.1387.

Melting Point: 70.5-72.0 °C.

IR (cm^{-1}, thin film in $CDCl_3$): 3289 (b, m), 3064 (w), 2955 (s), 2255(m), 2216 (m), 1636 (s), 1540 (s), 1473 (m), 1365 (m), 1309 (m), 1286 (m), 1189 (w), 1075 (w).

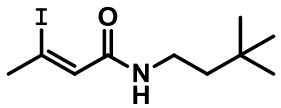

64

Synthesized from **63** by General Protocol C. 93% yield. Compound is a pale brown oil.

^{1}H-NMR ($CDCl_3$, 500 MHz): δ 6.21 (q, 1H, *J* = 1.5 Hz, vinyl C*H*), 6.02 (bs, 1H, N*H*), 3.31-3.27 (m, 2H), 2.61 (d, 3H, *J* = 1.5 Hz, NCH_3), 1.44-1.41 (m, 2H), 0.89 (s, 9H).

^{13}C-NMR ($CDCl_3$, 125 MHz): δ 164.78, 129.39, 105.53, 43.17, 36.31, 35.77, 30.02, 29.50.

HRMS (ESI-TOF) calcd for $C_{10}H_{19}NOI$ $(M+H)^+$: 296.0511, found: 296.0513.

Melting Point Not determined (oil).

IR (cm^{-1}, thin film, neat): 3289 (b, m), 3073 (w), 2955 (s), 2857 (m), 1653 (s), 1621 (m), 1541 (s), 1474 (w), 1431 (w), 1364 (w), 1333(w), 1229 (m), 1074 (w).

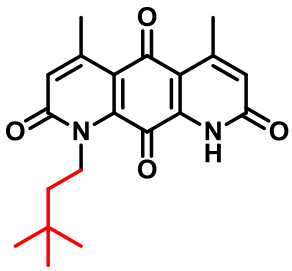

23

Synthesized from **70**, (Z)-3-iodo-N-(4-methoxybenzyl)but-2-enamide, and **64** by General Protocols D, E, F, and H. 17% yield over 4 steps. Compound is a red solid.

^{1}H-NMR (2:1 $CDCl_3$:CD_3OD, 500 MHz): δ 6.75 (d, 1H, *J* = 1.0 Hz, vinyl C*H*), 6.66 (d, 1H, *J* = 1.0 Hz, vinyl C*H*), 4.57-4.53 (m, 2H), 2.63 (d, 3H, *J* = 1.0 Hz, allylic CH_3), 2.62 (d, 3H, *J* = 1.0 Hz, allylic CH_3), 1.66 (m, 2H, $CH_2CH_2C(CH_3)_3$, 1.07 (s, 9H, $C(CH_3)_3$).

^{13}C-NMR (2:1 $CDCl_3$:CD_3OD, 125 MHz): δ 181.46, 174.98, 161.81, 161.60, 151.64, 149.82, 139.35, 138.45, 127.38, 127.21, 119.53, 114.74, 43.73, 41.45, 29.97, 28.87, 22.88, 21.81.

HRMS (ESI-TOF) calcd for $C_{20}H_{23}N_2O_4$ $(M+H)^+$: 355.1658, found: 355.1664.

Melting Point: >290 °C.

IR (cm^{-1}, thin film in $CDCl_3$): 2940 (w), 1652 (b, s), 1614 (w), 1583 (w), 1386 (w), 1372 (w), 1331 (w), 1293 (w), 1177 (w), 1108 (w).

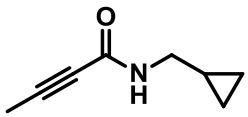

65

Synthesized from ethyl-2-butynoate and cyclopropylmethanamine by General Protocol A. 94% yield. Compound is a clear, colorless oil.

^{1}H-NMR ($CDCl_3$, 500 MHz): δ 5.94 (bs, 1H, major rotamer N*H*), 5.91 (bs, 1H, minor rotamer N*H*), 3.25 (dd, 2H, *J* = 5.5 and 1.5 Hz, minor rotamer NCH_2CH), 3.13 (dd, 2H, *J* = 5.5 Hz and 1.5 Hz, major rotamer NCH_2CH), 1.99 (s, 3H, minor rotamer CH_3), 1.92 (s, 3H, major rotamer CH_3), 0.92 (m, 1H, *J* = 0.9 Hz, $NCH_2CH(CH_2)_2$), 0.48 (m, 2H, $NCH_2CH(CH_2)_2$), 0.19 (m, 2H, $NCH_2CH(CH_2)_2$).

^{13}C-NMR ($CDCl_3$, 125 MHz): δ 153.47 (major), 83.15 (major), 76.90 (major), 48.22 (minor), 44.66 (major), 11.52 (minor), 10.55 (major), 3.73 (major), 3.52 (major).

HRMS (ESI) calcd for $C_8H_{12}NO$ $(M+H)^+$: 138.0919, found: 138.0916.

Melting Point Not determined (oil).

IR (cm^{-1}, thin film in CCl_4): 3276 (b, m), 3080 (b, w), 2964 (w), 2253 (m), 2217 (m), 1632 (s), 1536 (s), 1437 (m) 1287 (s), 1168 (w).

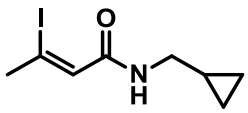

66

Synthesized from **65** by General Protocol C. 65% yield. Compound is a yellow/orange oily solid.

^{1}H-NMR ($CDCl_3$, 500 MHz): δ 6.24 (d, 1H. *J* = 1.5 Hz, vinyl C*H*), 5.80 (bs, 1H, N*H*), 3.20 (dd, 2H, *J* = 5.5 and 1.0 Hz, NCH_2CH), 2.66 (d, 3H, *J* = 1.5 Hz, allylic CH_3), 1.01 (m, 1H, $NCH_2CH(CH_2)_2$), 0.53 (m, 2H, $NCH_2CH(CH_2)_2$), 0.24 (m, 2H, $NCH_2CH(CH_2)_2$).

^{13}C-NMR ($CDCl_3$, 125 MHz): δ 164.81, 129.47, 105.71, 44.41, 35.76, 10.63, 3.64.

HRMS (ESI-TOF) calcd for $C_8H_{13}NOI$ $(M+H)^+$: 266.0042, found: 266.0041.

Melting Point Not determined.

IR (cm^{-1}, thin film in $CHCl_3$): 3438 (w), 2960 (w), 1655 (s), 1620 (m), 1560 (w), 1508 (m) 1466 (m), 1381 (w), 1208 (w), 1094 (w).

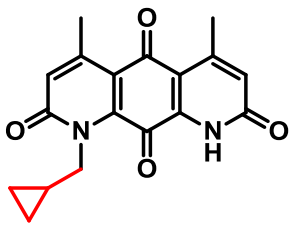

24

Synthesized from **70**, (Z)-3-iodo-N-(4-methoxybenzyl)but-2-enamide, and **66** by General Protocols D, E, G, and H. 16% yield over 4 steps. Compound is an orange solid.

^{1}H-NMR ($CDCl_3$, 500 MHz): δ 6.78 (d, 1H, *J* = 1.0 Hz, vinyl C*H*), 6.69 (d, 1H, *J* = 1.5 Hz, vinyl C*H*), 4.61 (d, *J* = 7.0 Hz, 2H), 2.62 (d, 3H, *J* = 1.0 Hz, allylic CH_3), 2.61 (d, 3H, *J* = 1.0 Hz, allylic CH_3), 1.19 (sept, 1H, *J* = 6.5 Hz, C*H*), 0.50 (d, *J* = 6.5 Hz 4H, CH(CH_2)$_2$).

^{13}C-NMR ($CDCl_3$, 125 MHz): δ 181.73, 175.33, 161.55, 160.55, 151.25, 149.24, 138.83, 137.76, 128.96, 128.46, 119.99, 114.54, 49.24, 23.51, 22.37, 11.54, 4.35. 6-29-11_BIP2-77_13C_u500

HRMS (ESI-TOF) calcd for $C_{18}H_{17}N_2O_4$ $(M+H)^+$: 325.1188, found: 325.1181.

Melting Point: >260 °C.

IR (cm^{-1}, thin film in $CDCl_3$): 1677 (w), 1651 (s), 1632 (w), 1604 (w), 1392 (w), 1375 (w), 1358 (w), 1293 (w), 1205 (w), 1167 (w), 1098 (w).

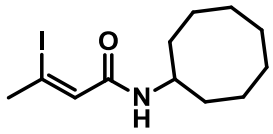

67

Synthesized from (Z)-3-iodobut-2-enoic acid and cyclooctylamine by General Protocols B. 92% yield. Compound is a yellow/brown oil.

^{1}H-NMR ($CDCl_3$, 500 MHz): δ 6.19 (d, 1H. *J* = 1.5 Hz, vinyl C*H*), 5.81 (bs, 1H, N*H*), 4.06 (m, 1H, NC*H*), 2.61 (d, 3H, *J* = 1.5 Hz, allylic CH_3) 1.86 (m, 2H), 1.65 (m, 2H), 1.54 (m, 10H).

^{13}C-NMR ($CDCl_3$, 125 MHz): δ 163.76, 129.87, 105.07, 49.56, 35.67, 32.05, 27.27, 25.46, 23.76.

HRMS (ESI-TOF) calcd for $C_{12}H_{21}NOI$ $(M+H)^+$: 322.0668, found: 322.0667.

Melting Point: Not determined (oil).

IR (cm^{-1}, thin film in $CHCl_3$): 3424 (w), 3293 (b, m), 3060 (w), 2923 (w), 1649 (s), 1624 (s), 1539 (s), 1473 (m), 1447 (m), 1426 (m), 1375 (w), 1351 (w), 1226 (s), 1128 (w), 1081 (m).

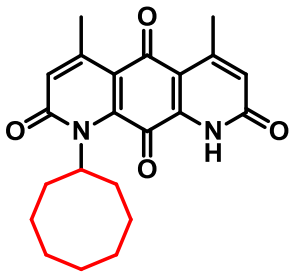

25

Synthesized from **70**, (Z)-3-iodo-N-(4-methoxybenzyl)but-2-enamide, and **67** by General Protocols D, E, G, and H. 4% yield over 4 steps. Compound is a yellow/orange oily solid.

^{1}H-NMR ($CDCl_3$, 400 MHz): δ 6.65 (d, 1H, *J* = 1.0 Hz, vinyl C*H*), 6.63 (d, 1H, *J* = 1.5 Hz, vinyl C*H*), 5.02 (m, 1H), 2.60 (d, 3H, *J* = 1.0 Hz, allylic CH_3), 2.55 (d, 3H, *J* = 1.0 Hz, allylic CH_3), 1.79 (m, 14 HCH_2)$_7$),

^{13}C-NMR ($CDCl_3$, 125 MHz): δ 181.71, 175.87, 161.81, 161.07, 151.51, 148.69, 141.52, 138.64, 129.80, 128.02, 120.01, 114.55, 32.97, 26.60, 26.56, 26.31, 23.24, 22.42.

HRMS (ESI-TOF) calcd for $C_{22}H_{25}N_2O_4$ $(M+H)^+$: 381.1814, found: 381.1820.

Melting Point: >250 °C.

IR (cm^{-1}, thin film in $CHCl_3$): 2925 (m), 1666 (s), 1651 (s), 1611 (m), 1587 (w), 1470 (w), 1397 (w), 1375 (w), 1354 (w), 1295 (w), 1170 (w), 1110 (w).

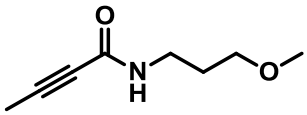

68

Synthesized from ethyl-2-butynoate and 3-methoxypropan-1-amine by General Protocol A. 65% yield. Compound is a clear, colorless oil.

^{1}H-NMR ($CDCl_3$, 500 MHz): δ 6.27 (bs, 1H, major rotamer N*H*), 6.02 (bs, 1H, minor rotamer N*H*), 3.46 (t, 2H, *J* = 6.0 Hz), 3.38 (q, 2H, *J* = 6.5 Hz), 3.34 (s, 3H), 1.92 (s, 3H), 1.77 (pent, 2H, *J* = 6.0 Hz).

^{13}C-NMR ($CDCl_3$, 125 MHz): δ 156.37 (minor), 153.62 (major), 89.82 (minor), 82.95 (major), 75.00 (major), 72.58 (minor), 71.28 (major), 70.45 (minor), 58.77 (major), 41.34 (minor), 38.04 (major), 30.15 (minor), 28.87 (major), 3.97 (minor), 3.64 (major).

HRMS (ESI-TOF) calcd for $C_8H_{14}NO_2$ $(M+H)^+$: 156.1025, found: 156.1029.

Melting Point Not determined (oil).

IR (cm^{-1}, thin film, neat): 3491 (b, m), 3273 (s), 3064 (w), 2928 (s), 2829 (w), 2255 (m), 2222 (m), 1651 (s), 1539 (s), 1446 (m), 1391 (w), 1287 (m), 1225 (w), 1191 (w), 1114 (m), 1029 (w).

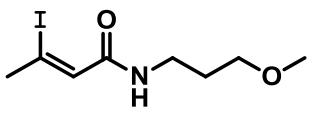

69

Synthesized from **68** by General Protocol C. 96% yield. Compound is a light yellow oil.

^{1}H-NMR ($CDCl_3$, 500 MHz): δ 6.26 (bs, 1H, N*H*), 6.21 (d, 1H. *J* = 1.0 Hz, vinyl C*H*), 3.49 (t, 2H, *J* = 6.0 Hz), 3.42 (q, 2H, *J* = 6.5 Hz), 3.34 (s, 3H), 2.64 (d, 3H, *J* = 1.5 Hz), 1.81 (pent, 2H, *J* = 6.0 Hz).

^{13}C-NMR ($CDCl_3$, 125 MHz): δ 164.90, 129.40, 105.51, 71.65, 58.93, 38.02, 35.78, 29.07.

HRMS (ESI-TOF) calcd for $C_8H_{15}NO_2I$ $(M+H)^+$: 284.0148, found: 284.0147.

Melting Point Not determined (oil).

IR (cm^{-1}, thin film, neat): 3491 (m), 3290 (s), 3069 (m), 2927 (s), 2872 (s), 1651 (s), 1538 (s), 1434 (m), 1374 (w), 1336 (w), 1229 (s), 1190 (m), 1080 (m), 1031 (w).

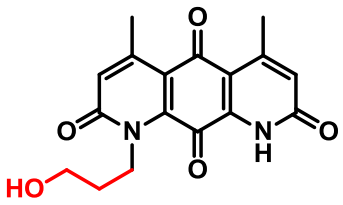

26

Synthesized from **70**, (Z)-3-iodo-N-(4-methoxybenzyl)but-2-enamide, and **69** by General Protocols D, E, G, and H. 22% yield over 4 steps. Compound is an orange solid.

^{1}H-NMR (2:1 $CDCl_3$:CD_3OD, 500 MHz): δ 6.76 (d, 1H, *J* = 1.0 Hz, vinyl C*H*), 6.65 (d, 1H, *J* = 1.0 Hz, vinyl C*H*), 4.58 (t, 2H, *J* = 7.5 Hz), 3.70 (t, 2H, *J* = 6.0 Hz), 2.63 (d, 3H, *J* = 1.0 Hz, allylic CH_3), 2.63 (d, 3H, *J* = 1.0 Hz, allylic CH_3), 2.06-2.01 (m, 2H).

^{13}C-NMR ($CDCl_3$, 125 MHz): δ 181.76, 175.59, 162.35, 151.91, 150.60, 140.16, 139.33, 127.45, 127.40, 119.76, 115.06, 59.79, 44.48, 31.66, 23.21, 22.15.

HRMS (ESI-TOF) calcd for $C_{17}H_{17}N_2O_5$ $(M+H)^+$: 329.1137, found: 329.1129.

Melting Point: >270 °C.

IR (cm^{-1}, thin film in $CHCl_3$): 3446 (b, s), 1646 (s), 1642 (s), 1635 (s), 1392 (w), 1373 (w), 1306 (w), 1292 (w).

2.6 References

(1) Bair, J. S.; Palchaudhuri, R.; Hergenrother, P. J. Chemistry and biology of deoxynyboquinone, a potent inducer of cancer cell death. *J Am Chem Soc* **2010**, *132*, 5469-5478.

(2) Gutierrez, P. L. The metabolism of quinone-containing alkylating agents: free radical production and measurement. *Front Biosci* **2000**, *5*, D629-638.

(3) Parkinson, E. I.; Bair, J. S.; Cismesia, M.; Hergenrother, P. J. Efficient NQO1 substrates are potent and selective anticancer agents. *ACS Chem Biol* **2013**, *8*, 2173-2183.

(4) Huang, X.; Dong, Y.; Bey, E. A.; Kilgore, J. A.; Bair, J. S.; Li, L. S.; Patel, M.; Parkinson, E. I.; Wang, Y.; Williams, N. S.; Gao, J.; Hergenrother, P. J.; Boothman, D. A. An NQO1 substrate with potent antitumor activity that selectively kills by PARP1-induced programmed necrosis. *Cancer Res* **2012**, *72*, 3038-3047.

(5) Li, L. S.; Bey, E. A.; Dong, Y.; Meng, J.; Patra, B.; Yan, J.; Xie, X. J.; Brekken, R. A.; Barnett, C. C.; Bornmann, W. G.; Gao, J.; Boothman, D. A. Modulating endogenous NQO1 levels identifies key regulatory mechanisms of action of beta-lapachone for pancreatic cancer therapy. *Clin Cancer Res* **2011**, *17*, 275-285.

(6) Yan, C.; Kepa, J. K.; Siegel, D.; Stratford, I. J.; Ross, D. Dissecting the role of multiple reductases in bioactivation and cytotoxicity of the antitumor agent 2,5-diaziridinyl-3-(hydroxymethyl)-6-methyl-1,4-benzoquinone (RH1). *Mol Pharmacol* **2008**, *74*, 1657-1665.

(7) Vichai, V.; Kirtikara, K. Sulforhodamine B colorimetric assay for cytotoxicity screening. *Nat Protoc* **2006**, *1*, 1112-1116.

(8) Dong, Y.; Bey, E. A.; Li, L. S.; Kabbani, W.; Yan, J.; Xie, X. J.; Hsieh, J. T.; Gao, J.; Boothman, D. A. Prostate cancer radiosensitization through poly(ADP-Ribose) polymerase-1 hyperactivation. *Cancer Res* **2010**, *70*, 8088-8096.

(9) Siegel, D.; Beall, H.; Senekowitsch, C.; Kasai, M.; Arai, H.; Gibson, N. W.; Ross, D. Bioreductive activation of mitomycin C by DT-diaphorase. *Biochemistry* **1992**, *31*, 7879-7885.

(10) Fitzsimmons, S. A.; Workman, P.; Grever, M.; Paull, K.; Camalier, R.; Lewis, A. D. Reductase enzyme expression across the National Cancer Institute Tumor cell line panel: correlation with sensitivity to mitomycin C and EO9. *J Natl Cancer Inst* **1996**, *88*, 259-269.

(11) Heeres, J. T.; Hergenrother, P. J. Poly(ADP-ribose) makes a date with death. *Curr Opin Chem Biol* **2007**, *11*, 644-653.

(12) Galluzzi, L.; Vitale, I.; Abrams, J. M.; Alnemri, E. S.; Baehrecke, E. H.; Blagosklonny, M. V.; Dawson, T. M.; Dawson, V. L.; El-Deiry, W. S.; Fulda, S.; Gottlieb, E.; Green, D. R.; Hengartner, M. O.; Kepp, O.; Knight, R. A.; Kumar, S.; Lipton, S. A.; Lu, X.; Madeo, F.; Malorni, W.; Mehlen, P.; Nunez, G.; Peter, M. E.; Piacentini, M.; Rubinsztein, D. C.; Shi, Y.; Simon, H. U.; Vandenabeele, P.; White, E.; Yuan, J.; Zhivotovsky, B.; Melino, G.; Kroemer, G. Molecular definitions of cell death subroutines: recommendations of the Nomenclature Committee on Cell Death 2012. *Cell Death Differ* **2012**, *19*, 107-120.

(13) Tegeris, A. S. Effect of sodium nitrite, primaquine, and menadione on TPN-methemoglobin reductase in vitro. *Toxicol Appl Pharmacol* **1966**, *8*, 6-12.

(14) Bodansky, O. Methemoglobinemia and methemoglobin-producing compounds. *Pharmacol Rev* **1951**, *3*, 144-196.

(15) Shahal, Y.; Zmora, E.; Katz, M.; Mazor, D.; Meyerstein, N. Effect of vitamin K on neonatal erythrocytes. *Biol Neonate* **1992**, *62*, 373-378.

(16) Lopez-Shirley, K.; Zhang, F.; Gosser, D.; Scott, M.; Meshnick, S. R. Antimalarial quinones: redox potential dependence of methemoglobin formation and heme release in erythrocytes. *J Lab Clin Med* **1994**, *123*, 126-130.

(17) Kruger-Zeitzer, E.; Sullivan, S. G.; Stern, A.; Munday, R. Effects of 1,4-naphthoquinone derivatives on red blood cell metabolism. *J Appl Toxicol* **1990**, *10*, 129-133.

(18) Goldberg, B.; Stern, A. Production of superoxide anion during the oxidation of hemoglobin by menadione. *Biochim Biophys Acta* **1976**, *437*, 628-632.

(19) Stolk, J. M.; Smith, R. P. Species differences in methemoglobin reductase activity. *Biochem Pharmacol* **1966**, *15*, 343-351.

(20) Jaffe, E. R. Methaemoglobinaemia. *Clin Haematol* **1981**, *10*, 99-122.

(21) Miodovnik, A. The biochemistry, diagnosis, and treatment of nitrate toxicity. *Virtual Mentor* **2009**, *11*, 451-455.

(22) Wright, R. O.; Lewander, W. J.; Woolf, A. D. Methemoglobinemia: etiology, pharmacology, and clinical management. *Ann Emerg Med* **1999**, *34*, 646-656.

(23) Harley, J. D.; Robin, H. The effect of menadione on the reduction of methaemoglobin. *Aust J Exp Biol Med Sci* **1962**, *40*, 473-483.

(24) Jaffe, E. R.; Neurmann, G. A Comparision of the Effect of Menadione, Methylene Blue and Ascorbic Acid on the Reduction of Methemoglobin in Vivo. *Nature* **1964**, *202*, 607-608.

(25) Evelyn, K. A.; Malloy, H. T. Microdetermination of oxyhemoglobin, methemoglobin, and sulfhemoglobin in a single sample of blood. *Journal of Biological Chemistry* **1938**, *126*, 655-662.

(26) Li, R.; Bianchet, M. A.; Talalay, P.; Amzel, L. M. The three-dimensional structure of NAD(P)H:quinone reductase, a flavoprotein involved in cancer chemoprotection and chemotherapy: mechanism of the two-electron reduction. *Proc Natl Acad Sci U S A* **1995**, *92*, 8846-8850.

(27) Faig, M.; Bianchet, M. A.; Talalay, P.; Chen, S.; Winski, S.; Ross, D.; Amzel, L. M. Structures of recombinant human and mouse NAD(P)H:quinone oxidoreductases: species comparison and structural changes with substrate binding and release. *Proc Natl Acad Sci U S A* **2000**, *97*, 3177-3182.

(28) Faig, M.; Bianchet, M. A.; Winski, S.; Hargreaves, R.; Moody, C. J.; Hudnott, A. R.; Ross, D.; Amzel, L. M. Structure-based development of anticancer drugs: complexes of NAD(P)H:quinone oxidoreductase 1 with chemotherapeutic quinones. *Structure* **2001**, *9*, 659-667.

(29) Vilar, S.; Cozza, G.; Moro, S. Medicinal chemistry and the molecular operating environment (MOE): application of QSAR and molecular docking to drug discovery. *Curr Top Med Chem* **2008**, *8*, 1555-1572.

(30) Mendoza, M. F.; Hollabaugh, N. M.; Hettiarachchi, S. U.; McCarley, R. L. Human NAD(P)H:quinone oxidoreductase type I (hNQO1) activation of quinone propionic acid trigger groups. *Biochemistry* **2012**, *51*, 8014-8026.

(31) Bair, J. S. The Development of Deoxynyboquinone as a Personalized Anticancer Compound, University of Illinois at Urbana-Champaign, 2012.

(32) Li, S.; Tian, X.; Niu, S.; Zhang, W.; Chen, Y.; Zhang, H.; Yang, X.; Li, W.; Zhang, S.; Ju, J.; Zhang, C. Pseudonocardians A-C, new diazaanthraquinone derivatives from a deap-sea actinomycete Pseudonocardia sp. SCSIO 01299. *Marine drugs* **2011**, *9*, 1428-1439.

(33) Parkinson, E. I.; Bair, J. S.; Nakamura, B. A.; Lee, H. Y.; Kuttab, H. I.; Southgate, E. H.; Lezmi, S.; Lau, G. W.; Hergenrother, P. J. Deoxynybomycins inhibit mutant DNA gyrase and rescue mice infected with fluoroquinolone-resistant bacteria. *Nat Commun* **2015**, *6*, 6947.

(34) Marin, A.; Lopez de Cerain, A.; Hamilton, E.; Lewis, A. D.; Martinez-Penuela, J. M.; Idoate, M. A.; Bello, J. DT-diaphorase and cytochrome B5 reductase in human lung and breast tumours. *Br J Cancer* **1997**, *76*, 923-929.

(35) Siegel, R. L.; Miller, K. D.; Jemal, A. Cancer statistics, 2015. *CA Cancer J Clin* **2015**, *65*, 5-29.

(36) Perou, C. M.; Sorlie, T.; Eisen, M. B.; van de Rijn, M.; Jeffrey, S. S.; Rees, C. A.; Pollack, J. R.; Ross, D. T.; Johnsen, H.; Akslen, L. A.; Fluge, O.; Pergamenschikov, A.; Williams, C.; Zhu, S. X.; Lonning, P. E.; Borresen-Dale, A. L.; Brown, P. O.; Botstein, D. Molecular portraits of human breast tumours. *Nature* **2000**, *406*, 747-752.

(37) Sorlie, T.; Perou, C. M.; Tibshirani, R.; Aas, T.; Geisler, S.; Johnsen, H.; Hastie, T.; Eisen, M. B.; van de Rijn, M.; Jeffrey, S. S.; Thorsen, T.; Quist, H.; Matese, J. C.; Brown, P. O.; Botstein, D.; Eystein Lonning, P.; Borresen-Dale, A. L. Gene expression patterns of breast carcinomas distinguish tumor subclasses with clinical implications. *Proc Natl Acad Sci U S A* **2001**, *98*, 10869-10874.

(38) Liedtke, C.; Mazouni, C.; Hess, K. R.; Andre, F.; Tordai, A.; Mejia, J. A.; Symmans, W. F.; Gonzalez-Angulo, A. M.; Hennessy, B.; Green, M.; Cristofanilli, M.; Hortobagyi, G. N.; Pusztai, L.

Response to neoadjuvant therapy and long-term survival in patients with triple-negative breast cancer. *J Clin Oncol* **2008**, *26*, 1275-1281.

(39) Verma, S.; Provencher, L.; Dent, R. Emerging trends in the treatment of triple-negative breast cancer in Canada: a survey. *Curr Oncol* **2011**, *18*, 180-190.

(40) Nanda, R. "Targeting" triple-negative breast cancer: the lessons learned from BRCA1-associated breast cancers. *Semin Oncol* **2011**, *38*, 254-262.

(41) Carey, L. A.; Dees, E. C.; Sawyer, L.; Gatti, L.; Moore, D. T.; Collichio, F.; Ollila, D. W.; Sartor, C. I.; Graham, M. L.; Perou, C. M. The triple negative paradox: primary tumor chemosensitivity of breast cancer subtypes. *Clin Cancer Res* **2007**, *13*, 2329-2334.

(42) Dent, R.; Trudeau, M.; Pritchard, K. I.; Hanna, W. M.; Kahn, H. K.; Sawka, C. A.; Lickley, L. A.; Rawlinson, E.; Sun, P.; Narod, S. A. Triple-negative breast cancer: clinical features and patterns of recurrence. *Clin Cancer Res* **2007**, *13*, 4429-4434.

(43) Duffy, M. J.; McGowan, P. M.; Crown, J. Targeted therapy for triple-negative breast cancer: Where are we? *Int J Cancer* **2012**.

(44) Tutt, A.; Robson, M.; Garber, J. E.; Domchek, S. M.; Audeh, M. W.; Weitzel, J. N.; Friedlander, M.; Arun, B.; Loman, N.; Schmutzler, R. K.; Wardley, A.; Mitchell, G.; Earl, H.; Wickens, M.; Carmichael, J. Oral poly(ADP-ribose) polymerase inhibitor olaparib in patients with BRCA1 or BRCA2 mutations and advanced breast cancer: a proof-of-concept trial. *Lancet* **2010**, *376*, 235-244.

(45) Lehmann, B. D.; Bauer, J. A.; Chen, X.; Sanders, M. E.; Chakravarthy, A. B.; Shyr, Y.; Pietenpol, J. A. Identification of human triple-negative breast cancer subtypes and preclinical models for selection of targeted therapies. *Journal of Clinical Investigation* **2011**, *121*, 2750-2767.

(46) Dorssers, L. C.; Van der Flier, S.; Brinkman, A.; van Agthoven, T.; Veldscholte, J.; Berns, E. M.; Klijn, J. G.; Beex, L. V.; Foekens, J. A. Tamoxifen resistance in breast cancer: elucidating mechanisms. *Drugs* **2001**, *61*, 1721-1733.

(47) Vu, T.; Claret, F. X. Trastuzumab: updated mechanisms of action and resistance in breast cancer. *Front Oncol* **2012**, *2*, 62.

(48) Bentle, M. S.; Reinicke, K. E.; Bey, E. A.; Spitz, D. R.; Boothman, D. A. Calcium-dependent modulation of poly(ADP-ribose) polymerase-1 alters cellular metabolism and DNA repair. *J. Biol. Chem.* **2006**, *281*, 33684-33696.

(49) Bey, E. A.; Reinicke, K. E.; Srougi, M. C.; Varnes, M.; Anderson, V. E.; Pink, J. J.; Li, L. S.; Patel, M.; Cao, L.; Moore, Z.; Rommel, A.; Boatman, M.; Lewis, C.; Euhus, D. M.; Bornmann, W. G.; Buchsbaum, D. J.; Spitz, D. R.; Gao, J.; Boothman, D. A. Catalase abrogates beta-lapachone-induced PARP1 hyperactivation-directed programmed necrosis in NQO1-positive breast cancers. *Molecular cancer therapeutics* **2013**, *12*, 2110-2120.

(50) Andrez, J. C. Mitomycins syntheses: a recent update. *Beilstein J Org Chem* **2009**, *5*, 33.

(51) Gustafson, D. L.; Siegel, D.; Rastatter, J. C.; Merz, A. L.; Parpal, J. C.; Kepa, J. K.; Ross, D.; Long, M. E. Kinetics of NAD(P)H:quinone oxidoreductase I (NQO1) inhibition by mitomycin C in vitro and in vivo. *J Pharmacol Exp Ther* **2003**, *305*, 1079-1086.

(52) Gustafson, D. L.; Beall, H. D.; Bolton, E. M.; Ross, D.; Waldren, C. A. Expression of human NAD(P)H: quinone oxidoreductase (DT-diaphorase) in Chinese hamster ovary cells: effect on the toxicity of antitumor quinones. *Mol Pharmacol* **1996**, *50*, 728-735.

(53) Pan, S. S.; Iracki, T.; Bachur, N. R. DNA alkylation by enzyme-activated mitomycin C. *Mol Pharmacol* **1986**, *29*, 622-628.

(54) Keyes, S. R.; Rockwell, S.; Sartorelli, A. C. Enhancement of mitomycin C cytotoxicity to hypoxic tumor cells by dicoumarol in vivo and in vitro. *Cancer Res* **1985**, *45*, 213-216.

(55) Belcourt, M. F.; Hodnick, W. F.; Rockwell, S.; Sartorelli, A. C. Bioactivation of mitomycin antibiotics by aerobic and hypoxic Chinese hamster ovary cells overexpressing DT-diaphorase. *Biochem Pharmacol* **1996**, *51*, 1669-1678.

(56) Nemeikaite-Ceniene, A.; Sarlauskas, J.; Anusevicius, Z.; Nivinskas, H.; Cenas, N. Cytotoxicity of RH1 and related aziridinylbenzoquinones: involvement of activation by NAD(P)H:quinone oxidoreductase (NQO1) and oxidative stress. *Arch Biochem Biophys* **2003**, *416*, 110-118.

(57) Begleiter, A.; Leith, M. K.; Patel, D.; Hasinoff, B. B. Role of NADPH cytochrome P450 reductase in activation of RH1. *Cancer Chemother Pharmacol* **2007**, *60*, 713-723.

(58) Tudor, G.; Alley, M.; Nelson, C. M.; Huang, R.; Covell, D. G.; Gutierrez, P.; Sausville, E. A. Cytotoxicity of RH1: NAD(P)H:quinone acceptor oxidoreductase (NQO1)-independent oxidative stress and apoptosis induction. *Anticancer Drugs* **2005**, *16*, 381-391.

(59) Winski, S. L.; Swann, E.; Hargreaves, R. H.; Dehn, D. L.; Butler, J.; Moody, C. J.; Ross, D. Relationship between NAD(P)H:quinone oxidoreductase 1 (NQO1) levels in a series of stably transfected cell lines and susceptibility to antitumor quinones. *Biochem Pharmacol* **2001**, *61*, 1509-1516.

(60) Dehn, D. L.; Inayat-Hussain, S. H.; Ross, D. RH1 induces cellular damage in an NAD(P)H:quinone oxidoreductase 1-dependent manner: relationship between DNA cross-linking, cell cycle perturbations, and apoptosis. *J Pharmacol Exp Ther* **2005**, *313*, 771-779.

(61) Dehn, D. L.; Winski, S. L.; Ross, D. Development of a new isogenic cell-xenograft system for evaluation of NAD(P)H:quinone oxidoreductase-directed antitumor quinones: evaluation of the activity of RH1. *Clin Cancer Res* **2004**, *10*, 3147-3155.

(62) Sharp, S. Y.; Kelland, L. R.; Valenti, M. R.; Brunton, L. A.; Hobbs, S.; Workman, P. Establishment of an isogenic human colon tumor model for NQO1 gene expression: application to investigate the role of DT-diaphorase in bioreductive drug activation in vitro and in vivo. *Mol Pharmacol* **2000**, *58*, 1146-1155.

(63) Plumb, J. A.; Workman, P. Unusually marked hypoxic sensitization to indoloquinone EO9 and mitomycin C in a human colon-tumour cell line that lacks DT-diaphorase activity. *Int J Cancer* **1994**, *56*, 134-139.

(64) Kim, J. Y.; Patterson, A. V.; Stratford, I. J.; Hendry, J. H. The importance of DT-diaphorase and hypoxia in the cytotoxicity of RH1 in human breast and non-small cell lung cancer cell lines. *Anticancer Drugs* **2004**, *15*, 71-77.

(65) Hussein, D.; Holt, S. V.; Brookes, K. E.; Klymenko, T.; Adamski, J. K.; Hogg, A.; Estlin, E. J.; Ward, T.; Dive, C.; Makin, G. W. Preclinical efficacy of the bioreductive alkylating agent RH1 against paediatric tumours. *Br J Cancer* **2009**, *101*, 55-63.

(66) Beall, H. D.; Murphy, A. M.; Siegel, D.; Hargreaves, R. H.; Butler, J.; Ross, D. Nicotinamide adenine dinucleotide (phosphate): quinone oxidoreductase (DT-diaphorase) as a target for bioreductive antitumor quinones: quinone cytotoxicity and selectivity in human lung and breast cancer cell lines. *Mol Pharmacol* **1995**, *48*, 499-504.

(67) Yee, S. B.; Pritsos, C. A. Comparison of oxygen radical generation from the reductive activation of doxorubicin, streptonigrin, and menadione by xanthine oxidase and xanthine dehydrogenase. *Arch Biochem Biophys* **1997**, *347*, 235-241.

(68) Lewis, A. M.; Ough, M.; Hinkhouse, M. M.; Tsao, M. S.; Oberley, L. W.; Cullen, J. J. Targeting NAD(P)H:quinone oxidoreductase (NQO1) in pancreatic cancer. *Mol Carcinog* **2005**, *43*, 215-224.

(69) Dehn, D. L.; Siegel, D.; Swann, E.; Moody, C. J.; Ross, D. Biochemical, cytotoxic, and genotoxic effects of ES936, a mechanism-based inhibitor of NAD(P)H:quinone oxidoreductase 1, in cellular systems. *Mol Pharmacol* **2003**, *64*, 714-720.

(70) Pink, J. J.; Planchon, S. M.; Tagliarino, C.; Varnes, M. E.; Siegel, D.; Boothman, D. A. NAD(P)H:Quinone oxidoreductase activity is the principal determinant of beta-lapachone cytotoxicity. *J Biol Chem* **2000**, *275*, 5416-5424.

(71) Bey, E. A.; Bentle, M. S.; Reinicke, K. E.; Dong, Y.; Yang, C. R.; Girard, L.; Minna, J. D.; Bornmann, W. G.; Gao, J.; Boothman, D. A. An NQO1- and PARP-1-mediated cell death pathway induced in non-small-cell lung cancer cells by beta-lapachone. *Proc Natl Acad Sci U S A* **2007**, *104*, 11832-11837.

(72) Blanco, E.; Bey, E. A.; Khemtong, C.; Yang, S. G.; Setti-Guthi, J.; Chen, H.; Kessinger, C. W.; Carnevale, K. A.; Bornmann, W. G.; Boothman, D. A.; Gao, J. Beta-lapachone micellar nanotherapeutics for non-small cell lung cancer therapy. *Cancer Res* **2010**, *70*, 3896-3904.

(73) Botham, R. C.; Fan, T. M.; Im, I.; Borst, L. B.; Dirikolu, L.; Hergenrother, P. J. Dual small-molecule targeting of procaspase-3 dramatically enhances zymogen activation and anticancer activity. *J Am Chem Soc* **2014**, *136*, 1312-1319.

(74) Munck, C.; Gumpert, H. K.; Wallin, A. I.; Wang, H. H.; Sommer, M. O. Prediction of resistance development against drug combinations by collateral responses to component drugs. *Sci Transl Med* **2014**, *6*, 262ra156.

(75) Rouleau, M.; Patel, A.; Hendzel, M. J.; Kaufmann, S. H.; Poirier, G. G. PARP inhibition: PARP1 and beyond. *Nat Rev Cancer* **2010**, *10*, 293-301.

(76) In *New and Events*; FDA: Silver Spring, MD, 2014; Vol. 2015.

(77) Weil, M. K.; Chen, A. P. PARP inhibitor treatment in ovarian and breast cancer. *Curr Probl Cancer* **2011**, *35*, 7-50.

(78) Rajan, A.; Carter, C. A.; Kelly, R. J.; Gutierrez, M.; Kummar, S.; Szabo, E.; Yancey, M. A.; Ji, J.; Mannargudi, B.; Woo, S.; Spencer, S.; Figg, W. D.; Giaccone, G. A phase I combination study of olaparib with cisplatin and gemcitabine in adults with solid tumors. *Clin Cancer Res* **2012**, *18*, 2344-2351.

(79) Hergenrother, P. J.; Boothman, D. A.; Bair, J. S.; Cao, L.; Gao, J.; Huang, X.; Luo, X.; Ma, X.; Moore, Z.; Parkinson, E. I.: USA, 2014.

(80) Moore, Z.; Chakrabarti, G.; Luo, X.; Ali, A.; Hu, Z.; Fattah, F. J.; Vemireddy, R.; DeBerardinis, R. J.; Brekken, R. A.; Boothman, D. A. NAMPT inhibition sensitizes pancreatic adenocarcinoma cells to tumor-selective, PAR-independent metabolic catastrophe and cell death induced by beta-lapachone. *Cell Death Dis* **2015**, *6*, e1599.

(81) Chakrabarti, G.; Gerber, D. E.; Boothman, D. A. Expanding antitumor therapeutic windows by targeting cancer-specific nicotinamide adenine dinucleotide phosphate-biogenesis pathways. *Clin Pharmacol* **2015**, *7*, 57-68.

(82) Warburg, O. On the origin of cancer cells. *Science* **1956**, *123*, 309-314.

(83) Calvaresi, E. C.; Granchi, C.; Tuccinardi, T.; Di Bussolo, V.; Huigens, R. W., 3rd; Lee, H. Y.; Palchaudhuri, R.; Macchia, M.; Martinelli, A.; Minutolo, F.; Hergenrother, P. J. Dual targeting of the Warburg effect with a glucose-conjugated lactate dehydrogenase inhibitor. *Chembiochem* **2013**, *14*, 2263-2267.

(84) Granchi, C.; Roy, S.; Giacomelli, C.; Macchia, M.; Tuccinardi, T.; Martinelli, A.; Lanza, M.; Betti, L.; Giannaccini, G.; Lucacchini, A.; Funel, N.; Leon, L. G.; Giovannetti, E.; Peters, G. J.; Palchaudhuri, R.; Calvaresi, E. C.; Hergenrother, P. J.; Minutolo, F. Discovery of N-hydroxyindole-based inhibitors of human lactate dehydrogenase isoform A (LDH-A) as starvation agents against cancer cells. *J Med Chem* **2011**, *54*, 1599-1612.

(85) Le, A.; Cooper, C. R.; Gouw, A. M.; Dinavahi, R.; Maitra, A.; Deck, L. M.; Royer, R. E.; Vander Jagt, D. L.; Semenza, G. L.; Dang, C. V. Inhibition of lactate dehydrogenase A induces oxidative stress and inhibits tumor progression. *Proc Natl Acad Sci U S A* **2010**, *107*, 2037-2042.

(86) Tannehill-Gregg, S. H.; Levine, A. L.; Rosol, T. J. Feline head and neck squamous cell carcinoma: a natural model for the human disease and development of a mouse model. *Vet Comp Oncol* **2006**, *4*, 84-97.

(87) Hall, S. R.; Blundon, H. L.; Ladda, M. A.; Robertson, A. W.; Martinez-Farina, C. F.; Jakeman, D. L.; Goralski, K. B. Jadomycin breast cancer cytotoxicity is mediated by a copper-dependent, reactive oxygen species-inducing mechanism. *Pharmacol Res Perspect* **2015**, *3*, e00110.

(88) Liou, G. Y.; Storz, P. Reactive oxygen species in cancer. *Free Radic Res* **2010**, *44*, 479-496.

(89) Gargouri, B.; Lassoued, S.; Ben Mansour, R.; Ayadi, W.; Idriss, N.; Attia, H.; El Feki Ael, F. High levels of autoantibodies against catalase and superoxide dismutase in nasopharyngeal carcinoma. *South Med J* **2009**, *102*, 1222-1226.

(90) Cai, C. Y.; Zhai, L. L.; Wu, Y.; Tang, Z. G. Expression and clinical value of peroxiredoxin-1 in patients with pancreatic cancer. *Eur J Surg Oncol* **2015**, *41*, 228-235.

(91) Dietlein, F.; Thelen, L.; Reinhardt, H. C. Cancer-specific defects in DNA repair pathways as targets for personalized therapeutic approaches. *Trends Genet* **2014**, *30*, 326-339.

(92) Gudmundsdottir, K.; Ashworth, A. The roles of BRCA1 and BRCA2 and associated proteins in the maintenance of genomic stability. *Oncogene* **2006**, *25*, 5864-5874.

(93) Elstrodt, F.; Hollestelle, A.; Nagel, J. H.; Gorin, M.; Wasielewski, M.; van den Ouweland, A.; Merajver, S. D.; Ethier, S. P.; Schutte, M. BRCA1 mutation analysis of 41 human breast cancer cell lines reveals three new deleterious mutants. *Cancer Res* **2006**, *66*, 41-45.

(94) Eccles, D. M.; Mitchell, G.; Monteiro, A. N.; Schmutzler, R.; Couch, F. J.; Spurdle, A. B.; Gomez-Garcia, E. B. BRCA1 and BRCA2 genetic testing-pitfalls and recommendations for managing variants of uncertain clinical significance. *Ann Oncol* **2015**.

(95) Feiner, J. R.; Bickler, P. E.; Mannheimer, P. D. Accuracy of methemoglobin detection by pulse CO-oximetry during hypoxia. *Anesth Analg* **2010**, *111*, 143-148.

(96) *Basic & Clinical Pharmacology, 13th Edition*; 13 ed.; Katzung, B.; Trevor, A., Eds.; McGraw-Hill Education, 2015.

(97) Uhlen, M.; Fagerberg, L.; Hallstrom, B. M.; Lindskog, C.; Oksvold, P.; Mardinoglu, A.; Sivertsson, A.; Kampf, C.; Sjostedt, E.; Asplund, A.; Olsson, I.; Edlund, K.; Lundberg, E.; Navani, S.; Szigyarto, C. A.; Odeberg, J.; Djureinovic, D.; Takanen, J. O.; Hober, S.; Alm, T.; Edqvist, P. H.; Berling, H.; Tegel, H.; Mulder, J.; Rockberg, J.; Nilsson, P.; Schwenk, J. M.; Hamsten, M.; von Feilitzen, K.; Forsberg, M.; Persson, L.; Johansson, F.; Zwahlen, M.; von Heijne, G.; Nielsen, J.; Ponten, F. Proteomics. Tissue-based map of the human proteome. *Science* **2015**, *347*, 1260419.

(98) Ma, X.; Huang, X.; Moore, Z.; Huang, G.; Kilgore, J. A.; Wang, Y.; Hammer, S.; Williams, N. S.; Boothman, D. A.; Gao, J. Esterase-activatable beta-lapachone prodrug micelles for NQO1-targeted lung cancer therapy. *J Control Release* **2015**, *200*, 201-211.

(99) Pink, J. J.; Planchon, S. M.; Tagliarino, C.; Varnes, M. E.; Siegel, D.; Boothman, D. A. NAD(P)H:Quinone oxidoreductase activity is the principal determinant of beta-lapachone cytotoxicity. *J. Biol. Chem.* **2000**, *275*, 5416-5424.

(100) Vichai, V.; Kirtikara, K. Sulforhodamine B colorimetric assay for cytotoxicity screening. *Nat. Protocols* **2006**, *1*, 1112-1116.

(101) Wuerzberger, S. M.; Pink, J. J.; Planchon, S. M.; Byers, K. L.; Bornmann, W. G.; Boothman, D. A. Induction of apoptosis in MCF-7:WS8 breast cancer cells by beta-lapachone. *Cancer Res* **1998**, *58*, 1876-1885.

(102) Bey, E. A.; Bentle, M. S.; Reinicke, K. E.; Dong, Y.; Yang, C. R.; Girard, L.; Minna, J. D.; Bornmann, W. G.; Gao, J.; Boothman, D. A. An NQO1- and PARP-1-mediated cell death pathway induced in non-small-cell lung cancer cells by beta-lapachone. *Proc. Natl. Acad. Sci. U. S. A.* **2007**, *104*, 11832-11837.

(103) Bentle, M. S.; Reinicke, K. E.; Bey, E. A.; Spitz, D. R.; Boothman, D. A. Calcium-dependent modulation of poly(ADP-ribose) polymerase-1 alters cellular metabolism and DNA repair. *J Biol Chem* **2006**, *281*, 33684-33696.

Chapter 3. Deoxynybomycins as antibacterial agents for fluoroquinolone resistant bacteria

Portions of this Chapter are reprinted with permission from Parkinson, E. I.; Bair, J. S.; Nakamura, B.; Lee, H. Y.; Kuttab, H. I.; Southgate, E. H.; Lezmi, S. Lau, G. W.; Hergenrother, P. J. *Nat. Commun*. **2015**, *6*, 6947. Copyright 2015 Nature Publishing Group. Contributions of others are noted when applicable.

3.1 Limitations of deoxynybomycin

As has been discussed in Chapter 1.2, antibiotic resistance is one of the largest challenges facing the healthcare community. Previous reports describing the small molecule deoxynybomycin (DNM) have shown it to have antibacterial activity against a variety of bacteria including *M. smegmatis*, *Bacillus* species, as well as fluoroquinolone resistant (FQR) *S. aureus*.[1-2] More recent studies show it specifically targets the mutant DNA gyrase responsible for FQR (see Ch. 1.2.2 for more details).[2] While these activities are very promising, at least two main hurdles exist for the translation of DNM from a laboratory curiosity to a potentially useful antibiotic: 1) Challenges in obtaining large quantities of pure material and 2) Poor solubility of the natural products. We hypothesized that we could access large quantities of DNM from a late stage intermediate of the DNQ synthesis[3] developed by Dr. Joseph Bair and that we could utilize the modular synthesis to develop DNM derivatives that would retain activity while possessing better solubility profiles. Described in this Chapter are our efforts towards overcoming these challenges and biological evaluations of the promising derivatives that we found.

3.1.1 Challenges in obtaining DNM

Both isolation and synthesis of DNM have been described in the literature.[1,4-6] However, until now (see section 3.2), neither strategy has been able to efficiently produce large quantities of pure DNM. This point is made clear in a paper describing a complex purification procedure for DNM and the related nybomycin that states “Nybomycin and [DNM] do not yet have a real application because an efficient production (fermentation and synthesis) and downstream process does not exist.”[4]

Isolation of DNM was first described by Umezawa and co-workers from an Okinawan soil *Streptomyces*.[1] Since then the isolation of DNM has been reported by others[2,4-6] but they have not reported yields. Instead, one isolation report notes that "Deoxynybomycin is not normally detected in thin-layer chromatograms of ethanol extracts from fermentation broths, possibly because of its low concentration,"[6] causing one to suspect that the yields are not provided because they are very poor.

Until our total synthesis (described in 3.2),[7] the only total synthesis of DNM was that developed by Prof. Kenneth Rinehart.[8-9] While this synthesis was quite impressive for the time, it required 10 steps and had an overall yield of 0.83%. The low yield combined with the fact that the synthesis was not amenable to the development of derivatives limited its use in the further study of DNM as an antibacterial agent.

3.1.2 Poor solubility of DNM

In addition to being difficult to obtain, DNM is also extremely insoluble in almost all solvents. The initial isolation of DNM reported it to be soluble in hydrochloric and acetic acid with limited to no solubility in water, methanol, ethyl acetate, chloroform, acetone, as well as other organic solvents.[1] We have also found this to be true and this is further highlighted in section 3.2. A potential reason for this insolubility is that DNM is likely able to π-stack with itself in the solid state. A similar π-stacking has been seen in the crystal structure of the structurally related DNQ reported by Li and co-workers.[10] Previously, we were able to develop DNQ derivatives with extended alkyl chains capable of breaking up this π-stacking allowing for improved aqueous and organic solubility (see Chapter 2.2.5).[11] We hypothesized that we would likely be able to do the same with DNM.

3.2 Synthesis of DNM and DNM derivatives with improved solubility profiles[7]

Due to the documented difficulty of isolating DNM from natural sources,[4,6] we aimed to develop an efficient, modular, and flexible synthesis of DNM that could also be used to construct derivatives. Dr. Joseph Bair, a previous graduate student in the Hergenrother laboratory, developed a synthesis of the natural product deoxynyboquinone (DNQ) that relies on a mixed Suzuki cross coupling followed by a palladium-catalyzed ring closing and deprotection to give diazaanthracenol (**1** in Fig. 3.1A, see section 3.12 General Procedures A and B for the full synthesis).[3] To construct DNQ, **1** is oxidized to give the desired quinone.[3] We found that **1** could be converted to DNM in a single step by insertion of the methylene bridge in a reaction inspired by Rinehart's degradation studies and by bridge insertions in similar systems.[12-14] Reaction of **1** with dibromomethane gave DNM in a 73% yield (Fig. 3.1A). Through this route, DNM was obtained in 7 steps with an overall yield of 11%, an improvement over the only other reported total synthesis (10 steps, 0.83% overall yield).[12-13]

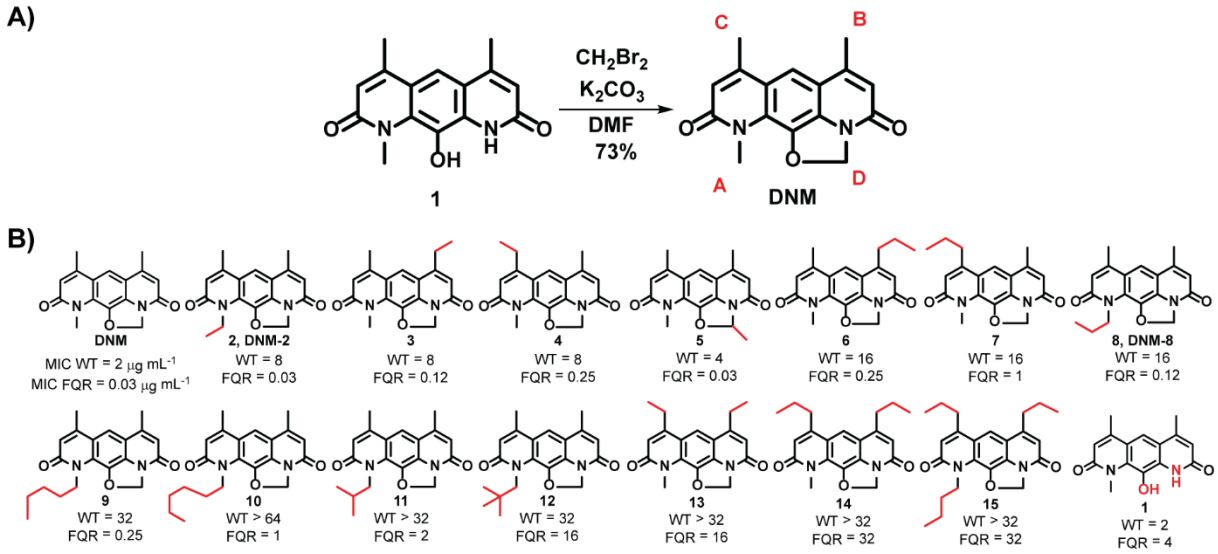

Figure 3.1. Synthesis and antibacterial activity of DNM and derivatives. (**A**) Final step in the synthesis of DNM. The letters A, B, C, and D around the structure of DNM denote sites of derivitization. (**B**) Structure of DNM and derivatives and their activities against wild type *S. aureus* (ATCC 29213, WT) and fluoroquinolone resistant *S. aureus* (NRS3, FQR). Activity is from three independent replicates of the microdilution broth assay and is reported as the MIC in μg mL^{-1}.

This flexible synthetic route also allowed for rapid generation of a variety of unnatural derivatives. We hypothesized that addition of alkyl chains would disrupt π-stacking between DNM molecules, thus increasing both aqueous and organic solubility, similar to what was observed with DNQ derivatives (see Chapter 2.2.5).[11] By changing the iodoamides used in the Suzuki cross coupling (see section 3.12 General Procedure A), three compounds were synthesized that substituted ethyl for methyl at positions *A*, *B*, and *C* (compounds **2**, **3**, and **4** respectively, Fig. 3.1B). The derivative with a methyl substitution at *D* was generated by using 1,1-dibromoethane in place of dibromomethane in the final step to provide compound **5** (Fig. 3.1B). Other compounds with single sites of derivatization (**6**-**12**) and multiple sites of derivatization (**13-15**) were also constructed. Full synthetic routes along with experimental details and characterization data can be found in the Materials and Methods Section (Section 3.12). Compounds with small alkyl appendages have markedly improved solubility (3 to 13 fold) in pH 7.4 phosphate buffered saline relative to DNM (Table 3.1), and all compounds synthesized also have improved DMSO solubility compared to the parent compound (Table 3.1).

Table 3.1. Solubility and activity of DNM and its derivatives

CIP	DAPT	VANC	LINEZ	DNM	2	3	4	5	6	7	8	9	10	11	12	13	14	15
Solubility in pH 7.4 PBS (μM)																		
				9 ± 3	121 ± 4	27 ± 1	53 ± 8	ND	ND	ND	68 ± 9	ND	ND	ND	ND	48 ± 8	<1	ND
Solubility in DMSO (mM)																		
				0.2	4	1.3	4.7	3.4	6.4	5.8	11.3	26.9	56.7	7.1	38.7	5.2	18.3	4.2
MIC against S. aureus 29213 (μg mL^{-1}) WT GyrA and WT ParC																		
0.25-0.5	2	1	2	>1	8	8	8	4	16	16	16	32	>64	>32	32	>32	>32	>32
MIC against S. aureus NRS3 (μg mL^{-1}) S84L GyrA and S80F ParC																		
>64	8	8	0.5	0.03	0.03	0.12	0.25	0.03	0.25	1	0.12	0.25	1	2	16	16	32	32

The solubility in PBS (pH 7.4) was determined by weighing a small amount of compound (0.5 – 2.0 mg) into a 1.7 mL Eppendorf tube. Enough PBS was added to make a 1 mg/mL solution. Compounds were then assessed by LC-MS and compared to a calibration curve to determine the solubility. More details can be found in the Supplementary Materials and Methods. Data shown is from three independent replicates ± SEM. ND = not determined. DMSO solubility of compounds was determined by weighing a small amount of compound (typically 1-2 mg) into a glass vial and adding DMSO dropwise until the compound was fully dissolved. Between DMSO additions, the vial was vortexed and sonicated. MICs with ciprofloxacin (CIP), daptomycin (DAPT), vancomycin (VANC), linezolid (LINEZ), deoxynybomycin (DNM), and DNM derivatives were determined using the microdilution broth method as outlined by the Clinical and Laboratory Standards Institute (CLSI).[15]

3.3 Evaluation of DNM and derivatives against FQR Gram-positive bacteria

Gram-positive bacteria (so named because they are stained by crystal violet dye) have a single cell membrane surrounded by a thick layer of peptidoglycan.[16] The CDC estimates that in 2013 approximately 64% of the 2,049,442 illnesses and 85% of the 23,488 deaths due to antibiotic resistant bacteria were due to Gram-positive infections. Specifically, methicillin-resistant *S. aureus* (MRSA) was estimated to cause 80,461 illnesses (~4%) and 11,285 deaths (~49%) while vancomycin-resistant *Enterococcus* (VRE) were estimated to cause 20,000 illnesses (~1%) and 1,300 deaths (~6%).[17] While some antibiotics are still effective against these infections (e.g. vancomycin, daptomycin and linezolid), further resistance has been observed even to these agents.[18-22] Additionally, linezolid is the only agent effective against these resistant pathogens that

is available for oral administration, highlighting the desperate need for novel orally available antibiotics.[23] For this reason, we chose to explore the potency of DNM against FQR Gram-positive bacteria.

3.3.1 Activity of DNM and derivatives against clinical isolates of *S. aureus*[7]

Previously, Hiramatsu and co-workers had demonstrated that DNM and nybomycin isolated from *Streptomyces* both showed excellent activity against FQR *S. aureus* with a S84L gyrA mutation.[2] Our synthetic DNM showed a similar activity profile. DNM was evaluated against both FQ sensitive *S. aureus* (ATCC 29213) and FQR MRSA (NRS3 which has GyrA S84L and ParC S80F). DNM showed modest activity against the FQ-sensitive (FQS) strain 29213 (MIC > 1 μg/mL). However, DNM showed excellent activity against the FQR NRS3 (MIC = 0.03 μg mL^{-1}, Fig. 3.1B and 3.2A). This MIC compares favorably with standard of care treatments for Gram-positive infections including vancomycin (VANC, MIC for NRS3 = 8 μg mL^{-1}), daptomycin (DAPT, MIC for NRS3 = 8 μg mL^{-1}) and linezolid (LINEZ, MIC for NRS3 = 0.5 μg mL^{-1}, Figure 3.2B). DNM derivatives were also evaluated against both FQ sensitive *S. aureus* (ATCC 29213) and FQR MRSA (NRS3), and their MIC values are listed in Figure 3.1B. Similar to DNM, most derivatives showed significantly enhanced activity against FQR NRS3 compared to FQS 29213. In general, compounds with a single methyl addition retained good activity against NRS3 (**2**-**5**). Further substitution at *B* was relatively well tolerated (**6**), while substitution at *C* was generally less well tolerated (**7**). Compounds possessing longer chains at *A* generally retained potency (**8-10**). However, compounds with bulky substitutions at *A* (**11-12**), multiple substitutions (**13-15**), or without the methylene bridge (**1**) were less active.

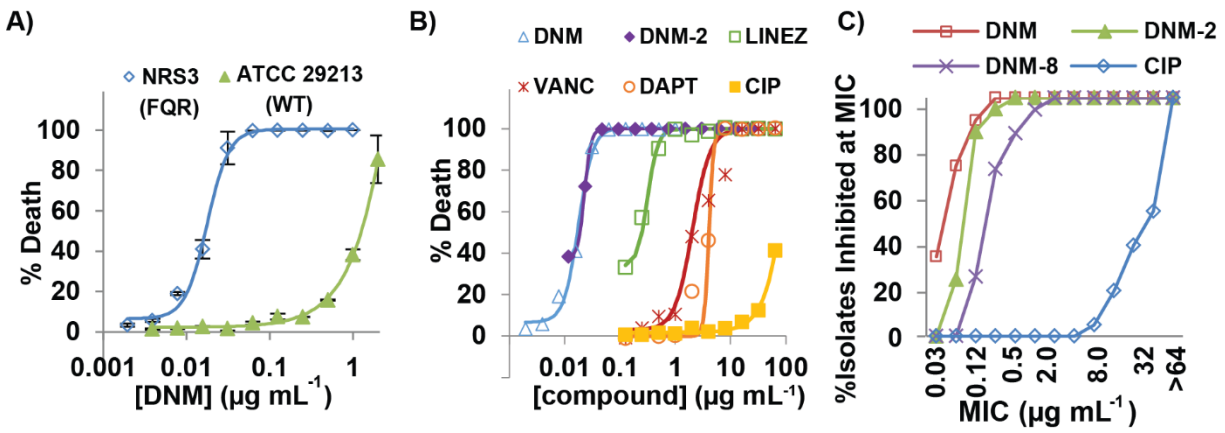

Figure 3.2. Sensitivity of MRSA isolates to DNM, DNM-2, DNM-8, ciprofloxacin (CIP), and other Gram-positive antibiotics. (**A**) Dose response curves for FQ sensitive *S. aureus* (29213) and FQR *S. aureus* (NRS3) treated with DNM. Data shown is from three independent replicates ± the standard error (SEM). (**B**) Dose response curves for FQR *S. aureus* (NRS3) treated with DNM, DNM-2, linezolid (LINEZ), vancomycin (VANC), daptomycin (DAPT) and CIP. (**C**) The percentage of MRSA clinical isolates (n = 21) with an MIC at or lower than the concentration shown.

DNM and two of the most potent derivatives (DNM-2 and DNM-8) were evaluated against a panel of MRSA clinical isolates (Fig. 3.2C and Table 3.2) by Cubist Pharmaceuticals. As shown in Fig. 3.2C, all MRSA strains were sensitive to these compounds and resistant to ciprofloxacin (CIP). In order to understand this selectivity, the quinolone resistance determining regions (QRDRs) of GyrA and ParC for many of these isolates were sequenced (Table 3.2). While different substitution patterns were found for MRSA ParC, all sequenced strains have the same mutation in GyrA (S84L) consistent with the notion that this mutation sensitizes bacteria to DNM. The activity of the DNM-2 and DNM-8 against these panels of clinical isolates closely mirrors that of DNM (Fig. 3.2C). Full details of the sensitivity of each strain can be found in Table 3.2.

Table 3.2. Sensitivity of MRSA clinical isolates to CIP, DNM, DNM derivatives, and other antibiotics and tabulated data from Figure 3.2C

Strain ID	CIP S/I/R	CIP MIC (μg mL^{-1})	DNM MIC (μg mL^{-1})	DNM-2 MIC (μg mL^{-1})	DNM-8 MIC (μg mL^{-1})	Vanc MIC (μg mL^{-1})	Amp MIC (μg mL^{-1})	Novo MIC (μg mL^{-1})	gyrA mutations	parC mutations
SAU.42	S	0.25	1	2	8	1	2	0.5	ND	ND
SAU.1118	S	0.5	1	2	8	2	>64	0.5	ND	ND
SAU.3017	S	1	1	4	4	1	>64	0.5	ND	ND
SAU.3021	R	8	0.031	0.063	0.125	1	>64	0.25	ND	ND
SAU.446	R	16	0.25	0.125	0.25	2	>64	0.5	ND	ND
SAU.491	R	16	0.125	0.125	0.5	2	>64	0.5	Ser84Leu	Ser80Phe
SAU.555	R	16	0.125	0.25	0.5	1	>64	0.25	ND	ND
SAU.493	R	32	0.063	0.125	0.25	1	>64	0.5	Ser84Leu	Ser80Phe
SAU.710	R	32	0.031	0.063	0.125	2	>64	0.5	Ser84Leu	Ser80Phe
SAU.3024	R	32	0.031	0.125	0.125	2	>64	0.5	ND	ND
SAU.3026	R	32	0.125	0.125	0.25	1	>64	0.5	ND	ND
SAU.419	R	64	0.125	0.063	0.25	4	>64	0.25	ND	ND
SAU.846	R	64	0.031	0.25	0.5	8	>64	0.125	ND	ND
SAU.2996	R	64	0.25	0.5	2	1	>64	0.5	ND	ND
SAU.447	R	>64	0.063	0.125	1	2	>64	0.25	ND	ND
SAU.489	R	>64	0.031	0.125	0.25	2	>64	0.25	Ser84Leu	Ser80Tyr
SAU.492	R	>64	0.063	0.125	ND	1	>64	0.5	Ser84Leu	Ser80Tyr
SAU.494	R	>64	0.063	0.125	0.25	1	>64	0.125	Ser84Leu	Ser80Phe
SAU.495	R	>64	0.063	0.125	0.25	2	>64	0.5	Ser84Leu	Ser80Phe
SAU.496	R	>64	0.063	0.125	0.25	1	>64	0.5	Ser84Leu	Ser80Phe
SAU.669	R	>64	0.031	0.063	0.125	2	>64	0.5	ND	ND
SAU.708	R	>64	0.063	0.125	1	2	64	0.25	Ser84Leu	Ser80Phe Glu84Lys
SAU.709	R	>64	0.063	0.125	0.25	1	>64	0.5	Ser84Leu	Ser80Tyr Glu84Gly
SAU.3025	R	>64	0.031	0.063	0.125	1	64	0.25	ND	ND

The ciprofloxacin (CIP) sensitivity where a strain was considered sensitive (S) if it had an MIC ≤ 4 μg mL^{-1}, intermediate (I) with a 16 > MIC > 4 μg mL^{-1}, or resistant (R) with a MIC ≥ 16 μg mL^{-1}. MICs with CIP, DNM, DNM-2, DNM-8, Vancomycin (Vanc), Ampicillin (Amp), and Novobiocin (Novo) were determined using the microdilution broth method as outlined by the CLSI.[15] QRDR mutations were determined as described in the text using primers (primer sequences can be found in Table 3.13). Clinical isolates were obtained from Cubist Pharmaceuticals (Lexington, MA). ND = not determined. CIP resistant strains are graphed in Figure 3.2C.

3.3.2 Activity of DNM and derivatives against FQR *Enterococcus*[7]

The sensitivity of FQR VRE was also explored. DNM had no detectable activity against FQ sensitive *Enterococcus* (ATCC 29212, MIC > 1.0 μg mL^{-1}), but it potently inhibited the growth of FQR VRE (clinical isolate S235 which has GyrA S83I and ParC S80I, MIC = 0.125 μg mL^{-1}, Fig. 3.3A). After discovering that DNM has activity against FQR VRE, DNM, DNM-2, and DNM-8 were evaluated against a panel of VRE clinical isolates (Fig. 3.3B).

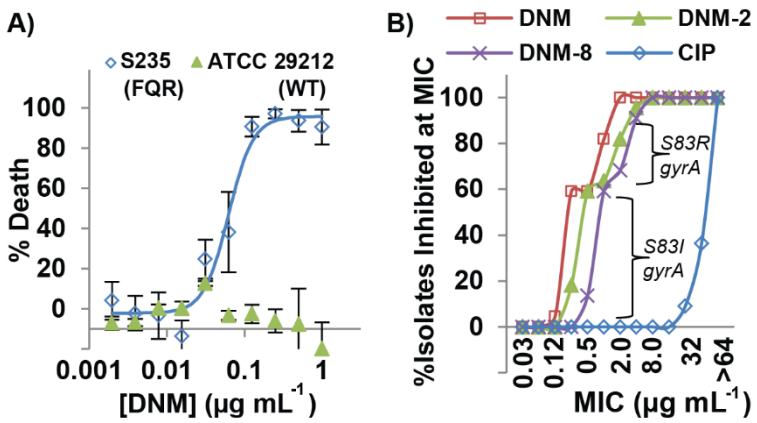

Figure 3.3. Sensitivity of VRE clinical isolates to DNM, DNM-2, DNM-8, and ciprofloxacin (CIP). (**A**) Dose response curves for FQ sensitive *Enterococcus* (29212) and FQR *Enterococcus* (S235) treated with DNM. Data shown is from three independent replicates ± SEM. (**B**) The percentage of VRE clinical isolates (n = 22) with an MIC at or lower than the concentration shown.

Similar to MRSA, all VRE strains are sensitive to these compounds, resistant to CIP, and have many different substitutions in ParC which do not appear to correlate with sensitivity. Unlike the MRSA isolates, the majority of VRE isolates have two different substitutions for GyrA (S83I or S83R). The sensitivity of these strains is affected by this substitution, with VRE harboring the S83I mutation being very sensitive to DNM (MIC = 0.125 to 1 µg mL^{-1}) and those with the S83R mutation being less sensitive (MIC ≥ 1 µg mL^{-1}). Again, the activity of DNM-2 and DNM-8 are similar to that of DNM (Fig. 3.3B). Full details of the sensitivity and QRDR mutational status of each strain can be found in Table 3.3.

Table 3.3. Sensitivity of ATCC strains and VRE clinical isolates to CIP, DNM, and DNM derivatives and tabulated data from Figure 3.3B

Strain	Species	CIP (S/I/R)	Cipro MIC (μg mL^{-1})	DNM MIC (μg mL^{-1})	DNM-2 MIC (μg mL^{-1})	DNM-8 MIC (μg mL^{-1})	gyrA mutations	parC mutations
ATCC 29212	*E. faecalis*	S	0.5-2	>1	8	8	WT	WT
ATCC 19433	*E. faecalis*	S	2	>1	8	16	WT	WT
S235	*E. faecium*	R	>64	0.125	0.5	1	Ser83Ile	Ser80Ile
S51	*E. faecium*	R	>64	0.25	0.5	1	Ser83Ile	Ser80Ile
S122	*E. faecium*	R	64	0.25	0.5	1	Ser83Ile	Ser80Ile
S226	*E. faecium*	R	64	0.25	0.5	1	Ser83Ile	Ser80Ile
S344	*E. faecium*	R	>64	0.25	0.5	1	Ser83Ile	Ser80Ile
S234	*E. faecalis*	R	32	0.25	0.25	0.5	Ser83Ile	Ser80Ile Glu84Asp
S557	*E. faecium*	R	>64	0.25	0.25	0.5	Ser83Ile	Ser80Ile
C27569	*E. faecium*	R	>64	0.25	0.25	1	Ser83Ile	Ser80Ile
C28535	*E. faecalis*	R	32	0.25	0.25	1	Ser83Ile	Ser80Ile
D1	*E. faecium*	R	>64	0.25	0.5	0.5	Ser83Ile	Ser80Ile
C21667	*E. faecalis*	R	>64	0.25	0.5	1	Ser83Ile	Ser80Ile
C28036	*Ent. Spp.*	R	64	0.25	0.5	1	Ser83Ile	Ser80Ile
SL152	*E. faecium*	R	>64	0.25	0.5	1	Ser83Ile	Ser80Ile
S206	*E. faecalis*	R	64	1	2	4	Ser83Arg	Ser80Ile
U63	*E. faecium*	R	>64	1	4	4	Ser83Arg	Ser80Ile
U275	*E. faecium*	R	>64	1	2	4	Ser83Cys Glu87Gly	Ser80Ile
U464	*E. faecium*	R	>64	1	2	2	Ser83Arg	Ser80Ile
S34	*E. faecium*	R	64	1	1	2	Ser83Ile	Ser80Arg
C27282	*E. faecium*	R	64	>1	4	8	Ser83Arg	Ser80Arg
U503	*E. faecium*	R	>64	>1	4	4	Ser83Arg	Ser80Ile
U563	*E. faecium*	R	>64	>1	2	4	Ser83Arg	Ser80Ile
C21190	*E. faecium*	R	>64	>1	8	8	Ser83Arg	Ser80Ile

The ciprofloxacin (CIP) sensitivity where a strain was considered sensitive (S) if it had an MIC ≤ 4 μg mL^{-1}, intermediate (I) with a 16 > MIC > 4 μg mL^{-1}, or resistant (R) with a MIC ≥ 16 μg mL^{-1}. MICs with CIP, DNM, DNM-2, and DNM-8 were determined using the microdilution broth method as outlined by the CLSI.[15] QRDR mutations were determined as described in the text using primers (primer sequences can be found in Table 3.13). CIP resistant strains are graphed in Figure 3.3B.

3.3.3 Activity of DNM and derivatives against other *Staphylococcus* species

In addition to analyzing *S. aureus* strains, Cubist Pharmaceuticals also tested DNM, DNM-2, and DNM-8 against several coagulase-negative *Staphylococcus* species including FQR *S. epidermis* and *S. haemolyticus*. Coagulase-negative *Staphylococcus* are *Staphyloccus* species that do not produce the enzyme coagulase which causes blood to clot. They are normally found in the skin and mucous membranes of humans, but can cause life-threatening bactermia in hospital settings, especially for immunocompromised patients and neonates.[24-25] In recent years,

high rates of antibiotic resistance have been observed in these bacteria with ~50-80% of the clinical isolates being FQR.[24-25] While we were not provided with the gyrA mutational status of these strains, generally the gyrA mutations observed for these FQR strains are as follows: FQR *S. haemolyticus* generally mutates S84 to either L (82-100%) or F (0-18%).[26-27] *S. epidermis* gyrA S84 generally has mutations to either Y (0-30%) or F (70-100%).[26-29] As expected, none of the FQS strains were particularly sensitive to DNM or its derivatives (Table 3.4). Both of the FQR *S. haemolyticus* strains had good sensitivity to DNM and its derivatives. The *S. haemolyticus* strains likely have a S84L mutation similar to *S. aureus* thus explaining their sensitivities. One of the FQR *S. epidermis* strains showed good sensitivity to DNM while the other two strains were more similar to the FQS strain. The FQR *S. epidermis* strains almost certainly have a different mutation than *S. aureus* and *S. haemolyticus* (S84Y/F instead of S84L) and this difference may explain the generally lower sensitivities seen with these strains. In vitro inhibition studies with the mutant enzymes support this hypothesis (see section 3.6.1). Further evaluation of FQR Coagulase-negative *Staphylococcus* species with known mutational statuses are needed to confirm this.

Table 3.4. Sensitivity of coagulase-negative *Staphylococcus* clinical isolates to CIP, DNM, DNM derivatives, and other antibiotics

Strain ID	Species	CIP S/I/R	CIP MIC (μg mL^{-1})	DNM MIC (μg mL^{-1})	DNM-2 MIC (μg mL^{-1})	DNM-8 MIC (μg mL^{-1})	Vanc MIC (μg mL^{-1})	Linez MIC (μg mL^{-1})	Novo MIC (μg mL^{-1})
SEP.5	*S. epidermidis*	S	0.125	>1	4	8	2	1	0.125
SSA.1960	*S. saprophyticus*	S	0.5	>1	4	8	2	4	32
SSA.1953	*S. saprophyticus*	S	0.5	>1	4	8	2	4	32
SHE.1682	*S. haemolyticus*	R	16	0.25	0.5	2	4	2	0.5
SHE.1245	*S. haemolyticus*	R	64	0.25	0.5	1	>64	2	2
SEP.714	*S. epidermidis*	R	>64	0.25	1	2	4	2	0.25
SEP.718	*S. epidermidis*	R	8	1	4	8	2	2	0.25
SEP.713	*S. epidermidis*	R	64	1	2	8	4	2	0.25

The ciprofloxacin (CIP) sensitivity where a strain was considered sensitive (S) if it had an MIC ≤ 4 μg mL^{-1}, intermediate (I) with a 16 > MIC > 4 μg mL^{-1}, or resistant (R) with a MIC ≥ 16 μg mL^{-1}. MICs with CIP, DNM, DNM-2, and DNM-8 were determined using the microdilution broth method as outlined by the CLSI.[15]

3.3.4 Activity of DNM and derivatives against FQR *B. anthracis*

While natural resistance of *B. anthracis* to FQs has not occurred, it has been generated in a laboratory setting.[30] There is fear that such strains could be used for a bioterrorist attack, especially since the front-line treatment for exposure to anthrax is ciprofloxacin. Similar to *S. aureus* and *S. haemolyticus*, FQR *B. anthracis* strains also have the characteristic S85L gyrA mutation (analogous to S84L in *S. aureus*).[30] Additionally, previous reports showed activity of DNM against *B*. *anthracis* as well as other *Bacillus* species.[1] Together these data strongly suggested that *B. anthracis* would be sensitive to DNM and its derivatives.

Table 3.5. Sensitivity of FQS & FQR *B. anthracis* to CIP & DNM-2

Strain	CIP S/I/R	CIP MIC (μg/mL)	DNM-2 MIC (μg/mL)	gyrA	parC
Sterne	S	<0.125	4.0	WT	WT
M5	R	16.0	4.0	E89K	WT
M12	R	8.0	1.0	S85L	WT
M16	R	64.0	2.0	S85L	WT

The ciprofloxacin (CIP) sensitivity where a strain was considered sensitive (S) if it had an MIC ≤ 4 μg mL^{-1}, intermediate (I) with a 16 > MIC > 4 μg mL^{-1}, or resistant (R) with a MIC ≥ 16 μg mL^{-1}. MICs with CIP and DNM-2 were determined using the microdilution broth method as outlined by the CLSI.[15] QRDR mutations were determined as described in the text using primers (primer sequences can be found in Table 3.13).

FQS and FQR *B. anthracis* strains were obtained from the Mitchell lab (UIUC), who originally obtained them from Lawrence Livermore National Labs. After sequencing the strains and finding several with either WT (S85) or S85L mutant gyrA, we tested these strains for sensitivity to CIP and DNM-2 (Table 3.5). CIP sensitivity was as expected with mutant strains being resistant to CIP. Addtionally, potency of DNM-2 against *B. anthracis* strains with WT S85 gyrA was comparable to the activities seen with FQS *S. aureus*. However, DNM-2 was less effective against the S85L gyrA *B. anthracis* strains compared to the S84L gyrA *S. aureus* strains. The reason for this remains unclear but is likely due to differences in DNA gyrase for *S. aureus* and *B. anthracis*. Uniprot alignment shows that gyrA for the two enzymes have ~62% identity and the QRDRs (amino acids 68-106) are 82% identical (see Figure 3.4A for sequence alignment).

While this is a relatively high level of identity, it is possible that some of the differences that exist are important for activity. Another possibility is that a difference exists in the other subunit of DNA gyrase, gyrB. Upon examination of a crystal structure of *S. aureus* DNA gyrase bound to DNA and CIP, a few main contacts with CIP were found to be important for binding. These include contacts with a Mn ion, the DNA, S84 on gyrA and R458 and E477 on gyrB (Figure 3.4B-C). Sequence alignment of gyrB from different bacteria revealed that there may be a correlation between the residue analogous to R458 in *S. aureus* and sensitivity of the bacteria to DNM-2. Specifically, when the residue is R458, there appears to be good sensitivity to DNM-2 (e.g. *S. aureus*, *Enterococcus* sp., and *M. tuberculosis* discussed in section 3.4). Alternatively, when the residue is R458 (*S. aureus* numbering), DNM-2 appears to be less potent (e.g. *B. anthracis*, *N. gonorrhoeae*, and the Gram-negative bacteria). More investigations into this observation are needed to confirm this correlation and determine an explanation for it.

A)

```
S. aureus........NEQGMTPDKSYKKSARIVGDVMGKYHPHGDSSIYEAMVRMAQDFSYRYPLVDGQGNFGSM 113
E. faecium.......NELGVTPDKAHKKSARIVGDVMGKYHPHGDSAIYESMVRMAQPFSYRYMLVDGHGNFGSV 113
E. faecalis......NELGVTPDKPHKKSARIVGDVMGKYHPHGDSAIYESMVRMAQPFSYRAMLVDGHGNFGSV 113
B. anthracis.....NDLGITADKAYKKSARIVGEVIGKYHPHGDSAVYETMVRMAQDFSQRYMLVDGHGNFGSV 114
S. pneumonia.....NELGVTPDKPHKKSARITGDVMGKYHPHGDSSIYEAMVRMAQWWSYRYMLVDGHGNFGSM 110
M. tuberculosis..FDSGFRPDRSHAKSARSVAETMGNYHPHGDASIYDSLVRMAQPWSLRYPLVDGQGNFGSP 119
N. gonorrhea.....HELKNNWNAAYKKSARIVGDVIGKYHPHGDSAVYDTIVRMAQNFAMRYVLIDGQGNFGSV 120
E. coli..........NVLGNDWNKAYKKSARVVGDVIGKYHPHGDSAVYDTIVRMAQPFSLRYMLVDGQGNFGSI 112
P. aeruginosa....SELGNDWNKPYKKSARVVGDVIGKYHPHGDTAVYDTIVRMAQPFSLRYMLVDGQGNFGSV 112
A. baumannii.....HELGNDYNKAYKKSARVVGDVIGKYHPHGDSAVYETIVRMAQDFSLRYLLVDGQGNFGSI 110
                      :  : **** ..:.:*:*******:::*:::***** :: *  *:**:*****
```

B)

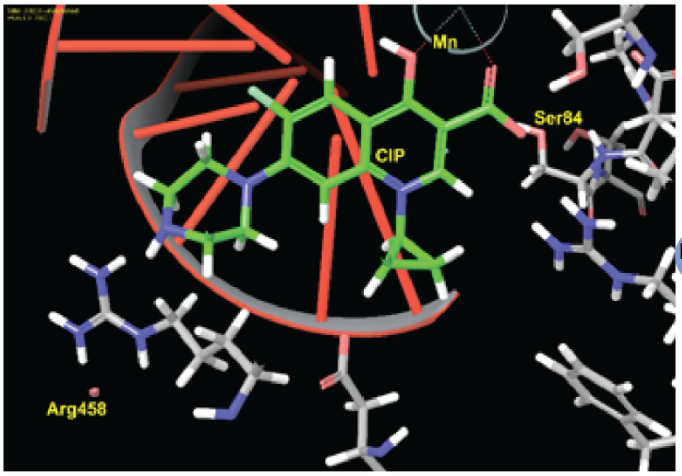

C)

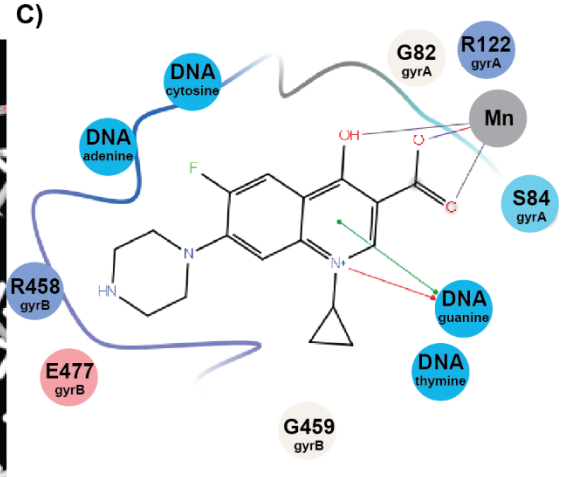

D)

```
S. aureus........RTQAILPLRGKILNVEKARLDRILNNNEIRQMITAFGTGIGG-DFDLAKARYHKIVIMTD 508
E. faecium.......EFQAILPIRGKILNVEKASMDKILANEEIRSLFTAMGTGFGE-DFDVSKARYHKLVIMTD 507
E. faecalis......EFQAILPIRGKILNVEKASMDKILANEEIRSLFTAMGTGFGE-DFDVSKARYHKLVIMTD 501
B. anthracis.....HFQAILPLKGKIINVEKARLDKILSNDEVRTIITAIGTNIGG-DFDIEKARYHKVIIMTD 503
S. pneumonia.....EFQAILPIRGKILNVEKASMDKILANEEIRSLFTAMGTGFGA-EFDVSKARYQKLVLMTD 506
M. tuberculosis..MFQAILPLRGKIINVEKARIDRVLKNTEVQAIITALGTGIHD-EFDIGKLRYHKIVLMAD 532
N. gonorrhea.....KFQAILPLKGKILNVEKARFEKMLASQEVATLITALGAGIGKEEFNPEKLRYHRIIIMTD 501
E. coli..........KNQAILPLKGKILNVEKARFDKMLSSQEVATLITALGCGIGRDEYNPDKLRYHSIIIMTD 498
P. aeruginosa....RTQAILPLKGKILNVEKARFDKMLSSQEVGTLITALGCGIGREEYNIDKLRYHNIIIMTD 500
A. baumannii.....KMQAILPLKGKILNVERARFDKMISSQEVGTLITALGCGIGREEYNPDKLRYHKII---- 388
                  *****::***:***:* ::::: . *:  ::**:*  :   :::  * **: ::
```

Figure 3.4. Comparison of DNA gyrase for *B. anthracis, S. aureus,* and other bacteria. (**A**) Sequence alignment of QRDR for gyrA of various bacteria. Key serine (S84 for *S. aureus*) or analogous residue is highlighted in red. (**B**) The crystal structure of *S. aureus* DNA gyrase with DNA (red) and CIP (green). Image generated with Maestro 9.7. (**C**) The ligand interaction map for B generated using Maestro. (**D**) The sequence alignment for gyrB for several species with the key arginine/lysine (R458 for *S. aureus*) highlighted in red.

3.3.5 Activity of DNM and derivatives against FQR *S. pneumoniae*

S. pneumoniae is one of the main causes of pneumonia, bacteremia, otitis media, and meningitis.[31] Fluoroquinolones (e.g. moxifloxacin or levofloxacin) are commonly prescribed for *S. pneumonia* infections.[31-32] While clinical isolates of FQR *S. pneumonia* are still relatively rare (≤1% worldwide),[31,33] more widespread resistance has been observed in some countries (e.g. 10.1% Israel, 14.1% Japan, and 22.3% Hong Kong, Emerging Infectious Diseases • www.cdc.gov/eid • Vol. 10, No. 10, October 2004) and is likely to increase with continued use of these agents. Similar to *S. epidermidis*, the most common gyrA mutations observed are S81F and S81Y.[34-35] Both Cubist Pharmaceuticals and UT Health Science Center (San Antonio, TX) tested DNM and its derivatives DNM-2 and DNM-8 against isolates of *S. pneumoniae* along with class A (e.g. *S. pyogenes*) and B *Streptococcus* (Table 3.6).

Table 3.6. Sensitivity of *Streptococcus* clinical isolates to CIP, DNM, DNM derivatives, and other antibiotics

Strain ID	Species	CIP S/I/R	CIP MIC (μg mL^{-1})	DNM MIC (μg mL^{-1})	DNM-2 MIC (μg mL^{-1})	DNM-8 MIC (μg mL^{-1})	Vanc MIC (μg mL^{-1})	Linez MIC (μg mL^{-1})	Novo MIC (μg mL^{-1})
SPN.31	S. pneumoniae	S	1	1	2	4	0.5	2	1
ATCC 49619	S, pneumoniae	S	ND	2	ND	ND	0.125	ND	ND
SPN.1007	S. pneumoniae	R	64	1	2	4	0.5	4	0.5
CO 314937	S. pneumoniae	R	ND	2	ND	ND	0.25	ND	ND
MD77773	S. pneumoniae	ND	ND	1	ND	ND	0.25	ND	ND
MD77841	S. pneumoniae	ND	ND	2	ND	ND	0.25	ND	ND
SPY.10	S. pyogenes	S	0.5	1	4	4	0.5	2	0.5
SPY.1055	S. pyogenes	S	0.5	>1	8	8	0.5	4	2
SPY.1465	S. pyogenes	S	0.5	>1	8	8	0.25	2	2
SPY.1469	S. pyogenes	S	1	>1	8	8	0.5	16	2
2008-1732	Group A Strep	WT	ND	>2	ND	ND	0.25	ND	ND
2008-818	Group A Strep	ND	ND	>2	ND	ND	0.25	ND	ND
2008-87	Group B Strep	WT	ND	>2	ND	ND	0.5	ND	ND
2009-61	Group B Strep	ND	ND	>2	ND	ND	0.5	ND	ND

CIP sensitivity where a strain was considered sensitive (S) if it had an MIC ≤ 4 μg mL^{-1}, intermediate (I) with a 16 > MIC > 4 μg mL^{-1}, or resistant (R) with a MIC ≥ 16 μg mL^{-1}. . MICs with CIP, DNM, DNM-2, and DNM-8 were determined using the microdilution broth method as outlined by the CLSI.[15]

Most of the strains tested were sensitive to CIP and showed sensitivity to DNM similar to WT *S. aureus* (MIC ≥ 1 μg/mL). Only two strains (SPN.1007 and CO 314937) are FQR, but their mutational status is unknown. Neither of these strains showed sensitization to DNM suggesting

that either they do not have the gyrA mutation or DNM is not as good an inhibitor of the S→F/Y compared to the S→L gyrA. The latter explanation is supported by in vitro evidence which shows poor inhibition of S83F/Y DNA gyrase by DNM (section 3.6.1), but further evaluation of FQR *Streptococcus* strains with known mutational statuses is needed to confirm this.

3.4 Evaluation of DNM and derivatives against atypical Gram-negative bacteria

Normal Gram-negative bacteria have an inner membrane surrounded by a thin layer peptidoglycan and a second outer membrane. On the outside of this second membrane, the bacteria normally have lipopolysacchardies (LPS) made up of lipid A, an inner core of conserved sugars such as KDO, an outer core of sugars, and a highly variable O-polysaccharide chain.[36] Atypical Gram-negative bacteria are similar to Gram-negative bacteria in that they are not colored by staining with crystal violet. However, their outer membranes typically differ from that of normal Gram-negative bacteria. For example, instead of the LPS, *Mycobacteria* have a layer of mycolic acid covalently linked to the arabinogalactan-peptidoglycan inner leaflet.[37] This difference in cell wall and its greater impermeability compared to LPS is thought to be the reason that *Mycobacteria* are less susceptible to traditional antibiotics than normal Gram-negative bacteria. Alternatively, *Neisseria* have lipooligosaccharides (LOS) instead of LPS. LOS differs from LPS in that they lack the O-polysaccharide chain.[36] This difference in structure helps to explain the greater permeability of *Neisseria* compared to typical Gram-negative bacteria.[38] Both *Mycobacteria* (especially *M. tuberculosis*) and *Neisseria* (especially *N. gonorrhoeae*) are serious health threats, and antibiotic resistant strains are particularly worrying. We chose to investigate whether DNM might be effective against these atypical Gram-negative bacteria.

3.4.1 *Mycobacteria*

In 2013, TB was the second leading cause of death from an infection worldwide with 9.0 million new cases and 1.5 million deaths.[39] 480,000 of the new cases and 210,000 of the deaths are multidrug-resistant (MDR, resistant to at least 2 of the first-line treatments) with ~9% of the MDR cases being extensively drug-resistant (XDR, also resistant to fluoroquinolones and at least

one injectable second-line treatment).[39] Based on previous data suggesting than *M. smegmatis* is sensitive to DNM,[1] we hypothesized that DNM and its active derivatives may be active against FQR TB. We collaborated with the Global TB Alliance who tested these compounds against WT and FQR TB. Specifically, they tested active DNM derivatives DNM-2, DNM-3, and DNM-8 along with inactive derivatives DNM-12, DNM-13, and DNM-14 in the microplate alamar blue assay (MABA[40]) which mimics the active infection, and the low oxygen recovery assay (LORA[41]) which mimics the latent infection.

Table 3.7. Sensitivity of *Mycobacteria* to moxifloxacin (MOX), DNM, DNM derivatives, and other antibiotics

Strain ID	Assay	FQR S/I/R	Compound MIC (μg mL^{-1})									
			MOX	DNM-2	DNM-3	DNM-8	DNM-12	DNM-13	DNM-14	RMP	INH	BDQ
M. tuberculosis H37 Rv	MABA	S	0.04	0.43-0.94	0.22-1.4	0.11-0.89	>32	14.3	14.8	0.02-0.08	0.03-0.71	0.016-0.11
M. tuberculosis H37 Rv	LORA	S	ND	3.9-6.9	6.6-7.6	>8	>32	>32	>32	0.189-0.92	>35-256	0.02-0.25
M. tuberculosis rMox #3	MABA	R	7.2	1.0	ND	ND	ND	ND	ND	0.10	0.27	ND
M. abscessus	MABA	R	5.59	>16	ND	ND	ND	ND	ND	>3.3	>1.1	0.12
M. chelonae	MABA	S	0.12	>16	ND	ND	ND	ND	ND	>3.3	>1.1	0.06
M. marinum	MABA	R	2.04	>16	ND	ND	ND	ND	ND	>3.3	>1.1	0.25
M. avium	MABA	S	0.29	>16	ND	ND	ND	ND	ND	0.18	>1.1	0.008
M. kansasii	MABA	S	<0.063	7.74-7.76	ND	ND	ND	ND	ND	0.10	>1.1	0.004
M. bovis	MABA	S	<0.063	1.95-1.98	ND	ND	ND	ND	ND	<0.013	0.18	0.06

Interestingly, DNM-2 and DNM-3 were active against both WT and FQR TB in both MABA and LORA (Table 3.7). This may be due to the fact that TB naturally has an A (not S!) at the gyrA position, which is commonly mutated.[42-43] The lack of a Ser at this position may sensitize the WT TB to DNM. Only one FQR strain (rMox #3) was examined and it had a similar sensitivity to WT TB. The gyrA mutational status of rMox #3 is unknown. Approximately 20% of FQR TB are predicted to have an A90V (analogous to the S84L mutation in *S. aureus*) while other FQR strains have different mutations in gyrA (Note: *M. tuberculosis* do not have topoisomerase IV and therefore mutations in parC are not a cause of FQR).[43] Further analysis of other FQR TB strains

with known gyrA statuses is necessary to determine what effect the A90V mutation will have on sensitivity to DNM. Kobayashi and co-workers recently found that nybomycin also has activity against WT TB although it is less potent than DNM-2 (H37 Rv MIC = 4.2 µg/mL).[5]

```
M. tuberculosis   MFDSGFRPDRSHAKSARSVAETMGNYHPHGDASIYDSLVRMAQPWSLRYPLVDGQGNFGS 118
M. bovis          MFDSGFRPDRSHAKSARSVAETMGNYHPHGDASIYDTLVRMAQPWSLRYPLVDGQGNFGS 118
M. avium          MYDSGFRPDRSHAKSARSVAETMGNYHPHGDASIYDTLVRMAQPWSLRYPLVDGQGNFGS 119
M. marinum        MYDSGFRPDRSHAKSARSVAETMGNYHPHGDASIYDTLVRMAQPWSLRYPLVDGQGNFGS 119
M. ulcerans       MYDSGFRPDHSHAKSARSVAETMGNYHPHGDASIYDTLVRMAQPWSLRYPLVDGQGNFGS 119
M. chelonae       MYDSGFRPDRSHAKSARSVAETMGNYHPHGDASIYDTLVRMAQPWSLRYPLVDGQGNFGS 120
S. aureus         LNEQGMTPDKSYKKSARIVGDVMGKYHPHGDSSIYEAMVRMAQDFSYRYPLVDGQGNFGS 112
                  : :.*: **:*: **** *.:.**:******:***:::***** :* ************
```

Figure 3.5. Sequence alignment of the quinolone resistance determining region of DNA gyrase for *Mycobacteria* and *S. aureus*. The key A/S is in red.

The TB alliance also examined the sensitivity of other *Mycobacteria* including *M. bovis* (causes tuberculosis in cows) as well as nontuberculous mycobacteria such as *M. abscesuss, M. chelonae, M. marinum, M. avium,* and *M. kansasii* to DNM-2 (Table 3.7). All of these strains have very good homology to *M. tuberculosis* in the region of A90 (see Figure 3.5). While *M. bovis* was relatively sensitive to DNM-2 (MIC ~ 2 µg/mL), none of the nontuberculous *Mycobacteria* were sensitive to DNM-2. Additionally, none of the nontuberculous *Mycobacteria* were sensitive to isoniazid (INH), one of the first-line therapies for TB. There is evidence to suggest that the nontuberculous *Mycobacteria* have a different outer membrane that causes them to be even less permeable than *M. tuberculosis*.[44-45] This impermeability may explain their lack of sensitivity to DNM derivatives and *M. tuberculosis* standard-of-care agents such as INH.

3.4.2 *N. gonorrhoeae*

In 2013, the CDC put out a report detailing the state of antibiotic-resistant bacteria in the United States. In this report, they categorized drug-resistant *N. gonorrhoeae* as an urgent threat (the highest level they assigned). Of the estimated 820,000 infections per year, 246,000 (30%) are drug resistant and ~1% of the resistant infections are resistant to ceftriaxone, the currently recommended treatment and the last line of defense against *N. gonorrhoeae*. The fact that resistant *N. gonorrhoeae* strains have been observed for all available antibiotics demonstrates

the extreme need for a new antibiotic. FQs were previously a recommended treatment for *N. gonorrhoeae* but when FQR reached ~10% in 2007, the CDC announced that FQs should no longer be used for *N. gonorrhoeae*.[46] Nearly all of the FQR *N. gonorrhoeae* have a mutation in S91 (analogous to S84 in *S. aureus*) with it going to either F (98-100%) or Y (0-2%) in the majority of cases.[47-48] Initially, I tested a WT *N. gonorrhoeae* strain (MS11) for its sensitivity to DNM-2 and found it to have an MIC of 2 µg/mL. The fact that this value is comparable to the MIC of DNM-2 against WT *S. aureus* suggests that DNM-2 is capable of getting past the outer membrane of *N. gonorrhoeae* and suggests that it might have activity against FQR clinical isolates. We collaborated with the NIH/NIAID who tested DNM-2 against 94 clinical isolates of *N. gonorrhoeae* (93% of which were FQR).The MIC_{50} and MIC_{90} for these strains was 8 µg/mL and there was no apparent correlation between FQR and sensitivity to DNM-2 (Table 3.8). Similar to *S. epipdermidis* and *S. pneumonia,* this lack of sensitivity may be because of the different mutation (S91F/Y vs. S84L for *S. aureus*) that is common for *N. gonorrhoeae*.

Table 3.8. Sensitivity of *N. gonorrhoeae* to DNM-2, CIP and other antibiotics

CDC ID	Compound MIC (μg mL^{-1})						
	DNM-2	CIP	Azi	Cfx	Cro	Pen	Tet
GCREF2012010	2	16	0.13	0.25	0.06	4	2
GCREF2012007	4	16	0.13	0.13	0.03	4	2
GCREF2012011	4	< 0.008	8	0.03	< 0.002	0.25	0.25
GCREF2012012	4	> 16	0.13	0.13	0.06	4	2
GCREF2012015	4	< 0.008	8	0.03	0.00	0.50	1
GCREF2012025	4	16	0.13	0.13	0.13	4	2
GCREF2012029	4	< 0.008	0.13	0.03	0.03	2	1
GCREF2012030	4	16	0.25	1.00	0.13	2	0.50
GCREF2013008	4	< 0.008	0.13	< 0.008	< 0.002	< 0.008	< 0.008
GCREF2013033	4	< 0.008	0.13	0.06	< 0.002	0.25	0.25
GCREF2013035	4	< 0.008	< 0.31	0.02	0.02	0.13	0.25
GCREF2012016	8	> 16	0.13	0.13	0.06	2	1
GCREF2012045	8	> 16	0.13	0.13	0.03	4	2
GCREF2013013	8	16	0.13	0.13	0.06	4	2
GCREF2013030	8	> 16	0.13	0.13	0.03	4	1
GCREF2012001	8	> 16	0.50	0.25	0.06	4	4
GCREF2012002	8	> 16	0.13	0.13	0.06	4	2
GCREF2012004	8	> 16	0.13	0.13	0.03	2	2
GCREF2012005	8	16	0.13	0.25	0.06	4	2
GCREF2012006	8	> 16	0.13	0.13	0.03	4	4
GCREF2012008	8	> 16	0.13	0.13	0.03	2	1
GCREF2012009	8	> 16	0.13	0.13	0.06	4	2
GCREF2012017	8	< 0.008	> 16	0.03	0.03	0.25	1
GCREF2012018	8	> 16	0.50	0.25	0.06	4	2
GCREF2012019	8	> 16	0.50	0.13	0.01	0.50	0.25
GCREF2012020	8	16	0.13	0.25	0.03	4	2
GCREF2012021	8	16	0.13	0.13	0.13	4	2
GCREF2012022	8	16	1	0.25	0.13	4	2
GCREF2012024	8	16	0.50	0.25	0.13	4	4
GCREF2012028	8	16	0.25	0.25	0.03	4	4
GCREF2012031	8	16	0.25	1	0.13	4	1
GCREF2012032	8	16	0.50	0.25	0.13	8	4
GCREF2012033	8	8	8	0.13	0.06	2	1
GCREF2012034	8	16	0.50	0.13	0.06	4	4
GCREF2012035	8	16	0.50	0.13	0.06	4	4
GCREF2012036	8	16	1	0.25	0.13	4	4
GCREF2012037	8	16	4	0.25	0.13	4	2
GCREF2012038	8	16	8	0.06	0.03	0.25	0.25
GCREF2012039	8	16	0.50	0.25	0.13	4	2
GCREF2012040	8	> 16	0.25	0.25	0.03	4	2
GCREF2012042	8	> 16	0.50	0.25	0.13	4	4
GCREF2012043	8	16	0.13	0.13	0.03	1	0.13
GCREF2012046	8	16	0.25	0.13	0.03	2	1
GCREF2012047	8	> 16	0.50	0.25	0.03	4	4
GCREF2012048	8	16	0.25	0.25	0.03	2	2
GCREF2012049	8	16	0.25	0.25	0.03	4	2
GCREF2012050	8	16	0.25	0.25	0.03	4	1

CDC ID	Compound MIC (μg mL^{-1})						
	DNM-2	Cip	Azi	Cfx	Cro	Pen	Tet
GCREF2012052	8	16	0.50	0.25	0.03	4	2
GCREF2013002	8	16	0.13	0.25	0.03	2	2
GCREF2013003	8	0.06	0.13	0.02	< 0.002	1	0.50
GCREF2013044	8	8	0.50	0.02	< 0.002	1	>16
GCREF2013007	8	> 16	0.50	0.02	< 0.002	0.25	0.25
GCREF2013009	8	0.02	2	0.03	0.004	1	2
GCREF2013010	8	8	4	0.02	0.004	1	1
GCREF2013011	8	16	8	0.02	< 0.002	0.25	0.50
GCREF2013014	8	> 16	2	0.06	0.02	1	1
GCREF2013016	8	> 16	0.50	0.25	0.03	2	2
GCREF2013017	8	16	0.50	0.25	0.06	2	2
GCREF2013018	8	> 16	8	0.13	0.03	2	2
GCREF2013019	8	0.02	2	0.02	0.004	1	1
GCREF2013020	8	0.13	1	0.25	0.02	4	2
GCREF2013021	8	0.02	2	0.03	0.01	1	2
GCREF2013022	8	16	2	0.03	0.004	1	2
GCREF2013023	8	0.02	2	0.03	0.004	1	1
GCREF2013024	8	0.25	2	0.03	0.004	1	2
GCREF2013025	8	> 16	8	< 0.008	< 0.002	0.50	0.13
GCREF2013026	8	4	1	0.13	0.01	0.50	0.25
GCREF2013027	8	> 16	0.25	0.25	0.03	4	2
GCREF2013028	8	4	16	< 0.008	< 0.002	4	0.25
GCREF2013029	8	> 16	0.50	0.25	0.06	4	2
GCREF2013031	8	16	8	0.06	0.06	2	2
GCREF2013032	8	< 0.008	0.13	0.02	< 0.002	0.50	1
GCREF2013036	8	16	0.25	0.25	0.06	4	2
GCREF2013038	8	> 16	8	0.06	0.06	2	2
GCREF2013039	8	> 16	0.25	0.25	0.25	4	4
GCREF2013040	8	16	0.13	0.13	0.06	1	2
GCREF2013041	8	> 16	0.13	0.06	0.06	2	2
GCREF2013042	8	16	4	0.25	0.13	2	2
GCREF2013043	8	< 0.008	8	0.02	< 0.002	0.50	0.50
GCREF2013045	8	> 16	0.25	0.25	0.02	4	2
GCREF2013046	8	> 16	0.13	0.13	0.03	1	2
GCREF2013047	8	> 16	0.13	0.13	0.03	0.50	2
GCREF2013048	8	> 16	0.25	0.06	0.03	4	2
GCREF2013012	8	< 0.008	8	0.02	< 0.002	0.50	0.25
GCREF2013015	8	16	0.25	0.13	0.03	2	2
GCREF2012014	16	16	0.50	0.25	0.13	8	4
GCREF2012023	16	8	1	0.13	0.06	1	0.25
GCREF2012027	16	> 16	0.25	0.06	0.03	4	2
GCREF2012044	16	16	0.50	0.13	0.03	1	1
GCREF2012051	16	16	0.50	0.25	0.03	4	4
GCREF2013001	16	16	0.50	0.25	0.03	4	2
GCREF2013004	16	> 16	0.25	0.25	0.02	4	2
GCREF2013005	16	16	0.25	0.13	0.03	2	2
GCREF2013006	16	16	0.50	0.06	0.03	8	4

CIP = ciprofloxacin, Azi = azithromycin, Cfx = Cefixime, Cro = Ceftriaxone, Pen = penicillin, Tet = tetracycline. MICs were determined using the agar dilution method as outlined by the CLSI.[15]

3.5 Evaluation of DNM and derivatives against Gram-negative bacteria

Gram-negative bacteria are another class of bacteria that are rapidly developing resistance to standard-of-care antibiotics. While the CDC estimates that antibiotic resistant Gram-negative bacteria currently cause fewer infections (490,100 or 24%) and deaths (3328 or 14%) than Gram-positive infections (Note: These numbers do not include healthcare associated *C. difficile* infections. When they are included, Gram-negative bacteria account for 32% of antibiotic resistant infections and 46% of deaths due to antibiotic resistant bacteria), Gram-negative bacteria are generally more difficult to treat due to their difficult to penetrate LPS layer. This is evidenced by the large number of antibiotics that are not effective against Gram-negative bacteria and the difficulty of developing novel Gram-negative antibiotics.[49] Fluoroquinolones have historically been very active against Gram-negative bacteria,[50] which has resulted in extensive FQR in Gram-negative bacteria.[17] Due to the activity of DNM against FQR Gram-positive bacteria, we chose to evaluate the activity of DNM against FQR Gram-negative bacteria.

3.5.1 Single agent activity of DNM-2 against Gram-negative bacteria

DNM-2 was evaluated against a panel of Gram-negative bacteria (Table 3.8). It showed no detectable activity against wild type or FQR *P. aeruginosa* or *A. baumannii*. Moderate activity consistent with the activity seen in WT Gram-positive bacteria was seen with DNM-2 against a FQS permeabilized strain of *E. coli* (MIC = 2 µg/mL), suggesting that DNM-2 is unable to penetrate Gram-negative bacteria.

Table 3.9. Sensitivity of Gram-negative bacteria to CIP and DNM-2 along with gyrA and parC mutations

Strain	CIP (S/R)	CIP MIC (µg mL^{-1})	DNM-2 MIC (µg mL^{-1})	gyrA mutation	parC mutation
P. aeruginosa 1000	R	32	>24	S83I	S80L
P. aeruginosa1586	R	>64	>24	S83I	E84K
A. baumannii KB349	R	>32	>24	S83L	none
A. baumannii KB304	R	24	>24	S83L	none
E. coli MG1655	S	0.025	>24	none	none
E. coli MG1655 ΔAcrB	S	0.008	2	none	none

3.5.2 Permeability of DNM-2 in *E. coli*

In order to further explore the possibility that the lack of DNM-2 activity in Gram-negative bacteria is due to an inability to get into Gram-negative bacteria, Michelle Richter tested DNM-2 for its ability to accumulate in *E. coli* (Figure 3.6). She found that it accumulated to a similar level to other low accumulating compounds (e.g. Gram-positive only antibiotic erythromycin). However, upon co-treatment with twice the MIC of colistin (COL), a polymixin antibiotic known to permeabilize the outer membrane of Gram-negative bacteria,[51-52] for ten minutes DNM-2 accumulates to a similar level as high accumulating compounds (e.g. ciprofloxacin and tetracycline).

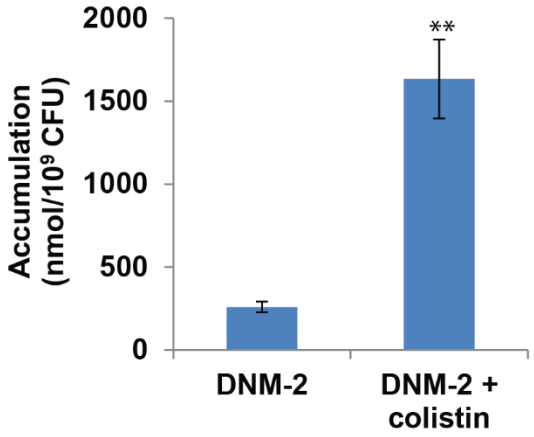

Figure 3.6. Accumulation of DNM-2 (40 µM) in MG1655 *E. coli* alone and after 10 min pre-treatment with 2X MIC of colistin. ** p<0.005

3.5.3 Activity of DNM-2 in combination with COL against Gram-negative bacteria

Previously, COL was found to sensitize *A. baumannii* to Gram-positive antibiotics such as vancomycin (VANC) by permeabilizing their outer membrane allowing for accumulation of these otherwise impermeable compounds.[53-54] After confirming that COL is able to permeabilize Gram-negative bacteria allowing for accumulation of DNM-2 (Fig. 3.3), we chose to examine the ability of COL to sensitize Gram-negative bacteria to DNM-2.

3.5.3.1 *A. baumannii*

We chose to examine the ability of COL to sensitize clinical isolates of *A. baumannii* to DNM-2. First, the single agent sensitivities of the strains to COL, CIP, VANC, and DNM-2 were determined (Table 3.10). The gyrA and parC mutational status of these strains had previously been determined.[55] All six strains have similar sensitivity to COL (MIC = 0.25 to 0.38 µg/mL). As expected, those with mutations in gyrA and parC were resistant to CIP (MIC = 16 to >64 µg/mL) while those with WT gyrA and parC were sensitive to CIP (MIC = 0.25 to 0.5 µg/mL). All strains were resistant to the Gram-positive antibiotic VANC. Most strains were completely resistant to DNM-2 with two strains (BD335 and WO22) showing very weak sensitivity (MIC = 24 µg/mL).

Table 3.10. Sensitivity of ATCC strains and clinical isolates of *A. baumannii* to colistin (COL), ciprofloxacin (CIP), vancomycin (VANC) and DNM-2 along with previously reported gyrA and parC mutations[55]

Strain	COL MIC (µg/mL)	CIP MIC (µg/mL)	VANC MIC (µg/mL)	DNM-2 MIC (µg/mL)	gyrA mutations	parC mutations
IF101	0.38	64	>64	>24	S83L	S80L
KB349	0.38	16	>64	>24	S83L	WT
BD335	0.38	32	>64	24	S83L	S80L
WO22	0.38	>64	>64	24	S83L	E84K
LU324	0.25	0.25	>64	>24	WT	WT
19606	0.38	0.5	>64	>24	WT	WT

After determining that the strains had similar sensitivity to COL, the ability of COL to sensitize strains to DNM-2 was explored utilizing a checkerboard assay similar to previous studies.[53-54] The results of the checkerboard assay with the strain IF101 are shown in Figure 3.7A. As can be seen, COL successfully sensitized the strain to DNM-2. This sensitization was synergistic in the IF101 strain of *A. baumannii* as evidenced by the combination index values (Figure 3.7B) calculated using Compusyn software which indicate strong synergism for combinations of sub-MIC COL (<0.375 µg/mL) and DNM-2.

Another way of determining synergistic interactions is to use the Bliss independence values.[56] Bliss independence assumes that the relative effect of one drug is independent of that of the other. Bliss independence values are calculated using the equation $E_{ind} = (E_A + E_B) – (E_A \times E_B)$ where E_{ind} = the effect if the two drugs act independently, E_A = effect of drug A alone, and E_B = effect of drug B alone. If $E_{ind} > 0$ then the drugs act synergistically and if $E_{ind} < 0$ then they act antagonistically. Bliss independence calculations for DNM-2 in combination with ¼ MIC of COL (lines in Figure 3.7C and Figure 3.7D) for IF101 suggest strong synergism. Similar results were seen for other *A. baumannii* strains (Figure 3.7E-L). This sensitization provides further confirmation that the lack of activity observed in Gram-negative bacteria is likely due to an inability to penetrate the outer membrane. Interestingly, no significant difference was observed for strains containing the S83L gyrA (IF101, KB349, BD335, and WO22) mutation compared to strains that are WT for gyrA (LU324 and 19606, not shown). This could mean that DNM-2 is capable of inhibiting both WT and S83L gyrA mutants in *A. baumannii*. Development of Gram-negative penetrant DNM derivatives is in progress and will aid in the examination of this.

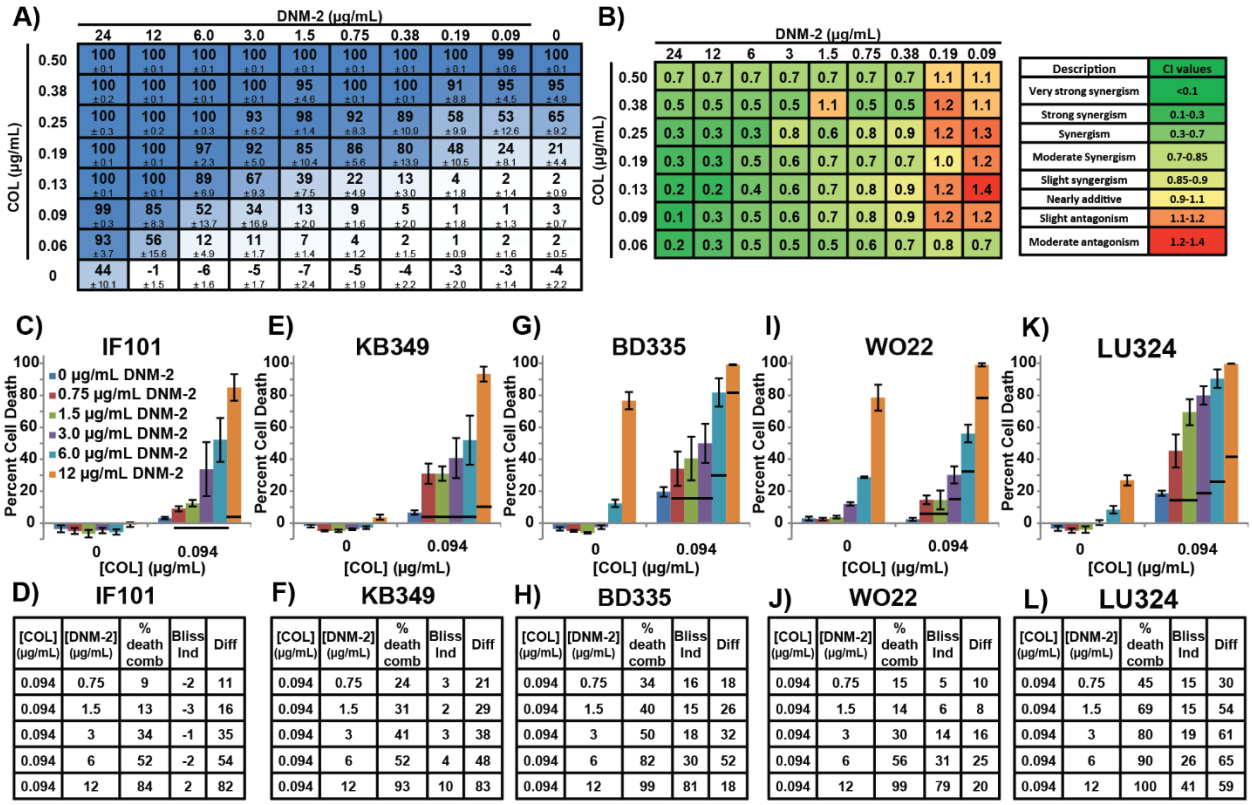

Figure 3.7. Sensitization of *A. baumannii* to DNM-2 by co-treatment with colistin (COL). (**A**) Checkerboard assay of strain IF101 with DNM-2 and COL. Percentage dead bacteria are shown for each combination ± SEM. Each combination is also color-coded with blue being 100% dead and white being 100% alive. (**B**) Combination index values of DNM-2 and COL against IF101. Green indicates strong synergism and red indicates antagonism. (**C**) Percent cell death observed for IF101 with the indicated treatments of COL and DNM-2. The lines indicate the expected percent cell death if the compounds were additive calculated using the Bliss Independence Equation. (**D**) Table of the percent death for the indicated combination (% death comb), the calculated Bliss independence value (Bliss Ind), and the difference between these values (Diff). (**E**) Like C but for strain KB349. (**F**) Like D but for strain KB349. (**G**) Like C but for strain BD335. (**H**) Like D but for strain BD335. (**I**) Like C but for strain WO22. (**J**) Like D but for strain WO22. (**K**) Like C but for strain LU324. (**L**) Like D but for strain LU324.

3.5.3.2 *P. aeruginosa*

After examining *A. baumannii*, the ability to sensitize *P. aeruginosa* to DNM-2 with COL was investigated. Initially, single agent sensitivity of a set of *P. aeruginosa* isolates (obtained from Cubist Pharmaceuticals) and gyrA and parC mutational status was determined (Table 3.11). All

strains were similarly sensitive to COL (MIC = 0.25 to 0.5 µg/mL). The strains with mutations in gyrA and parC showed the expected CIP resistance (MIC = 32 to >64 µg/mL). Unsurprisingly, none of the strains showed sensitivity to either VANC or DNM-2.

Table 3.11. Sensitivity of clinical isolates of *P. aeruginosa* to colistin (COL), ciprofloxacin (CIP), vancomycin (VANC) and DNM-2 along with gyrA and parC mutations

Strain	COL MIC (µg/mL)	CIP MIC (µg/mL)	VANC MIC (µg/mL)	DNM-2 MIC (µg/mL)	gyrA	parC
PA1000	0.38	32	>64	>24	S83I	S80L
PA1586	0.50	>64	>64	>24	S83I	E84K
PA1591	0.38	>64	>64	>24	S83I	S80L
PA1592	0.50	32	>64	>24	S83I	S80L
PAO1	0.25	0.25	>64	>24	WT	WT

Similar to the *A. baumannii* studies, a checkerboard assay was performed with the *P. aeruginosa* strains. Unlike *A. baumannii*, potent sensitization to DNM-2 upon co-treatment with sub-MIC COL was not observed. For the 1592 strain of *P. aeruginosa*, combination indices suggest no real synergism (Figure 3.8A-B). However, the values obtained were not in the usual range of numbers and may represent a failure of the software. For this reason, Bliss independence values were also examined. DNM-2 in combination with 0.09 ug/mL COL (~1/4 MIC COL) did not result in higher cell death for any of the *P. aeruginosa* strains than expected by the Bliss Independence calculations (data not shown). However, some synergy was observed at ½ MIC of COL with higher concentrations of DNM-2 for 1592 (Figure 3.8C-D) and the other strains examined (Figure 3.8E-L). While this initially was disappointing, previous reports show that COL does not significantly sensitize *P. aeruginosa* to Gram-positive bacteria antibiotics such as VANC.[53] We confirmed this by also analyzing VANC in combination with COL (Figure 3.8M) and saw similar results to those observed for DNM-2, suggesting that *P. aeruginosa* strains seem to be resistant to permeabilization by COL even though they are not resistant to cell death induced by COL.

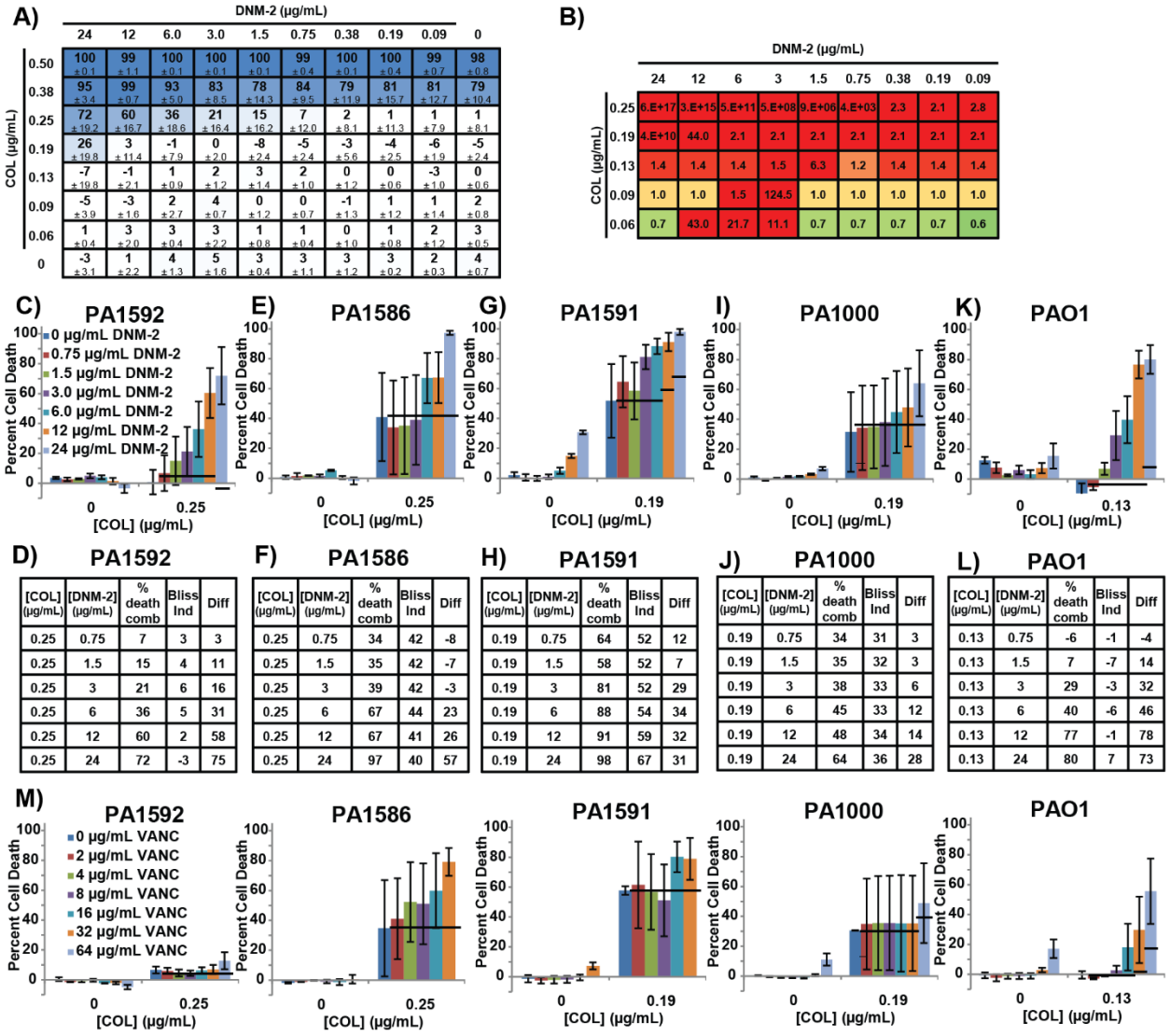

Figure 3.8. Sensitization of *P. aeruginosa* to DNM-2 and VANC by co-treatment with colistin (COL). (**A**) Checkerboard assay of strain PA1592 with DNM-2 and COL. Percentage dead bacteria are shown for each combination ± SEM. Each combination is also color-coded with blue being 100% dead and white being 100% alive. (**B**) Combination index values of DNM-2 and COL against PA1592. Green indicates strong synergism and red indicates antagonism. (**C**) Percent cell death observed for PA1592 with the indicated treatments of COL and DNM-2. The lines indicate the expected percent cell death if the compounds were additive calculated using the Bliss Independence Equation. (**D**) Table indicating the percent death for the indicated combination (% death comb), the calculated Bliss independence value (Bliss Ind), and the difference between these values (Diff). (**E**) Like C but for strain PA1586. (**F**) Like D but for strain PA1586. (**G**) Like C but for strain PA1591. (**H**) Like D but for strain PA1591. (**I**) Like C but for strain PA1000. (**J**) Like D but for strain PA1000. (**K**) Like C but for strain PAO1. (**L**) Like D but for strain PAO1. (**M**) Percent cell death observed for indicated *P. aeruginosa* strains with the indicated treatments of COL and VANC. The lines indicate the expected percent cell death if the compounds were additive calculated using the Bliss Independence Equation.

3.6 *In vitro* investigation of inhibition of mutant gyrA by DNM and its derivatives

In order to further investigate the importance of the GyrA mutation for DNM activity, the ability of DNM, DNM-2, and CIP to inhibit DNA gyrase was determined utilizing an in vitro DNA cleavage assay. In this assay, DNA gyrase is coincubated with supercoiled DNA and the compound of interest. Inhibition at the cleavage complex of DNA gyrase leads to an increase in either doubly nicked linear (L) DNA (e.g. inhibition by CIP[57]) or singly nicked open circular (OC) DNA (e.g. inhibition by GSK299423[58]). GSK299423 is a recently discovered DNA gyrase inhibitor that is hypothesized to stabilize the DNA-enzyme complex either pre-cleavage or after the formation of a single strand break resulting in a buildup of OC DNA [58].

3.6.1 *E. coli* DNA gyrase cleavage assay[7]

For the first studies, we chose to examine the effect of CIP, DNM, and DNM-2 on *E. coli* DNA gyrase, the enzyme typically used in inhibition studies. Similar to previous studies, we found that CIP potently inhibits WT DNA gyrase with a greater than seven-fold increase in L DNA being observed at concentrations as low as 0.68 μM (Fig. 3.9A). Additionally, in a time course assay, inhibition of WT DNA gyrase by CIP resulted in a time dependent buildup of L DNA (Fig. 3.9B). Alternatively when either DNM or DNM-2 was incubated with WT DNA gyrase, neither showed similar increases in L or OC DNA, suggesting that these compounds are poor inhibitors of WT DNA gyrase (Fig. 3.6A). Additionally, during the time course study with these compounds, buildup of L DNA was only observed at later time points and to a smaller degree (Fig. 3.9B).

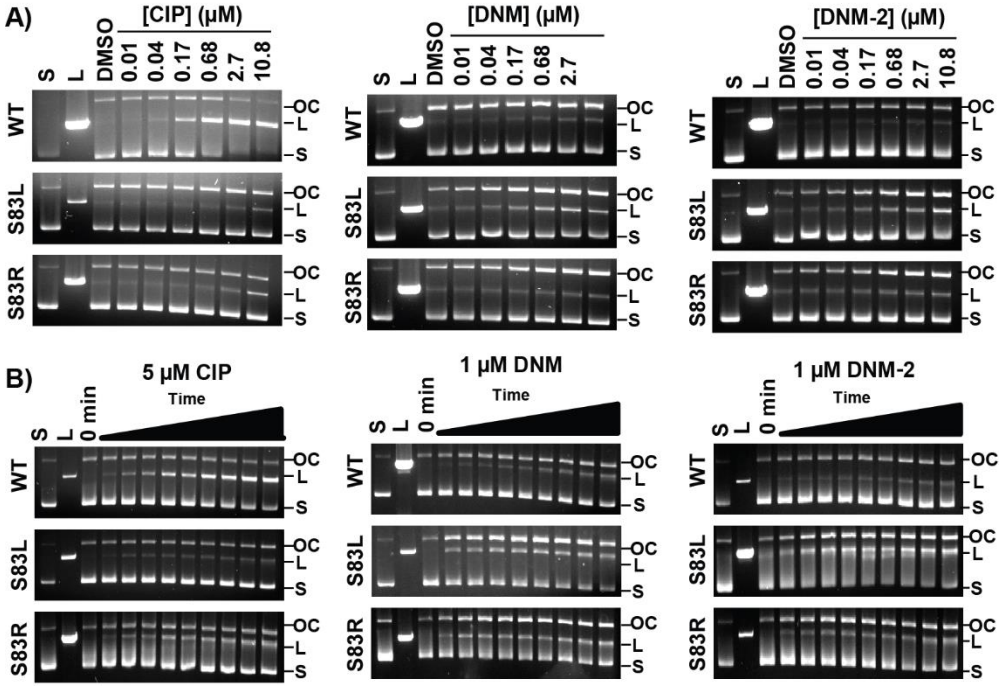

Figure 3.9. Inhibition of WT and mutant DNA gyrase. (**A**) DNA cleavage assay with WT, S83L, and S83R *E. coli* DNA gyrase in the presence of increasing concentrations of CIP, DNM, and DNM-2. Concentrations were 0.01, 0.04, 0.017, 0.68, 2.7, and 10.8 μM except for DNM which was 8.9 μM for the highest concentration. Experiments were performed at 30ºC for 25 min. S = supercoiled, L = linear, and OC = open circular or nicked DNA. (**B**) Timecourse of DNA cleavage with WT, S83L and S83R *E. coli* DNA gyrase in the presence of 5 μM CIP, 1 μM DNM, and 1 μM DNM-2. Experiments were performed at 30ºC, and timepoints were 0, 1, 3, 5, 10, 15, 20, 30 ,60, and 90 min. All gels are representative data from at least three independent experiments.

The ability of CIP, DNM, and DNM-2 to inhibit S83L or S83R DNA gyrase was then determined. CIP was much less effective at inhibiting either S83L or S83R DNA gyrase compared to WT with only small increases in L DNA being observed (Fig. 3.9A). Additionally, minimal change was observed with 5 μM CIP at up to 1.5 h (Fig. 3.9B). Time course studies performed with an increased concentration of CIP (200 μM) and S83L DNA gyrase revealed a similar pattern of inhibition to that of WT DNA gyrase suggesting that the residual inhibition goes through a similar mechanism (Fig. 3.10A). DNM and DNM-2 induce only small increases in L DNA with S83L DNA gyrase (Fig. 3.9A). Instead, DNM inhibition of S83L DNA gyrase led to a significant buildup of OC DNA at 0.17 μM ($P < 0.05$) with a similar increase observed for DNM-2 (Fig. 3.9A). This buildup

does not diminish over time (Fig. 3.9B) suggestive of a mode of inhibition more similar to GSK 299423 than to CIP. Increasing concentrations of DNM-2 to 200 µM and increasing the time up to 2 h confirmed that this OC buildup is not a fleeting event as occurs with CIP (Fig. 3.10B). DNM or DNM-2 inhibition of S83R also led to a buildup of OC DNA similar to that seen with S83L DNA gyrase only at a slightly higher concentration or longer time points, consistent with the activity of these compounds against VRE with the S83R DNA gyrase. Overall, these results are consistent with clinical isolate data, supporting the critical importance of a mutant DNA gyrase for sensitizing bacteria to DNM. Further studies with *S. aureus* and *Enterococcus* DNA gyrase would be useful to confirm that they behave similarly to *E. coli* DNA gyrase in these assays.

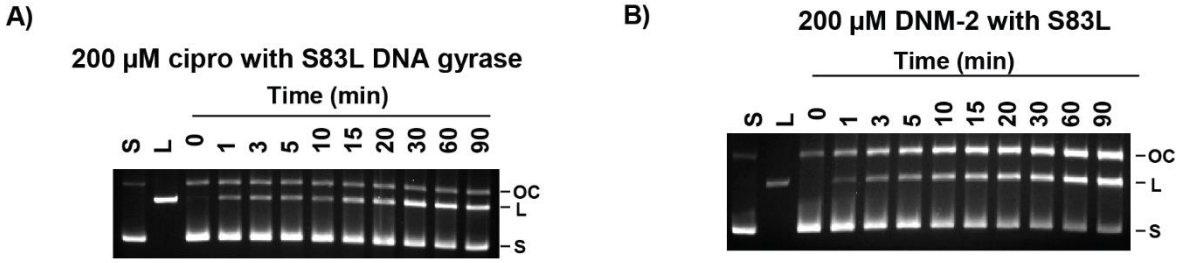

Figure 3.10. Cleavage assay time course with increased concentrations of CIP and DNM-2. (**A**) Time course of DNA cleavage of 200 µM CIP with S83L DNA gyrase. Time points were 0, 1, 3, 5, 10, 15, 20, 30 ,60, and 90 min at 30ºC. (**B**) Time course of DNA cleavage of 200 µM DNM-2 with S83L DNA gyrase. Time points were 0, 1, 3, 5, 10, 15, 20, 30 ,60, and 90 min at 30ºC. Longer time points (120 and 180 min) were also investigated with little change being observed (data not shown). One representative gel shown out of at least three independent experiments.

We then chose to investigate the effect of S83 mutations other than L and R. Specifically, we evaluated the sensitivity of S83Y and S83F since those are common mutations which, at least in *S. epidermidis* (Table 3.4), *S. pneumoniae* (Table 3.6), and *N. gonorhoeae* (Table 3.8), do not appear to sensitize the bacteria to DNM. Evaluation *E. coli* DNA gyrase with S83Y and S83F showed that both of these enzymes were not as efficiently inhibited by DNM compared to either the S83L or S83R (Figure 3.11). Further studies with the enzymes from each species of bacteria would be valuable to confirm that there is not a difference between them and *E. coli* DNA gyrase in this assay.

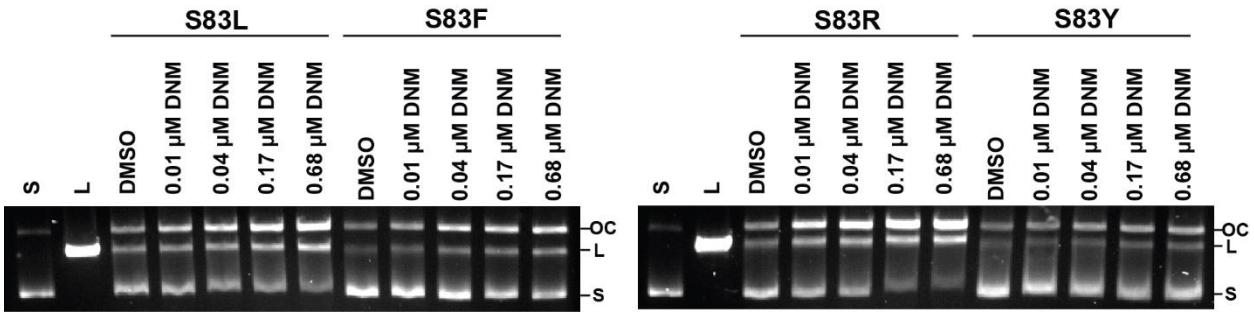

Figure 3.11. Inhibition of mutant DNA gyrase. DNA cleavage assay with S83L, S83F, S83R and S83Y *E. coli* DNA gyrase in the presence of increasing concentrations of DNM. Concentrations were 0.01, 0.04, 0.017, and 0.68 µM. Experiments were performed at 37ºC for 30 min. S = supercoiled, L = linear, and OC = open circular or nicked DNA. One representative gel shown out of at least three independent experiments.

3.6.2 Human topoisomerase II inhibition assay[7]

Finally, in order to determine the selectivity of DNM and derivatives for bacterial DNA gyrase, a decatenation assay with human topoisomerase II was performed. While doxorubicin inhibited human topoisomerase II at concentrations as low as 3 µM, DNM-2 showed no significant inhibition at concentrations up to 30 µM (Figure 3.12). While others have found that DNM-2 is capable of inhibiting mammalian topoisomerase I,[59] our toxicity studies (see Section 3.9) suggest that it likely does not occur at the concentrations where antibacterial activity is observed.

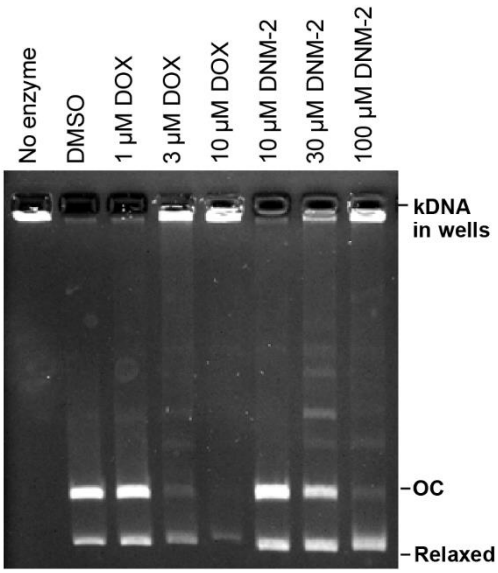

Figure 3.12. Inhibition of human topoisomerase II. A decatenation assay was performed with human topoisomerase II in the presence of either DMSO, doxorubicin (DOX) or DNM-2 at the indicated concentrations. One representative gel shown out of at least three independent experiments.

3.7 Resistance development to DNM

One of the primary ways to fight antibiotic resistant bacteria is to develop new antibiotics that are capable of killing the resistant bacteria. However, this leads to a problem because eventually the bacteria will develop resistance to the new antibiotic as well leading to what has colloquially been termed a superbug. DNM is unique in that it targets the enzyme which leads to FQR opening up the possibility of resistance cycling where a bacteria which is sensitive to CIP will be resistant to DNM and vice versa (Figure 3.13A).[2,7] Hiramatsu had previously shown that developing resistance to DNM in FQR bacteria results in re-sensitization to CIP.[2] Here we explore a full resistance cycle.

3.7.1 Resistance cycling with CIP and DNM[7]

In order to explore the development of resistance to both CIP and DNM in *S. aureus*, resistant strains of ATCC 29213 were generated. Consistent with previous reports [60-61], high level resistance to CIP was generally not achieved in a single step. Instead, low level resistance (CIP

MIC = 4-8 µg mL^{-1}) was usually achieved with the first step and corresponded to a mutation in ParC (e.g. E84K or S80F, Fig. 3.13A-B). Unsurprisingly, these low level resistant strains that do not have the S84L mutation in GyrA were not sensitive to DNM or DNM-2. Development of high level CIP resistance (CIP MIC = 16-64 µg mL^{-1}) similar to what is often seen in clinical isolates [2,62-63] was observed at the second step and corresponded to an S84L mutation in GyrA. These high level CIP resistant strains were extremely sensitive to DNM (MIC = 0.03-0.06 µg mL^{-1}) and DNM-2 (MIC = 0.06-0.12 µg mL^{-1}). These FQR bacteria were then exposed to DNM in an effort to create DNM resistant isolates. The development of DNM resistance in high level CIP resistant strains was a rare event with resistance frequencies ranging from 1×10^{-10} to 7×10^{-10} (Fig. 3.13A-B). When these strains were found, they showed dramatically improved sensitivity to CIP (MIC = 0.25 – 8.0 µg mL^{-1}). All these strains had reverted to WT GyrA (Ser84), with the more CIP sensitive strains also having WT ParC, and the less CIP sensitive strains retaining ParC mutations (Fig. 3.13A-B). This complete cycle of complementary resistance/sensitivity of CIP and DNM is shown in Figure 3.8A, and the complete list of resistant strains generated and the sequences of their QRDR is in Figure 3.13B.

A)

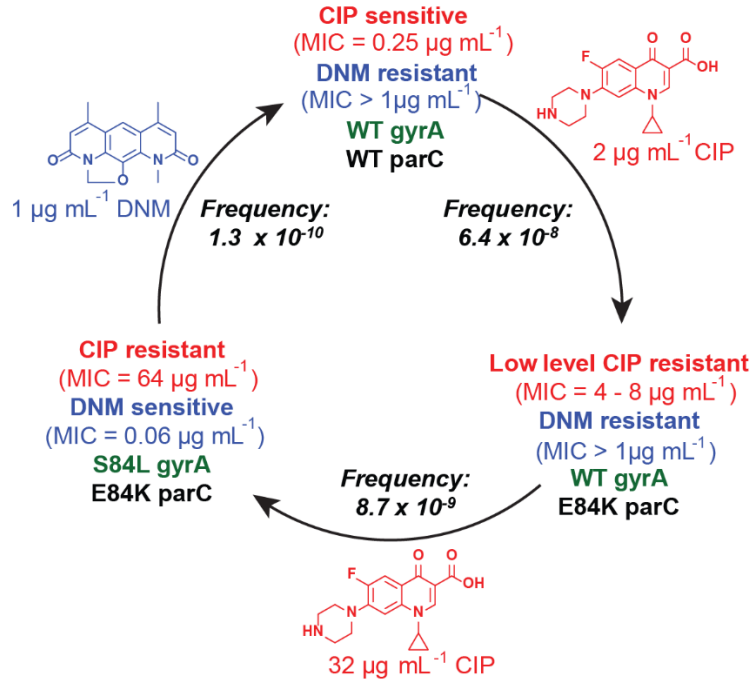

B)

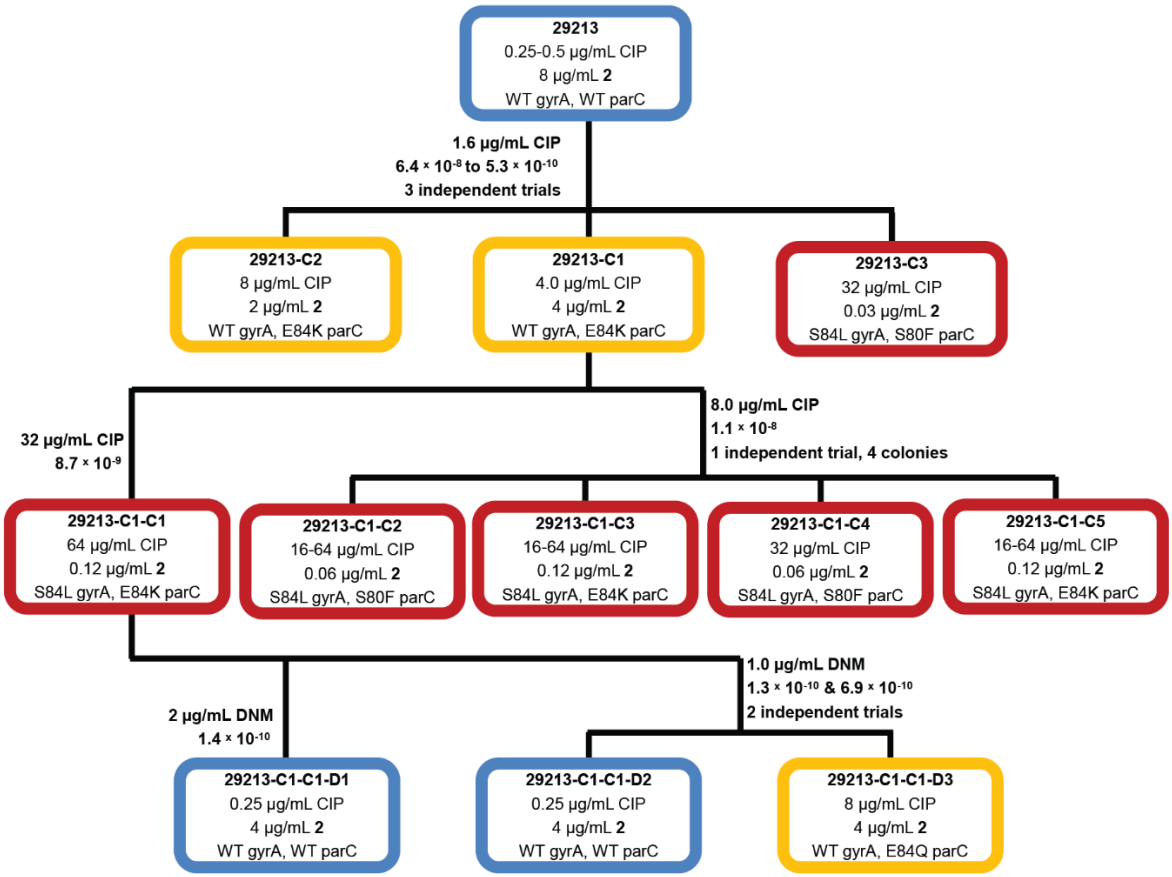

Figure 3.13. Resistance cycling of CIP and DNM with *S. aureus* strain ATCC 29213.

Figure 3.13. (cont.) (**A**) Representative data of the resistance cycle observed when bacteria are sequentially treated with CIP then DNM. Each strain generated is listed with the MIC of CIP (red), DNM (blue), as well as mutation status of the QRDR of GyrA (green) and ParC (black) shown below. The selection pressure used in each step is shown over the arrow along with the mutation frequency. (**B**) Conditions for selection along with resistance frequency are indicated above the boxes to which they correspond. In each box is the strain name, MIC for CIP, MIC for DNM-2, and the mutations in the QRDR of gyrA and parC. Blue = CIP sensitive (MIC < 4 μg mL^{-1}), Yellow = low level CIP resistance (16 > MIC ≥ 4 μg mL^{-1}), Red = high level CIP resistance (MIC ≥ 16 μg mL^{-1}).

3.7.2 Resistance to co-treatment with CIP and DNM[7]

Resistance development upon co-treatment with CIP and DNM-2 was also explored (Figure 3.8C). A low level CIP resistant strain (29213-C1) was utilized in these studies. Upon treatment with either CIP or DNM-2 resistant colonies were observed. However, no colonies were observed upon co-treatment (resistance frequency < 1.0 X 10^{-10}). While it is likely that resistance could eventually be generated, it appears to be a very rare event.

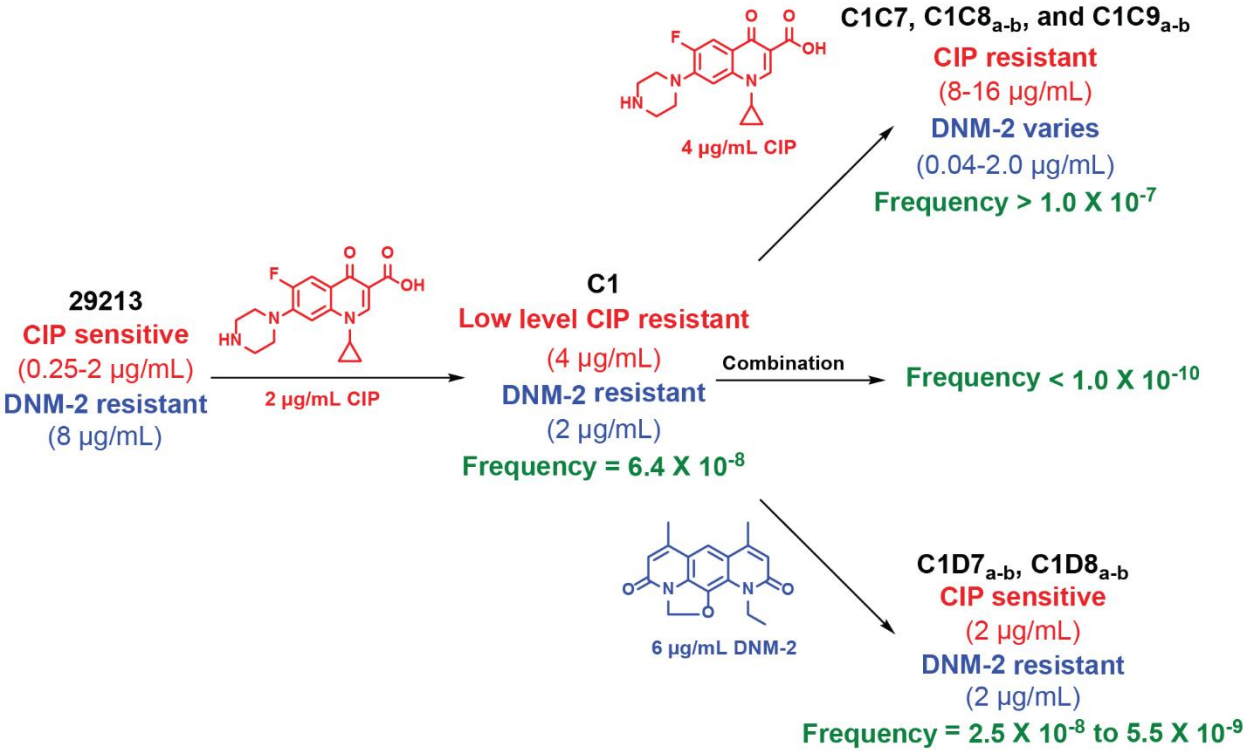

Figure 3.14. Development of co-resistance to CIP and DNM-2 with *S. aureus* strain ATCC 29213. Initially, a low level CIP resistant mutant (C1) was generated. This strain was then treated with CIP alone, DNM-2 alone, or a combination. Along each arrow is indicated the conditions used to

Figure 3.14. (cont.) select for resistance. Below each strain (black) is listed the CIP MIC (red), DNM-2 MIC (blue), and the frequency of the mutation observed (green).

3.8 Pharmacokinetics and solubility of DNM and its derivatives[7]

As discussed earlier, there is a desperate need for orally available Gram-positive antibiotics. The ability of DNM or its derivatives to fill this need depends upon its ability to be well tolerated and bioavailable. Before this study, little to no data existed about the administration of DNM to animals. However, a related but less potent compound nybomycin (*C* = CH_2OH) has been examined in mice. It was found to be well tolerated when dosed either subcutaneously, orally, or by IP injection[64]. However, it showed no activity in mice infected with various bacteria (*K. pneuomoniae, S. aureus,* or *M. tuberculosis*), leading Brock and Sokolski to suggest that this high tolerability and lack of efficacy is likely a result of the very poor solubility of nybomycin (similar to DNM it is only soluble in concentrated acid) and thus lack of absorption[64].

Dr. Hyang Yeon Lee treated mice with increasing concentrations of DNM, DNM-2, and DNM-3 and showed that all three compounds were well tolerated up to the highest dose evaluated (50 mg kg^{-1} by oral gavage). Dr. Lee in collaboration with Prof. Levent Dirikolu performed pharmacokinetic studies on DNM, DNM-2, and DNM-3. While DNM itself showed very low serum exposure (C_{max} < 0.20 µM or 0.060 µg mL^{-1}) after a 50 mg kg^{-1} oral dose, DNM-2 showed good bioavailability with a peak serum concentration of 42.6 µM (12.8 µg mL^{-1}) and an AUC of 44 h µg mL^{-1} (Figure 3.15A-B).

A)

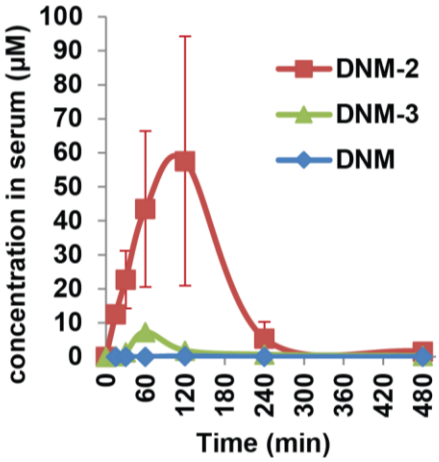

B)

Pharmacokinetic parameters for DNM, DNM-2, and DNM-3					
	Dose (mg kg^{-1})	$t_{1/2}$ (hr)	AUC (hr ng mL^{-1})	C_{max} (ng mL^{-1})	T_{max} (hr)
DNM	50			< 60	
DNM-2	50	0.9	44000	12800	1.2
DNM-3	50	1.2	4000	1260	1.1

C)

Pharmacokinetic parameters for DNM-2 and DNM-8 by Global TB Alliance					
	Dose (mg kg^{-1})	$t_{1/2}$ (hr)	AUC (hr ng mL^{-1})	C_{max} (ng mL^{-1})	T_{max} (hr)
DNM-8	50	2.2	12000	5500	0.7
DNM-8	200	1.1	75000	21700	0.7
DNM-2	50	1.5	33000	10500	1.0
DNM-2	200	4.1	278000	31900	1.0

D)

Pharmacokinetic parameters for DNM-2			
	Dose (mg kg^{-1})	MIC for AUC/MIC = 35 (μg mL^{-1})	MIC for AUC/MIC = 125 (μg mL^{-1})
DNM-2	50	0.9 – 1.25	0.26 – 0.35
DNM-2	200	7.9	2.2

Figure 3.15. Pharmacokinetic analysis of DNM, DNM-2, DNM-3 and DNM-4. (A) C57/BL6 mice were treated with 50 mg kg^{-1} DNM, DNM-2, or DNM-3 via oral gavage. After the indicated time points (15, 30, 60, 120, 240, and 480 min), mice were sacrificed and the serum concentrations of DNM, DNM-2, and DNM-3 was determined by HPLC. (B) Pharmacokinetic parameters determined from curves presented in A. (C) Pharmacokinetic parameters determined from curves obtained by the Global TB Alliance. (D) Prediction for in vivo efficacy based on AUC/MIC.

DNM-3 showed an intermediate level of bioavailability with a peak serum concentration of 4.3 μM (1.26 μg mL^{-1}) and an AUC of 4 h μg mL^{-1}. The bioavailability of these compounds mirrors the aqueous solubility suggesting that at least for this limited set of compounds aqueous solubility could be a reasonable predictor of oral bioavailability.

After these studies were performed, the Global TB Alliance did further MTD and PK studies on both DNM-2 and DNM-8. They found that 200 mg/kg (oral gavage) of either compound was well tolerated. Additionally, for DNM-2 this higher dose greatly extended the half-life (~3-4 fold) and allowed for an increase AUC (~6 fold, Figure 3.15C). This is particularly promising given the fact that AUC/MIC is very predictive of in vivo efficacy of antibiotics. For animal models with fluoroquinolones, an AUC/MIC ~30-35 is associated with clinically significant decreases in

mortality from Gram-positive infections while mortality is completely prevented with an AUC/MIC of ~100-125 in a variety of different mouse models including Gram-negative infections.[65-66] Assuming that DNM-2 and the fluoroquinolones act similarly, with the 50 mg/kg dose of DNM-2, we would expect to see good in vivo activity in FQR MRSA (Figure 3.15D and Table 3.2) and FQR VRE (Figure 3.15D and Table 3.3). Specifically, using the MIC_{50} for FQR MRSA strains with DNM-2 (0.125 µg/mL), the AUC/MIC is 264-352. This is well above the amount needed for a response in vivo. Using the MIC_{90} of FQR MRSA strain treated with DNM-2 (0.25 µg/mL), the AUC/MIC (132-176) is still well within the range expected to show potent in vivo activity. Similar results are seen for FQR VRE. Using the MIC_{50} for FQR VRE (0.5 µg/mL), the AUC/MIC is 66-88. This is still well above the ~30-35 associated with clinical response. Using the MIC_{90} for FQR VRE (4.0 µg/mL), the AUC/MIC is 8-11. This no longer is expected to have good in vivo activity. However, with the increased AUC associated with the 200 mg/kg dose, in vivo efficacy is expected for nearly all of the bacteria tested with DNM-2 thus far including FQR VRE, coagulase negative *Staphylococcus*, *B. anthracis*, *S. pneumoniae,* and *M. tuberculosis*.

3.9 Mammalian toxicity of the deoxynybomycins

As a prelude to exploring in vivo efficacy, the toxicity of DNM and key derivatives was evaluated.

3.9.1 *In vitro* toxicity[7]

Treatment of red blood cells with DNM and key derivatives indicated that none of these compounds induce hemolysis at the highest doses possible to test (Figure 3.16A). Additionally, DNM-2 demonstrated no significant DNA intercalation at concentrations up to 30 µM (9 µg mL^{-1}, Figure 3.16B). No mutagenesis was observed at concentrations up to 120 µg/mL of DNM-2 as evidenced by the Ames test performed by the Global TB Alliance (Figure 3.16C). Data from the Global TB Alliance did indicate slight hERG inhibition at the highest dose tested (20% at 3 ug mL^{-1}, Figure 3.16D). They also found that DNM-2 was positive for the micronucleus test (Figure 3.16E). Further in vitro and in vivo toxicity studies are needed to thoroughly explore these observations.

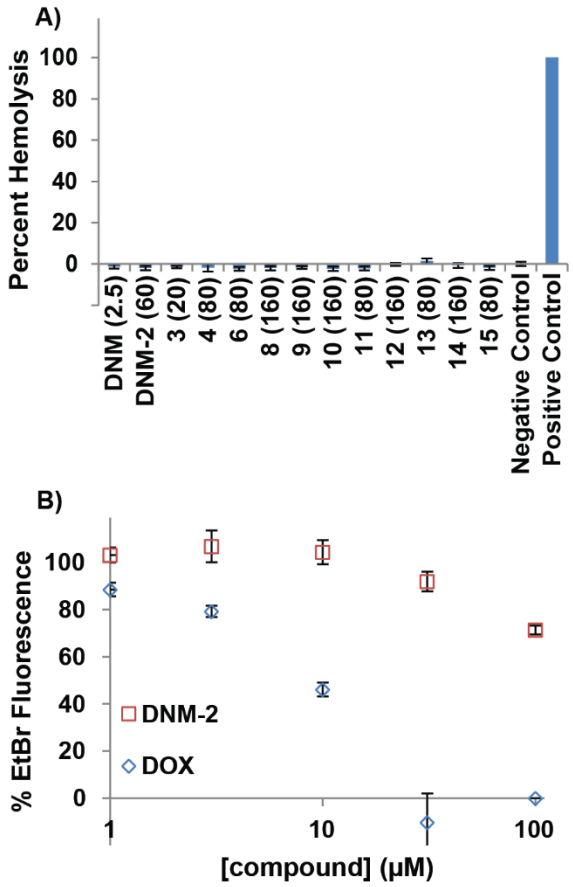

C)

Ames Test				
Compound	**Test Strain**	**S9**	**Conc (μg/mL)**	**AMES result**
2-nitrofluorine + 4-nitroquinoline N-oxide	TA98	no	4 + 2	Positive
2-nitrofluorine + 4-nitroquinoline N-oxide	TA100	no	4 + 2	Positive
aminoanthracene	TA98	yes	5.0	Positive
aminoanthracene	TA100	yes	5.0	Positive
DNM-2	TA98	no	125.0	Negative
DNM-2	TA100	no	125.0	Negative
DNM-2	TA98	yes	125.0	Negative
DNM-2	TA100	yes	125.0	Negative

D)

hERG inhibition			
Compound	**Conc (μM)**	**Conc (μg/mL)**	**% Inhibition**
Amitriptyline (positive control)	1	0.3	13 ± 3
	10	2.8	86 ± 3
DNM-2	1	0.3	4 ± 2
	3	0.9	6.4 ± 0.4
	5	1.5	5 ± 4
	10	3.0	20 ± 6

E)

Micronucleus Test					
Compound	**S9**	**MNT**	**First Response**		
			Conc (μM)	**% MN**	**Fold**
Cyclophosphamide	no	-	-	-	-
Cyclophosphamide	yes	+	200	3.1	6.45
Etoposide	no	+	0.4	6.6	14.00
Etoposide	yes	±	0.0004	0.7	2.00
DNM-2	no	+	2 (0.6 μg/mL)	6.1	12.90
DNM-2	yes	+	5.0 (1.5 μg/mL)	3.8	7.90

Figure 3.16. In vitro toxicity of DNM and select derivatives. (**A**) Hemolysis assay. Human red blood cells were co-incubated with compound. After incubation for 2 h at 37°C, the supernatant was analyzed for hemolysis. Each compound was tested either at 160 μg mL^{-1} or at the highest concentration which its solubility allowed. Concentrations (μg mL^{-1}) are indicated in parenthesis. The negative control is DMSO and the positive control is water. Data shown is from three independent replicates ± SEM. (**B**) Ethidium bromide (EtBr) intercalation assay. Compounds were incubated with Herring Sperm DNA, ethidium bromide, and compound of interest for 30 minutes. The solutions were then analyzed for ethidium bromide fluorescence. Any decrease in percentage fluorescence is indicative of compound intercalation. Doxorubicin (DOX) was used as a positive control. (**C**) In vitro Ames test for mutagenicity with or without S9 fraction of rat livers. 2-nitrofluorene + 4-nitroquinoline N-oxide were used as the positive control without the S9 fraction. 2-aminoanthracene was used as the positive control with the S9 fraction. S. typhimurium TA98: hisD3052, rfa, uvrB / pKM101; detects frame-shift mutations. S. typhimurium TA100: hisG45, rfa, uvrB / pKM101; detects base-pair substitutions. (**D**) In vitro hERG inhibition assay with amitriptyline as a positive control. (**E**) In vitro micronucleus test performed with and without S9 fraction rat livers with cyclophosphamide as the S9+ positive control and etoposide as the

Figure 3.16. (cont.) S9-positive control. % MN = Percentage of targeted cells with observed micronuclei. Fold = Fold elevation above vehicle control. Yes (+) = Strong positive response at least 3-fold higher than controls. Yes (±) = Weak positive response at least 2-fold higher than controls. No (-) = Negative response (less than 2-fold higher than controls).

3.9.2 Cell culture toxicity

Next, the effect of DNM on mammalian cells in culture was evaluated. While DNM does eventually kill mammalian cells,[67] it is at higher concentrations and longer time points compared to bacterial cells (Figure 3.17A-B). Specifically, when HEK293 cells (a human cell line derived from embryonic kidney cells) are treated with 0.5 µg/mL DNM for 24 h, only 32% of the cells are killed compared to when NRS3 bacterial cells are treated with 0.06 µg/mL DNM for 24h all of the cells were dead (Figure 3.2A). Additionally, treatment of HEK293 cells with 12 µg/mL DNM-2 (~C_{max} for 50 mg/kg treatment) for 4 h (~3X the $t_{1/2}$ for the 50 mg/kg treatment) resulted in only 26% cell death (data not shown). This is in stark contrast to treatment of NRS3 with 0.12 µg/mL DNM (~100 fold less compound) for 4h which results in a 2-log reduction in the number of colony forming units (cfu, Figure 3.17B). These data combined with previously published data showing that deoxynybomycin is non-toxic to normal (i.e. non-cancerous) cell lines[67] suggests that these compounds would likely be well-tolerated in vivo at concentrations expected to show antibacterial efficacy.

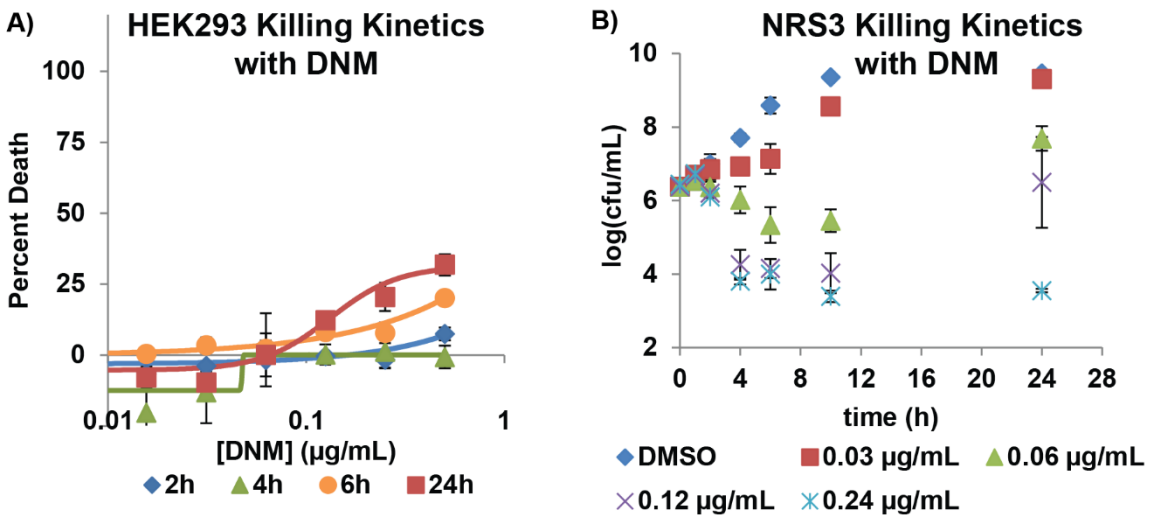

Figure 3.17. Comparison of mammalian and bacterial cell culture toxicity. (**A**) Killing kinetics for HEK293 cells treated with DNM. 10,000 cells/well were plated in a 96 well plate. Cells were then treated with DNM for the indicated times. Viability was assessed by Alamar blue. Data shown is from three independent replicates ± SEM. (**B**) Killing kinetics for NRS3 MRSA bacteria. ~1 X 10^7 cfu/mL were incubated with either DMSO or DNM at the indicated concentrations for the indicated times. Aliquots were taken, diluted and plated on MH plates to determine number of viable bacteria. Data shown is from three independent replicates ± SEM.

3.9.3 *In vivo* toxicity[7]

While in vitro and cell culture toxicities are informative, the best test of mammalian toxicity is to examine the effect that a compound has on an animal. Dr. Hyang Yeon Lee treated mice with increasing concentrations of DNM, DNM-2, and DNM-3 and found that all three compounds were well tolerated up to the highest dose evaluated (50 mg kg^{-1} by oral gavage, single dose).

Table 3.12. Hematologic Toxicity of DNM-2

	Vehicle	DNM-2 (50 mg kg^{-1})	Normal values[57] (Range)
RBC ($X10^6/\mu L$)	7.35 ± 0.2*	8.5 ± 0.2*	9.07 ± 0.49 (7.77 - 9.77)
Hemoglobin (g/dL)	12.8 ± 0.5	14.2 ± 0.3	13.4 ± 0.616 (12.0 - 14.5)
Hematocrit (%)	38.3 ± 1	40 ± 1	44.9 ± 2.09 (39.8 - 48.6)
Platelet (cells/μL)	330,000 ± 162,000*	60,000 ± 10,000*	1,310,000 ± 188,000 (990,000 - 1,840,000)
Mean Cell Volume (fl)	52.1 ± 0.6	47.3 ± 0.4	50 ± 0.64 (49 - 51)
WBC (cells/μL)	4970 ± 1240	3800 ± 300	5800 ± 810 (4400 - 7200)
Neutrophil (% of WBC)	11.2 ± 4.5	18 ± 3	14 ± 7.9 (2.0 - 30)
Lymphocyte (% of WBC)	85.2 ± 3	81 ± 3	81 ± 8.7 (60 - 98)
ALT (U/L)	32 ± 4	36 ± 1	39 ± 7.9 (28 - 57)
ALP (U/L)	160 ± 50	60 ± 10	72 ± 13 (40 - 90)
Albumin (g/dL)	2.2 ± 0.2	3.2 ± 0.1	2.7 ± 0.23 (2.4 - 3.0)
Globulin (g/dL)	2.7 ± 0.1	2.62 ± 0.05	1.2 ± 0.25 (0.8 - 1.5)
Total Bilirubin (mg/dL)	0.43 ± 0.07	0.7 ± 0.1	0.2 ± 0.04
BUN (Urea, mg/dL)	29 ± 1	32.0 ± 0.4	29 ± 4.9 (24 - 40)
Creatine (mg/dL)	0.17 ± 0.03	0.2 ± 0.0	0.6 ± 0.2 (0.4 - 1.0)

Hematologic toxicity of DNM-2. No clinically significant evidence for myelosuppression, renal injury, or hepatic toxicity was identified in any of the treatment groups. *Platelet cell counts were low because many platelet clumps were observed. This was reflected in lower RBC counts. Total bilirubin increases were observed for both vehicle and DNM-2-treated mice due to hemolysis during blood collection. Normal values were reported by Schnell and Wilson.[68]

To explore the effect of sustained treatments *in vivo*, Prof. Gee Lau administered DNM-2 to mice once-a-day for 10 days (via oral gavage at 50 mg kg^{-1}). Prof. Stéphane Lezmi, a board certified pathologist, then examined the mice for markers of hematological and non-hematological toxicity. No clinically significant evidence for myelosuppression, renal injury, or hepatic toxicity was identified (Table 3.12). No long-term pathologic effects were noted in the kidney, brain, lung, liver, spleen, heart, or stomach. In small intestine sections, mild intestinal dilation associated with

villi atrophy was noted (Figure 3.18). Also noted was increased vacuolation of white and brown adipocytes with a minimal increase in triglyceride levels. These changes were likely indirectly related to the drug, and possibly due to the antibiotic effects on the intestinal flora. As none of the mice showed any clinical symptoms, these changes were considered of minimal significance.

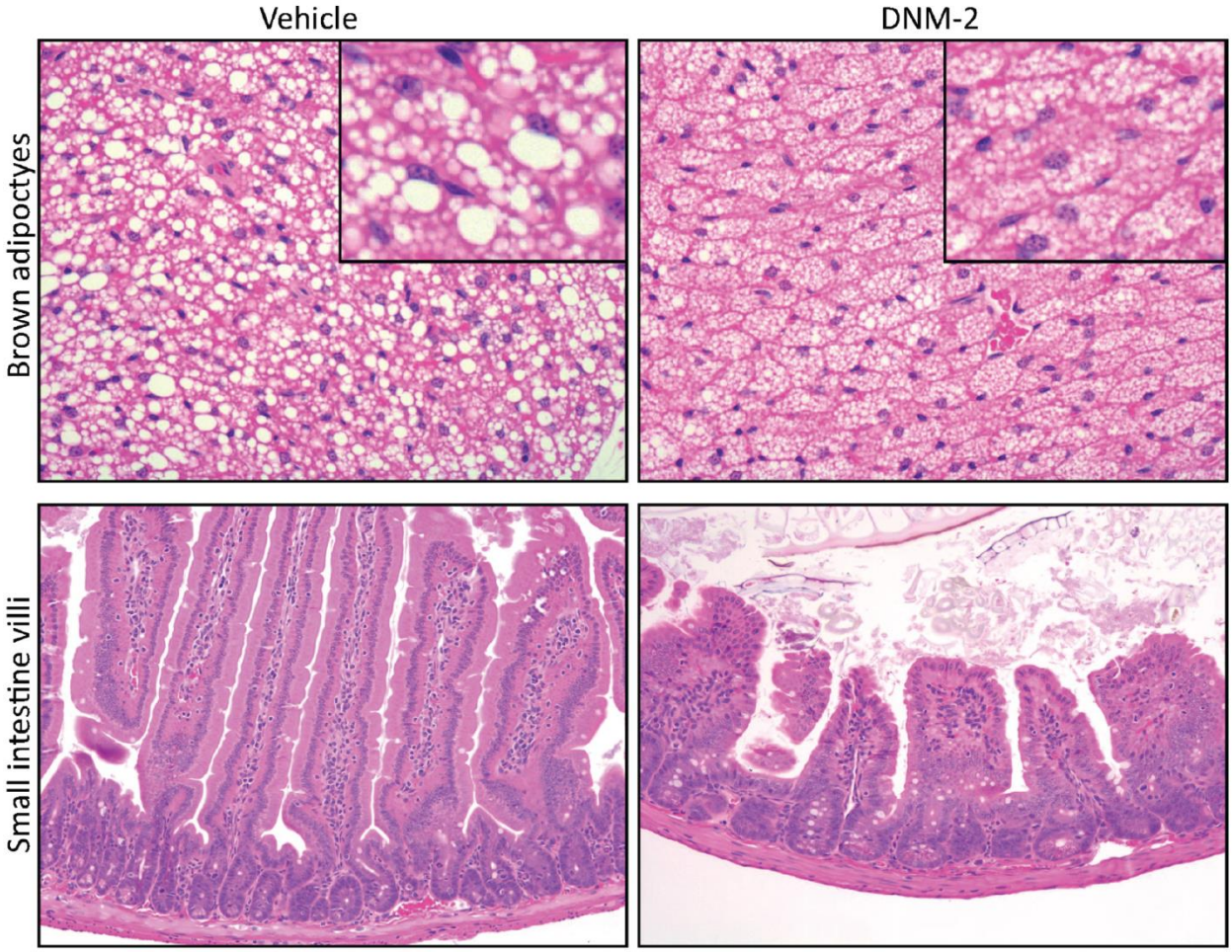

Figure 3.18. In vivo toxicity studies. After euthanasia, mouse organs were collected for histopathological analyses. Tissue sections were stained with hematoxylin and eosin. All slides were systematically evaluated for evidence of acute or chronic inflammation and toxicity. No long-term pathologic effects were noted in kidneys, brains, lungs, livers, spleens, hearts, and stomachs. In small intestine sections, mild intestinal dilation associated with villi atrophy was noted. Also noted was increased vacuolation of white and brown adipocytes. These changes were considered of minimal significance.

3.10 *In vivo* efficacy

With the indication that DNM-2 offered good exposure upon oral dosing with no observable in vivo toxicity, Prof. Gee Lau conducted an in vivo model of mouse sepsis. Mice were infected with FQR MRSA (NRS3) via tail vein injection. Mice were treated with CIP (50 mg kg^{-1}, oral gavage), DNM-2 (50 mg kg^{-1}, oral gavage), or vehicle control once-a-day for 10 days. As shown by the Kaplan-Meier survival curve in Figure 3.11B, mice treated with DNM-2 showed a significant survival difference relative to both CIP and vehicle treated control ($P < 0.005$, Fig. 3.19).

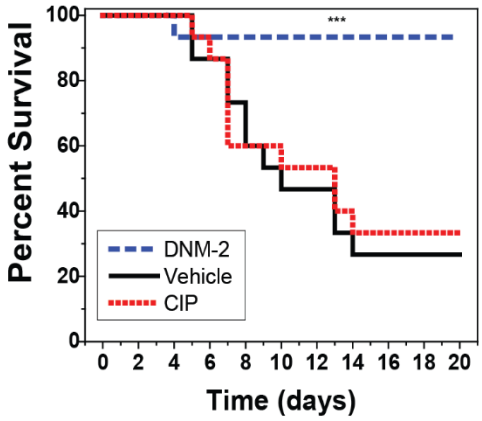

Figure 3.19. Kaplan-Meier curves showing the survival rates of mice infected with MRSA (NRS3, FQR). The mice received vehicle alone, 50 mg kg^{-1} CIP, or 50 mg kg^{-1} DNM-2 by oral gavage once-a-day for 10 days; n = 15 for each group. ***P < 0.005 versus vehicle and CIP, Log Rank Survival Test.

3.11 Conclusions and future directions

In conclusion, we developed a facile chemical route to produce DNM and derivatives with better solubility and pharmacokinetic properties. These compounds possess excellent activity against FQR MRSA, VRE, and *M. tuberculosis* while showing more modest activity against other Gram-positive and atypical Gram-negative bacteria like *B. anthracis*, *S. pneumoniae,* and *N. gonorrhoeae*. Through in vitro assays and resistance development, we demonstrated that these compounds work by inhibiting mutant DNA gyrase. Interestingly, based on the pattern of DNA observed in the in vitro assay, it appears that DNM may inhibit DNA gyrase differently than the

FQs (and perhaps more similarly to GSK299423, see Chapter 1.2.1.3). Further investigation into the mode of inhibition (e.g. a crystal structure) is needed to definitely show this. In vitro data combined with cell culture activity assays suggests that DNM and its derivative DNM-2 are best at inhibiting bacteria where the S84 of gyrA is mutated to a hydrophobic residue such as L, I, A, or V. Bacteria that typically mutate S84 to a different residue (e.g. F/Y/R) tend to be less sensitive. Further exploration of the reason for this selectivity is needed. A crystal structure of DNM bound to DNA gyrase would be very informative. Additionally, further in vitro studies with DNA gyrase enzymes from the individual species may also aid in answering these questions.

In addition to examining Gram-positive and atypical Gram-negative bacteria, we also examined typical Gram-negative bacteria. We found that DNM-2 shows little-to-no activity against typical Gram-negative bacteria such as *P. aeruginosa* and *A. baumannii.* Further examination revealed that this is most likely due to an inability to penetrate their cell membrane. Co-treatment with COL sensitized the bacteria to DNM-2 but this is likely not a good long term solution given the toxicity of COL. Development of novel DNM derivatives capable of penetrating the Gram-negative membrane while still retaining activity against DNA gyrase could greatly improve treatment options for these difficult to treat bacteria. Compounds with lower cLogD values have previously been shown to penetrate Gram-negative bacteria more effectively.[69-70] For this reason, DNM derivatives with more polar functionality are currently being explored.

One of the most intriguing aspects of DNM is its ability to resistance cycle. Bacteria that are resistant to fluoroquinolones are sensitive to DNM. When bacteria develop resistance to DNM, they are re-sensitized to fluoroquinolones suggesting that resistance that emerges to DNM would be treatable. This idea of developing molecules to specifically target the mutated target responsible for antibiotic resistance is an intriguing concept that could potentially be used to treat different types of antibiotic resistant bacteria (see Ch. 1.2.1.3). Below are a few potential areas in addition to FQR where it could be applied:

1) Targeting Sulfonamide Resistance. Clinically relevant Gram-negative bacteria primarily develop sulfonamide resistance via accumulation of plasmids which encode drug resistant versions of the target DHPS.[71] Specifically, *sul1* and *sul2* together are responsible for nearly 100% of sulfonamide resistant Gram-negative bacteria.[72] Developing small molecule inhibitors that are specific for these sulfonamide-resistant DHPSs may be an excellent strategy for targeting these resistant bacteria and could put selective pressure to lose the plasmids which encode these resistant sulfonamide-resistant DHPSs. The loss of these plasmids would result in re-sensitization to the sulfonamides.
2) Targeting Macrolide Resistance. The primary mechanism of high level resistance to macrolides is via target site modification by an rRNA methyltransferase (Erm responsible for methylation of the 23S rRNA at A2058).[73] Discovery of a small molecule which could inhibit translation by interacting with this modified rRNA site would likely pressure the bacteria to lose this resistance mechanism and potentially resensitize bacteria to the macrolides. One could search for such compounds by screening isogenic bacteria with and without Erm. Compounds which show selective activity for the bacteria containing the Erm would then need to be further analyzed to ensure one was not simply selecting for a methyltransferase inhibitor.
3) Targeting Linezolid Resistance-Part 1. Similar to the macrolides, one of the major forms of resistance to linezolid is methylation of the rRNA. A majority of linezolid-resistant bacteria express a methyltransferase (the chloramphenicol-florfenicol resistance (*cfr*) methyltransferase) which inhibits binding of these antibiotics via methylation of the target rRNA (A2503 of the 23S rRNA).[74-75] Again, similar to with the macrolides, discovery of a small molecule capable of targeting the methylated rRNA may be able to pressure bacteria back to the WT linezolid-sensitive phenotype.

4) Targeting Linezolid Resistance-Part 2. Another common cause of linezolid-resistant bacteria is mutation in the target rRNA (most commonly C2534U) along with mutations in ribosomal proteins L3 and L4. It may be possible to target this mutant ribosome similarly to how DNM targets the mutated gyrA of DNA gyrase. Screening for such a compound could be performed with WT and mutant isogenic pairs of bacteria.

5) Targeting Rifamycin Resistance. Resistance to rifamycin is primarily via point mutations in its target the β-subunit of the DNA-dependent RNA polymerase.[76] Specifically, 41% of rifamycin-resistant clinical isolates have a mutation at S455, 36% at H440, and 9% at D430.[77] These three sites are known to hydrogen bond with rifamycin thus explaining the acquired resistance.[76] Development of a small molecule capable of inhibiting these mutant DNA-dependent RNA polymerase may have similar activity against rifamycin-resistant bacteria as DNM has against bacteria with S83 gyrA mutantions.

Finally, utilizing a DNM derivative, the first in vivo efficacy of the nybomycin class is demonstrated in a mouse infection model. However, thus far the only in vivo model has been a sepsis model utilizing the NRS3 strain of MRSA. Another important future direction will be further evaluation of efficacy of DNM-2 in other in vivo models including other *S. aureus* models, *Enterococcus* models, and *M. tuberculosis* models. Additionally, in vivo models that evaluate the rate of resistance development and the ability to prevent resistance development through co-treatment with DNM and CIP would be very interesting to perform. Overall, the data presented suggest the promise of DNM derivatives for the treatment of FQR infections.

3.12 Materials and methods

General chemical reagents were purchased from Sigma Aldrich. Metal catalysts and ligands were purchased from Strem Chemicals Inc. (Newburyport, MA). Alkynes were purchased from GFS Chemicals (Powell, OH) and bis-pinacolboronate was purchased from Frontier Scientific (Logan, UT). All reagents were used without further purification unless otherwise noted.

^{1}H-NMR and ^{13}C-NMR spectra were recorded on Varian Unity spectrometers at 500 MHz and 125 MHz, respectively. Spectra generated from a solution of $CDCl_3$ were referenced to residual chloroform (^{1}H: δ 7.26 ppm, ^{13}C: δ 77.16 ppm). Spectra generated in mixtures of $CDCl_3$ and CD_3OD were referenced to C*D*$_3$OD (^{1}H: δ 3.31 ppm, ^{13}C: δ 49.0 ppm).

General protocol A: Synthesis of diazaanthracenols

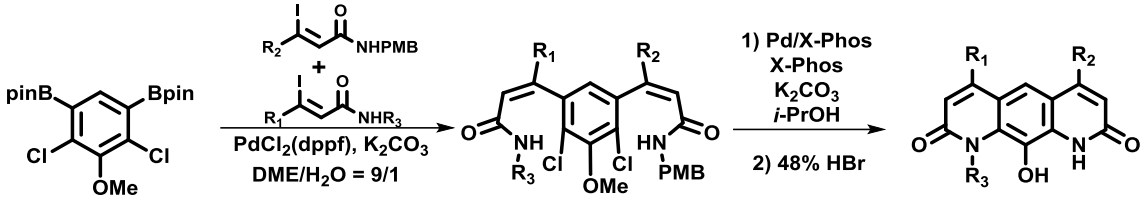

The synthesis of these diazaanthracenols has been previously described by Hergenrother and co-workers.[3,11] The only alteration from these protocols was that the phenols were further purified by reversed phase chromatography (10:90 MeCN:H_2O to 100:0 MeCN:H_2O) using a CombiFlash Rf (Teledyne Isco).

General protocol B: Synthesis of deoxynybomycins

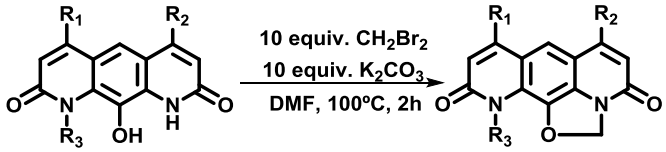

To a 20-mL vial was added diazaanthracenol (1 equiv.) and potassium carbonate (10 equiv.). The vial was evacuated and filled with argon three times. Degassed DMF (90 mL per mmol diazaanthracenol) was added followed by dibromomethane (10 equiv.). The only difference was with **5** in which 100 equiv of 1,1-dibromoethane were used in place of the dibromomethane. The vial was plunged into an oil bath preheated to 100 °C. The reaction was monitored by TLC (10% MeOH in CH_2Cl_2) with starting material appearing under UV as a green spot at the baseline and product appearing under UV as a bright blue spot at R_f = 0.5. When starting material was no longer visible by TLC (usually after 2-3 h), the solvent was evaporated and the residue was

purified by silica gel chromatography (0 to 5% MeOH in CH_2Cl_2). DNM and derivatives were collected as off-white solids.

Tabulated spectra

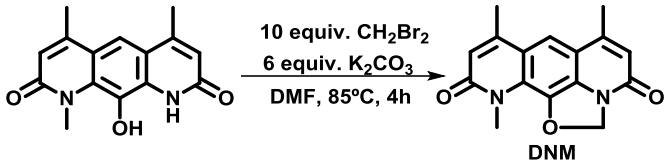

Synthesized from bispinacolborane,[3] (Z)-3-iodo-N-(4-methoxybenzyl)but-2-enamide,[3] and (Z)-3-iodo-N-methylbut-2-enamide,[3] by General Protocols A and B. 73% yield for methylene bridge insertion. 16% yield over 4 steps. 11% overall yield from commercially available starting material. Product is an off-white solid.

mp: >350 °C, 358-360 °C resulted in decomposition; ^{1}H NMR (400 MHz, 2:1 $CDCl_3$:CD_3OD): δ 7.55 (s, 1H), 6.49 (d, *J* = 1.0 Hz, 1H), 6.47 (d, *J* = 1.0 Hz, 1H), 6.39 (s, 2H), 3.92 (s, 3H), 2.54 (d, *J* = 1.0 Hz, 3H), 2.52 (d, *J* = 1.0 Hz, 3H); IR (neat, cm^{-1}): 1651 (s), 1625 (s), 1593 (s), 1558 (s), 1485 (m), 1445 (m), 1351 (s), 1327 (m), 1291 (w), 1154 (w); HRMS (m/z, ESI-TOF): $(M+H)^+$ calcd for $C_{16}H_{15}N_2O_3$, 283.1094; found, 283.1083.

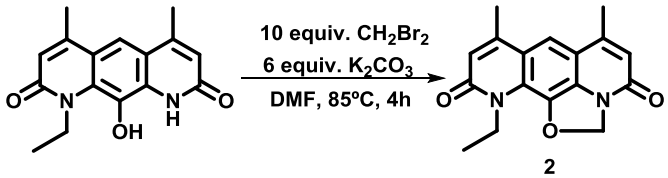

Synthesized from bispinacolborane,[3] (Z)-3-iodo-N-(4-methoxybenzyl)but-2-enamide,[3] and (Z)-N-ethyl-3-iodobut-2-enamide[11], by General Protocols A and B. 64% yield for methylene bridge insertion. 11% yield over 4 steps. Product is an off-white solid.

mp: >250 °C, 253 – 255 °C resulted in decomposition; ^{1}H NMR (500 MHz, $CDCl_3$): δ 7.47 (s, 1H), 6.52 (d, *J* = 1.0 Hz, 1H), 6.46 (d, *J* = 1.0 Hz, 1H), 6.40 (s, 2H), 4.54 (q, *J* = 7.0 Hz, 2H), 2.52 (d, *J* = 1.0 Hz, 3H), 2.50 (d, *J* = 1.0 Hz, 3H), 1.36 (t, *J* = 7.0 Hz, 3H); ^{13}C NMR (125 MHz, $CDCl_3$): δ 161.63, 158.64, 147.63, 146.74, 135.05, 132.32, 125.06, 121.34, 121.05, 120.79, 113.62, 113.42, 86.10, 40.27, 20.34, 18.00, 14.96; IR (neat, cm^{-1}): 1668 (m), 1657 (s), 1625 (s), 1596 (s), 1561 (m), 1485 (w), 1447 (2) 1419 (w), 1394 (m), 1380 (m), 1351 (s), 1322 (m), 1282 (w), 1243 (w), 1148 (w); HRMS (m/z, ESI-TOF): $(M+H)^+$ calcd for $C_{17}H_{17}N_2O_3$, 297.1239; found, 297.1246.

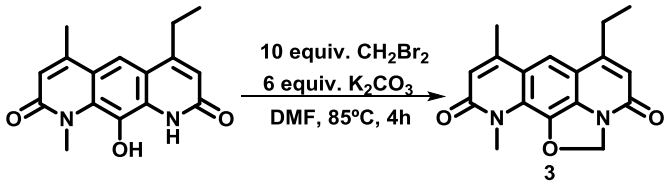

Synthesized from bispinacolborane,[3] (Z)-3-iodo-N-(4-methoxybenzyl)pent-2-enamide,[11] and (Z)-3-iodo-N-methylbut-2-enamide,[3] by General Protocols A and B. 72% yield for methylene bridge insertion. 13% yield over 4 steps. Product is an off-white solid.

mp: >250 °C, 274 – 275 °C resulted in decomposition; ^{1}H NMR (500 MHz, $CDCl_3$): δ 7.47 (s, 1H), 6.50 (d, *J* = 1.0 Hz, 1H), 6.47 (d, *J* = 1.0 Hz, 1H), 6.37 (s, 2H), 3.91 (s, 3H), 2.90 (q, *J* = 7.5 Hz, 2H), 2.47(s, 3H), 1.37 (t, *J* = 7.5 Hz, 3H); ^{13}C NMR (125 MHz, $CDCl_3$) δ 161.98, 158.86, 153.03, 146.76, 135.79, 132.48, 125.65, 120.71, 120.50, 119.43, 113.05, 112.86, 86.03, 32.60, 24.46, 20.27, 12.82; IR (neat, cm^{-1}): 1675 (w), 1658 (s), 1631 (s), 1598 (m), 1559 (w), 1491 (w), 1440 (w), 1414 (m), 1383 (w), 1342 (w), 1291 (2), 1147 (w); HRMS (m/z, ESI-TOF): $(M+H)^+$ calcd for $C_{17}H_{17}N_2O_3$, 297.1239; found, 297.1247

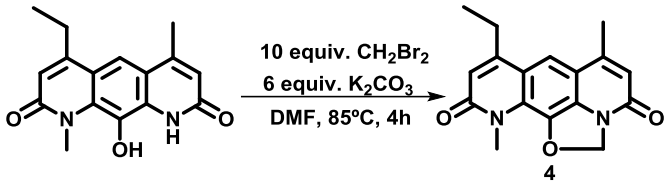

Synthesized from bispinacolborane,[3] (Z)-3-iodo-N-(4-methoxybenzyl)but-2-enamide,[3]and (Z)-3-iodo-N-methylpent-2-enamide,[11] by General Protocols A and B. 2% yield over 4 steps. Product is an off-white solid.

mp: >250 °C, 269 – 270 °C resulted in decomposition; ^{1}H NMR (500 MHz, $CDCl_3$): δ 7.51 (s, 1H), 6.53 (d, *J* = 1.0 Hz, 1H) 6.46 (d, *J* = 1.0 Hz, 1H), 6.38 (s, 2H), 3.94 (s, 3H), 2.88 (q, *J* = 7.5 Hz, 2H), 2.51 (d, *J* = 1.0 Hz, 3H), 1.36 (t, *J* = 7.5 Hz, 3H); ^{13}C NMR (125 MHz, $CDCl_3$) δ 162.38, 158.69, 151.94, 147.66, 135.89, 132.29, 126.09, 121.53, 120.09, 118.50, 113.56, 112.87, 86.15, 32.71, 25.95, 18.06, 12.93; IR (neat, cm^{-1}): 1651 (s), 1621 (s), 1594 (s), 1557 (w), 1490 (w), 1421 (m), 1354 (m), 1328 (m), 1292 (w), 1154 (w); HRMS (m/z, ESI-TOF): $(M+H)^+$ calcd for $C_{17}H_{17}N_2O_3$, 297.1239; found: 297.1234

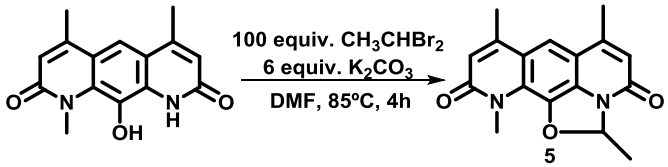

Synthesized from bispinacolborane,[3] (Z)-3-iodo-N-(4-methoxybenzyl)but-2-enamide,[3] and (Z)-3-iodo-N-methylbut-2-enamide,[3] by General Protocols A and B. General Protocol B was altered slightly. Specifically, 1,2-dibromoethane was used in place of dibromomethane and 100 equivalents were used instead of 10. 4% yield over 4 steps. Product is a yellow/off-white solid.

^{1}H NMR (500 MHz, $CDCl_3$): δ 7.43 (s, 1H), 6.80 (q, *J* = 5.5 Hz, 1H), 6.51 (d, *J* = 1.0 Hz, 1H), 6.44 (d, *J* = 1.0 Hz, 1H), 3.93 (s, 3H), 2.50 (d, *J* = 1.0 Hz, 3H), 2.49 (d, *J* = 1.0 Hz, 3H), 1.96 (d, *J* = 5.5 Hz, 3H); ^{13}C NMR (125 MHz, $CDCl_3$) δ 163.09, 159.71, 148.92, 148.49, 135.09, 132.19, 125.52,

121.65, 121.45, 119.96, 114.40, 113.74, 96.44, 32.99, 20.34, 20.22, 17.92; HRMS (m/z, ESI-TOF): $(M+H)^+$ calcd for $C_{17}H_{17}N_2O_3$, 297.1239; found, 297.1244.

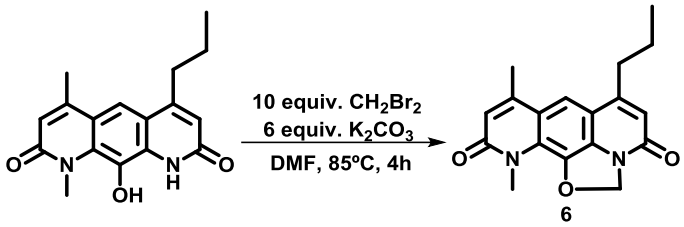

Synthesized from bispinacolborane,[3] (Z)-3-iodo-N-(4-methoxybenzyl)hex-2-enamide,[11] and (Z)-3-iodo-N-methylbut-2-enamide,[3] by General Protocols A and B. 2% yield over 4 steps. Product is an off-white solid.

mp: >200 °C, 228 – 230 °C resulted in decomposition; ^{1}H NMR (500 MHz, $CDCl_3$) δ 7.48 (s, 1H), 6.52 (1H), 6.46 (1H), 6.39 (s, 2H), 3.93 (s, 3H), 2.83 (t, *J* = 7.5 Hz, 2H), 2.49 (3H), 1.80 (m, 2H), 1.06 (t, *J* = 7.5 Hz, 3H); ^{13}C NMR (125 MHz, $CDCl_3$): δ 162.01, 158.76, 151.62, 146.73, 135.84, 132.60, 125.70, 120.74, 120.55, 120.40, 113.24, 113.01, 86.06, 33.39, 32.61, 21.96, 20.24, 14.05; IR (neat, cm^{-1}): 1660 (s), 1636 (s), 1600 (s), 1558 (w), 1489 (w), 1442 (w), 1416 (w), 1382 (w), 1344 (m), 1277 (w), 1148 (w); HRMS (m/z, ESI-TOF): $(M+H)^+$ calcd for $C_{18}H_{19}N_2O_3$, 311.1396; found: 311.1405

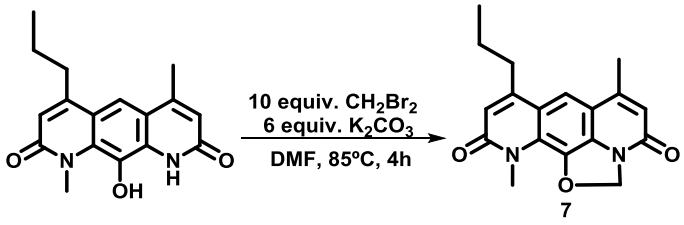

Synthesized from bispinacolborane,[3] (Z)-3-iodo-N-(4-methoxybenzyl)but-2-enamide,[3]and (Z)-3-iodo-N-methylhex-2-enamide,[11] by General Protocols A and B. 1% yield over 4 steps. Product is an off-white solid.

^{1}H NMR (500 MHz, $CDCl_3$): δ 7.51 (s, 1H), 6.52 (d, *J* = 1.0 Hz, 1H), 6.46 (d, *J* = 1.0 Hz, 1H), 6.39 (s, 2H), 3.95 (s, 3H), 2.81 (t, 2H, *J* = 7.5 Hz), 2.52 (d, 3H, *J* = 1.0 Hz, allylic C*H*$_3$), 1.78 (m, 2H),

1.07 (t, 3H, *J* = 7.5 Hz); ^{13}C NMR (125 MHz, $CDCl_3$): δ 162.16, 158.61, 150.46, 147.57, 135.82, 132.19, 126.09, 121.43, 120.03, 119.38, 113.46, 113.01, 86.07, 34.98, 32.64, 21.83, 17.97, 14.19; HRMS (m/z, ESI-TOF): $(M+H)^+$ calcd for $C_{18}H_{19}N_2O_3$, 311.1396; found, 311.1393.

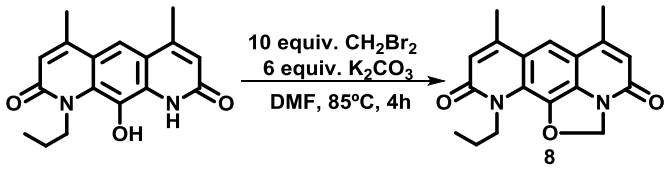

Synthesized from bispinacolborane,[3] (Z)-3-iodo-N-(4-methoxybenzyl)but-2-enamide,[3] and (Z)-3-iodo-N-propylbut-2-enamide,[11] by General Protocols A and B. 2% yield over 4 steps. Product is an off-white solid.

mp: >250 °C, 248 – 250 °C resulted in decomposition; ^{1}H NMR (500 MHz, $CDCl_3$): δ 7.46 (s, 1H), 6.51(1H), 6.46 (1H), 6.39 (s, 2H), 4.42 (m, 2H), 2.52 (3H), 2.49 (3H), 1.78 (m, 2H), 1.00 (t, *J* = 7.5 Hz, 3H); ^{13}C NMR (125 MHz, $CDCl_3$): δ 161.82, 158.67, 147.68, 146.74, 135.16, 132.35, 125.33, 121.37, 121.03, 120.80, 113.68, 113.43, 86.10, 46.43, 23.07, 20.42, 18.07, 11.36; IR (neat, cm^{-1}): 1655 (s), 1623 (s), 1594 (m), 1556 (w), 1485 (w), 1439 (w), 1399 (w), 1352 (m), 1229 (w), 1154 (w); HRMS (m/z, ESI-TOF): $(M+H)^+$ calcd for $C_{18}H_{19}N_2O_3$, 311.1396; found, 311.1398

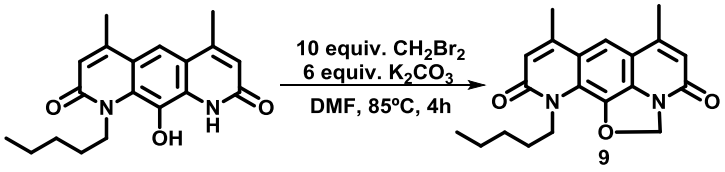

Synthesized from bispinacolborane,[3] (Z)-3-iodo-N-(4-methoxybenzyl)but-2-enamide,[3]and (Z)-3-iodo-N-pentylbut-2-enamide,[11] by General Protocols A and B. 6% yield over 4 steps. Product is an off-white solid.

^{1}H NMR (500 MHz, $CDCl_3$): δ 7.47 (s, 1H6.54 (d, *J* = 1.0 Hz, , 1H), 6.47 (d, *J* = 1.0 Hz, 1H), 6.40 (s, 2H), 4.46 (m, 2H), 2.52 (d, *J* = 1.0 Hz, 3H), 2.50 (d, *J* = 1.0 Hz, 3H), 1.74 (pent, *J* = 7.5 Hz,

2H) , 1.38 (m, 4H), 0.91 (t, *J* = 7.0 Hz, 3H); ^{13}C NMR (125 MHz, $CDCl_3$): δ 161.78, 158.67, 147.64, 146.64, 135.17, 132.37, 125.34, 121.38, 121.07, 120.83, 113.68, 113.43, 86.06, 45.06, 29.44, 29.11, 22.62, 20.35, 18.00, 14.22; HRMS (m/z, ESI-TOF): $(M+H)^+$ calcd for $C_{20}H_{23}N_2O_3$, 339.1709; found, 339.1704.

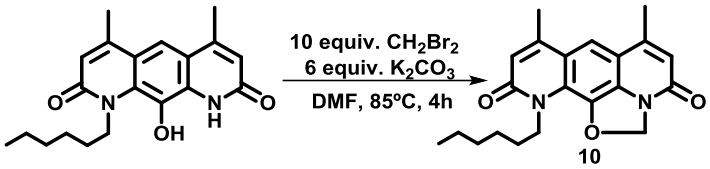

Synthesized from bispinacolborane,[3] (Z)-3-iodo-N-(4-methoxybenzyl)but-2-enamide,[3] and (Z)-N-hexyl-3-iodobut-2-enamide,[11] by General Protocols A and B. 20% yield over 4 steps. Product is an off-white solid.

^{1}H NMR (500 MHz, $CDCl_3$): δ 7.47 (s, 1H), 6.52 (d, *J* = 1.0 Hz, 1H), 6.46 (d, *J* = 1.0 Hz, 1H), 6.39 (s, 2H), 4.46 (m, 2H), 2.52 (d, *J* = 1.0 Hz, 3H), 2.49 (d, *J* = 1.0 Hz, 3H), 1.73 (pent, *J* = 7.5 Hz, 2H), 1.42 (pent, *J* = 7.5 Hz, 2H), 1.33 (m, 4H), 0.89 (t, *J* = 7.0 Hz, 3H); HRMS (m/z, ESI-TOF): $(M+H)^+$ calcd for $C_{21}H_{25}N_2O_3$, 353.1865; found: 353.1870

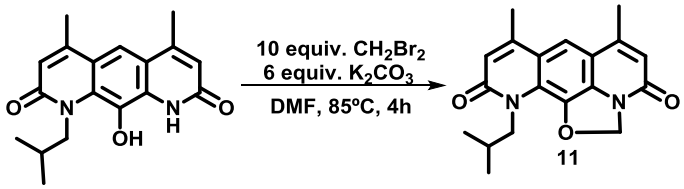

Synthesized from bispinacolborane,[3] (Z)-3-iodo-N-(4-methoxybenzyl)but-2-enamide,[3]and (Z)-3-iodo-N-isobutylbut-2-enamide,[11] by General Protocols A and B. 62% yield for methylene bridge insertion. 6% yield over 4 steps. Product is an off-white solid.

^{1}H NMR (400 MHz, $CDCl_3$): δ 7.47 (s, 1H), 6.52 (d, *J* = 1.0 Hz, 1H 6.46 (d, *J* = 1.0 Hz, 1H), 6.39 (s, 2H), 4.38 (d, *J* = 7.2 Hz, 2H), 2.52 (d, *J* = 1.0 Hz, 3H), 2.50 (d, *J* = 1.0 Hz, 3H), 2.17 (sept, *J* = 7.2 Hz, 1H), 0.95 (d, *J* = 6.8 Hz, 1H); ^{13}C NMR (125 MHz, $CDCl_3$): δ 162.13, 158.65, 147.58,

146.51, 135.23, 132.38, 125.61, 121.34, 121.02, 120.81, 113.68, 113.40, 85.91, 50.88, 29.08, 20.33, 19.87, 17.96; HRMS (m/z, ESI-TOF): $(M+H)^+$ calcd for $C_{19}H_{21}N_2O_3$, 325.1552; found, 325.1553.

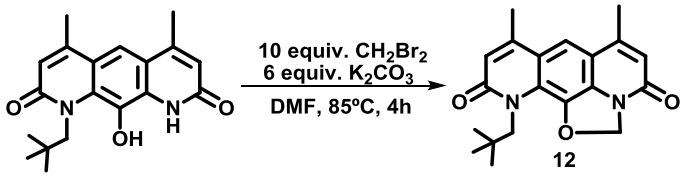

Synthesized from bispinacolborane,[3] (Z)-3-iodo-N-(4-methoxybenzyl)but-2-enamide,[3] and (Z)-3-iodo-N-neopentylbut-2-enamide,[11] by General Protocols A and B. 30% yield over 4 steps. Product is an off-white solid.

mp: >200 °C, 210 – 213 °C resulted in decomposition; ^{1}H NMR (500 MHz, $CDCl_3$): δ 7.46 (s, 1H), 6.53 (d, *J* = 1.0 Hz, 1H), 6.45 (d, *J* = 1.0 Hz, 1H), 6.38 (s, 2H), 4.56 (bs, 1H), 2.52 (d, *J* = 1.0 Hz, 3H), 2.50 (d, *J* = 1.0 Hz, 3H), 0.95 (s, 9H); ^{13}C NMR (125 MHz, $CDCl_3$): δ 162.91, 158.73, 147.68, 146.69, 135.45, 132.34, 126.92, 121.34, 121.08, 121.03, 113.69, 113.38, 85.69, 53.00, 35.34, 28.36, 20.42, 18.06; IR (neat, cm^{-1}): 1698 (w), 1658 (s), 1631 (s), 1606 (s), 1560 (w), 1474 (w), 1447 (w), 1353 (m), 1313 (w), 1258 (w), 1137 (m); HRMS (m/z, ESI-TOF): $(M+H)^+$ calcd for $C_{20}H_{23}N_2O_3$, 339.1709; found, 339.1715.

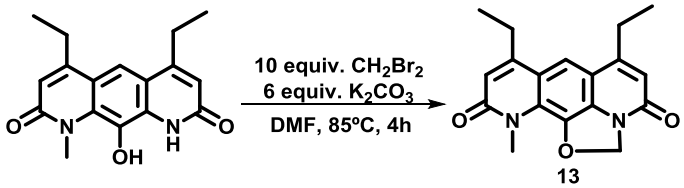

Synthesized from bispinacolborane,[3] (Z)-3-iodo-N-(4-methoxybenzyl)pent-2-enamide,[11] and ((Z)-3-iodo-N-methylpent-2-enamide,[11] by General Protocols A and B. 7% yield over 4 steps. Product is an off-white solid.

mp: >200 °C, 214 – 215 °C resulted in decomposition; ^{1}H NMR (500 MHz, $CDCl_3$): δ 7.54 (s, 1H), 6.52 (1H), 6.46 (1H), 6.37 (s, 2H), 3.92 (s, 3H), 2.88 (dq, *J* = 1.0 Hz, 7.5 Hz, 2H), 2.87 (dq, *J* = 1.0 Hz, 7.5 Hz, 2H), 1.36 (t, *J* = 7.5 Hz, 3H), 1.34 (t, *J* = 7.5 Hz, 3H); ^{13}C NMR (125 MHz, $CDCl_3$): δ 162.28, 158.87, 153.03, 151.86, 135.92, 132.32, 125.84, 119.93, 119.44, 118.39, 112.81, 112.49, 86.00, 32.60, 25.91, 24.52, 12.88; IR (neat, cm^{-1}): 1682 (w), 1657 (s), 1631 (s), 1595 (s), 1558 (w), 1455 (w), 1416 (m), 1370 (w), 1339 (m), 1261 (w), 1145 (w); HRMS (m/z, ESI-TOF): $(M+H)^+$ calcd for $C_{18}H_{19}N_2O_3$, 311.1396; found, 311.1393

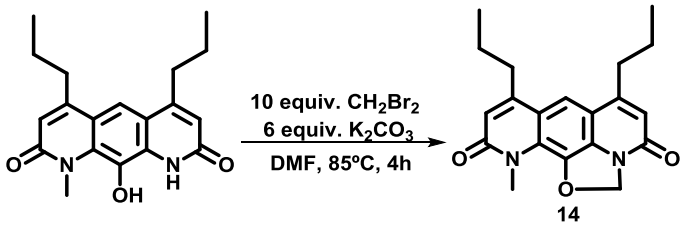

Synthesized from bispinacolborane,[3] (Z)-3-iodo-N-(4-methoxybenzyl)hex-2-enamide,[11] and (Z)-3-iodo-N-methylhex-2-enamide,[11] by General Protocols A and B. 5% yield over 4 steps. Product is an off-white solid.

mp: 171-173 °C; ^{1}H NMR (500 MHz, $CDCl_3$): δ 7.53 (s, 1H), 6.51 (1H), 6.45 (1H), 6.38 (s, 2H), 3.94 (s, 3H), 2.82 (t, *J* = 7.5 Hz, 2H), 2.80 (t, *J* = 7.5 Hz, 2H), 1.78 (m, 4H), 1.06 (t, *J* = 7.5 Hz, 6H); ^{13}C NMR (125 MHz, $CDCl_3$): δ 161.96, 158.57, 151.44, 150.30, 135.78, 132.25, 125.76, 120.25, 119.75, 119.23, 112.79, 112.75, 85.92, 34.90, 33.29, 32.48, 21.91, 21.78, 14.07, 13.95; IR (neat, cm^{-1}): 1652 (s), 1627 (s), 1596 (s), 1556 (w), 1487 (w), 1458 (w), 1427 (m), 1378 (w), 1340 (m), 1326 (m), 1282 (w), 1143 (w); HRMS (m/z, ESI-TOF): $(M+H)^+$ calcd for $C_{20}H_{23}N_2O_3$, 339.1709; found, 339.1717

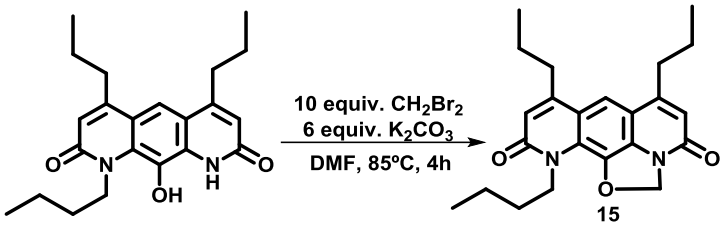

Synthesized from bispinacolborane,[3] (Z)-3-iodo-N-(4-methoxybenzyl)hex-2-enamide,[11] and (Z)-N-butyl-3-iodohex-2-enamide[11] by General Protocols A and B. 6% yield over 4 steps. Product is an off-white solid.

mp: 156-158 °C; ^{1}H NMR (500 MHz, $CDCl_3$) δ 7.56 (s, 1H), 6.53(1H), 6.46(1H), 6.40(s, 2H), 4.48 (m, 2H), 2.83 (t, *J* = 7.5 Hz, 2H), 2.81 (t, *J* = 7.5 Hz, 2H), 1.70-1.83 (m, 6H), 1.45 (sext, *J* = 7.5 Hz, 2H), 1.07 (t, *J* = 7.5 Hz, 3H), 1.06 (t, *J* = 7.5 Hz, 3H), 0.97 (t, *J* = 7.5 Hz, 3H); ^{13}C NMR (125 MHz, $CDCl_3$): δ 161.92, 158.77, 151.57, 150.33, 135.42, 132.38, 125.38, 120.36, 120.18, 119.60, 113.19, 112.81, 85.94, 44.88, 35.14, 33.46, 31.84, 22.10, 21.97, 20.21, 14.23, 14.08; IR (neat, cm^{-1}): 1658 (s), 1629 (s), 1596 (m), 1557 (w), 1485 (w), 1445 (w), 1422 (w), 1397 (w), 1336 (w), 1315 (w), 1271 (w), 1219 (w); HRMS (m/z, ESI-TOF): $(M+H)^+$ calcd for $C_{23}H_{29}N_2O_3$, 381.2178; found, 381.2167

Bacterial strains

MRSA and *P. aeruginosa* isolates were from Cubist Pharmaceuticals. VRE isolates were from a previously published collection.[78]. *B. anthracis* strains and the *N. gonorrheae* strain (MS11) were obtained from Prof. Douglass Mitchell (UIUC). Prof. Mitchell originally obtained the *B. anthracis* strains from (Lawrence Livermore National Labs). *E. coli* strains were obtained either from ATCC or Prof. Cari Vanderpool (UIUC). *A. baumannii* isolates were obtained from Dr. John Quale.[55]

Antibiotic susceptibility tests

Susceptibility testing for all bacteria except for *N. gonorrhoeae* was performed in triplicate using the microdilution broth method as outlined by the Clinical and Laboratory Standards Institute

CLSI.[15] MH broth was used. Briefly, 2 µL of a 50X compound stock (usually in DMSO or water) was added to the wells of a 96-well round well plate. Live and dead controls received 2 µL of vehicle. 88 µL of MH broth were added to all wells except the dead control wells which received 98 µL of MH broth. 100 uL of an overnight culture of bacteria was then added to 10 mL of MH broth and grown until the culture reached a turbidity equal to 1 X 10^7 – 2 X 10^8 cfu/mL (based on a previously determined calibration curve). The culture was then diluted to 5 X 10^6 cfu/mL and 10 µL of this solution was added to each well except the dead controls for a final of 5 X 10^5 cfu/mL. Plates were incubated at 37 ºC for 16-20 h. Absorbance was then read on a Molecular Devices SpectraMax Plus 384 Microplate reader at λ = 600 nm. MIC values were defined as the lowest concentration of compound that resulted in ≥ 90% growth inhibition.

N. gonorrhoeae was assessed by agar dilution method as outlined by the CLSI and the CDC.[15,79] GC agar with 1% IsoVitaleX growth supplement was used. The agar was prepared, autoclaved, and cooled to 50 ºC in a waterbath. 20 µL of a 100X DMSO stock and 20 µL of freshly made IsoVitaleX supplement was added to each well of a 12 well plate. To this was added 1960 µL of GC agar and the agar was gently rocked to mix. A colony of *N. gonorrhoeae* from a freshly streaked chocolate agar (GC agar with 1% bovine hemoglobin and 1% IsoVitaleX grown in 5% CO_2 at 35-36 ºC) was resuspended in MH broth and adjusted to OD450 ~ 0.15 which is equivalent to 10^8 cfu/mL according to the CDC.[79] The culture was then diluted 1:10 to give 10^7 cfu/mL and 5 uL of this solution was plated 3X on each concentration of agar to give 5 X 10^4 cfu per spot. The plates were allowed to air dry in a sterile biosafety cabinet for ~15 minutes before inverting and placing in an incubator with 5% CO_2 at 35-36 ºC for 24 h. Plates were examined for growth and recorded as good (+, 3/3 spots grew), poor (±, 1 or 2/3 spots grew), or no growth (-, no spots grew).

Testing for clinical isolates of MRSA (other than NRS3), Coagulase-negative *Staphylococcus*, and a portion of the *Streptococcus* species was performed by Cubist Pharmaceuticals. The other *Streptococcus* species were tested by the UT Health Science Center

(San Antonio, TX). *Mycobacteria* species were tested by the Global TB Alliance. The *N. gonorrhoeae* clinical isolates were examined by NIH/NIAID in collaboration with the Southern Research Institute.

DMSO Solubility Determination

A small amount of solid compound (generally ~2 mg) was measured into a 7 mL glass vial. The vial was then tared. DMSO was added dropwise, sonicated, vortexed, and examined visually for undissolved compound. When compound had completely gone into solution, the vial was weighed to obtain a weight for the DMSO. The density of DMSO was then used to calculate the volume of DMSO added and subsequently the solubility of the compound in DMSO.

Aqueous Solubility Determination

Initially a small amount of solid compound (generally 0.5 to 1.5 mg) was measured into a 1.7 mL Eppendorf tube. Phosphate buffered saline (pH 7.4) was added to give a maximum final concentration of 1 mg/mL of compound. The compound was vortexed for ~30 seconds before being placed into a bath sonicator (Cole Parmer, ultrasonic cleaner) for 1 h. Longer incubation times (up to 24 h) were performed with select compounds and no difference in solubility was observed so 1 h was used for all subsequent testing. The tubes were vortexed again for 30 s before being centrifuged at maximum speed (13,000 $\times$ g) for 10 minutes. The supernatant was then filtered through a 0.22 µm syringe filter (Millipore Millex MP). The filtrate was then analyzed by LC-MS (λ = 254 nm, ESI-TOF in positive mode, Agilent Technologies 6230 TOF LC/MS). The filtrate was diluted 1:2 and 1:4 and all three samples (1X, 0.5X and 0.25X) were analyzed in triplicate. Three independent replicates of each compound were performed. A calibration curve for each compound was generated from 1 – 40 µM by dissolving the compound in DMSO and making dilutions of the stock in DMSO. The calibration curve (measured by UV absorbance) was

linear over this range. The concentration of the samples was calculated based on the calibration curves.

Compound Accumulation Assay

These studies were performed by Michelle Richter. Briefly, accumulation was studied for *E. coli* strain MG1655. Bacteria were treated for 10 minutes with either 40 µM DNM-2 alone or 40 µM DNM-2 with 2X MIC of COL. After treatment, cells were washed and lysed. Lysates were analyzed by LC-MS/MS for presence of compound and compared to a calibration curve to determine the concentration of the compound.

Checkerboard Assay

Checkerboard assays were performed by first adding 2 µL of a 50X COL stock (dissolved in sterile filtered MilliQ water) to the appropriate wells. 2 µL of a 50X DNM-2 stock (dissolved in DMSO) or 2 µL of a VANC stock (dissolved in sterile filtered MilliQ water) were added to the appropriate wells. 2 µL of MilliQ water and 2 µL of DMSO were added for the live and dead controls. 86 µL of MH broth were added to all wells except the dead control wells which received 96 µL of MH broth. 10 µL of a 5 X 10^6 cfu/mL was added to each well except the dead controls for a final of 5 X 10^5 cfu/mL as outlined in the CLSI guidelines.[15]

DNA amplification and sequencing analysis

A single colony of *S. aureus* grown on MH agar or isolated DNA provided by Cubist, a single colony of *Enterococcus* grown on BHI agar, a single colony of *P. aeruginosa* grown on Tryptic Soy agar, or a single colony of *B. anthracis* grown on MH agar was suspended in 50 µL of the PCR mixture containing the primers (Table 3.13) and PCR master mix (Platinum *Taq*DNA Polymerase, invitrogen). PCR amplification was performed using the following protocol:

1) An initial denaturation step of 94°C for 2 minutes
2) 94°C for 30 s
3) 51°C (*E. coli*), 52°C (*S. aureus*, *Enterococcus faecalis, B. anthracis*, and *N. gonorhoeae*), 58°C (*Enteroccocus faecium*) or 59°C (*P. aeruginosa*) for 30 s
4) 72 °C for 60 s.
5) Repeat 2-4 34 more times for a total of 35 cycles
6) For *P. aeruginosa*, there was an addition 72 °C extension after the 35 cycles for 7 min.
7) Hold at 4 °C until purification

PCR products were purified further on a 1% agarose gel and DNA was extracted (QIAquick Gel Extraction Kit, Qiagen). DNA sequencing was performed by the W. M. Keck Center for Comparative and Functional Genomics (UIUC). The NCBI standard nucleotide BLAST database was used to verify the identity of the PCR products and determine mutations within the sequences.

Table 3.13. Primers used for sequencing and for site directed mutagenesis

Primer	Sequence	Reference
Bacillus anthracis gyrA-F	5'-CGGCTCTCTTTCAGAACCAT-3'	*Antimicrob. Agents Chemother.* 2004, *48*, 3024
Bacillus anthracis gyrA-R	5'-AAAACCTGTGCATCGTAGGG-3'	*Antimicrob. Agents Chemother.* 2004, *48*, 3024
Bacillus anthracis parC-F	5'-CGTGACGGCTTAAAACCAGTA-3'	*Antimicrob. Agents Chemother.* 2004, *48*, 3024
Bacillus anthracis parC-R	5'-TTCCGTATAACGCATTGCTG-3'	*Antimicrob. Agents Chemother.* 2004, *48*, 3024
Enterococcus faecalis_gyrA_F	5'-ATGAGTGAAGAAATTAAAGAAAACATTCA-3'	Antimicrob. Agents Chemother. 2002, 46, 1800
Enterococcus faecalis_gyrA_R	5'-ACTCATACGTGCTTCGGTATAACGC-3'	Antimicrob. Agents Chemother. 2002, 46, 1800
Enterococcus faecalis_parC_F	5'-GTGACAATTTTGGAAAAACGCCAAG-3'	Antimicrob. Agents Chemother. 2002, 46, 1800
Enterococcus faecalis_parC_R	5'-CACCACTTAACTGTGATAAACGAGC-3'	Antimicrob. Agents Chemother. 2002, 46, 1800
Enterococcus faecium_gyrA_F	5'-CGGGATGAACGAATTGGGTGTGA-3"	J. Chemotherapy. 2011, 23, 87-91
Enterococcus faecium_gyrA_R	5'-AATTTTACTCATACGTGCTTCGG-3'	J. Chemotherapy. 2011, 23, 87-91
Enterococcus faecium_parC_F	5'-TTCCCGTGCATTTCGATCAGTACTTC-3'	J. Chemotherapy. 2011, 23, 87-91
Enterococcus faecium_parC_R	5'-CGTATGACAAAGGATTCGGTAAATC-3'	J. Chemotherapy. 2011, 23, 87-91
Escherichia coli_gyrA_F	5'-TGCCAGATGTCCGAGAT-3'	Antimicrob. Agents Chemother. 2001, 45, 1515.
Escherichia coli_gyrA_R	5'-GTATAACGCATTGCCGC-3'	Antimicrob. Agents Chemother. 2001, 45, 1515.
Escherichia coli_parC_F	5'-TATGCGATGTCTGAACTGGG-3'	Antimicrob. Agents Chemother. 2001, 45, 1515.
Escherichia coli_parC_R	5'-GCTCAATAGCAGCTCGGAAT-3'	Antimicrob. Agents Chemother. 2001, 45, 1515.
Neisseria gonorrhoeae_gyrA_F	5'-CGGCGCGTACTGTACGCGATGCA-3'	J. Clin. Microbiol. 2000, 38, 521-525.
Neisseria gonorrhoeae_gyrA_R	5'-AATGTCTGCCAGCATTTCATGTGAGA-3'	J. Clin. Microbiol. 2000, 38, 521-525.
Neisseria gonorrhoeae_parC_F	5'-ATGCGCGATATGGGTTTGAC-3'	J. Clin. Microbiol. 2000, 38, 521-525.
Neisseria gonorrhoeae_parC_R	5'-GGACAACAGCAATTCCGCAA-3'	J. Clin. Microbiol. 2000, 38, 521-525.
Pserudomonas aeruginosa_gyrA_F	5'-TTA TGC CAT GAG CGA GCT GGG CAA CGA CT -3'	Microb. Drug Resistance. 1993, 4, 257 Antimicrob. Agents Chemother. 2000, 44, 710
Pserudomonas aeruginosa_gyrA_R	5'-AAC CGT TGA CCA GCA GGT TGG GAA TCT T -3'	Microb. Drug Resistance. 1993, 4, 257 Antimicrob. Agents Chemother. 2000, 44, 710
Pserudomonas aeruginosa_parC_F	5'-CTG GAT GCC GAT TCC AAG CA -3'	Microb. Drug Resistance. 1993, 4, 257 Antimicrob. Agents Chemother. 2000, 44, 710
Pserudomonas aeruginosa_parC_R	5'-GAA GGA CTT GGG ATC GTC CG -3'	Microb. Drug Resistance. 1993, 4, 257 Antimicrob. Agents Chemother. 2000, 44, 710
Staphylococcus aureus_gyrA_F	5'-GGATTAAATGAACAAGGTATGACACCG-3'	Int. J. Antimicrob. Agents 2012, 39, 478-485
Staphylococcus aureus_gyrA_R	5'-TAGTCATACGCGCTTCAGTATAACG-3'	Int. J. Antimicrob. Agents 2012, 39, 478-485
Staphylococcus aureus_parC_F	5'-TTAGGTGATCGCTTTGGAAGATATAG-3'	Int. J. Antimicrob. Agents 2012, 39, 478-485
Staphylococcus aureus_parC_R	5'-TACCATTGGTTCGAGTGTCG-3'	Int. J. Antimicrob. Agents 2012, 39, 478-485
E coli S83L sense for gyrA site-directed mutagenesis	5'-AATACCATCCCCATGGTGACTTGGCGGTCTATG-3'	Agilent QuikChange Primer Design
E coli S83L antisense for gyrA site-directed mutagenesis	5'-CATAGACCGCCAAGTCACCATGGGGATGGTATT-3'	Agilent QuikChange Primer Design
E coli S83R sense for gyrA site-directed mutagenesis	5'-CATCCCCATGGTGACAGGGCGGTCTATGACAC-3'	Agilent QuikChange Primer Design
E coli S83R antisense for gyrA site-directed mutagenesis	5'-GTGTCATAGACCGCCCTGTCACCATGGGGATG-3'	Agilent QuikChange Primer Design
E coli S83F sense for gyrA site-directed mutagenesis	5'-CATGGTGACTtcGCGGTCTATG-3'	NEB Base Changer
E coli S83F antisense for gyrA site-directed mutagenesis	5'-GGGATGGTATTTACCGATTAC-3'	NEB Base Changer
E coli S83Y sense for gyrA site-directed mutagenesis	5'-CATGGTGACTatGCGGTCTATG-3'	NEB Base Changer
E coli S83Y antisense for gyrA site-directed mutagenesis	5'-GGGATGGTATTTACCGATTAC-3'	NEB Base Changer

Sequence alignments

Protein sequences for sequence alignments were found on the Uniprot website. Sequence alignments were performed using the Uniprot align tool.

Site directed mutagenesis

pTRCHisA-GyrA plasmid containing the gene for *E. coli* gyrase A was kindly provided by Prof. David Hooper [80]. Primers for mutagenesis were designed using either QuikChange Primer Design (Agilent) or NEB base changer and their sequences can be found in Table 3.13. Site directed mutagenesis was carried out with the QuikChange Lightning Site-Directed Mutagenesis Kit (Agilent) or NEB Q5 Site-Directed Mutagenesis Kit according to the manufacturer's instructions with the modification that NEB Turbo Competent *E. coli* were used as the host strain. All clones were confirmed by sequencing.

E. coli DNA gyrase expression

Expression of WT *E. coli* gyrase A and gyrase B was performed as previously described [80]. Briefly, pTRCHisA-GyrA, pTRCHisA-GyrAS83L, pTRCHisA-GyrAS83R, pTRCHisA-GyrAS83F, pTRCHisA-GyrAS83Y, or pTRCHisA-GyrB were introduced into One Shot BL21 Star (DE3) (NEB) by chemical transformation. Transformed cells were selected for on an LB ampicillin plate. Single colonies from a fresh plate were inoculated into 50 mL of LB with 50 µg/mL ampicillin and incubated aerobically at 37°C with shaking at 250 rpm overnight (14-16 h). The overnight culture was then used to inoculate 1L LB with 50 µg/mL ampicillin. The culture was grown aerobically with shaking at 250 rpm until A_{600} reached 0.4-0.6. Protein expression was induced with a final concentration of 0.5 mM of IPTG at 37°C with shaking at 250 rpm for 4h. The culture was harvested by centrifugation at 5000 × g for 5 min at 4 °C. Cell pellets were frozen at –20 °C, thawed on ice for 30 min, and resuspended in TGN_{150} (20 mM Tris-HCl [pH 7.5], 10% glycerol,

150 mM NaCl) with 0.5 mg/mL lysozyme with 2 µg/mL aprotinin, 1 µg/mL leupeptin, 1 µg/mL pepstatin A, and 100 µM phenylmethanesulfonylfluoride. Cells were lysed by sonication at 35% amplitude (10 s pulse with 30 s rest, 6 times). The lysate was cleared by centrifugation at 35,000 ^{x} g for 30 min at 4 °C. The supernatant was batch-loaded onto 1 mL of 1:1 Ni-NTA agarose (Qiagen) at 4 °C for 30 min with inversion. The resin was washed with 20 mL TGN_{150} with 10 mM imidazole followed by 10 mL of wash buffer (20 mM Tris-HCl (pH 7.5), 10% glycerol, 300 mM NaCl, 10 mM imidazole) and eluted with TGN150 containing imidazole concentrations of 25, 50, 100, 200, 300, and 500 mM. Eluted fractions were assessed by sodium dodecyl sulfate-polyacrylamide gel electrophoresis (SDS-PAGE) using 4-20% TGX Mini-PROTEAN gels (Bio-Rad). Fractions containing pure protein were pooled and dialyzed against TDEN buffer (50 mM Tris-HCl [pH 7.5], 5 mM dithiothreitol, 1 mM EDTA, 150 mM NaCl) overnight at 4°C utilizing a Slide-A-Lyzer Dialysis Cassette, 10 000 MWCO (Thermo Scientific) and concentrated to ~0.5-1 mL using an Amicon Ultra-15 50K Centrifugal Filter Device. The concentration was determined by Bradford assay (Sigma) using bovine serum albumin (BSA, Thermo Scientific) as the control.Expression of S83L and S83R GyrA was performed identically to expression of the WT GyrA.

DNA gyrase cleavage assay

DNA gyrase cleavage assays were performed as previously described with minor changes [57,81-82]. 10 µg/mL supercoiled DNA (pBR322, Inspiralis) was added to buffer (35 mM TrisHCl pH 7.5, 24 mM KCl, 4 mM $MgCl_2$, 2 mM DTT, 1.8 mM spermidine, 6.5% glycerol, 0.1 mg/mL albumin) with compound or vehicle. Compound concentrations were 0.01, 0.04, 0.17, 0.68, 2.7, and 10.8 µM except for DNM which was 8.9 µM for its highest concentration. DNA gyrase was added to a final concentration of 16 nM gyrA and 32 nM gyrA (giving a final concentration of A_2B_2 of 8 nM) for 25 min at 30 °C. Linear product was revealed by addition of 0.2% SDS and 0.1 µg/mL proteinase K for 30 min at 37 °C. DNA loading dye (Thermo Scientific) was added to the samples

and they were run on 1% agarose gels containing 0.5 µg/mL ethidium bromide. Gels were imaged on a Molecular Imager Gel Doc XR+ (Biorad) and bands were quantified using ImageJ[83]. Percent of type of DNA was calculated with total DNA in each lane being 100%. For time-course cleavage assays, the same protocol was followed except that the initial incubation was for varying times (0, 1, 3, 5, 10, 15, 20, 30, 60, 90, 120, and 180 min) instead of 25 min.

Human topoisomerase decatenation assay

The decatenation assay was performed with the Human Topo II Decatenation Assay Kit (Inspiralis) according to the manufacturer's instructions with minor modifications. First, a master mix was made containing 2 µL 10X assay buffer (500 mM Tris.HCl, pH 7.5, 1250 mM NaCl, 100 mM $MgCl_2$, 50 mM DTT, 1000 µg/mL albumin), 0.67 µL 30 mM ATP, 1.34 µL 0.1 ng/µL kDNA, and 14.3 µL of nuclease free water per sample is made. DMSO or 30X compound is added to a 0.5 mL eppendorf tube (0.67 µL per tube). The master mix is then added to each tube (18.3 µL per tube). Finally, 1 U of human topoisomerase (1 µL of 1 U/µL stock) is added to each tube for a final volume of 20 µL. The tubes are then incubated at 37°C for 30 min. Reactions are stopped by the addition of 20 µL of 24:1 chloroform: isoamyl alcohol and 20 µL of stop dye (40% sucrose, 1 mM EDTA, 100 mM TrisHCl pH 7.5, 0.5 µg/mL bromophenol blue). Samples were run on 1% agarose gels containing 0.5 µg/mL ethidium bromide for 1 h at 110V or until the dye front was approximately halfway down the gel. Gels were imaged on a Molecular Imager Gel Doc XR+ (Biorad).

Resistant mutant generation

Agar plates (15 cm) were prepared containing MH broth and antibacterial compounds at concentrations detailed in the Figure 3.8B-C. 40 mL of an overnight bacterial culture was centrifuged at 3000 ^{x} g for 10 min and resuspended in 0.4 mL of sterile PBS. Plates were inoculated with 100 µL of bacteria in PBS by spreading with beads. Inoculated plates were then

incubated at 37 °C for 72 h and the number of resistant colonies was counted. To determine the number of viable colonies spread onto each plate, dilutions of the overnight culture in sterile PBS were spread onto nonselective MH agar plates and plates were incubated overnight at 37 °C before counting colonies.

Pharmacokinetic assessment

The animal studies (PK, in vivo toxicity and in vivo efficacy) were carried out in strict accordance with the recommendations in the Guide for the Care and Use of Laboratory Animals of the National Institutes of Health. The protocol was approved by the Institutional Animal Care and Use Committee (IACUC) at the University of Illinois at Urbana-Champaign (Protocol Number: 13406). In these studies, 10-12 week old female C57BL/6 mice purchased from Charles River were used. DNM, DNM-2, and DNM-3 were formulated as slurries at 8.3 mg mL^{-1} in 25% Cremophor RH40/water (v/v). Before beginning the pharmacokinetic assessment, mice were first tested for their ability to tolerate the DNM, DNM-2, and DNM-3 at 50 mg kg^{-1} (p.o.). After establishing that this dose was well tolerated, mice were treated with DNM, DNM-2, or DNM-3 (all 50 mg kg^{-1}) via oral gavage with 3 mice per time point (15, 30, 60, 120, 240, and 480 min). At specified time points, mice were sacrificed and blood was collected, centrifuged, and the serum was frozen at -80 ℃ until analysis. The proteins in a 50 µL aliquot of serum were precipitated by the addition of 50 µL of acetonitrile and the sample was centrifuged to remove the proteins. Serum concentrations of DNM, DNM-2, and DNM-3 were determined by HPLC. PK parameters were determined using GraphPad Prism Version 5.00 for Windows. Other PK studies investigating DNM-2 and DNM-8 at 50 and 200 mg kg^{-1} (p.o.) were performed by the Global TB Alliance.

In vitro hemolysis assay

Hemolysis assays were performed as previously described [84]. Briefly, assays were performed using human erythrocytes within three days of receipt. One milliliter of human blood purchased

from Bioreclamation, Inc. (Hicksville, NY) was centrifuged (10 000 x g, 2 min). The pellet was washed three times with sterile saline (0.9% NaCl in water) by repeated gentle suspension and centrifugation. The pellet was resuspended in red blood cell (RBC) buffer (10 mM Na_2HPO_4, 150 mM NaCl, 1 mM $MgCl_2$, pH 7.4). To evaluate hemolytic activity of DNM and derivatives, 1 µL either 3.2 mg/mL DMSO stock (or the most concentrated stock of the compound available if not soluble at 3.2 mg/mL in DMSO) was transferred to 0.5 mL Eppendorf tubes containing 19 µL RBC buffer. Negative control tubes contained 1 µL DMSO and 19 µL RBC buffer and positive control tubes contained 1 µL DMSO and 19 µL sterile deionized water. A suspension of washed erythrocytes (10 µL) was added to each tubes and samples were incubated at 37 °C for 2h. Samples were centrifuged at 10,000 x g for 2 min and the supernatants from each sample (25 µL) were transferred to a clear, sterile 384-well plate. The absorbance of these supernatants was measured at 540 nm using a SpectraMaxPlus384 absorbance plate reader (Molecular Devices). Percent hemolysis of each sample was calculated relative to the average absorbance values measured for positive controls.

Intercalation Assay

Intercalation assays were performed as previously described [3]. The ability of DNM-2 to intercalate into DNA was measured by an ethidium bromide displacement assay. Herring Sperm DNA (34 µg/mL final) was premixed with buffer containing ethidium bromide (50 mM Tris base, 100 mM NaCl, 1 mM EDTA, 5 µM EtBr, pH =7.5). 95 µL of this solution was added to a 96 well plate containing 5 µL of DMSO solutions of compounds. In addition to vehicle controls, wells lacking either DNA or EtBr were also used to ensure that these did not have an effect on fluorescence. Doxorubicin was used as a positive control. The reactions were allowed to incubate for 30 minutes. Fluorescence was then read on a Gemini microplate reader (Molecular Devices, excitation = 545 nm, emission = 595 nm).

Ames Test

These tests were performed by Cytoprex (Watertown, MA) and the Global TB Alliance. Ten million bacteria (either S. typhimurium TA98: hisD3052, rfa, uvrB / pKM101 to detect frame-shift mutations or S. typhimurium TA100: hisG45, rfa, uvrB / pKM101 to detects base-pair substitutions) are exposed in triplicate to test agent (six concentrations), anegative control (vehicle) and a positive control (2-aminoanthracene or 2-nitrofluorene and 4-nitroquinoline N-oxide) for 90 minutes in medium containing a low concentration of histidine (sufficient for about 2 doublings.) The cultures are then diluted into indicator medium lacking histidine, and dispensed into 48 wells of a 384 well plate (micro-plate format, MPF). The plate is incubated for 48 hr at 37°C, and cells that have undergone a reversion will grow in a well, resulting in a color change in wells with growth. The number of wells showing growth are counted and compared to the vehicle control. An increase in the number of colonies of at least two-fold over baseline (mean + SD of the vehicle control) and a dose response indicates a positive response. An unpaired, one-sided Student's T-test is used to identify conditions that are significantly different from the vehicle control. Where indicated, S9 fraction from the livers of Aroclor 1254-treated rats is included in the incubation at a final concentration of 4.5%. An NADPH-regenerating system is also included to ensure a steady supply of reducing equivalents.

hERG inhibition

These tests were performed by WuXi AppTec (Shanghai) Co., Ltd. and the Global TB Alliance. Amitriptyline was used as a positive control. No further information about these tests was provided.

Micronucleus Test

These tests were performed by Cytoprex (Watertown, MA) and the Global TB Alliance. CHO-K1 cells are incubated with test compound over a 10 point concentration range in duplicate. The in vitro micronucleus test (MNT) method uses automated fluorescent cellular imaging (Thermo Scientific Cellomics ArrayScanr VTI HCS Reader) to assess cytotoxicity and quantification of micronuclei (genotoxicity). For the tests without S9 fraction, cells were incubated with compound for 24h. For tests with S9 fractions, cells were incubated with compound and S9 for 3h followed by a 21h recovery.

Mammalian Cell Killing Kinetics

HEK293 cells were plated at 10,000 cells/well in 50 µL of EMEM and allowed to attached for ~2h. To each well was added 50 µL of a 2X compound EMEM solution (final 1% DMSO) with 3 wells per compound concentration. Approximately one hour before the indicated time, 10 uL of alamar blue (i.e. 440 µM resazurin in sterile PBS) was added. The cells were then read 1 h after the indicated times. Fluorescence was read on an Analyst HT and normalized to the average untreated wells (i.e. 1% DMSO control, 0% cell death) and wells without cells (100% cell death). The data were plotted as compound concentration versus percent dead cells and fitted to a logistic-dose response curve using OriginPro. The data were generated in triplicate.

Bacterial Cell Killing Kinetics

10 mL of MH was inoculated with 100 µL of an overnight culture of NRS3. When it reached an OD = 0.16, 5 mL of this culture was added to 45 mL of MH broth. 10 mL of this culture was then added to a 50 mL vial with either DMSO or compound stock in DMSO so that the final concentrations were 0.03 µg/mL, 0.06 µg/mL, 0.12 µg/mL or 0.24 µg/mL DNM (final 0.5% DMSO). These vials were incubated at 37ºC with shaking (250 rpm). 100 µL aliquots were taken at the

indicated times, diluted, plated on non-selective MH agar, and incubated at 37ºC overnight. The next morning, the number of colonies was counted.

In vivo toxicity assessment

The protocol was approved by the Institutional Animal Care and Use Committee (IACUC) at the University of Illinois at Urbana-Champaign (Protocol Number: 14032). Six-week old male pathogen-free BALB/c mice were purchased from Taconics Biosciences (Albany, NY). All animals were housed in a pathogen free environment and received sterile food and water. Mice (n=5) were treated once daily for 10 days with 50 mg kg^{-1} DNM-2 or vehicle (25 % Cremophor RH 40 / PBS (v/v)) by oral gavage. Toxicity was assessed as previously described[85]. Specifically, heparinized whole blood was collected for assessment of total white blood cells, neutrophils, lymphocytes, hematocrit, platelets, creatinine, blood urea, nitrogen, albumin, alanine aminotransferase, alkaline phosphatase, and total bilirubin. Mice were euthanized by overdosing with Ketamine/Xylazine, and heart, lung, kidney, liver, spleen, gastrointestinal tract and brain were collected for histopathology. Tissue samples were fixed 24 hours in 10% neutral buffered formalin, processed, and paraffin embedded, sectioned (5 µm thickness) and stained with hematoxylin and eosin. All slides were systematically evaluated by a single board certified veterinary anatomic pathologist (SL) for evidence of acute or chronic inflammation and toxicity. All lesions were characterized, recorded, and scored for severity (minimal = 1, mild = 2, moderate = 3, and severe = 4).

In vivo efficacy

The protocol was approved by the Institutional Animal Care and Use Committee (IACUC) at the University of Illinois at Urbana-Champaign (Protocol Number: 14032). Six-week old male pathogen-free BALB/c mice were purchased from Harlan Sprague-Dawley (Indianapolis, IN). All animals were housed in a pathogen free environment and received sterile food and water. For

the inoculation, overnight cultures of S. aureus clinical isolate NRS3 were diluted 1:100 into fresh tryptic soy broth (TSB) and grown for 2 h at 37° C. Bacteria were washed and resuspended in sterile PBS. The mice were anesthetized with ketamine and xylazine. The mouse tails were pre-warmed in 45°C for 5 minutes before 1.2 x 10^8 CFU of S. aureus in 50 µL of PBS were injected into a tail vein using a 29-gauge needle. This number of bacteria was determined from a series of preliminary studies in which groups of mice were infected with a range of 10^6 to 10^9 CFU of S. aureus. Infected mice (15 mice per group) were then treated once daily for 10 days with 50 mg kg^{-1} DNM-2, 50 mg kg^{-1} CIP, or vehicle (25 % Cremophor RH 40 / PBS (v/v)) by oral gavage. For survival analyses a Kaplan-Meier Log Rank Survival Test was performed using OriginPro 9 (Northampton, MA).

3.13 References

(1) Naganawa, H.; Wakashiro, T.; Yagi, A.; Kondo, S.; Takita, T. Deoxynybomycin from a streptomyces. *J Antibiot (Tokyo)* **1970**, *23*, 365-368.

(2) Hiramatsu, K.; Igarashi, M.; Morimoto, Y.; Baba, T.; Umekita, M.; Akamatsu, Y. Curing bacteria of antibiotic resistance: reverse antibiotics, a novel class of antibiotics in nature. *Int J Antimicrob Agents* **2012**, *39*, 478-485.

(3) Bair, J. S.; Palchaudhuri, R.; Hergenrother, P. J. Chemistry and biology of deoxynyboquinone, a potent inducer of cancer cell death. *J Am Chem Soc* **2010**, *132*, 5469-5478.

(4) Adelmann, S.; Baldhoff, T.; Koepcke, B.; Schembecker, G. Selection of operating parameters on the basis of hydrodynamics in centrifugal partition chromatography for the purification of nybomycin derivatives. *J Chromatogr A* **2013**, *1274*, 54-64.

(5) Arai, M.; Kamiya, K.; Pruksakorn, P.; Sumii, Y.; Kotoku, N.; Joubert, J. P.; Moodley, P.; Han, C.; Shin, D.; Kobayashi, M. Anti-dormant mycobacterial activity and target analysis of nybomycin produced by a marine-derived Streptomyces sp. *Bioorg Med Chem* **2015**, *23*, 3534-3541.

(6) Pope, J. A., Jr.; Nelson, R. A.; Schaffner, C. P.; Rosen, R. T.; Pandey, R. C. Applications of thin layer chromatography, high performance liquid chromatography and mass spectrometry in the fermentation and isolation of the antibiotic nybomycin. *J Ind Microbiol* **1990**, *6*, 61-69.

(7) Parkinson, E. I.; Bair, J. S.; Nakamura, B. A.; Lee, H. Y.; Kuttab, H. I.; Southgate, E. H.; Lezmi, S.; Lau, G. W.; Hergenrother, P. J. Deoxynybomycins inhibit mutant DNA gyrase and rescue mice infected with fluoroquinolone-resistant bacteria. *Nat Commun* **2015**, *6*, 6947.

(8) Forbis, R. M.; Rinehart, K. L., Jr. Nybomycin. IV. Total synthesis of deoxynybomycin. *J Am Chem Soc* **1970**, *92*, 6995-6996.

(9) Forbis, R. M.; Rinehart, K. L., Jr. Nybomycin. VII. Preparative routes to nybomycin and deoxynybomycin. *J Am Chem Soc* **1973**, *95*, 5003-5013.

(10) Li, S.; Tian, X.; Niu, S.; Zhang, W.; Chen, Y.; Zhang, H.; Yang, X.; Li, W.; Zhang, S.; Ju, J.; Zhang, C. Pseudonocardians A-C, new diazaanthraquinone derivatives from a deap-sea actinomycete Pseudonocardia sp. SCSIO 01299. *Mar Drugs* **2011**, *9*, 1428-1439.

(11) Parkinson, E. I.; Bair, J. S.; Cismesia, M.; Hergenrother, P. J. Efficient NQO1 substrates are potent and selective anticancer agents. *ACS Chem Biol* **2013**, *8*, 2173-2183.

(12) Forbis, R. M.; Rinehart, K. L. Nybomycin .4. Total Synthesis of Deoxynybomycin. *J. Am. Chem. Soc.* **1970**, *92*, 6995-&.

(13) Forbis, R. M.; Rinehart, K. L. Nybomycin .7. Preparative Routes to Nybomycin and Deoxynybomycin. *J. Am. Chem. Soc.* **1973**, *95*, 5003-5013.

(14) Angibaud, P.; Bourdrez, X.; Devine, A.; End, D. W.; Freyne, E.; Ligny, Y.; Muller, P.; Mannens, G.; Pilatte, I.; Poncelet, V.; Skrzat, S.; Smets, G.; Van Dun, J.; Van Remoortere, P.; Venet, M.; Wouters, W. 5-imidazolyl-quinolinones, -quinazolinones and -benzo-azepinones as farnesyltransferase inhibitors. *Bioorg Med Chem Lett* **2003**, *13*, 1543-1547.

(15) Wikler, M. A.; Cockerill III, F. R.; Craig, W. A.; Dudley, M. N.; Eliopoulos, G. M.; Hecht, D. W.; Hindler, J. F.; Low, D. E.; Sheehan, D. J.; Tenover, F. C.; Turnidge, J. D.; Weinstein, M. P.; Zimmer, B. L. *Methods for dilution antimicrobial susceptibility tests for bacteria that grow aerobically; approved standard*; 7 ed.; Clinical and Laboratory Standards Institute: Waye, PA, 2006; Vol. 26.

(16) Lolis, E.; Bucala, R. Therapeutic approaches to innate immunity: severe sepsis and septic shock. *Nat Rev Drug Discov* **2003**, *2*, 635-645.

(17) CDC: Atlanta, GA, 2013.

(18) Courvalin, P. Vancomycin resistance in gram-positive cocci. *Clin Infect Dis* **2006**, *42 Suppl 1*, S25-34.

(19) Marshall, C. G.; Broadhead, G.; Leskiw, B. K.; Wright, G. D. D-Ala-D-Ala ligases from glycopeptide antibiotic-producing organisms are highly homologous to the enterococcal vancomycin-resistance ligases VanA and VanB. *Proc Natl Acad Sci U S A* **1997**, *94*, 6480-6483.

(20) Gaupp, R.; Lei, S.; Reed, J. M.; Peisker, H.; Boyle-Vavra, S.; Bayer, A. S.; Bischoff, M.; Herrmann, M.; Daum, R. S.; Powers, R.; Somerville, G. A. Staphylococcus aureus Metabolic Adaptations during the Transition from a Daptomycin Susceptibility Phenotype to a Daptomycin Nonsusceptibility Phenotype. *Antimicrob Agents Chemother* **2015**, *59*, 4226-4238.

(21) Wilson, D. N. Ribosome-targeting antibiotics and mechanisms of bacterial resistance. *Nat Rev Microbiol* **2014**, *12*, 35-48.

(22) Billal, D. S.; Feng, J.; Leprohon, P.; Legare, D.; Ouellette, M. Whole genome analysis of linezolid resistance in Streptococcus pneumoniae reveals resistance and compensatory mutations. *BMC Genomics* **2011**, *12*, 512.

(23) Talbot, G. H.; Bradley, J.; Edwards, J. E., Jr.; Gilbert, D.; Scheld, M.; Bartlett, J. G. Bad bugs need drugs: an update on the development pipeline from the Antimicrobial Availability Task Force of the Infectious Diseases Society of America. *Clin Infect Dis* **2006**, *42*, 657-668.

(24) Koksal, F.; Yasar, H.; Samasti, M. Antibiotic resistance patterns of coagulase-negative staphylococcus strains isolated from blood cultures of septicemic patients in Turkey. *Microbiol Res* **2009**, *164*, 404-410.

(25) May, L.; Klein, E. Y.; Rothman, R. E.; Laxminarayan, R. Trends in antibiotic resistance in coagulase-negative staphylococci in the United States, 1999 to 2012. *Antimicrob Agents Chemother* **2014**, *58*, 1404-1409.

(26) Kern, A.; Perreten, V. Clinical and molecular features of methicillin-resistant, coagulase-negative staphylococci of pets and horses. *J Antimicrob Chemother* **2013**, *68*, 1256-1266.

(27) Dubin, D. T.; Fitzgibbon, J. E.; Nahvi, M. D.; John, J. F. Topoisomerase sequences of coagulase-negative staphylococcal isolates resistant to ciprofloxacin or trovafloxacin. *Antimicrob Agents Chemother* **1999**, *43*, 1631-1637.

(28) Bispo, P. J.; Alfonso, E. C.; Flynn, H. W.; Miller, D. Emerging 8-methoxyfluoroquinolone resistance among methicillin-susceptible Staphylococcus epidermidis isolates recovered from patients with endophthalmitis. *J Clin Microbiol* **2013**, *51*, 2959-2963.

(29) Sreedharan, S.; Peterson, L. R.; Fisher, L. M. Ciprofloxacin resistance in coagulase-positive and -negative staphylococci: role of mutations at serine 84 in the DNA gyrase A protein of Staphylococcus aureus and Staphylococcus epidermidis. *Antimicrob Agents Chemother* **1991**, *35*, 2151-2154.

(30) Price, L. B.; Vogler, A.; Pearson, T.; Busch, J. D.; Schupp, J. M.; Keim, P. In vitro selection and characterization of Bacillus anthracis mutants with high-level resistance to ciprofloxacin. *Antimicrob Agents Chemother* **2003**, *47*, 2362-2365.

(31) Lupien, A.; Billal, D. S.; Fani, F.; Soualhine, H.; Zhanel, G. G.; Leprohon, P.; Ouellette, M. Genomic characterization of ciprofloxacin resistance in a laboratory-derived mutant and a clinical isolate of Streptococcus pneumoniae. *Antimicrob Agents Chemother* **2013**, *57*, 4911-4919.

(32) Mandell, L. A.; Wunderink, R. G.; Anzueto, A.; Bartlett, J. G.; Campbell, G. D.; Dean, N. C.; Dowell, S. F.; File, T. M., Jr.; Musher, D. M.; Niederman, M. S.; Torres, A.; Whitney, C. G. Infectious Diseases Society of America/American Thoracic Society consensus guidelines on the management of community-acquired pneumonia in adults. *Clin Infect Dis* **2007**, *44 Suppl 2*, S27-72.

(33) Domenech, A.; Tirado-Velez, J. M.; Fenoll, A.; Ardanuy, C.; Yuste, J.; Linares, J.; de la Campa, A. G. Fluoroquinolone-resistant pneumococci: dynamics of serotypes and clones in Spain in 2012 compared with those from 2002 and 2006. *Antimicrob Agents Chemother* **2014**, *58*, 2393-2399.

(34) Bast, D. J.; Low, D. E.; Duncan, C. L.; Kilburn, L.; Mandell, L. A.; Davidson, R. J.; de Azavedo, J. C. Fluoroquinolone resistance in clinical isolates of Streptococcus pneumoniae: contributions of type II topoisomerase mutations and efflux to levels of resistance. *Antimicrob Agents Chemother* **2000**, *44*, 3049-3054.

(35) Pan, X. S.; Ambler, J.; Mehtar, S.; Fisher, L. M. Involvement of topoisomerase IV and DNA gyrase as ciprofloxacin targets in Streptococcus pneumoniae. *Antimicrob Agents Chemother* **1996**, *40*, 2321-2326.

(36) Erridge, C.; Bennett-Guerrero, E.; Poxton, I. R. Structure and function of lipopolysaccharides. *Microbes Infect* **2002**, *4*, 837-851.

(37) Sarathy, J. P.; Dartois, V.; Lee, E. J. The role of transport mechanisms in mycobacterium tuberculosis drug resistance and tolerance. *Pharmaceuticals (Basel)* **2012**, *5*, 1210-1235.

(38) *Neisseria: Molecular Mechanisms of Pathogenesis*; Genco, C.; Wetzler, L., Eds.; CAISTER ACADEMIC PRESS: Norfolk, England, 2010, pp 1-270.

(39) Dean, A.; Dias, H. M.; Falzon, D.; Floyd, K.; Raviglione, M.; Weil, D.; Weyer, K.; Zignol, M. "Drug-Resistant TB: Surveillance and Response," World Health Organization, 2014.

(40) Collins, L.; Franzblau, S. G. Microplate alamar blue assay versus BACTEC 460 system for high-throughput screening of compounds against Mycobacterium tuberculosis and Mycobacterium avium. *Antimicrob Agents Chemother* **1997**, *41*, 1004-1009.

(41) Cho, S. H.; Warit, S.; Wan, B.; Hwang, C. H.; Pauli, G. F.; Franzblau, S. G. Low-oxygen-recovery assay for high-throughput screening of compounds against nonreplicating Mycobacterium tuberculosis. *Antimicrob Agents Chemother* **2007**, *51*, 1380-1385.

(42) Li, J.; Gao, X.; Luo, T.; Wu, J.; Sun, G.; Liu, Q.; Jiang, Y.; Zhang, Y.; Mei, J.; Gao, Q. Association of gyrA/B mutations and resistance levels to fluoroquinolones in clinical isolates of Mycobacterium tuberculosis. *Emerg Microbes Infect* **2014**, *3*, e19.

(43) Avalos, E.; Catanzaro, D.; Catanzaro, A.; Ganiats, T.; Brodine, S.; Alcaraz, J.; Rodwell, T. Frequency and geographic distribution of gyrA and gyrB mutations associated with fluoroquinolone resistance in clinical Mycobacterium tuberculosis isolates: a systematic review. *PLoS One* **2015**, *10*, e0120470.

(44) Morris, S. L.; Rouse, D. A. The genetics of multiple drug resistance in Mycobacterium tuberculosis and the Mycobacterium avium complex. *Res Microbiol* **1996**, *147*, 68-73.

(45) Brennan, P. J.; Nikaido, H. The envelope of mycobacteria. *Annu Rev Biochem* **1995**, *64*, 29-63.

(46) Update to CDC's sexually transmitted diseases treatment guidelines, 2006: fluoroquinolones no longer recommended for treatment of gonococcal infections. *MMWR Morb Mortal Wkly Rep* **2007**, *56*, 332-336.

(47) Tanaka, M.; Nakayama, H.; Haraoka, M.; Saika, T. Antimicrobial resistance of Neisseria gonorrhoeae and high prevalence of ciprofloxacin-resistant isolates in Japan, 1993 to 1998. *J Clin Microbiol* **2000**, *38*, 521-525.

(48) Vernel-Pauillac, F.; Hogan, T. R.; Tapsall, J. W.; Goarant, C. Quinolone resistance in Neisseria gonorrhoeae: rapid genotyping of quinolone resistance-determining regions in gyrA and parC genes by melting curve analysis predicts susceptibility. *Antimicrob Agents Chemother* **2009**, *53*, 1264-1267.

(49) Brown, D. G.; May-Dracka, T. L.; Gagnon, M. M.; Tommasi, R. Trends and exceptions of physical properties on antibacterial activity for Gram-positive and Gram-negative pathogens. *J Med Chem* **2014**, *57*, 10144-10161.

(50) *Basic & Clinical Pharmacology, 13th Edition*; 13 ed.; Katzung, B.; Trevor, A., Eds.; McGraw-Hill Education, 2015.

(51) Schindler, M.; Osborn, M. J. Interaction of divalent cations and polymyxin B with lipopolysaccharide. *Biochemistry* **1979**, *18*, 4425-4430.

(52) Lim, L. M.; Ly, N.; Anderson, D.; Yang, J. C.; Macander, L.; Jarkowski, A., 3rd; Forrest, A.; Bulitta, J. B.; Tsuji, B. T. Resurgence of colistin: a review of resistance, toxicity, pharmacodynamics, and dosing. *Pharmacotherapy* **2010**, *30*, 1279-1291.

(53) Vidaillac, C.; Benichou, L.; Duval, R. E. In vitro synergy of colistin combinations against colistin-resistant Acinetobacter baumannii, Pseudomonas aeruginosa, and Klebsiella pneumoniae isolates. *Antimicrob Agents Chemother* **2012**, *56*, 4856-4861.

(54) Gordon, N. C.; Png, K.; Wareham, D. W. Potent synergy and sustained bactericidal activity of a vancomycin-colistin combination versus multidrug-resistant strains of Acinetobacter baumannii. *Antimicrob Agents Chemother* **2010**, *54*, 5316-5322.

(55) Bratu, S.; Landman, D.; Martin, D. A.; Georgescu, C.; Quale, J. Correlation of antimicrobial resistance with beta-lactamases, the OmpA-like porin, and efflux pumps in clinical isolates of Acinetobacter baumannii endemic to New York City. *Antimicrob Agents Chemother* **2008**, *52*, 2999-3005.

(56) Yeh, P. J.; Hegreness, M. J.; Aiden, A. P.; Kishony, R. Drug interactions and the evolution of antibiotic resistance. *Nat Rev Microbiol* **2009**, *7*, 460-466.

(57) Kampranis, S. C.; Maxwell, A. The DNA gyrase-quinolone complex. ATP hydrolysis and the mechanism of DNA cleavage. *J Biol Chem* **1998**, *273*, 22615-22626.

(58) Bax, B. D.; Chan, P. F.; Eggleston, D. S.; Fosberry, A.; Gentry, D. R.; Gorrec, F.; Giordano, I.; Hann, M. M.; Hennessy, A.; Hibbs, M.; Huang, J.; Jones, E.; Jones, J.; Brown, K. K.; Lewis, C. J.; May, E. W.; Saunders, M. R.; Singh, O.; Spitzfaden, C. E.; Shen, C.; Shillings, A.; Theobald, A. J.; Wohlkonig, A.; Pearson, N. D.; Gwynn, M. N. Type IIA topoisomerase inhibition by a new class of antibacterial agents. *Nature* **2010**, *466*, 935-940.

(59) Egawa, K.; Yamori, T.; Nosaka, C.; Kunimoto, S.; Takeuchi, T.; Nos, K. Deoxynybomycin is a selective anti-tumor agent inducing apoptosis and inhibiting topoisomerase I. *Biol Pharm Bull* **2000**, *23*, 1036-1040.

(60) Ferrero, L.; Cameron, B.; Crouzet, J. Analysis of gyrA and grlA mutations in stepwise-selected ciprofloxacin-resistant mutants of Staphylococcus aureus. *Antimicrob Agents Chemother* **1995**, *39*, 1554-1558.

(61) Hori, S.; Ohshita, Y.; Utsui, Y.; Hiramatsu, K. Sequential acquisition of norfloxacin and ofloxacin resistance by methicillin-resistant and -susceptible Staphylococcus aureus. *Antimicrob Agents Chemother* **1993**, *37*, 2278-2284.

(62) Kwak, Y. G.; Truong-Bolduc, Q. C.; Bin Kim, H.; Song, K. H.; Kim, E. S.; Hooper, D. C. Association of norB overexpression and fluoroquinolone resistance in clinical isolates of Staphylococcus aureus from Korea. *J Antimicrob Chemother* **2013**, *68*, 2766-2772.

(63) Costa, S. S.; Falcao, C.; Viveiros, M.; Machado, D.; Martins, M.; Melo-Cristino, J.; Amaral, L.; Couto, I. Exploring the contribution of efflux on the resistance to fluoroquinolones in clinical isolates of Staphylococcus aureus. *BMC Microbiol* **2011**, *11*, 241.

(64) Brock, T. D.; Sokolski, W. T. Biological studies on the antibiotic, nybomycin. *Antibiot Chemother (Northfield Ill)* **1958**, *8*, 631-636.

(65) Wise, R.; Honeybourne, D. Pharmacokinetics and pharmacodynamics of fluoroquinolones in the respiratory tract. *Eur Respir J* **1999**, *14*, 221-229.

(66) Rodvold, K. A.; Neuhauser, M. Pharmacokinetics and pharmacodynamics of fluoroquinolones. *Pharmacotherapy* **2001**, *21*, 233S-252S.

(67) Egawa K, Y. T., Nosaka C, Kunimoto S, Takeuchi T, Nos K. Deoxynybomycin is a selective anti-tumor agent inducing apoptosis and inhibiting topoisomerase I. *Biological & Pharmaceutical Bulletin* **2000**, *23*, 1036-1040.

(68) Schnell, M. A.; Hardy, C.; Hawley, M.; Propert, K. J.; Wilson, J. M. Effect of blood collection technique in mice on clinical pathology parameters. *Hum Gene Ther* **2002**, *13*, 155-161.

(69) O'Shea, R.; Moser, H. E. Physicochemical properties of antibacterial compounds: implications for drug discovery. *J Med Chem* **2008**, *51*, 2871-2878.

(70) Bazile, S.; Moreau, N.; Bouzard, D.; Essiz, M. Relationships among antibacterial activity, inhibition of DNA gyrase, and intracellular accumulation of 11 fluoroquinolones. *Antimicrob Agents Chemother* **1992**, *36*, 2622-2627.

(71) Skold, O. Sulfonamide resistance: mechanisms and trends. *Drug Resist Updat* **2000**, *3*, 155-160.

(72) Antunes, P.; Machado, J.; Sousa, J. C.; Peixe, L. Dissemination of sulfonamide resistance genes (sul1, sul2, and sul3) in Portuguese Salmonella enterica strains and relation with integrons. *Antimicrob Agents Chemother* **2005**, *49*, 836-839.

(73) Olivieri, R.; Morandi, M.; Zanchi, A.; Tordini, G.; Pozzi, G.; De Luca, A.; Montagnani, F. Evolution of macrolide resistance in Streptococcus pyogenes over 14-years in an area of central Italy. *J Med Microbiol* **2015**.

(74) Tewhey, R.; Gu, B.; Kelesidis, T.; Charlton, C.; Bobenchik, A.; Hindler, J.; Schork, N. J.; Humphries, R. M. Mechanisms of linezolid resistance among coagulase-negative staphylococci determined by whole-genome sequencing. *MBio* **2014**, *5*, e00894-00814.

(75) Gabriel, E. M.; Fitzgibbon, S.; Clair, J.; Coffey, A.; O'Mahony, J. M. Characterisation of clinical meticillin-resistant Staphylococcus epidermidis demonstrating high levels of linezolid resistance (>256 mug/ml) resulting from transmissible and mutational mechanisms. *J Infect Chemother* **2015**, *21*, 547-549.

(76) Kahne, D.; Leimkuhler, C.; Lu, W.; Walsh, C. Glycopeptide and lipoglycopeptide antibiotics. *Chem Rev* **2005**, *105*, 425-448.

(77) Floss, H. G.; Yu, T. W. Rifamycin-mode of action, resistance, and biosynthesis. *Chem Rev* **2005**, *105*, 621-632.

(78) Moritz, E. M.; Hergenrother, P. J. Toxin-antitoxin systems are ubiquitous and plasmid-encoded in vancomycin-resistant enterococci. *Proc Natl Acad Sci U S A* **2007**, *104*, 311-316.

(79) In *Gonorrhea Laboratory Information*; Centers for Disease Control and Prevention: Atlanta, GA, 2013; Vol. 2015.

(80) Tran, J. H.; Jacoby, G. A.; Hooper, D. C. Interaction of the plasmid-encoded quinolone resistance protein Qnr with Escherichia coli DNA gyrase. *Antimicrob Agents Chemother* **2005**, *49*, 118-125.

(81) Fisher, L. M.; Pan, X. S. Methods to assay inhibitors of DNA gyrase and topoisomerase IV activities. *Methods Mol Med* **2008**, *142*, 11-23.

(82) Barnard, F. M.; Maxwell, A. Interaction between DNA gyrase and quinolones: effects of alanine mutations at GyrA subunit residues Ser(83) and Asp(87). *Antimicrob Agents Chemother* **2001**, *45*, 1994-2000.

(83) Schneider, C. A.; Rasband, W. S.; Eliceiri, K. W. NIH Image to ImageJ: 25 years of image analysis. *Nat Methods* **2012**, *9*, 671-675.

(84) Eibergen, N. R.; Im, I.; Patel, N. Y.; Hergenrother, P. J. Identification of a novel protein synthesis inhibitor active against gram-positive bacteria. *Chembiochem* **2012**, *13*, 574-583, 490.

(85) Botham, R. C.; Fan, T. M.; Im, I.; Borst, L. B.; Dirikolu, L.; Hergenrother, P. J. Dual small-molecule targeting of procaspase-3 dramatically enhances zymogen activation and anticancer activity. *J Am Chem Soc* **2014**, *136*, 1312-1319.

Chapter 4. Phenotype-based screening for discovery of novel anticancer agents and determination of the mode of action of an actinophyllic acid analogue ersindole

Portions of this Chapter are reprinted with permission from Granger, B. A.; Jewett, I, T.; Butler, J. D.; Hua, B.; Knezevic, C. E.; Parkinson, E. I.; Hergenrother, P. J.; Martin, S. F. "Synthesis of (±)-Actinophyllic Acid and Analogs: Applications of Cascade Reactions and Diverted Total Synthesis" *J. Am. Chem. Soc.* **2013,** *135*, 12984-12986.[1] and Knezevic, C. E.; Parkinson, E. I.; Lee, H. Y.; Granger, B. A.; Hua, B.; Sahn, J. J.; Martin, S. F.; Hergenrother, P. J. "Examination of High Hill Slope and E_{max} Values as Anticancer Parameters Utilizing Diverted Intermediates of Actinophyllic Acid" *Angew. Chem*. Submitted **2015**.

4.1 High-throughput phenotypic screening

Screening of natural products and natural product-like compounds for cytotoxicity toward cancer cells has consistently led to the discovery of promising antitumor agents.[2-3] Cell viability is one of the most commonly used phenotypic screens and has been used to discover many potential anticancer compounds.[3]

4.1.1 Screening of the *ent*-kauranoids from the Reisman laboratory

The *ent*-kauranoids are a class of diterpenoids isolated from plants of the *Isodon* genus.[4] Many of the *ent*-kauranoids have bioactivity, including antibacterial, anti-inflammatory, and anticancer properties.[4-5] Recently, Prof. Reisman and coworkers developed novel syntheses of many of these *ent*-kauranoids, including (-)-maoecrystal Z,[5] (-)-trichorabdal A,[4] and (-)-longikaurin E[4] (See Figure 4.1A). After these syntheses were completed, the compounds and several synthetic intermediates (Figure 4.1B) were evaluated in biological assays at UIUC.

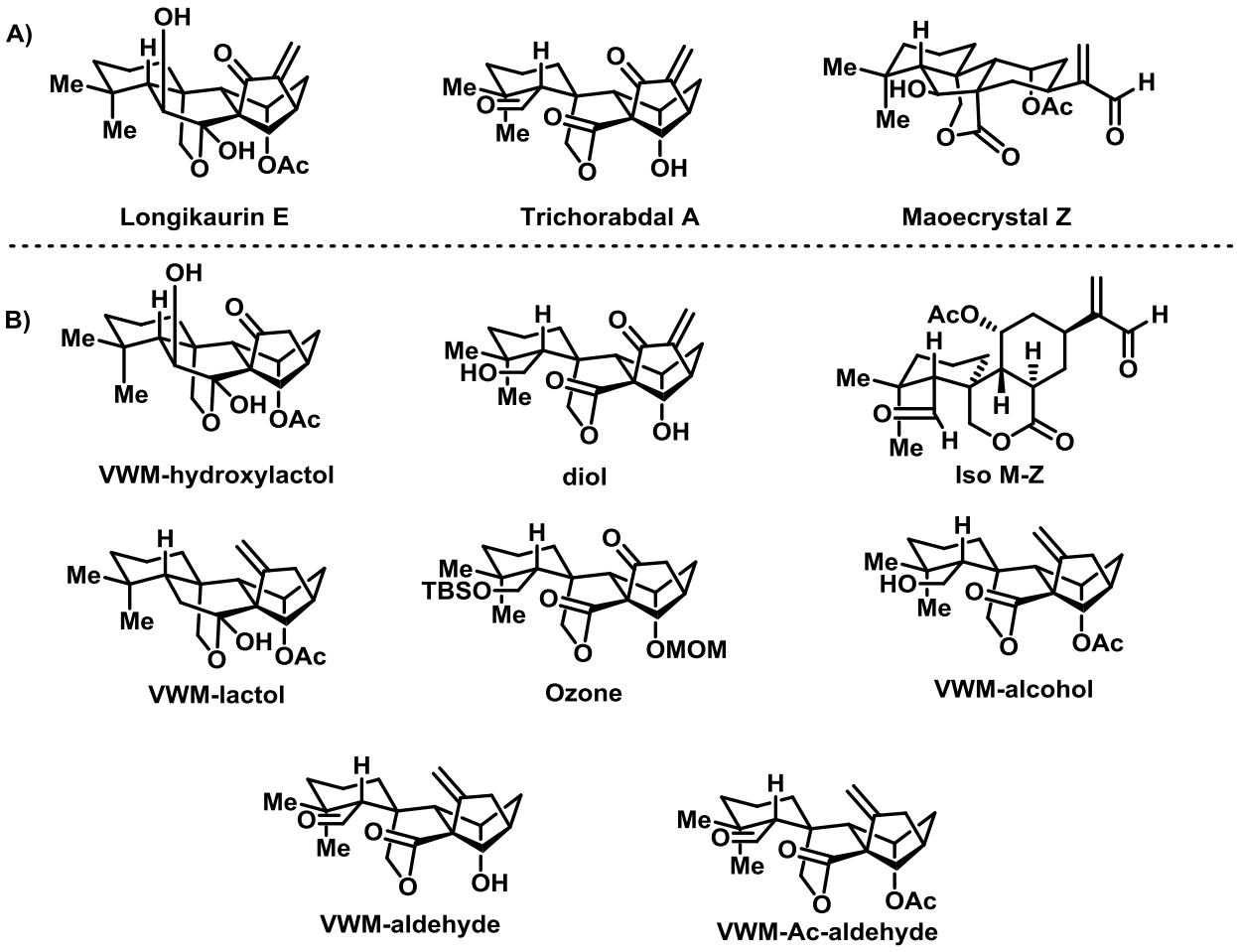

Figure 4.1. (**A**) Structures of *ent*-kauranoids synthesized by the Reisman laboratory. (**B**) Structures of synthetic intermediates to *ent*-kauranoids.

Initial screening of the natural products along with intermediates to these natural products was performed in U937 (human lymphoma), A549 (human lung cancer), and HeLa (human cervical cancer) cell lines. Initial screening was performed at 10 μM for 72 h in 384 well plates, and cell viability was determined by the Alamar Blue assay. Of the compounds, longikaurin E, diol, maoecrystal Z, iso M-Z, trichorabdal A, and ozone all were active (≥ 70% cell death at 10 μM) in at least one cell line. These compounds were further examined for their ability to induce dose-dependent cell death over 72 h. Longikaurin E was the most potent compound across the

three cell lines tested (IC_{50} < 4 μM, Table 4.1) with diol, maoecrystal Z, and iso M-Z also showing promising activity (Average IC_{50} for 3 cell lines ≤ 10 μM).

Table 4.1. Anticancer and hemolytic activity of *ent*-kauranoids and their intermediates

Compound	U937 IC_{50} (μM)	HeLa IC_{50} (μM)	A549 IC_{50} (μM)	% Hemolysis at 330 μM
Longikaurin E	2.0 ± 0.1	3.8 ± 0.9	3.2 ± 0.9	-3 ± 1
diol	7 ± 2	10 ± 2	9.8 ± 0.5	-1 ± 1
Maoecrystal Z	8 ± 5	16 ± 4	6 ± 2	-2.8 ± 0.3
Iso M-Z	8 ± 1	11 ± 4	6.7 ± 0.7	-2.9 ± 0.6
Trichorabdal A	20 ± 10	23 ± 10	17 ± 7	-5 ± 2
Ozone	22 ± 7	30 ± 1	14 ± 3	6 ± 3
VWM-aldehyde	>100	>100	>100	-2.8 ± 0.8
VWM-Ac-aldehyde	>100	>100	>100	-2.6 ± 0.8
VWM-alcohol	>100	>100	>100	5 ± 3
VWM-lactol	>100	>100	>100	-2 ± 1
VWM-hydroxylactol	>100	>100	>100	-1.5 ± 0.5
Doxorubicin	0.06 ± 0.02	0.05 ± 0.03	0.04 ± 0.02	ND

Screening was performed with compounds at 10 μM for 72 h. U937 cells were plated at 5000 cells/well in 384 well plates. A549 and HeLa cells were plated at 1000 cells/well in 384 well plates. Cell viability determined by the Alamar Blue assay with 100 μM doxorubicin as the 100% Dead and 1% DMSO as the 100% Alive. % Hemolysis was determined by adding 1 μL of a 10 mM DMSO stock to a 0.5 mL tube. To each tube was added 19 μL of red blood cell buffer and 10 μL of resuspended erythrocytes, which had previously been washed and resuspended in red blood cell buffer. They were incubated for 2h at 37°C. Samples were centrifuged and the absorbance of the supernatant at 540 nm was determined. DMSO alone with red blood cell buffer was the negative (0% Hemolysis) control and DMSO in water was the positive (100% hemolysis) control.

Trichorabdal A and ozone were less active (Average IC_{50} for 3 cell lines ≥ 20 μM), while the other compounds induced minimal cell death at concentrations up to 100 μM. The fact that longikaurin E shows potent activity but VWM-hydroxylactol does not strongly suggests that the α,β-unsaturated ketone is necessary for activity. A similar α,β-unsaturated ketone is also found in the highly active ent-kauranoids (diol, maoecrystal Z, iso M-Z) but not in the inactive compounds

(IC_{50} > 100 μM). This further supports the necessity of the α,β-unsaturated ketone for biological activity. However, the difference in potency observed between longikaurin E and trichorabdal A suggests that the anticancer activity of these compounds is not simply dependent upon having an α,β-unsaturated ketone. Instead, it is likely that the surrounding structure has an effect on activity as well.

The α,β-unsaturated ketone (i.e. the Michael acceptor) is typically avoided in drug discovery due to its high reactivity; it has even been marked as a subset of the PAINS (Pan Assay Interference Compounds), which are active in a variety of high-throughput screens.[6] However, others have demonstrated that the reactivity of this functional group can be modulated by the identity of the rest of the molecule.[7] Thus, it is possible for compounds containing the α,β-unsaturated ketone motif to advance to the clinic.[7] In fact, there are already many FDA-approved drugs that have an α,β-unsaturated ketone as their active moiety, including ethacrynic acid[7-8] and bardoxolone-methyl/RTA402[9-11](Figure 4.2). Therefore, this functional group alone does not preclude further investigations into these compounds.

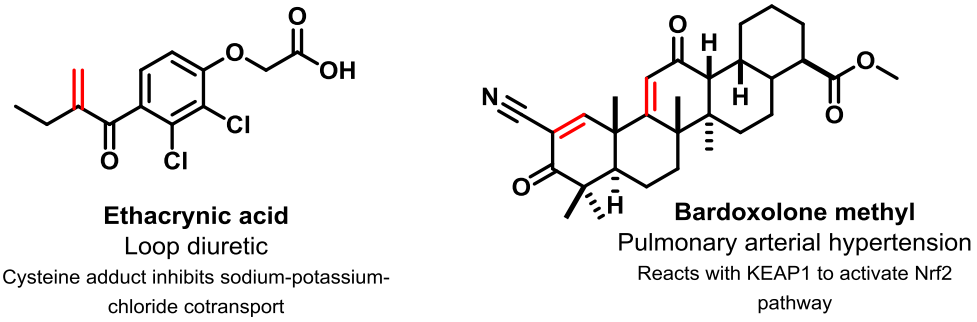

Figure 4.2. Structures of FDA approved drugs which have mechanisms of action dependent on their α,β-unsaturated ketones. Red indicates the α,β-unsaturated ketone which reacts to give the compound its activity.

In order to advance these anticancer compounds, they must not show high toxicity to normal cells. For this reason, we next investigated the effect of these compounds on red blood cells (RBCs). None of the compounds induced hemolysis of RBCs, suggesting that they may have a tolerable toxicity profile (Table 4.1). Future directions for these compounds include further

investigations into the toxicity to normal cells in culture, tolerability in mice, and mechanism of action.

4.1.2 Screening of the epipolythiodiketopiperazine compounds from the Movassaghi laboratory

The epipolythidiketopiperzines (ETPs) are a class of alkaloids produced by variety of filamentous fungi including *Chaetomium*, *Leptosphaeria*, *Aspergillus*, *Verticillium*, *Penicillium*, and *Pithomyces* genera.[12] Many of the ETPs have been found to have biological activity, including antibacterial, anticancer, antiviral, antiparasitic, antifungal, antimalarial, immunosuppressive, immunomodulatory, phytotoxic, nematicidal, antiplatelet, and anti-inflammatory effects.[12]

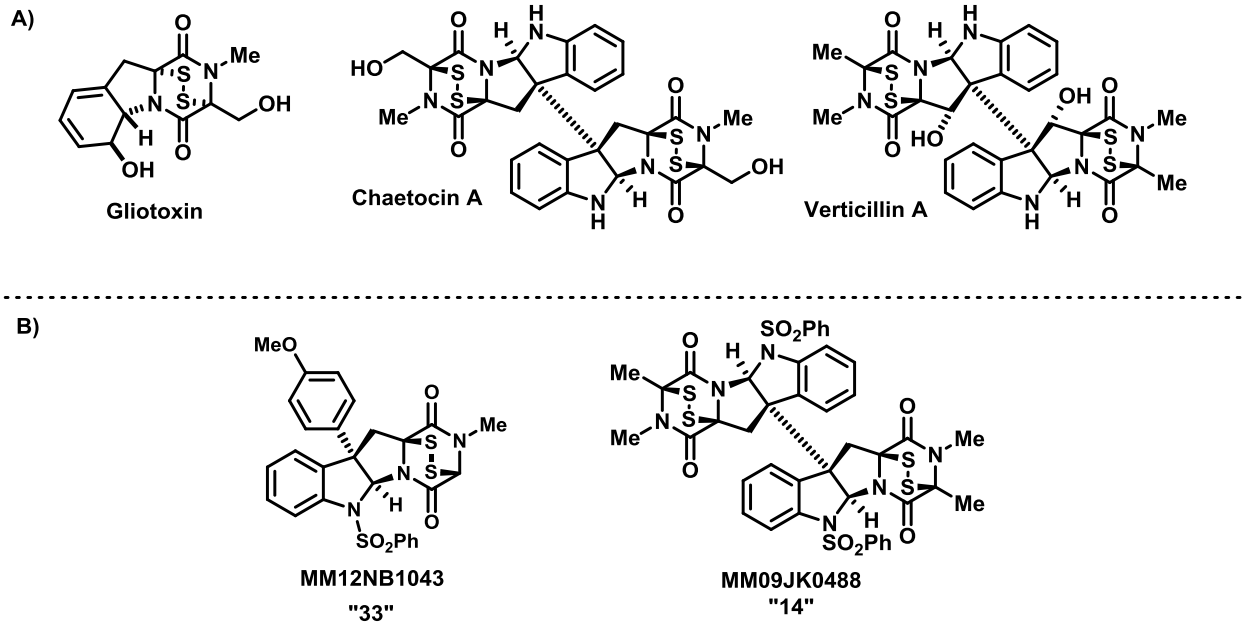

Figure 4.3 (**A**) Structure of natural product ETPs. (**B**) ETPs that were found to have excellent activity against cancer cells in culture.[12]

Recently, Prof. Movassaghi and his laboratory developed syntheses for many of the ETPs including chaetocin A and verticillin A (Figure 4.3A).[12] Additionally, they synthesized a collection of structurally-related ETPs that were evaluated in cell culture by Dr. Karen Morrison. Two compounds (compound 33 and 14, Figure 4.3B) showed high potency against cell lines derived from a variety of tumor types, including lymphoma, breast cancer, and lung cancer.[12] Further

analysis revealed that these compounds induce apoptotic cell death and do not result in hemolysis.[12] With these promising results, the Movassaghi laboratory synthesized more compounds (Figure 4.4) which were analyzed for bioactivity.

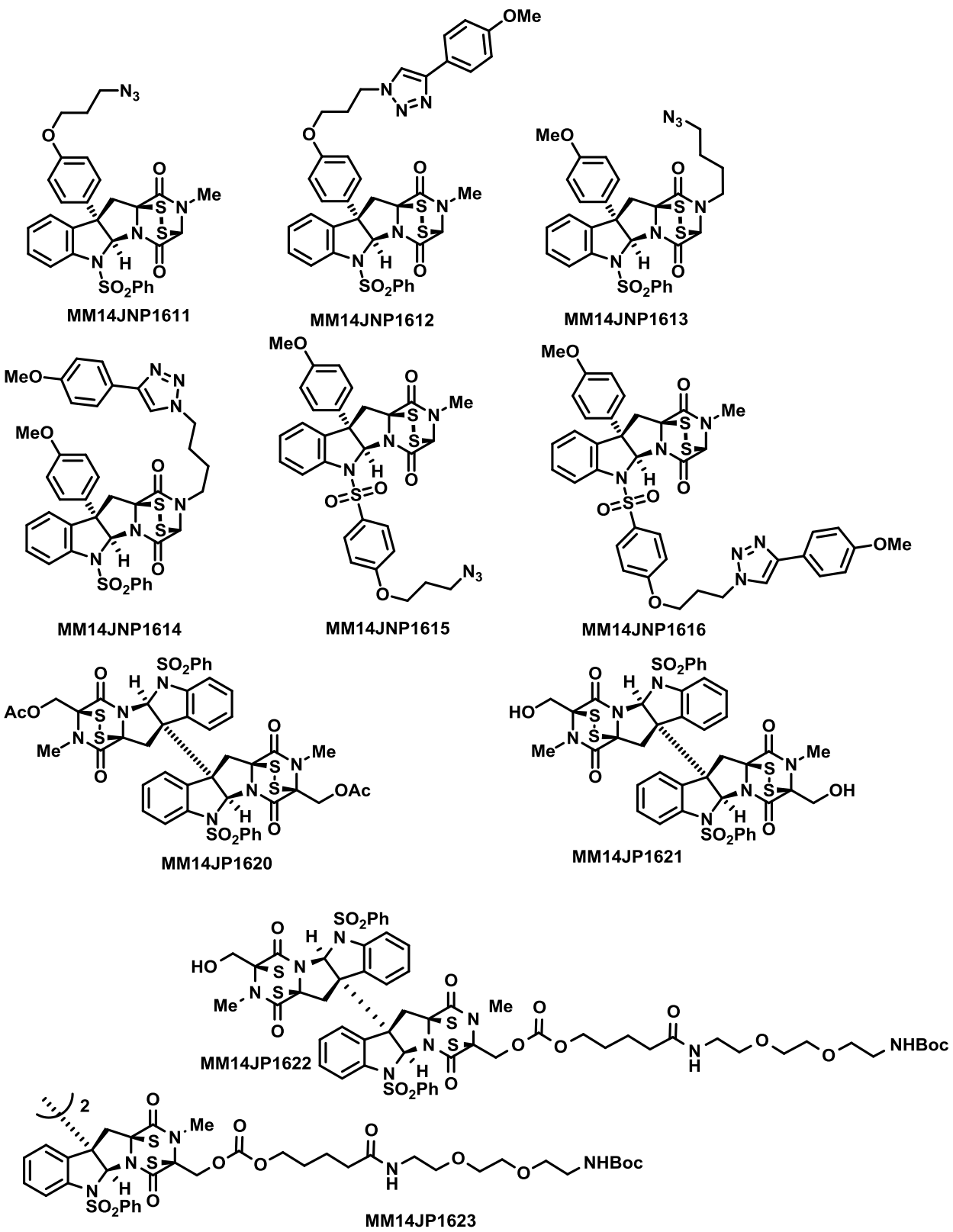

Figure 4.4. New ETPs for testing

The new compounds were tested for anticancer activity against H460 (human lung cancer), MCF7 (human breast cancer), and U937 (human lymphoma) cells. Testing was performed as previously reported.[12] All of the monomeric compounds were active, but not as active as compound 33 (Table 4.2), and none of the monomeric compounds induced hemolysis. Compound 33 is most likely the best lead compound in the monomeric series. However, some of these derivatives (e.g. 1611, 1613, and 1615) may be useful in target identification studies, given their activity and the presence of the azide, which could be used in bioorthogonal reactions for pull down or visualization purposes.

Table 4.2. Anticancer and hemolytic activity of the ETPs

Compound	monomer or dimer	H460 IC_{50} (nM)	MCF7 IC_{50} (nM)	U937 IC_{50} (nM)	% Hemolysis at 100 μM
1611	monomer	118*	129*	90 ± 10	-4 ± 3
1612	monomer	146*	109*	80 ± 10	-5 ± 3
1613	monomer	120*	135*	140 ± 20	-3 ± 2
1614	monomer	208*	103*	77 ± 9	-5 ± 3
1615	monomer	172*	186*	160 ± 40	-6 ± 3
1616	monomer	209*	130*	70 ± 20	-6 ± 3
33	monomer	45*	47*	68 ± 6	ND
1620	dimer	96*	341*	180 ± 60	ND
1621	dimer	7.6*	18*	17 ± 3	ND
1622	dimer	318*	357*	500 ± 100	ND
1623	dimer	>1000*	>1000*	>1000	ND
14	dimer	4.1*	4.6*	7 ± 1	ND

Cells were plated at 2000 cells/well (H460 and MCF7) or 5000 cells/well (U937) in 96 well plate for 72 h. Viability was assessed by SRB as previously described.[12] *Only 2 replicates. % Hemolysis was determined by adding 1 μL of a 3 mM DMSO stock to an 0.5 mL tube. To each tube was added 19 μL of red blood cell buffer and 10 μL of resuspended erythrocytes which had previously been washed and resuspended in red blood cell buffer. They were incubated for 2h at 37°C. Samples were centrifuged and the absorbance of the supernatant at 540 nm was determined. DMSO alone with red blood cell buffer was the negative (0% Hemolysis) control and DMSO in water was the positive (100% hemolysis) control.

Similar to the monomers, many of the new dimers also show potent activity. Compounds 1622 and 1623, both of which have long PEG linkers, were significantly less active. Compound

1621 is nearly as potent as compound 14; however, compound 14 remains the most potent of the compounds tested and remains the best candidate for *in vivo* evaluation.

4.1.3 Screening for compounds with potent activity against breast cancer cell lines

As described in Chapter 2.3.1, breast cancer is the most commonly diagnosed cancer in women, with 231,840 estimated new cases (29% of cancer diagnoses in women) and 40,290 predicted deaths (15% of cancer deaths in women) in the United States in 2015.[13] Therefore, the discovery of novel anticancer agents with activity against breast cancer is an important goal. Breast cancers have traditionally been classified based on the expression of three important receptors (Estrogen Receptor (ER) +/-, Progesterone Receptor (PR) +/-, HER2+/-); cancers expressing none of these receptors are referred to as triple negative breast cancer (TNBC). More recent studies based on gene expression signatures subdivide breast cancers even further into six subtypes (Basal, Erbb2, LumA, LumA/B, LumB, and mixed).[14] In collaboration with Claire Knežević breast cancer cell lines from different subtypes (HS578t, BT20, and BT549→Subtype 5, basal; HCC1954→Subtype 8, basal; MCF-7 and T47D→Subtype 4, luminal B) were screened. We focused most on the basal subtype because cancers of the basal subtype are often TNBC and are typically aggressive and difficult to treat.[14] Compounds from two sources were evaluated in these cell lines: 1) a plant extract library from Prof. Ikhlas Khan and Dr. Troy Smilie (University of Mississippi) and 2) the compound collection at the UIUC high-throughput screening facility (HTSF).

Natural products from plants have been a rich source of anticancer agents (e.g. paclitaxel from the bark of the Pacific yew *Taxus brevifolia*, vinca alkaloids from the periwinkle plant *Vinca rosea*, the camptothecins from the bark of the *Camptotheca acuminata* tree, and the epipodophyllotoxins from the root of the mayapple *Podophyllum peltatum*).[8,15] For this reason, we chose to test a library of plant extracts derived from *Dioscorea villosa* (Wild Yam), *Alangium salvifollium*, and other plants.

Table 4.3. Anticancer activity of the plant extracts

Cell Line	Subtype	Botanical IC_{50}s (µg/mL)							
		Dioscorea villosa			*Alangium salvifollium*		*Sida acuta*	*V. sitchensis*	*Coptis chinensis*
		Yam AB	Yam AC	Yam B	1215c:ALSAA	1215b:ALSAA	1226b:SIACM	*V. sitchensis*	840:COCHR
Hs578t	5, Basal	22.4	19.9	59.8	10.2	8.2	23.1	42.6	-
BT549	5, Basal	35.3	27.2	177	11.1	9.8	67.0	43.0	-
BT20	5, Basal	42	58	-	16	12	32	-	18.5
HCC 1954	8 , Basal	8.9	4.2	-	0.14	0.25	-	-	-
MDAMB436	14, Mixed	19.7	-	-	4.6	2.7	-	-	32
MCF7	4, Luminal B	7.0	10.4	-	0.39	2.9	-	-	-

Screening was performed with compounds at 40 µg/mL for 48 h. Extracts that induced >70% cell death were then analyzed for their IC_{50}s. Cells were plated at 2000 cells/well in 384 well plates. Percent viability determined by Alamar Blue with 100 µM DOX as the 100% Dead and 1% DMSO as the 100% Alive.

Some of the extracts showed moderate to potent activity against the breast cancer cell lines tested (Table 4.3). The root and bark extracts from *Alangium salvifollium* (1215c:ALSAA and 1215b:ALSAA, respectively) showed the best activity against the breast cancer cell lines tested with average IC_{50} < 10 µg/mL. The identification of the active components from these mixtures remains a challenge for further pursuit of these samples.

The second library that was tested was the UIUC High Throughput Screening Facility (HTSF) and Marvel compound libraries. Many promising anticancer agents have been discovered from these libraries, including the triphenylmethylamides[16] and the deoxynyboquinones.[17-19] Because synthetic laboratories from across the United States are continuing to contribute to the HTSF library, further screening efforts were conducted. For these studies, compounds from HTSF plates 1-17 were evaluated in Hs578t cells (subtype 5, basal). From these efforts, 19 hits were

found, and 9 of these compounds induced dose-dependent cell death. One of these nine compounds was the previously identified compound deoxynyboquinone. Of the other eight compounds, only four had potent activity (IC_{50} < 10 μM, Figure 4.5).

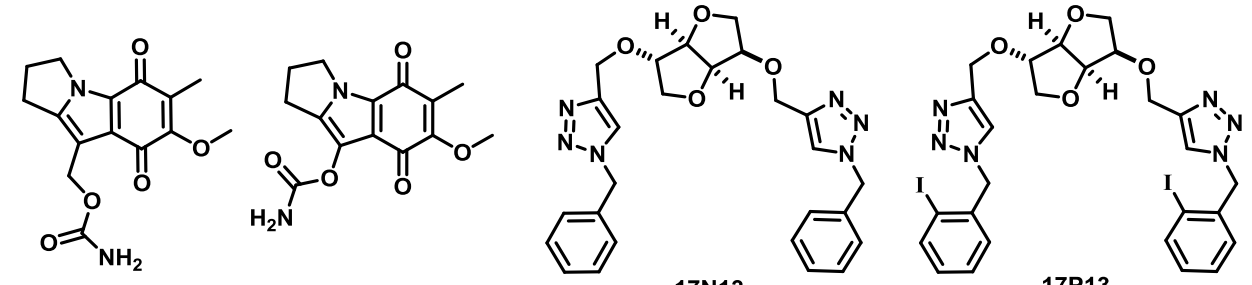

Figure 4.5. Structures of potent hits from the HTSF library against the Hs578t breast cancer cell line. Below each compound is the location in the library (plate number followed by the location in the plate), the origin of the compound, and the 48 h IC_{50} against Hs578t cells.

Two of the compounds were mitomycin C derivatives synthesized by the Coates laboratory (UIUC). One of the compounds (6B13) was previously published as a "barely active" derivative of mitomycin C which showed modest in vivo efficacy in a P388 murine model of leukemia (minimum effective dose = 51 mg/kg).[20] The other mitomycin C derivative (6C13) has never been reported in the literature, and no further information on the compound is known. The goal of this investigation was the discovery of structurally novel compounds, rather than the development of derivatives of known anticancer agents, so these compounds were not pursued further. The other two hits were compounds synthesized from isosorbide by Dr. Karen Morrison; evaluation of these compounds has been reported.[21]

Several additional hits from the screening efforts have been described elsewhere.[22] One of these compounds was compound **1227** (Figure 4.6), a diverted intermediate toward actinophyllic acid synthesized by the laboratory of Prof. Stephen Martin.[1] While the natural product actinophyllic acid showed no anticancer activity, **1227** has potent activity against a variety of breast cancer cell lines (48 h IC_{50} ranging from 13 to 63 μM, Figure 4.6).[22] Upon screening of

1227 derivatives, we found that a different derivative (**1257** or Ersindole, Figure 4.6) was more potent and was chosen for further analysis.

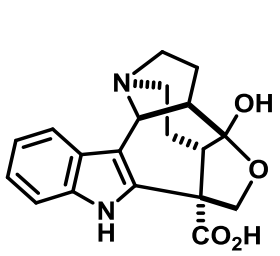

Actinophyllic acid
Martin Lab
Hs578t IC_{50} > 100 μM

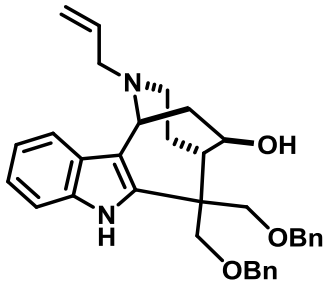

1227
Martin Lab
Hs578t IC_{50} = 63 μM
BT549 IC_{50} = 14 μM
T47D IC_{50} = 13 μM
MCF7 IC_{50} = 21 μM

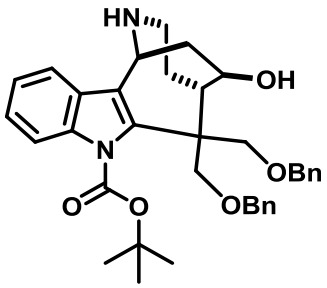

1257, Ersindole
Martin Lab
Hs578t IC_{50} = 7.7 μM
BT549 IC_{50} = 8.0 μM
T47D IC_{50} = 6.5 μM
MCF7 IC_{50} = 5.8 μM

Figure 4.6. Structure of actinophyllic acid, **1227**, and **1257** along with IC_{50} against the indicated cell lines at 48 h. Where error is indicated n=3, ± SEM, where error is not indicated n=1. Performed with Dr. Claire Knežević.

4.2 Characterization of ersindole

After it was determined that ersindole (ERS) would be the lead compound, further characterization of its mode of cell death was performed. Dr. Claire Knežević determined that ERS kills cancer cells rapidly with steep Hill slope and E_{max}.[22] Additionally, she found that it appears to kill via endoplasmic reticulum (ER) stress.[22] The rest of this chapter describes the experiments performed to support these findings.

4.2.1 Dose-response curves of ERS-treated cancer cells have steep Hill slopes and high E_{max} values

As described in Chapter 1.3, Hill slope and E_{max} values have recently been recognized as potentially important features for novel anticancer agents.[23] Upon treatment with ERS for 48 h, the breast cancer cell line MDA-MB-231 exhibits a steep dose response curve (HS = 15) and few

cells are able to survive concentrations above the IC_{50} value (E_{max} = 100, Figure 4.7A). This differs significantly from many commonly-used anticancer drugs[23] such as doxorubicin (DOX), cisplatin (CIS) and 5-fluorouracil (5-FU), which have shallower HS (~1) and lower Emax values (81, 90, and 59, respectively) than ERS (Figure 4.7A). Although the dose-response curves of cells treated with some anticancer drug classes show steep HS (e.g. Hsp90 inhibitors) or high E_{max} values (e.g. DNA crosslinking drugs), few exhibit both traits.[23] Additionally, for almost all compounds, these values vary across cell lines. Evaluation of a panel of cancer cell lines from different tumor types reveals that ERS is unique, in that both the steep HS (average = 8.4 ± 1.3) and high E_{max} (100) are consistent across all cell lines evaluated (Figures 4.7B-C) Average IC_{50} values show that ERS is less potent than DOX, similar in potency to CIS, and more potent than 5-FU (Figure 4.7D). Data from the individual cells lines can be seen in Figure 4.7E.

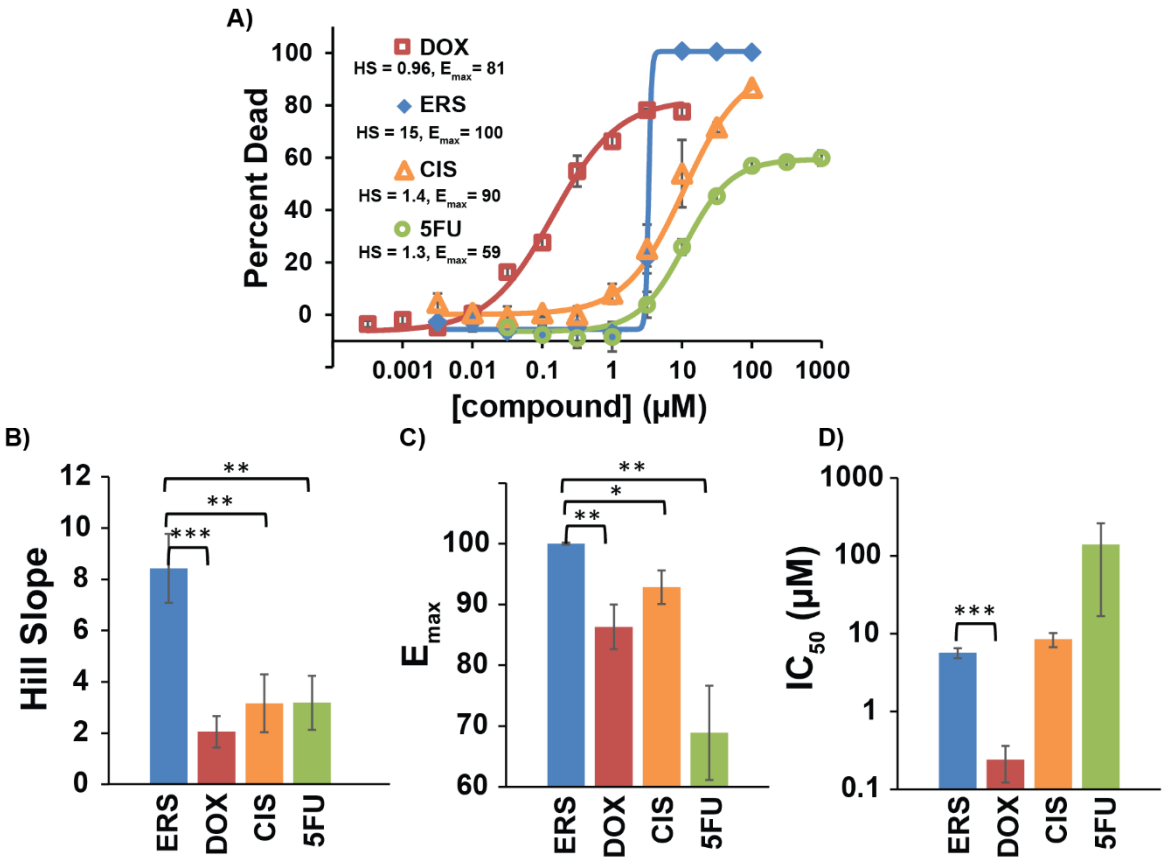

E)

Cell Line (tumor type)	Ersindole			Doxorubicin			5-Fluorouracil			Cisplatin		
	Hill Slope	E_{max}	IC_{50} (μM)	Hill Slope	E_{max}	IC_{50} (μM)	Hill Slope	E_{max}	IC_{50} (μM)	Hill Slope	E_{max}	IC_{50} (μM)
A549 (lung)	7.9 ± 3.2	100 ± 0.05	6.8 ± 1.3	0.91 ± 0.06	89.9 ± 0.5	0.19 ± 0.05	2.1 ± 0.84	73.6 ± 4.4	11 ± 5.4	2.6 ± 0.44	91.1 ± 3.6	8.6 ± 4.5
Hs578t (breast)	7.6 ± 2.3	100 ± 0.1	6.6 ± 0.67	1.3 ± 0.21	93 ± 3.0	0.16 ± 0.10	9.5 ± 4.0	69.4 ± 5.8	17 ± 11	3 ± 0.65	95.9 ± 1.6	9.6 ± 2.4
MCF-7 (breast)	3.3 ± 0.34	98.9 ± 0.2	4.3 ± 0.40	6.3 ± 2.5	65 ± 4.4	1.1 ± 0.21	1.8 ± 0.27	22.3 ± 3.3	>1000	0.94 ± 0.10	99.5 ± 6.5	18 ± 5.0
MDA-MB-231 (breast)	15 ± 0.47	100 ± 0.09	3.4 ± 0.023	0.96 ± 0.13	80.7 ± 0.47	0.29 ± 0.062	1.3 ± 0.082	59.3 ± 1.7	45 ± 11	1.4 ± 0.22	90.2 ± 3.9	11 ± 3.4
MIA PaCa-2 (pancreatic)	3.2 ± 0.32	100 ± 0.3	4.3 ± 0.24	1.9 ± 0.28	90.8 ± 0.93	0.021 ± 0.004	5.8 ± 3.8	80.8 ± 2.0	7.5 ± 2.5	1.6 ± 0.056	94.4 ± 0.35	6.3 ± 0.74
T47D (breast)	10 ± 2.9	99.9 ± 0.04	10 ± 2.3	1.8 ± 0.49	81.8 ± 1.8	0.092 ± 0.007	2.1 ± 0.12	65.3 ± 1.8	25 ± 3.2	10.9 ± 3.8	75.6 ± 1.9	8 ± 2.3
U937 (lymphoma)	11 ± 3.7	100 ± 0.2	3.3 ± 0.18	1.8 ± 0.12	98.3 ± 0.66	0.021 ± 0.001	1.8 ± 0.25	92 ± 5.5	10 ± 2.2	2.1 ± 0.34	100 ± 0.7	2.5 ± 1.0
4T1 (murine breast)	9.8 ± 4.1	100 ± 0.05	6.1 ± 1.5	1.5 ± 0.15	91.2 ± 1.3	0.11 ± 0.005	0.95 ± 0.063	88.5 ± 0.52	2.7 ± 0.31	2.8 ± 0.61	95.9 ± 0.64	3.5 ± 1.2

Figure 4.7. (**A**) Dose-response curves, HS, and E_{max} values of doxorubicin (DOX), ERS, cisplatin (CIS), and 5-fluorouracil (5FU) against human breast cancer MDA-MB-231 cells, n = 3, error bars = standard error of the mean (SEM). (**B**) Average HS for 8 cell lines (A549, Hs578t, MCF-7,

Figure 4.7. (cont.) MDA-MB-231, MIA PaCa-2, T47D, U937, and 4T1) treated with DOX, ERS, CIS, or 5FU for 48 h, n = 3, error bars = SEM. *P≤0.05, **P≤0.01, ***P ≤0.001, Student's t-test.(**C**) Average E_{max} values from data in part B. (**D**) Average IC_{50} values from data in part B. (**E**) Tabulated data from B-D. n = 3, mean ± SEM.

Previously ERS was found to rapidly induce cell death.[22] High HS and E_{max} values were also observed for ERS even after short incubations (1, 3, or 6h) for both MCF-7 (Figure 4.8A) and MIA PaCa-2 (Figure 4.8B-C).

A)

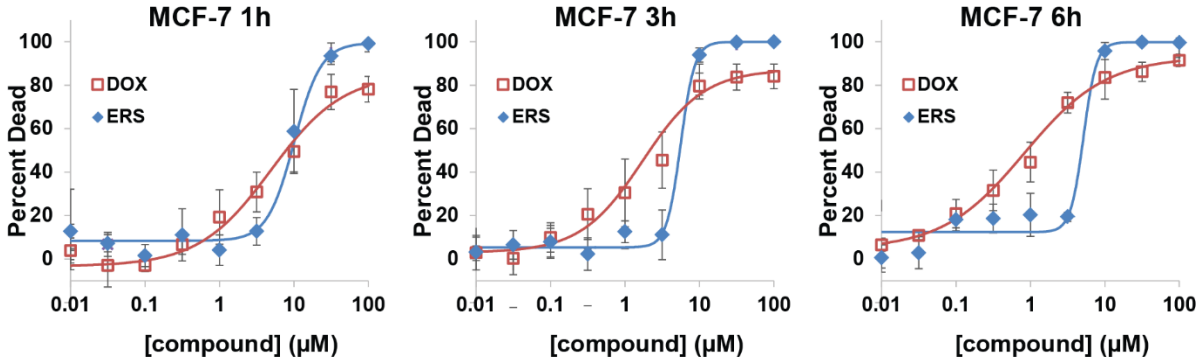

B)

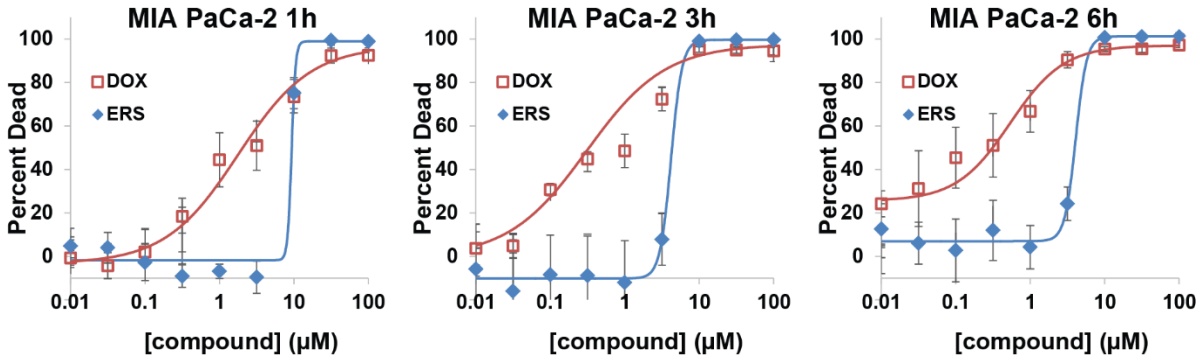

C)

Cell Line	treatment (h)	ERS			DOX		
		Hill Slope	Emax (%)	IC_{50} (μM)	Hill Slope	Emax (%)	IC_{50} (μM)
MCF-7							
	1	2.4	99	11 ± 2	0.9	85	10 8
	3	4.6	100	6 ± 2	1	87	3 ± 1
	6	5	100	3.6 ± 0.6	0.8	93	1.2 ± 0.4
MIA PaCa-2							
	1	16	99	9.2 ± 0.5	0.88	97	3 ± 1
	3	5.8	100	3.8 ± 0.4	0.83	98	0.9 ± 0.4
	6	5.9	100	3.7 ± 0.2	1.2	97	0.4 ± 0.2

Figure 4.8. Dose-response curves of doxorubicin (DOX) and ersindole (ERS), against (**A**) MCF-7 and (**B**) MIA PaCa-2 after the indicated treatment times. Cells were plated at 2,000 cells per

Figure 4.8. (cont.) well in a 96-well plate and allowed to attach overnight. Cells were then treated with compound for the indicated times. After treatment, fresh media was added and the cells were allowed to recover for a total of 48 h. Cell death was assessed by the sulforhodamine B assay. Data were fit to a logistical dose response curve with OriginPro 9 and values for E_{max}, Hill slope, and IC_{50} were obtained from these curves, n = 3, mean ± SEM. (**C**) Tabulated data from A and B.

4.2.2. ERS causes ER stress-dependent cancer cell death

As described in Chapter 1.3, cancer cells experience a higher basal level of ER stress than normal cells. Aggravation of this chronic ER stress and subsequent activation of pro-death signaling has been proposed as an anticancer strategy.[24-25] To further probe the mechanism of action of ERS, Dr. Claire Knezevic analyzed the cell death induced by this compound and the effect that small molecule inhibitors of various biological pathways had on its potency. Inhibition of ER stress with the PP1/GADD34 inhibitor salubrinal[26] drastically reduced sensitivity to ERS in both U937 and MIA PaCa-2 cells.[22] Additionally, U937 cells treated with ERS were studied via transmission electron microscopy. A large increase in ER size was observed, similar to the ER stress-inducing agent thapsigargin, and the increase in size was prevented by co-treatment with salubrinal.[22]

4.2.2.1 ERS causes increased phosphorylation of eIF2α

Due to the observed protection from ERS provided by co-treatment with the ER stress inhibitor salubrinal and the increase in size of the ER upon treatment with ERS, the ability of ERS to induce ER stress was explored further. As described in Chapter 1.3, both phosphorylation of IRE1α and eIF2α are signs of ER stress.[27] For this reason, we chose to examine the phosphorylation states of these proteins after treatment with ERS.

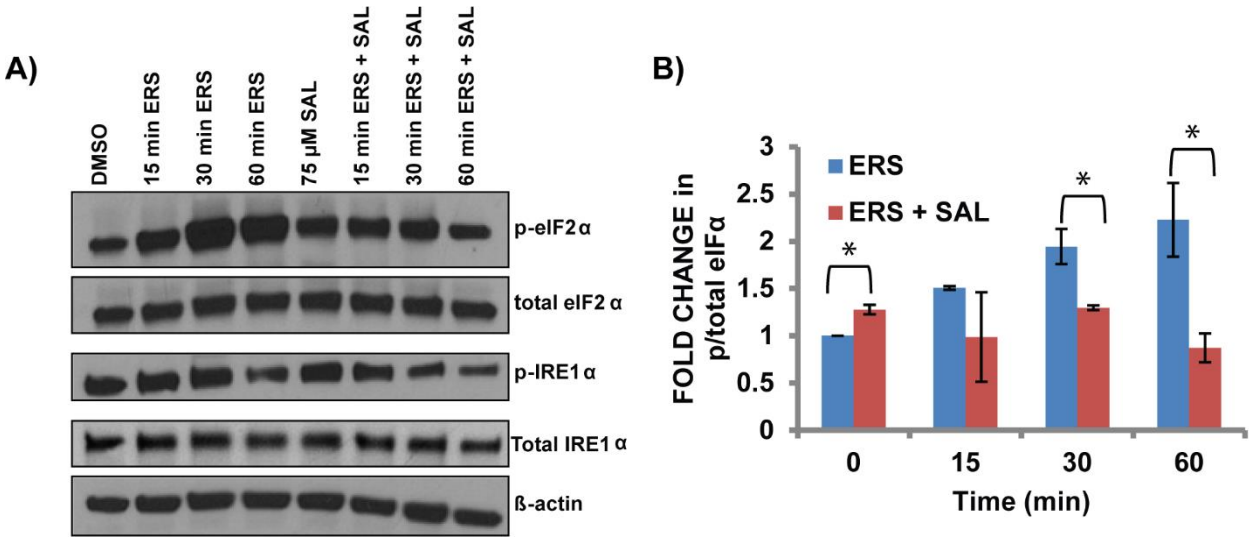

Figure 4.9. (**A**) Western blot analysis of U937 cells treated with vehicle (DMSO), 9 µM ersindole (ERS), or 75 µM Salubrinal and 9 µM ersindole (ERS + SAL). Cells were treated in 6-well plates at 300,000 cells/mL and harvested at the indicated times. Blot is representative of three independent experiments. (**B**) Quantification of triplicate blots was performed using ImageJ, ratio of phosphorylated protein to total protein, n = 3, mean ± SEM. *P ≤ 0.05, Student's t-test.

Western blots of U937 cells treated with ERS reveal an increase in p-eIF2α after only 15 min, with continuing increases after 30 and 60 min of treatment, consistent with induction of ER stress (Figure 4.9). Co-treatment with salubrinal prevented this increase in p-eIF2α throughout the 60 min period of treatment (Figure 4.9). This is unusual because salubrinal inhibits the phosphatase that dephosphorylates eIF2α, which usually causes an increase in p-eIF2α. Treatment with salubrinal for 3 h in the absence of ERS results in the expected small but significant increase in p-eIF2α that is due to prolonged inhibition of eIF2α dephosphorylation by PP1/GADD34. One possible explanation for this is that ERS may inhibit PP1/GADD34 at a site near the site of inhibition for salubrinal, but with higher efficiency. It is known that complete inhibition of this phosphatase is lethal to the cell. Specifically, genetic modulation of the site of phosphorylation of eIF2α revealed that mutation of the residue to a phospho-mimic (Asp) increased cell death, suggesting that while moderate levels of inhibition with agents such as salubrinal may be protective, high levels of inhibition are lethal.[28] Cells that were co-treated with salubrinal and ERS were first pre-treated with salubrinal at >8X the concentration used for ERS

for 2 h before the addition of ERS. Thus, it is possible that salubrinal outcompetes ERS for binding to PP1/GADD34 in the co-treatments. Studies utilizing siRNA against PP1 further support this (see section 4.2.2.2). Further studies using other PP1/GADD34 inhibitors such as guanabenz or sephin 1[29] should be performed in order to better understand this phenomenon. Also, studies to determine the ability of ERS to inhibit PP1/GADD34, similar to those previously performed with salubrinal,[26] would directly determine if this is in fact the mechanism of ERS.

In addition, no significant change in the level of IRE1α phosphorylation was observed over 60 minutes of treatment with ERS (Figure 4.9), which is unusual among ER stress-inducing agents. IRE1α phosphorylation is a common indicator of ER stress, but some suggest that it is difficult to observe.[30] Our results suggest that either ERS induces ER stress in a PERK dependent (and IRE1α independent) manner (consistent with inhibiting PP1/GADD34) or our technique for visualizing IRE1α phosphorylation was not sufficient. Future studies should examine the effects downstream of IRE1α phosphorylation, including XPB1 splicing.

4.2.2.2 shRNA screening and siRNA validation support that ERS induces ER stress

In order to understand the mechanism by which ERS induces ER stress, Dr. Claire Knezevic performed an shRNA screen for constructs that protect against ERS.[22] Many of the top constructs are related to ER stress, including ITPR3 (codes for the inositol 1,4,5-triphosphate receptor 3, a ligand gated calcium channel important in signaling for ER stress),[31] SGMS2 (codes for sphingomyelin synthase 2, an enzyme the production of sphingomyelin, a major component of cell and Golgi membranes),[32] and ESR1 (encodes ERα, an estrogen receptor recently shown to be involved in ER stress).[33]

To validate these results and confirm the role of these gene products in ERS-induced cell death, one or two siRNAs were obtained for 66 of the enriched genes. The toxicity of ERS at 6.5 μM in MIA PaCa-2 cells transfected with each of these siRNAs was determined (Figure 4.10).

Consistent with the protective action of the PP1/GADD34 inhibitor salubrinal, siRNA targeting PPP1R15A, the gene for PP1/GADD34, provided the most protection from ERS-induced cell death. Additionally, ITPR3 and ESR1, which both were ER-stress related genes found to be protective in the shRNA screen, were also identified as providing strong protection in the siRNA validation. Other genes whose silencing provided protection from ERS cytotoxicity are involved in membrane trafficking, such as the regulator of vesicle fusion RAB26, or protein degradation, such as the probable E3 ubiquitin ligase MKRN2.

Figure 4.10. Cell death of MIA PaCa-2 cells transfected with various siRNA constructs followed by treatment with 6.5 µM ERS for 3 h. AllStars Death (Qiagen) is a collection of siRNAs that target genes essential to survival. It was used alone (no ERS added) and was used to estimate transfection efficiency. Ave ERS death is the average death induced by 6.5 µM ERS under the assay conditions.

4.2.2.3 Comparison of ERS to tunicamycin and thapsigargin

The two most commonly-used chemical tools for the study of ER stress and its downstream effects are thapsigargin, a sarco/endoplasmic reticulum Ca^{2+}-ATPase (SERCA) inhibitor,[34] and tunicamycin, a heterogeneous natural product mixture that inhibits N-glycosylation.[35] After determining that ERS most likely causes cell death via induction of ER stress, we chose to compare ERS to these commonly used ER stress inducing agents.

A)

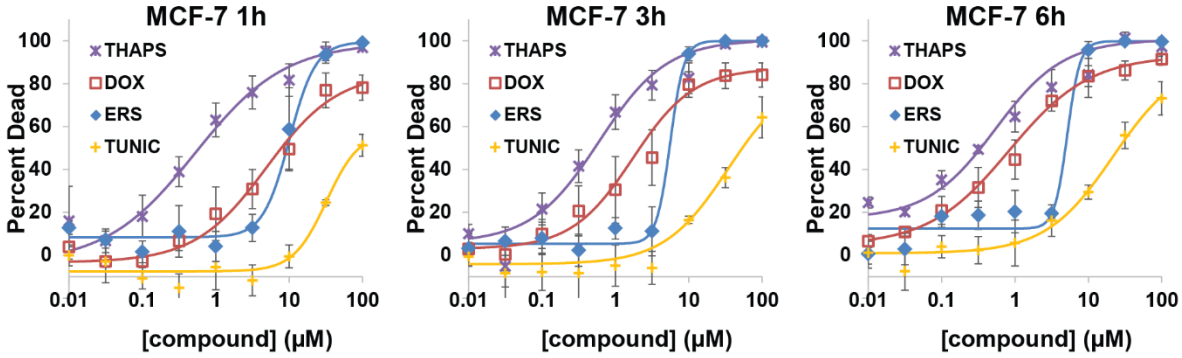

B)

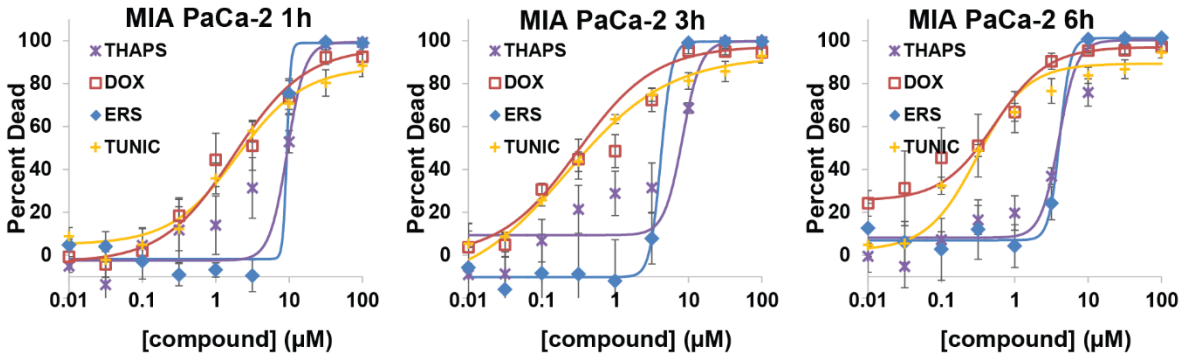

C)

Cell Line	treatment (h)	Ersindole			TUNIC			THAPS			DOX		
		Hill Slope	Emax (%)	IC_{50} (μM)	Hill Slope	Emax (%)	IC_{50} (μM)	Hill Slope	Emax (%)	IC_{50} (μM)	Hill Slope	Emax (%)	IC_{50} (μM)
MCF-7													
	1	2.4	99	11 ± 2	1.9	58	>100	0.7	99	0.8 ± 0.3	0.9	85	10 8
	3	4.6	100	6 ± 2	1	80	63 ± 16	0.9	100	0.6 ± 0.3	1	87	3 ± 1
	6	5	100	3.6 ± 0.6	0.9	91	26 ± 6	0.9	100	0.4 ± 0.1	0.8	93	1.2 ± 0.4
Mia PaCa-2													
	1	16	99	9.2 ± 0.5	0.96	88	2.3 ± 0.6	3.6	99	7 ± 3	0.88	97	3 ± 1
	3	5.8	100	3.8 ± 0.4	0.62	93	0.5 ± 0.1	3.5	100	4 ± 2	0.83	98	0.9 ± 0.4
	6	5.9	100	3.7 ± 0.2	1.3	89	0.4 ± 0.1	3.5	100	4.6 ± 0.8	1.2	97	0.4 ± 0.2

Figure 4.11. (**A**) Dose-response curves of doxorubicin (DOX), ersindole (ERS) tunicamycin (TUNIC) and thapsigargin (THAPS), against (**A**) MCF-7 and (**B**) MIA PaCa-2 after the indicated treatment times. Cells were plated at 2,000 cells per well in a 96-well plate and allowed to attach overnight. Cells were then treated with compound for the indicated times. After treatment, fresh media was added and the cells were allowed to recover for a total of 48 h. Cell death was assessed by the sulforhodamine B assay. Data were fit to a logistical dose response curve with OriginPro 9 and values for E_{max}, Hill slope, and IC_{50} were obtained from these curves, n = 3,

Figure 4.11. (cont.) mean ± SEM. (**C**) Tabulated data from A and B.

The high Hill slope and E_{max} are two defining features of ERS. For that reason, we chose to characterize the dose response curves for tunicamycin and thapsigargin and compare them to those of ERS and doxorubicin. As shown in Figure 4.11, ERS has a higher E_{max} than tunicamycin and a greater Hill slope than both tunicamycin and thapsigargin.

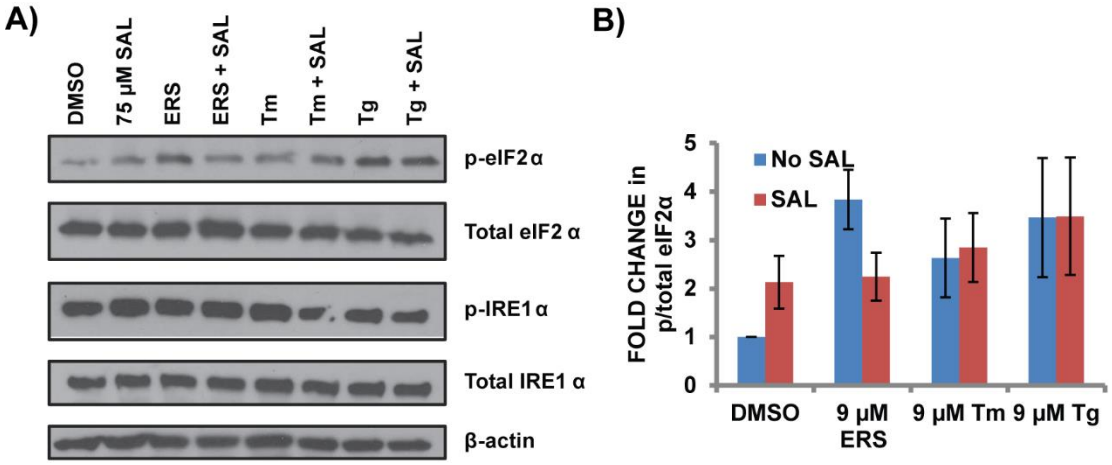

Figure 4.12. (**A**) U937 cells were pretreated with 75 µM salubrinal (SAL) or DMSO for 2h followed by 9 µM ER stress inducer tunicamycin (Tm), thapsigargin (Tg), or ersindole (ERS) for 30 min, then harvested for lysis and western blot analysis. (**B**) Quantification of triplicate blots using ImageJ, ratio of phosphorylated protein to total protein, n = 3, mean ± SEM.

Another important feature of ERS is its ability to rapidly induce phosphorylation of eIF2α. Both tunicamycin and thapsigargin also cause an increase in p-eIF2α after a 30 min treatment, demonstrating that all three compounds can rapidly induce ER stress (Figure 4.12). However, salubrinal is capable of preventing the increase in p-eIF2α induced by ERS, and not by tunicamycin or thapsigargin (Figure 4.12). This observation provides further evidence for a different mechanism of ER stress induction by ERS compared to either of these commonly-used agents.

We then compared the shRNA screening results for ERS to those for tunicamycin and thapsigargin. Of the enriched transcripts, only two were identified in common with tunicamycin and ERS samples (DEK and SGMS2), whereas 14 different enriched constructs were shared by

both thapsigargin and ERS, suggesting that the mode of ER stress induction by ERS may be more similar to thapsigargin than tunicamycin.

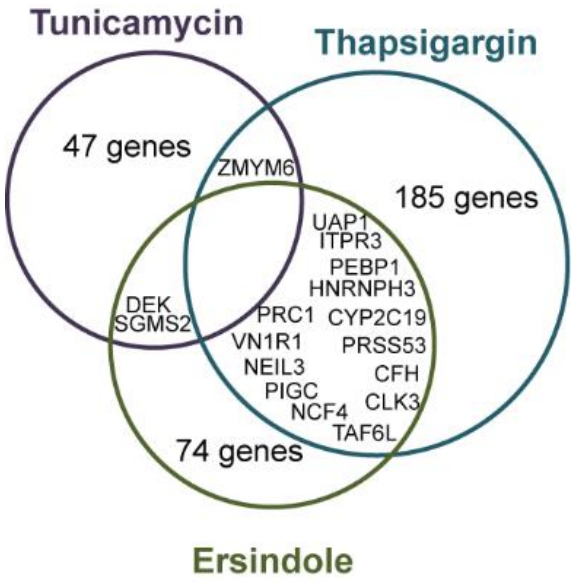

Figure 4.13. Venn diagram of enriched shRNA constructs identified from cells surviving treatment with thapsigargin, tunicamycin, and ERS.

4.3 In vivo analysis of ERS

ER stress-inducing agents are hypothesized to be excellent anticancer candidates due to their ability to overwhelm an already overloaded ER.[24-25] For this reason, the in vivo activity of this novel class of ER stress-inducing compounds was investigated. Before beginning in vivo work, Dr. Claire Knezevic investigated the effect of ERS on human red blood cells and found that it induced significant hemolysis at concentrations near the IC_{50} value. Additional derivatives of ERS were then synthesized by the Martin laboratory. We evaluated these derivatives against cancer cells and red blood cells in culture, with the objective of finding an active ERS derivative that does not induce hemolysis. One derivative (ERS-9, Figure 4.14) retained its potency against Hs578t cells in culture while inducing minimal hemolysis at concentrations up to 100 µM. Additionally, cell death induced by ERS-9 was still protected by treatment with salubrinal.[22] The rest of this section describes further evaluation of this compound both in cell culture and *in vivo*.

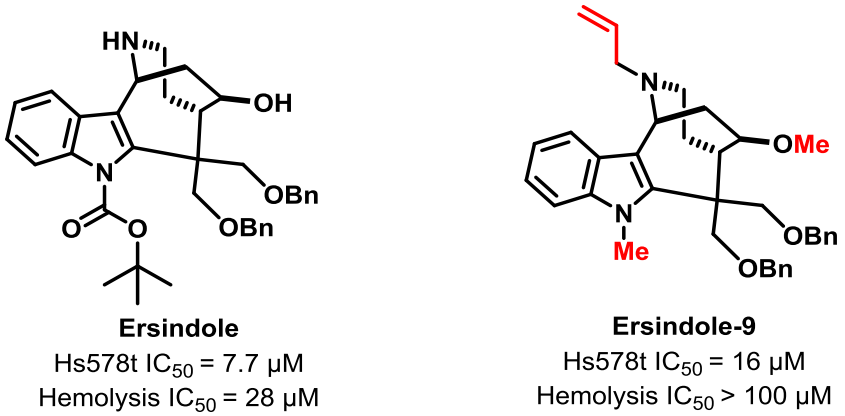

Ersindole
Hs578t IC_{50} = 7.7 μM
Hemolysis IC_{50} = 28 μM

Ersindole-9
Hs578t IC_{50} = 16 μM
Hemolysis IC_{50} > 100 μM

Figure 4.14. Structures, anticancer activity, and hemolysis induction of ERS and ERS-9.

4.3.1 Dose-response curves of ERS-9-treated cancer cells have steep Hill slopes and high E_{max} values

Similar to ERS, ERS-9 displays high Hill slope and E_{max} values in multiple cancer cell lines (Figure 4.15). However, ERS-9 is slightly less potent than ERS.

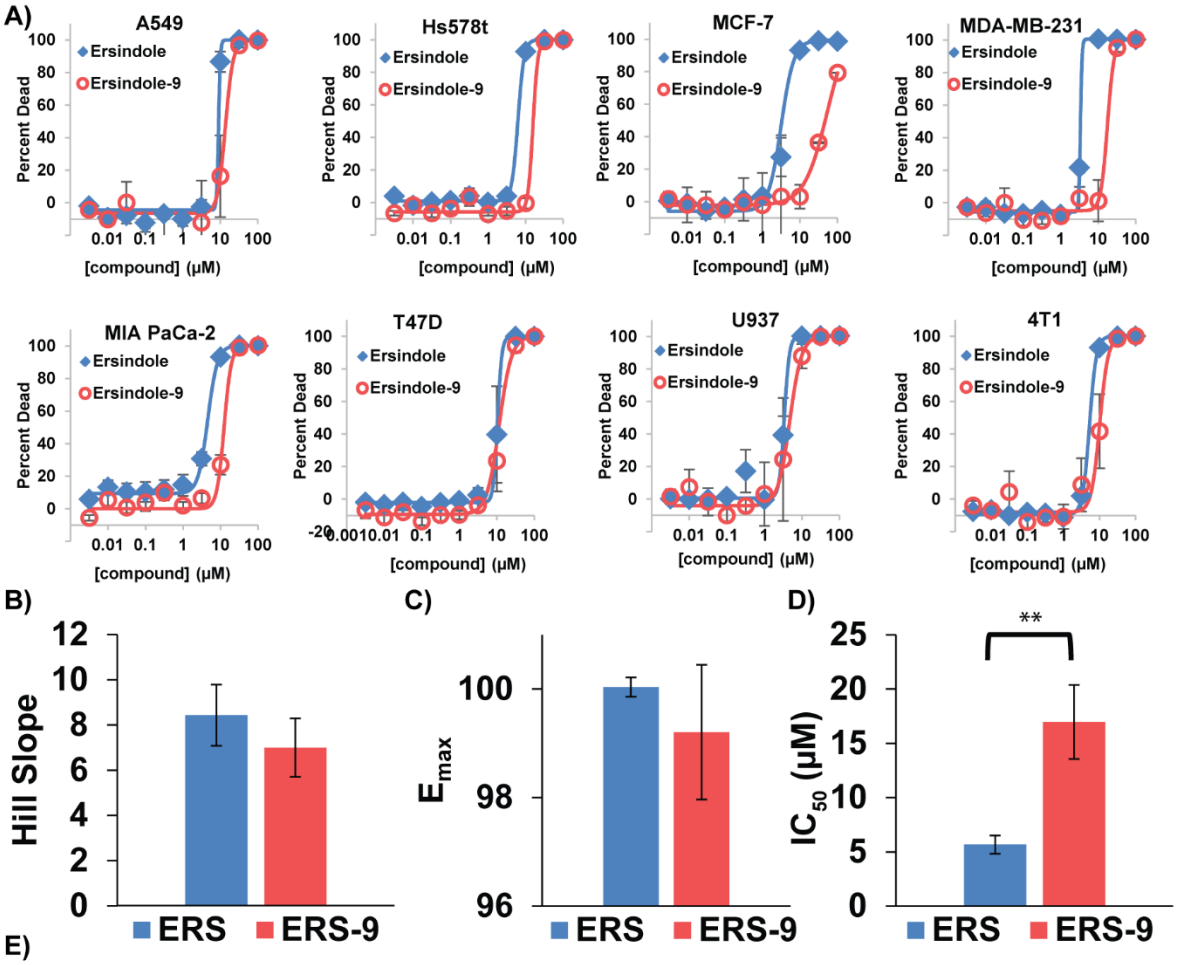

E)

Cell Line (tumor type)	ERS			ERS-9		
	Hill Slope	E_{max}	IC_{50} (μM)	Hill Slope	E_{max}	IC_{50} (μM)
A549 (lung)	7.9 ± 3.2	100 ± 0.05	6.8 ± 1.3	4.5 ± 1.5	100 ± 0.7	14 ± 3.7
Hs578t (breast)	7.6 ± 2.3	100 ± 0.1	6.6 ± 0.67	13 ± 3.8	99.9 ± 0.2	20 ± 2.9
MCF-7 (breast)	3.3 ± 0.34	98.9 ± 0.2	4.3 ± 0.40	6.3 ± 4.4	90.6 ± 9.6	37 ± 1.3
MDA-MB-231 (breast)	15 ± 0.47	100 ± 0.09	3.4 ± 0.023	12 ± 4.4	100 ± 0.7	22 ± 4.5
MIA PaCa-2 (pancreatic)	3.2 ± 0.32	100 ± 0.3	4.3 ± 0.24	4.4 ± 0.63	100 ± 0.3	13 ± 0.71
T47D (breast)	10 ± 2.9	99.9 ± 0.04	10 ± 2.3	3.6 ± 0.83	100 ± 0.6	14 ± 3.2
U937 (lymphoma)	11 ± 3.7	100 ± 0.2	3.3 ± 0.18	8.5 ± 5.3	99.9 ± 0.7	5.6 ± 2.3
4T1 (murine breast)	9.8 ± 4.1	100 ± 0.05	6.1 ± 1.5	4 ± 0.91	99.7 ± 0.5	10 ± 3.1

Figure 4.15. (**A**) Dose-response curves of ERS and ersindole-9 (ERS-9) against A549, Hs578t, MCF-7, MDA-MB-231, MIA PaCa-2, T47D, U937, and 4T1 cells after 48 h of treatment, n = 3,

Figure 4.15. (cont.) error bars = standard error of the mean (SEM). (**B**) Average HS from data in part A, n = 3, error bars = SEM. *P≤0.05, **P≤0.01, ***P ≤0.001, Student's t-test.(**C**) Average E_{max} values from data in part A. (**D**) Average IC_{50} values from data in part A. (**E**) Tabulated data from A. n = 3, mean ± SEM.

4.3.2 In vivo activity of ERS-9

Due to the favorable activity profile and minimal hemolytic activity of ERS-9 (Figure 4.13-14), the anticancer efficacy of ERS-9 was investigated in vivo. Dr. Hyang Yeon Lee performed all of the animal studies described in this section. The maximum tolerated dose of ERS-9 in C57BL/6 mice was 60 mg kg^{-1} for a single intraperitoneal (IP) injection, with no lasting adverse effects. Therefore, ERS-9 was assessed in an aggressive[36] 4T1 syngeneic model of breast cancer at this dose, with tumor-bearing mice receiving three treatments of ERS-9.

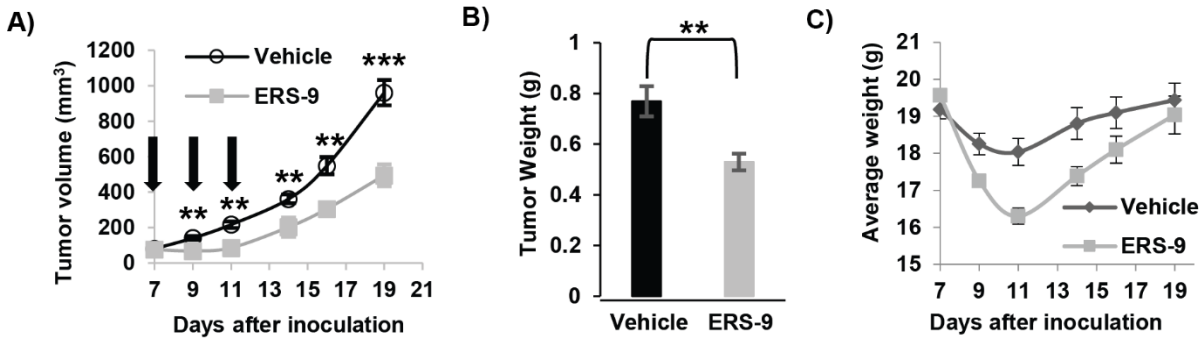

Figure 4.16. 8-week-old female Balb/c mice were subcutaneously inoculated with $1x10^6$ 4T1 murine breast cancer cells in the right flank. At 7, 9, and 11 days post-inoculation, mice were injected intraperitoneally with 60 mg/kg ERS-9 in PEG-400 or an equal volume of PEG-400 alone (vehicle). 5 mice per group. (**A**) Tumor growth curves of 4T1 syngeneic murine breast cancer model. Arrows indicate IP injections of 60 mg kg^{-1} ERS-9 in PEG-400 or an equal volume of PEG-400 alone (vehicle). Average ± SEM. (**B**) Tumor mass from day 19. Average ± SEM, **P≤0.01, ***P ≤0.001, Student's t-test. (**C**) Mice were weighed every 2-3 days and the average weight of each treatment group is shown. Values shown are mean ± SEM.

Tumor volumes in ERS-9-treated mice were significantly lower than those in vehicle-treated mice ($P < 0.01$, Figure 4.16A) and tumor mass measured after sacrifice was also lower ($P < 0.01$, Figure 4.16B). While treatment with ERS-9 initially resulted in weight loss, the weight of ERS-9 treated mice was similar to that of vehicle-treated mice by day 19 (Figure 4.16C), indicating no overt toxicity from treatment with ERS-9.

4.4 Analysis of third set of derivatives from the Martin laboratory

While ERS-9 showed significant activity against the aggressive 4T1 model, there was interest in finding ERS derivatives with better potency that retained the non-hemolytic phenotype of ERS-9. For this reason, the Martin laboratory synthesized additional derivatives (Figure 4.17).

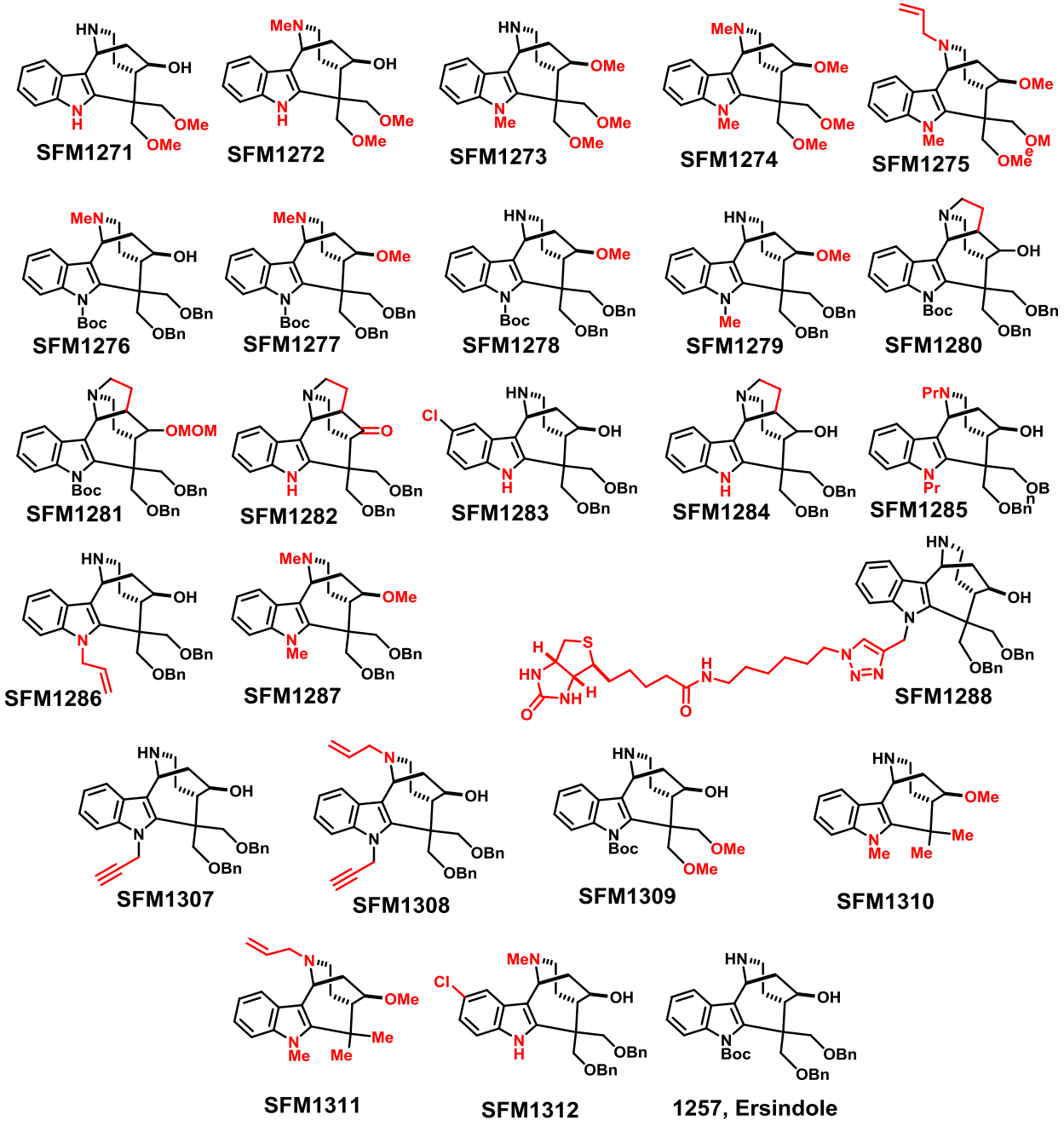

Figure 4.17. New ERS derivatives. Difference from ERS is highlighted in red.
Previously, a partial structure activity relationship (SAR) had been determined including:

1. Benzylation of the two primary alcohols is beneficial, as a compound with free alcohols showed minimal activity.
2. A carbamate moiety on the indole nitrogen atom is beneficial, but not essential, for anticancer activity.
3. Electron-withdrawing substituents on the secondary hydroxyl group are detrimental to activity.
4. *N*-propyl and *N*-allyl groups are generally tolerated, as is the formation of a fused pyrrolidine ring. The presence of an electron-withdrawing *N*-allyl carbamate group or an *N*-benzyl group on the nitrogen atom of the basic amino group yields inactive analogs.

These new derivatives have allowed us to further evaluate the SAR. Additionally, a few derivatives could be useful in target ID (e.g. the biotin-linked compound 1288 and the alkyne derivatives 1307 and 1308). First, the ability of new derivatives to kill the U937 lymphoma cell line and their ability to induce hemolysis were assessed (Table 4.4). Consistent with previous SAR studies, benzylation of the two primary alcohols appears to be essential for anticancer activity. Compounds with either methyl ethers (e.g. 1271, 1272, 1273, and 1274) or removed hydroxyl groups (e.g. 1275, 1310, and 1311) have minimal activity against U937 cells ($IC_{50} \geq 100$ μM). Interestingly, all of these compounds induced no hemolysis at up to the highest concentration tested (333 μM). Previously it was found that derivatives with a carbamate moiety on the indole nitrogen have anticancer activity, but replacement of the carbamate moiety with a hydrogen or a methyl group was tolerated. This set of derivatives shows a similar trend, as compounds with a carbamate on the indole nitrogen (e.g. 1276, 1278, and 1280) showed potent activity ($IC_{50} < 10$ μM against U937 cells). Additionally, compounds with a hydrogen (1283, 1312), an alkyl chain (1285, 1287) or an alkyne (1308) at this position also retain activity ($IC_{50} < 10$ μM against U937 cells). A long chain with a biotin attached, however, is not well tolerated (1288).

Table 4.4. Anticancer and hemolytic activity of new ERS derivatives

Compound	Hill slope	E_{max}	U937 IC_{50} (μM)	Hemolysis IC_{50} (μM)	Hemolysis/ U937 IC_{50}
ERS	10.9 ± 3.6	100.4 ± 0.2	3.3 ± 0.2	28	8
ERS-9	8.5 ± 5.3	99.9 ± 0.7	5.6 ± 2.3	>100	>18
1276	4.1 ± 0.1	99.9 ± 0.1	5.3 ± 0.1	140 ± 60	26
1277	1.4 ± 0.2	99.9 ± 0.1	57.0 ± 1.5	>333	>6
1278	5.7 ± 0.2	100.0 ± 0.1	4.0 ± 0.1	50 ± 12	13
1279	4.8 ± 0.6	100.6 ± 0.4	12.0 ± 0.2	170 ± 60	14
1280	3.3 ± 0.2	100.4 ± 0.2	6.9 ± 0.5	80 ± 10	12
1281	4.3 ± 0.1	100.6 ± 0.1	12.6 ± 0.1	140 ± 30	11
1282	4.4 ± 0.5	100.9 ± 0.3	12.1 ± 0.1	>333	>28
1283	5.1 ± 0.3	100.1 ± 0.1	6.0 ± 0.2	120 ± 20	20
1284	7.2 ± 3.1	100.5 ± 0.3	10.8 ± 0.3	210 ± 40	19
1285	7.2 ± 0.1	100.1 ± 0.1	4.0 ± 0.1	54 ± 9.8	14
1286	10.8 ± 3.7	100.4 ± 0.5	10.7 ± 0.4	110 ± 10	10
1287	3.2 ± 0.4	101.0 ± 0.5	8.5 ± 0.7	120 ± 40	14
1288	1.9 ± 0.2	101 ± 1.5	34.9 ± 6.1	310 ± 30	9
1307	9.3 ± 3.9	99.9 ± 0.1	22.5 ± 4.7	>333	>15
1308	3.3 ± 0.2	100.4 ± 0.1	9.4 ± 0.1	>333	>35
1312	4.1 ± 0.1	99.9 ± 0.1	4.9 ± 0.1	190 ± 60	39

For anticancer studies: U937 cells were plated at 5000 cells/well in 384 well plates. Percent viability determined by Alamar Blue with no cells as the 100% Dead and 1% DMSO as the 100% Alive. For hemolysis studies: % Hemolysis was determined by adding 1 μL of a DMSO stock to a well of a PCR plate. To each well was added 19 μL of red blood cell buffer and 10 μL of resuspended erythrocytes which had previously been washed and resuspended in red blood cell buffer. They were incubated for 2h at 37°C. Samples were centrifuged and the absorbance of the supernatant at 540 nm was determined.

Electron-withdrawing substituents on the secondary hydroxyl group were previously found to be detrimental to activity, but a methyl group was tolerated. Similarly, with these derivatives,

compounds with a free hydroxyl (1276, 1280, 1283, 1285, 1308, and1312) or those with a methyl group (1278, 1287) retained activity (IC_{50} < 10 μM). Compounds containing a methoxymethyl ether (1281) or with a ketone replacing the secondary alcohol (1282) have moderate activity (IC_{50} ~ 12 μM). Previous results indicated that *N*-propyl and *N*-allyl groups are generally well tolerated, as is the formation of a fused pyrrolidine ring. This study confirmed previous results, as compounds with no nitrogen substitution (1278, 1283), *N*-methyl (1276, 1287, 1312), *N*-propyl (1285), *N*-allyl (1308), and a fused pyrrolidine ring (1280) all showed potent activity against U937 cells (IC_{50} < 10 μM). Additionally, for the first time, we found that compounds with substitution on the phenyl ring (1283 and 1312) retain activity. A summary of the SAR for this compound is shown in Figure 4.18.

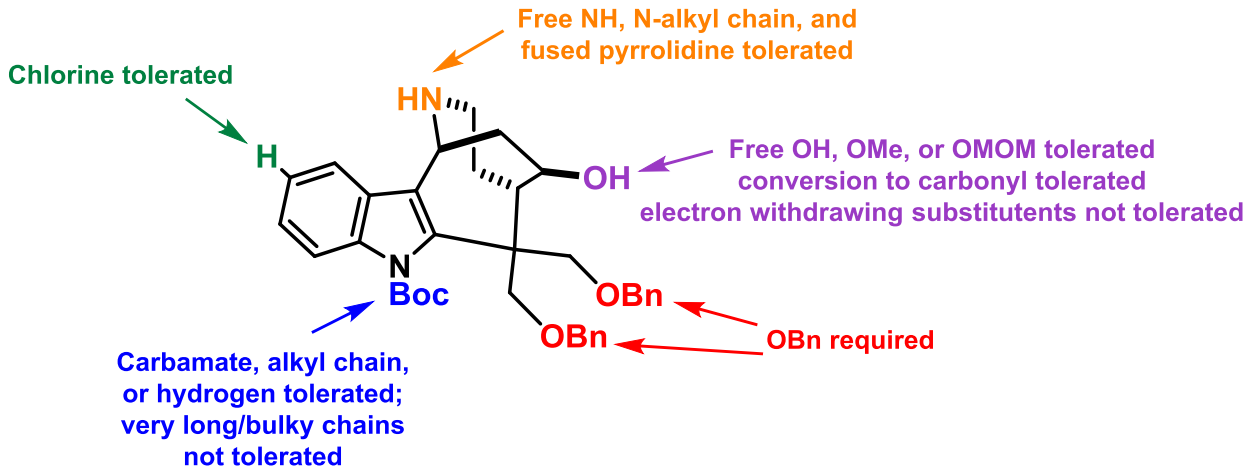

Figure 4.18. SAR for ERS.

After testing the compounds for their anticancer activity, their ability to induce hemolysis was assessed. In order to compare compounds, the ratio of hemolysis IC_{50} to U937 IC_{50} was used. For ERS, this ratio is 8, while for ERS-9 it is >18. Most compounds had ratios greater than 8, suggesting that they may have a greater therapeutic window than ERS. Ideally, a new lead would be more potent than ERS-9 (i.e. U937 IC_{50} < 5.6 μM), have a steep Hill slope and high E_{max}, and have similar or better selectivity (hemolysis/U937 IC_{50} ≥ 18). Only two compounds fulfill this requirement: 1276 and 1312. However, before advancing a lead compound, all of the derivatives

with promising hemolysis profiles (hemolysis IC_{50} > 100 μM), moderate potency against U937 (IC_{50} ≤ 25 μM), and high Hill slope and E_{max} should be tested in other cell lines (i.e. 1276, 1279, 1281, 1282, 1283, 1284, 1286, 1287, 1307, 1308, 1312). Additionally, the ability of salubrinal to protect against cell death should be evaluated, in order to ensure that they have the same mechanism of action as ERS and ERS-9.

4.5 Conclusions and future directions

Utilizing cell based phenotypic screening, we have identified several promising anticancer leads. Several of the *ent*-kauranoids synthesized in the laboratory of Prof. Sarah Reisman show promise as anticancer agents, including the natural products Longikaurin E and Maocrystal Z, as well as the synthetic compounds diol and Iso-M-Z. Because all of these compounds are Michael acceptors, further analysis of their effect on normal cells other than red blood cells is needed before other studies are performed. If the compounds show minimal toxicity in non-cancerous cells, studies should be performed to determine the mechanism of action. Studies evaluating novel ETPs from the laboratory of Prof. Mohammad Movassaghi show that they are not as potent as previous derivatives. However, some of these compounds (especially the ones with the azide handle) will likely be useful tools for determining the mechanism of action of these compounds. Screens of breast cancer cell lines with natural product extracts suggest that some of the extracts contain compounds with anticancer activity. Identification of the active components in these mixtures remains an area for future study.

The most promising lead anticancer compounds were identified in the screen of breast cancer cell lines against the HTSF library at UIUC. Dr. Claire Knezevic discovered that one of these compounds (**1227**) was a particularly promising lead. **1227** is a synthetic intermediate en route to actinophyllic acid from the laboratory of Prof. Stephen Martin. Testing of other intermediates allowed for the discovery of the more potent compound ERS. Studies that we performed revealed that this compound consistently and efficiently kills a variety of cancer cell types in culture, as evidenced by its uniformly steep Hill slope and high E_{max}. Additionally, we

found that ERS likely kills cancer cells via induction of ER stress. While ERS was not evaluated *in vivo* due to its induction of hemolysis *in vitro*, the derivative ERS-9 showed potent activity in an aggressive murine model of breast cancer. Screening of new derivatives has revealed several compounds with potent activity and low hemolysis. Further examination of the scope of activity and mechanism of these compounds is needed.

4.6 Materials and methods

General Biology Materials

Compounds were purchased from the following sources: staurosporine (Sigma Aldrich or Selleck Chemicals), doxorubicin (Sigma Aldrich), tunicamycin (Sigma Aldrich or Santa Cruz Biotechnology), thapsigargin (Santa Cruz Biotechnology), salubrinal (Selleck Chemicals), protease inhibitor cocktail (Calbiochem, 539134), phosphatase inhibitor cocktail (Calbiochem, 524625), PMSF (Sigma Aldrich), ß-mercaptoethanol (BME, Sigma Aldrich). Tetracyclic indole compounds, including ersindole, ersindole-9, and related analogs, were prepared by the Martin laboratory. 10 mM stocks in DMSO were prepared, aliquoted, and stored at -20 ˚C.

Antibodies were purchased from Cell Signaling Technology: actin (4970L), eIF2α (9722S), phospho-eIF2α (2298S), and secondary anti-rabbit IgG HRP conjugate (7074S). Antibodies were stored at either -20 or 4 ˚C according to manufacturer's instructions.

Hs578t, MCF-7, T47D, and U937 cells were obtained from ATCC. A549, MDA-MB-231, and MIA PaCa-2 cells were obtained from Professor David Boothman (UTSW). 4T1 cells were obtained from Prof. Jianjun Cheng (UIUC). MIA PaCa-2 (pancreatic cancer cells), Hs578t (human breast cancer), and HEK293TN (viral producer, embryonic kidney) cells were cultured in Dulbecco's modified Eagle medium (DMEM) containing 4.5 g/L glucose and supplemented with 10% (v/v) fetal bovine serum (Gemini Bio-Products, West Sacramento, CA), 1 mM sodium pyruvate, 100 U/ml penicillin (Cellgro, Manassas, VA), and 100 µg/mL streptomycin (Cellgro, Manassas, VA). MCF-7 (human breast cancer), Jurkat (human leukemia), T47D (human breast

cancer), U937 (human lymphoma), and A549 (human lung cancer) were grown in RPMI 1640 supplemented with 10% (v/v) fetal bovine serum, 100 µg/ml penicillin, and 100 µg/mL streptomycin. All cells were maintained in a humidified atmosphere with 95% air and 5% CO_2. All adherent cell lines were detached using 0.05% trypsin/EDTA, except for MIA PaCa-2 cells where 0.25% trypsin/EDTA was used.

Absorbance measurements were made on a Spectramax Plus or a Spectramax M3 (Molecular Devices, Sunnyvale, CA). Fluorescence measurements were made on an Analyst HT (LJL Biosciences) or a Spectramax M3 (Molecular Devices, Sunnyvale, CA).

High-throughput Screen for Cancer Cell Death. This protocol was used for the screening of the botanical extracts and the HTSF library. Screening of the Reisman compounds was performed as described for the Dose Response—384 well plates. Screening of the Movassaghi compounds was performed as described for the Dose Response—96 well plates. The protocol is the same as was previously used.[22] Briefly, 40 µL of media was added to all wells of a 384-well tissue culture-treated plate using an electronic multichannel pipette. 100 nL of compound in DMSO was then pin-transferred from compound storage plates into media-containing wells using the Platemate Plus at the UIUC HTSF. A 200,000 cells/mL suspension of breast cancer cells was prepared, and 10 µL was added to each well using an electronic multichannel pipette for a final concentration of 2000 cells/well. Doxorubicin and etoposide (100 µM final) were used as positive controls. Plates were sealed with gas-permeable seals and incubated at 37 °C for 48 h. After incubation, 5 µL of Alamar blue (440 µM resazurin in sterile PBS) was added and allowed to incubate for 2-5 h, until visible color change occurred.

Dose Response (IC_{50}) curves—384 well plates. This protocol was used for determining IC_{50}s for botanical extracts, HTSF compounds, **1227** and ersindole derivatives, and the Reisman compounds. To a 384-well plate, 40 µL of 1.25X compound dilution or 1.25% DMSO-containing media was added (final volume of 1% DMSO in all wells). The one exception to this was cisplatin,

which was dissolved in sterile saline. No DMSO was used in any wells containing cisplatin due to the ligand exchange that can occur. Concentrations of compounds tested were 1000 µM to 30 nM for 5-fluorouracil, 100 µM to 3 nM for cisplatin, ersindole, and all ersindole derivatives, and 10 µM to 0.3 nM for doxorubicin. On each plate at least 3 technical replicates were performed. Next, for HTSF compounds, 10 µL of either a 200,000 cells/mL (A549, Hs578t, MCF-7, MDA-MB-231, MIA PaCa-2, T47D, or 4T1) or 300,000 cells/mL (U937) suspension was added to each well, yielding a final concentration of 2,000 or 3,000 cells/well. For Reisman compounds, 10 uL of 100,000 cells/mL (A549 or HeLa) or 500,000 cells/mL (U937) was added to each well, yielding a final concentration of 1,000 or 5,000 cells/well. The final row of the plate received no cells and was used as the 100% dead control. To multiple wells in column 2 was added 0.5 µL of 10 mM doxorubicin (final concentration of 100 µM) and 0.5 µL of 1 mM bortezomib as positive controls that should result in cell death. Plates were sealed with gas-permeable seals and incubated at 37 ˚C for 48 h. At that time, 5 µL of Alamar blue (440 µM resazurin in sterile PBS) was added, the plates were re-sealed and incubated for 4-8 hours. Fluorescence was read on an Analyst HT or a Molecular Devices SpectraMax 3 (excitation = 555 nm, emission = 585 nm, emission cutoff = 570 nm). Wells were normalized to the average of non-edge untreated wells (0% cell death) and the average of no cells in wells (100% cell death). The data were plotted as compound concentration versus percent dead cells, and fitted to a logistic-dose response curve using either Table Curve (SYSTAT Software, Richmond, CA) or OriginPro (OriginLab, Northampton, MA). Hill Slope and E_{max} values were obtained from curves fitted by OriginPro. The data were generated in triplicate, and IC_{50} values, Hill slopes, and E_{max} values are reported as the average of three separate experiments along with standard error of the mean.

Dose Response (IC_{50}) curves—96 well plates. This protocol was used for determining IC_{50}s for the Movassaghi compounds. These experiments were performed as previously described.[12,21]

Briefly, adherent cell lines (H460 and MCF-7) were evaluated as follows: Cells (2000

cells/well) were added to 96 well plates in 99 µL of media and allowed to adhere for 2-3 hours. Compounds were solubilized in DMSO as 100X stocks and 1 µL of the stock was added directly to the cells (100 µL final volume). Concentrations tested ranged from 1 pM to 10 µM. DMSO and cell-free wells served as the live and dead controls, respectively. After 72 hours of continuous exposure, viability was assessed via the SRB colorimetric assay.[37] Cells were fixed by the addition of 50 µL of 10% trichloroacetic acid in water. After incubating at 4 °C for an hour, the plates were washed in water and allowed to dry. Sulforhodamine B was added as a 0.057% solution in 1% acetic acid (100 µL) and the plates were incubated for 30 minutes at room temperature. The plates were then washed in 1% acetic acid and allowed to dry. The dye was solubilized by adding 10 mM Tris base solution (pH 10.5, 200 µL) and incubating at room temperature for 30 minutes. Absorbance of the plate at 510 nm was then read. IC_{50} values were determined from three independent experiments using Origin (OriginLab, Northampton, MA).

Suspension cells (U937) were evaluated as follows: 1 µL of DMSO stock (100X concentration) was added to the wells of a 96 well plates for a final DMSO concentration of 1%. DMSO and cell-free wells served as the live and dead controls, respectively. U937 (5,000 cells/well) cells were distributed in 99 µL of media to the compound containing plate. After 72 hours, cell viability was assessed by Alamar blue. 10 µL of alamar blue (440 µM resazurin in sterile PBS) was added, and the plates were incubated for 4-8 hours. Fluorescence was read on a Molecular Devices SpectraMax 3 (excitation = 555 nm, emission = 585 nm, emission cutoff = 570 nm). The data were plotted as compound concentration versus percent dead cells, and fitted to a logistic-dose response curve using OriginPro (OriginLab, Northampton, MA).

Hemolysis Assay. Whole human blood in citrate phosphate dextrose was obtained from Bioreclamation LLC, stored at 4 ˚C and used before expiration date. Combined 100 µL of whole blood with 500 µL saline (0.9% NaCl), centrifuged for 5 min at 300xg. Carefully removed supernatant from erythrocyte pellet, discarded liquid. Washed pellet 3x in 500 µL saline. The

erythrocyte pellet was resuspended in 800 µL of Red Blood Cell Buffer (10 mM Na_2HPO_4, 150 mM NaCl, 1 mM $MgCl_2$, pH 7.4). To a 0.5 mL eppendorf tube or a PCR plate was added 1.0 µL of 30X compound in DMSO and 19 µL RBC Buffer. For negative controls, 1.0 µL DMSO was combined with 19 µL RBC buffer. For positive controls, either 20 µL MilliQ H_2O or 1.0 µL 30% Triton X-100 were combined with 19 µL RBC Buffer. Tubes or plates were briefly centrifuged. Next, 10 µL of washed erythrocyte suspension was added to each tube, then capped or sealed. After incubation at 37 ˚C for 2 h, samples were centrifuged for 5 min at 300xg, and 20 µL of supernatant was carefully removed and transferred to wells of a clear flat-bottomed 384-well plate. Absorbance was measured at 540 nm. Water and detergent controls were used for 100% hemolysis and DMSO vehicle controls were used for 0% hemolysis. The data were plotted as compound concentration versus percent hemolysis, and fitted to a logistic-dose response curve using either Table Curve (SYSTAT Software, Richmond, CA) or OriginPro (OriginLab, Northampton, MA).

Dose Response Timecourse. To a 96-well plate, 50 µL of media containing 40,000 cells/mL (MCF-7 or MIA PaCa-2) were added for a final seeding density of 2,000 cells/well. These cells were then allowed to attach overnight (typically ~12h). After adhering, 50 µL of media containing 2X compound dilution or 2% DMSO containing media was added to the cells. On each plate at least 3 wells per compound concentration were prepared. Compound concentrations tested were 100 µM to 3 nM for ersindole, tunicamycin, and thapsigargin and 10 µM to 0.3 nM for doxorubicin. Wells with just DMSO were used as 0% dead controls and wells without cells were used as the 100% dead controls. Plates were incubated at 37 ˚C for either 1, 3, or 6 h. At that time, media was removed from the wells, the wells were washed with 100 µL of fresh media, and then 200 µL of new media was added to the wells. Plates were then incubated at 37 ˚C until the live control wells were confluent (generally 48 h). The sulforhodamine B assay was then used to assess cell viability. Briefly, 100 µL of cold 10% trichloroacetic acid was added for a final concentration of

3.3% TCA and the plates were incubated at 4 °C for a minimum of 1 h. The plates were then washed with water and allowed to air dry. 100 µL of a 0.057% (w/v) sulforhodamine B and 1% (v/v) acetic acid solution were added and allowed to incubate at room temperature for 30 minutes. The plates were then rinsed 4 times with 1% (v/v) acetic acid and allowed to air dry. 200 µL of a 10 mM Tris base solution (pH ≥ 10.5) was added to each well and allowed to incubate for 30 minutes at room temperature. Absorbance at 510 nm was read on a Molecular Devices SpectraMax 3 and normalized to the average of non-edge untreated wells (0% cell death) and the average of no cells in wells (100% cell death). The data were plotted as compound concentration versus percent dead cells, and fitted to a logistic-dose response curve using OriginPro. IC_{50}, Hill Slope and E_{max} values were obtained from curves fitted by OriginPro. The data were generated in triplicate, and IC_{50} values, Hill slopes, and E_{max} values are reported as the average of three separate experiments along with standard error of the mean.

Western blotting. U937 cells at a density of 300,000 cells/mL were treated with indicated amounts of compound for indicated times in 6-well plates. Cells were then transferred to 15-mL conical tubes, centrifuged (3 min, 500xg), and the media was discarded. The cell pellet was resuspended in 1.0 mL sterile PBS and transferred to a 1.7-mL tube, centrifuged (3 min, 500xg) and PBS was discarded. The cell pellet was resuspended in RIPA lysis buffer (50 mM Tris, 150 mM NaCl, 1% Triton X-100, 0.5% Na-deoxycholate, 0.1% SDS, pH = 7.4) containing 1X protease inhibitor cocktail, 1X phosphatase inhibitor cocktail, and 1 mM PMSF. The suspension was vortexed for 3 seconds 3-5x over a 10 min incubation on ice. The lysate was clarified (15,000xg, 10 min) and the pellets were discarded. Protein concentration was determined by BCA assay and lysates were diluted with MilliQ H_2O to achieve a uniform protein concentration. Lysates were stored at -20 ˚C until use.

Gel samples were prepared by combining 13.5 µL of lysate with 2.5 µL 6X Laemmli dye containing 5% ß-mercaptoethanol (BME) in 0.5-mL tubes and heated to 95 ˚C for 5 min to

denature proteins. Once cooled, the samples were loaded onto a 4-20% Tris-HCl 15-well gel (Mini-Protean, TGX, Bio-Rad) and run at 120 V for 1 h. The gel was transferred to an activated PVDF membrane in Towbin transfer buffer (192 mM glycine, 25 mM Tris-HCl, 20% methanol, pH = 8.3) for 2 h at 45 V.

Membranes were blocked overnight at 4 ˚C in 5% milk or bovine serum albumin in TBST. Membranes were then washed quickly 2x with TBST (25 mM Tris, 150 mM NaCl, 0.1% Tween-20, pH = 7.6), then washed twice for 10 min in TBST, followed by an overnight incubation at 4 ˚C with 1:500-1:1000 dilution of primary antibody in 2% milk or bovine serum albumin in TBST. Next, membranes were washed 2x quickly and 2x 10 min with TBST, then incubated at room temperature for 2 h in a 1:10,000 dilution of secondary antibody (rabbit or mouse IgG horseradish peroxidase conjugate). Then membranes were washed 2x quickly and 2x 10 min with TBST, followed by 3-4 quick washes with PBS, then incubated for 3 min in SuperSignal West Pico Chemiluminescent Substrate (Thermo Scientific) mixture before visualization.

siRNA validation

siRNA were ordered from Qiagen in the FlexiPlate siRNA 384 well plate format with 0.1 nmol siRNA per well. When validated siRNAs were available, they were used. For transcripts that did not have validated siRNAs, two different siRNAs were ordered. See below for a table of the siRNAs that were used in this study. After thawing and centrifuging the plate of siRNAs, 50 µL of sterile RNAse free water was added to obtain a stock plate with 2 µM siRNA. The siRNA were allowed to dissolve for 30 minutes at 4 °C with occasional shaking. The plates were then centrifuged again and working plates were made. Then, 3.5 µL of siRNA was transferred to a sterile 96 well plate and 36.5 µL of sterile RNAse free water was added for a 175 nM stock.

Polyplus INTERFERin reverse transfection protocol was followed for the siRNA validation. Briefly, 2 µL of siRNA was added to a sterile RNAse free 96 well plate. AllStars Negative Control

siRNA was used for the live control and AllStars Hs Cell Death siRNA was used for the dead control. To the siRNA was added 96 µL of room temperature Optimem and 2 µL of INTERFERin. The solution was mixed by pipetting up and down and 50 µL was transferred to a new 96 well plate. Both plates were incubated at room temperature for 15-30 minutes.

While the plates were incubating, MIA PaCa-2 cells were trypsinized and then resuspended at 16,000 cells/mL in normal media. 125 µL of the cell suspension was then added to the plates for a final seeding density of 2000 cells/well. The plates were then incubated at 37 °C for 60 h. The plates were then treated with either DMSO or 6.5 µM ersindole for 3 h. After 3 h, media was removed, the plates were washed with 100 µL of fresh media and then 200 µL of media was added. Cells were allowed to recover until the live control was confluent (usually ~48 hours). Cell viability was then assessed using the sulforhodamine B assay. Briefly, 100 µL of cold 10% trichloroacetic acid was added for a final concentration of 3.3% TCA and the plates were incubated at 4 °C for a minimum of 1 h. The plates were then washed with water and allowed to air dry. 100 µL of a 0.057% (w/v) sulforhodamine B and 1% (v/v) acetic acid solution were added and allowed to incubate at room temperature for 30 minutes. The plates were then rinsed 4 times with 1% (v/v) acetic acid and allowed to air dry. 200 µL of a 10 mM Tris base solution (pH ≥ 10.5) was added to each well and allowed to incubate for 30 minutes at room temperature. Absorbance at 510 nm was read on a Molecular Devices SpectraMax 3 and normalized to the average of AllStars Negative Control siRNA (0% cell death) and the average of AllStars Hs Cell Death siRNA wells (100% cell death). Two independent replicates were performed.

Gene Symbol	**siRNA ID**
APAF1	Hs_APAF1_14
PPP1R15A	Hs_PPP1R15A_5

ESR1	Hs_ESR1_8
MGC26963	Hs_MGC26963_8
PERP	Hs_PERP_7
RAB26	Hs_RAB26_5
ITPR3	Hs_ITPR3_2
NCF4	Hs_NCF4_3
HMMR	Hs_HMMR_5
IDH3A	Hs_IDH3A_1
PEBP1	Hs_PEBP1_2
FLJ10858	Hs_FLJ10858_5
PPM1H	Hs_PPM1H_1
SLC7A6	Hs_SLC7A6_1
RTN3	Hs_RTN3_2
ARHGAP1	Hs_ARHGAP1_5
ITPR3	Hs_ITPR3_1
NCF4	Hs_NCF4_1
PPM1H	Hs_PPM1H_2
SLC7A6	Hs_SLC7A6_2
RTN3	Hs_RTN3_6
ARHGAP1	Hs_ARHGAP1_6
RNMT	Hs_RNMT_6
HNRPH3	Hs_HNRPH3_7
RASA1	Hs_RASA1_2
CACYBP	Hs_CACYBP_5
SLC22A4	Hs_SLC22A4_6
C1orf149	Hs_C1orf149_3
NCOA3	Hs_NCOA3_2
RBM35A	Hs_RBM35A_1
MKRN2	Hs_MKRN2_4
MAN1A2	Hs_MAN1A2_6

POU5F1	Hs_POU5F1_2
CDH18	Hs_CDH18_5
POLR2J2	Hs_POLR2J2_3
ZNF148	Hs_ZNF148_5
HYPE	Hs_HYPE_2
MTMR9	Hs_MTMR9_5
UAP1	Hs_UAP1_5
NIT2	Hs_NIT2_3
GANAB	Hs_GANAB_1
IL17RB	Hs_IL17RB_2
RNMT	Hs_RNMT_5
HNRPH3	Hs_HNRPH3_5
RASA1	Hs_RASA1_1
CACYBP	Hs_CACYBP_4
SLC22A4	Hs_SLC22A4_5
C1orf149	Hs_C1orf149_2
NCOA3	Hs_NCOA3_1
FLJ20171	Hs_FLJ20171_4
MKRN2	Hs_MKRN2_2
MAN1A2	Hs_MAN1A2_2
POU5F1	Hs_POU5F1_10
CDH18	Hs_CDH18_6
POLR2J2	Hs_POLR2J2_6
ZNF148	Hs_ZNF148_8
HYPE	Hs_HYPE_5
MTMR9	Hs_MTMR9_6
UAP1	Hs_UAP1_6
NIT2	Hs_NIT2_5
GANAB	Hs_GANAB_2
IL17RB	Hs_IL17RB_3

OSBPL7	Hs_OSBPL7_6
FLVCR	Hs_FLVCR_8
SATL1	Hs_SATL1_12
POL3S	Hs_POL3S_1
CCPG1	Hs_CCPG1_6
CYP2C19	Hs_CYP2C19_3
ELF1	Hs_ELF1_8
TAF6L	Hs_TAF6L_4
HS2ST1	Hs_HS2ST1_7
LAMP1	Hs_LAMP1_6
RNF4	Hs_RNF4_5
DEK	Hs_DEK_4
RPN2	Hs_RPN2_2
COL5A1	Hs_COL5A1_1
MCF2	Hs_MCF2_1
STX16	Hs_STX16_1
ELOVL6	Hs_ELOVL6_4
NFAT5	Hs_NFAT5_2
VN1R1	Hs_VN1R1_1
TSC2	Hs_TSC2_1
OSBPL7	Hs_OSBPL7_5
FLVCR	Hs_FLVCR_6
SATL1	Hs_SATL1_13
POL3S	Hs_POL3S_2
CCPG1	Hs_CCPG1_1
CYP2C19	Hs_CYP2C19_1
ELF1	Hs_ELF1_7
TAF6L	Hs_TAF6L_2
HS2ST1	Hs_HS2ST1_5
LAMP1	Hs_LAMP1_2

RNF4	Hs_RNF4_7
DEK	Hs_DEK_5
RPN2	Hs_RPN2_5
COL5A1	Hs_COL5A1_2
MCF2	Hs_MCF2_3
STX16	Hs_STX16_6
ELOVL6	Hs_ELOVL6_5
NFAT5	Hs_NFAT5_3
VN1R1	Hs_VN1R1_2
TSC2	Hs_TSC2_3
CLK3	Hs_CLK3_5
CLK3	Hs_CLK3_6
SLC25A20	Hs_SLC25A20_1
SUPT7L	Hs_SUPT7L_1
CFH	Hs_CFH_2
RRBP1	Hs_RRBP1_2
PPIE	Hs_PPIE_1
PIGC	Hs_PIGC_7
SLC25A20	Hs_SLC25A20_2
SUPT7L	Hs_SUPT7L_2
CFH	Hs_CFH_3
RRBP1	Hs_RRBP1_4
PPIE	Hs_PPIE_9
PIGC	Hs_PIGC_8
UBE1	Hs_UBE1_5
PRC1	Hs_PRC1_3
UBE1	Hs_UBE1_2
PRC1	Hs_PRC1_5

Murine Maximum Tolerated Dose Determination

Ersindole-9 was dissolved in PEG400 and administered to C57BL/6 female mice (10-12 week old, Charles River) intraperitoneally using a 1 mL syringe fitted with a 25 ga needle. The maximum tolerated dose of ersindole-9 was determined to be 60 mg/kg for a single dose.

Murine 4T1 Cancer Model

8 week old, female Balb/C mice (Charles River) were lightly sedated with i.p. xylazine/ketamine/saline solution and the right flank was shaved. Following sedation, 4T1 murine breast cancer cells suspended in chilled HBSS (1×10^6 cells in 100 µL) were injected subcutaneously into the right flank using an insulin syringe. On day 7 after inoculation, the mice were randomized with 8 mice per group for vehicle or 5 mice per group for ersindole-9 treatment. Vehicle (PEG400) or compound was administered intraperitoneally as a PEG400 solution (12 mg/mL in PEG400, 100 µL was injected per 20 g weight mouse for 60 mg/kg dosage) on days 7, 9, and 11. Tumor measurements were performed every 2 or 3 days using a caliper and tumor volume was calculated using the equation ($0.5 \times l \times w^2$). On day 19 after the 4T1 cells inoculation, the average tumor volume in the control group reached approximately 1000 mm^3 so all mice in both groups were sacrificed. The tumors were then surgically removed and their mass was measured.

4.7 References

(1) Granger, B. A.; Jewett, I. T.; Butler, J. D.; Hua, B.; Knezevic, C. E.; Parkinson, E. I.; Hergenrother, P. J.; Martin, S. F. Synthesis of (+/-)-actinophyllic acid and analogs: applications of cascade reactions and diverted total synthesis. *J Am Chem Soc* **2013**, *135*, 12984-12986.

(2) Zheng, W.; Thorne, N.; McKew, J. C. Phenotypic screens as a renewed approach for drug discovery. *Drug Discov Today* **2013**, *18*, 1067-1073.

(3) Moffat, J. G.; Rudolph, J.; Bailey, D. Phenotypic screening in cancer drug discovery - past, present and future. *Nat Rev Drug Discov* **2014**, *13*, 588-602.

(4) Yeoman, J. T.; Mak, V. W.; Reisman, S. E. A unified strategy to ent-kauranoid natural products: total syntheses of (-)-trichorabdal A and (-)-longikaurin E. *J Am Chem Soc* **2013**, *135*, 11764-11767.

(5) Cha, J. Y.; Yeoman, J. T.; Reisman, S. E. A concise total synthesis of (-)-maoecrystal Z. *J Am Chem Soc* **2011**, *133*, 14964-14967.

(6) Baell, J. B.; Holloway, G. A. New substructure filters for removal of pan assay interference compounds (PAINS) from screening libraries and for their exclusion in bioassays. *J Med Chem* **2010**, *53*, 2719-2740.

(7) Amslinger, S. The tunable functionality of alpha,beta-unsaturated carbonyl compounds enables their differential application in biological systems. *ChemMedChem* **2010**, *5*, 351-356.

(8) *Basic & Clinical Pharmacology, 13th Edition*; 13 ed.; Katzung, B.; Trevor, A., Eds.; McGraw-Hill Education, 2015.

(9) Avonto, C.; Taglialatela-Scafati, O.; Pollastro, F.; Minassi, A.; Di Marzo, V.; De Petrocellis, L.; Appendino, G. An NMR spectroscopic method to identify and classify thiol-trapping agents: revival of Michael acceptors for drug discovery? *Angew Chem Int Ed Engl* **2011**, *50*, 467-471.

(10) Lariat: Irving, TX, 2015; Vol. 2015; pp April 10, 2015.

(11) Dinkova-Kostova, A. T.; Liby, K. T.; Stephenson, K. K.; Holtzclaw, W. D.; Gao, X.; Suh, N.; Williams, C.; Risingsong, R.; Honda, T.; Gribble, G. W.; Sporn, M. B.; Talalay, P. Extremely potent triterpenoid inducers of the phase 2 response: correlations of protection against oxidant and inflammatory stress. *Proc Natl Acad Sci U S A* **2005**, *102*, 4584-4589.

(12) Boyer, N.; Morrison, K. C.; Kim, J.; Hergenrother, P. J.; Movassaghi, M. Synthesis and Anticancer Activity of Epipolythiodiketopiperazine Alkaloids. *Chem Sci* **2013**, *4*, 1646-1657.

(13) Siegel, R. L.; Miller, K. D.; Jemal, A. Cancer statistics, 2015. *CA Cancer J Clin* **2015**, *65*, 5-29.

(14) Gatza, M. L.; Lucas, J. E.; Barry, W. T.; Kim, J. W.; Wang, Q.; Crawford, M. D.; Datto, M. B.; Kelley, M.; Mathey-Prevot, B.; Potti, A.; Nevins, J. R. A pathway-based classification of human breast cancer. *Proc Natl Acad Sci U S A* **2010**, *107*, 6994-6999.

(15) Kinghorn, A. D.; Chin, Y. W.; Swanson, S. M. Discovery of natural product anticancer agents from biodiverse organisms. *Curr Opin Drug Discov Devel* **2009**, *12*, 189-196.

(16) Palchaudhuri, R.; Nesterenko, V.; Hergenrother, P. J. The complex role of the triphenylmethyl motif in anticancer compounds. *J Am Chem Soc* **2008**, *130*, 10274-10281.

(17) Bair, J. S.; Palchaudhuri, R.; Hergenrother, P. J. Chemistry and biology of deoxynyboquinone, a potent inducer of cancer cell death. *J Am Chem Soc* **2010**, *132*, 5469-5478.

(18) Huang, X.; Dong, Y.; Bey, E. A.; Kilgore, J. A.; Bair, J. S.; Li, L. S.; Patel, M.; Parkinson, E. I.; Wang, Y.; Williams, N. S.; Gao, J.; Hergenrother, P. J.; Boothman, D. A. An NQO1 substrate with potent antitumor activity that selectively kills by PARP1-induced programmed necrosis. *Cancer Res* **2012**, *72*, 3038-3047.

(19) Parkinson, E. I.; Bair, J. S.; Cismesia, M.; Hergenrother, P. J. Efficient NQO1 substrates are potent and selective anticancer agents. *ACS Chem Biol* **2013**, *8*, 2173-2183.

(20) Hodges, J. C.; Remers, W. A.; Bradner, W. T. Synthesis and antineoplastic activity of mitosene analogues of the mitomycins. *J Med Chem* **1981**, *24*, 1184-1191.

(21) Morrison, K. C. Chemical Diversification and Anticancer Activity of Natural Products, University of Illinois at Urbana-Champaign, 2013.

(22) Knezevic, C. E. Development of Poly(ADP-Ribose) Glycohydrolase Inhibitors and Tetracyclic Indoles as Anticancer Compounds, University of Illinois at Urbana-Champaign, 2014.

(23) Fallahi-Sichani, M.; Honarnejad, S.; Heiser, L. M.; Gray, J. W.; Sorger, P. K. Metrics other than potency reveal systematic variation in responses to cancer drugs. *Nat Chem Biol* **2013**, *9*, 708-714.

(24) Wang, G.; Yang, Z. Q.; Zhang, K. Endoplasmic reticulum stress response in cancer: molecular mechanism and therapeutic potential. *Am J Transl Res* **2010**, *2*, 65-74.

(25) Clarke, H. J.; Chambers, J. E.; Liniker, E.; Marciniak, S. J. Endoplasmic reticulum stress in malignancy. *Cancer Cell* **2014**, *25*, 563-573.

(26) Boyce, M.; Bryant, K. F.; Jousse, C.; Long, K.; Harding, H. P.; Scheuner, D.; Kaufman, R. J.; Ma, D.; Coen, D. M.; Ron, D.; Yuan, J. A selective inhibitor of eIF2alpha dephosphorylation protects cells from ER stress. *Science* **2005**, *307*, 935-939.

(27) Oslowski, C. M.; Urano, F. Measuring ER stress and the unfolded protein response using mammalian tissue culture system. *Methods Enzymol* **2011**, *490*, 71-92.

(28) Scheuner, D.; Patel, R.; Wang, F.; Lee, K.; Kumar, K.; Wu, J.; Nilsson, A.; Karin, M.; Kaufman, R. J. Double-stranded RNA-dependent protein kinase phosphorylation of the alpha-subunit of eukaryotic translation initiation factor 2 mediates apoptosis. *J Biol Chem* **2006**, *281*, 21458-21468.

(29) Das, I.; Krzyzosiak, A.; Schneider, K.; Wrabetz, L.; D'Antonio, M.; Barry, N.; Sigurdardottir, A.; Bertolotti, A. Preventing proteostasis diseases by selective inhibition of a phosphatase regulatory subunit. *Science* **2015**, *348*, 239-242.

(30) Samali, A.; Fitzgerald, U.; Deegan, S.; Gupta, S. Methods for monitoring endoplasmic reticulum stress and the unfolded protein response. *Int J Cell Biol* **2010**, *2010*, 830307.

(31) Kiviluoto, S.; Vervliet, T.; Ivanova, H.; Decuypere, J. P.; De Smedt, H.; Missiaen, L.; Bultynck, G.; Parys, J. B. Regulation of inositol 1,4,5-trisphosphate receptors during endoplasmic reticulum stress. *Biochim Biophys Acta* **2013**, *1833*, 1612-1624.

(32) Kajiwara, K.; Muneoka, T.; Watanabe, Y.; Karashima, T.; Kitagaki, H.; Funato, K. Perturbation of sphingolipid metabolism induces endoplasmic reticulum stress-mediated mitochondrial apoptosis in budding yeast. *Mol Microbiol* **2012**, *86*, 1246-1261.

(33) Raina, K.; Noblin, D. J.; Serebrenik, Y. V.; Adams, A.; Zhao, C.; Crews, C. M. Targeted protein destabilization reveals an estrogen-mediated ER stress response. *Nat Chem Biol* **2014**, *10*, 957-962.

(34) Wictome, M.; Henderson, I.; Lee, A. G.; East, J. M. Mechanism of inhibition of the calcium pump of sarcoplasmic reticulum by thapsigargin. *Biochem J* **1992**, *283 (Pt 2)*, 525-529.

(35) Duksin, D.; Mahoney, W. C. Relationship of the structure and biological activity of the natural homologues of tunicamycin. *J Biol Chem* **1982**, *257*, 3105-3109.

(36) Pulaski, B. A.; Ostrand-Rosenberg, S. Mouse 4T1 breast tumor model. *Current protocols in immunology / edited by John E. Coligan ... [et al.]* **2001**, *Chapter 20*, Unit 20 22.

(37) Vichai, V.; Kirtikara, K. Sulforhodamine B colorimetric assay for cytotoxicity screening. *Nat Protoc* **2006**, *1*, 1112-1116.